Exploration of N-Heterocyclic Carbenes for the Functionalization of Gold Surfaces and Their Metal Complexes

A Dissertation Presented for the
Doctor of Philosophy
Degree
The University of Tennessee, Knoxville

Shelby Lynne-Frances Strausser

May 2021

Copyright © 2021 by Shelby Lynne-Frances Strausser.
All rights reserved.

DEDICATION

I dedicate this page to my late grandfathers, Reed Foster Furman and Patrick Vincent Beuchert Sr.

ACKNOWLEDGEMENTS

In the five years of graduate school, there are a lot of people who helped me get to where I am today. I am dedicating this section of my dissertation to say thank you to every one of those people.

The first person I would like to thank is my husband, Jeffrey, I would not have been able to get through graduate school without him by my side. He has been my best friend, my rock, my shoulder to cry on, and the love of my life for the past 9 years. He is an incredible husband and dog father to Rocco. He has taken on the work of both of us in our home life in addition to working full-time so that I could finish my degree. I thank him for moving to Tennessee with me for this and Knoxville even became the place where we got married. I also thank him for allowing me to uproot our life again for a post-doc in Canada. Where hopefully his love of snowboarding will make up for it.

The next person I would like to think is my advisor, Dr. David Jenkins. I appreciate his support and efforts in allowing me to obtain my degree in his research group. He has helped me learn a lot more than I could ever know in organic and organometallic chemistry. I also completely appreciate his time and effort to help me finish my degree. I also appreciate our shared love for margaritas.

I would like to say thank you to my collaborators. Their work and expertise in their field has helped develop and expand the research of N-heterocyclic carbenes on gold surfaces. In particular, I would like to thank Dr. John Camden and his graduate students Mike Trujillo, Lindy Sherman, and Nathan Dominique at Notre Dame University, Dr. Bhavya Sharma and her graduate student Paula Pimiento at UTK, and Dr. Lasse Jensen and his graduate student Jeffrey Becca at Pennsylvania State University. Without our shared work, we would not have been able to expand this field of research.

I would like to thank my committee members, Dr. Bhavya Sharma, Dr. Ampofo Darko, and Dr. Cong Trinh. They have provided me with valuable advice and knowledge as I went along in my degree. Their time and efforts have given me the ability to become a better chemist and researcher.

I would like to thank my fellow colleagues in the Jenkins group. My friend, Joseph DeJesus, gave me the foundation and advice for this work presented in my dissertation and being my “marg. guy”. Xian Carrol taught me about X-ray crystallography and edited many drafts of my dissertation and I truly thank her. Kevin Blatchford and Vernon Stafford became close friends of mine and helped me survive graduate school by supporting my work and for the enlightening talks and venting. I would also like to thank the Long group at UTK. Dr. Long and his graduate students have helped with teaching me to build laboratory apparatus’ that were crucial for my work in isotope labeling. I would like to thank Justin Burroughs in the Long lab and his wife Karlie Burroughs. They have become amazing friends in Knoxville, and I can’t wait for our friendships to continue to grow in all of our future endeavors.

Lastly, I would like to thank my family for their encouragement to pursue my doctoral degree. They reminded me that even when things are difficult that everything works out in the end and made me the fighter and strong woman I am today through it all.

ABSTRACT

Gold surface chemistry has progressed considerably towards many applications in medicine. Due to the non-toxic nature of gold in the human body, gold surfaces have been investigated for biometric sensors and targeted drug therapy agents. While gold is relatively unreactive in its elemental form, gold surfaces (such as films or nanoparticles) require a ligand for stability and improved functionality. The typical ligand is thiols for self-assembled monolayers on gold surfaces. While thiol self-assembly on surfaces is well understood, thiols are known to degrade or leach under a wide variety of conditions, including both thermal and chemical, which is toxic in the body. For gold surfaces to be viable in the medical field, the surface ligands must be stable in a multitude of conditions. Thiols' degradation has resulted in the exploration for more stable ligands. Since N-heterocyclic carbene (NHC) ligands are strong σ-donors, they have the potential to replace thiols. In a short time, utilization of NHCs have greatly advanced the field of gold surface chemistry. These ligands have shown greater stability than thiols under a variety of conditions. Since these ligands are new to surface chemistry, research has not progressed past the traditional imidazolium and benzimidazolium based NHCs. However, variations from the traditional NHC ligands can be more effective in solution phase chemistry. The research presented in this dissertation will focus on synthesis, spectroscopy, and theory to understand the binding of NHCs to gold surfaces. The exploration of non-standard NHC ligands were also explored for functionalization of gold surfaces. The traditional NHC ligands were deuterated and bound to gold surfaces to aid in the assignment of their modes in SERS. Within the non-traditional NHC ligands, an imidazolinium NHC ligand was bound and the stability was tested on gold surfaces to show the first examples of non-standard NHC superior stability over and imidazolium NHC. In addition, using a conjugated six-membered NHC, four d^{10} metal complexes were synthesized and characterized through X-ray crystallography and NMR. Finally, a variety of functionalized NHC ligands are in the process of being synthesized for post-synthetic modification on gold surfaces.

Table of Contents

Chapter 1 : Introduction 1
References 2
Chapter 2 Using SERS to Understand the Binding of N-Heterocyclic Carbenes to Gold Surfaces 12
Abstract 13
Introduction 14
Experimental 24
References 67
Chapter 3 : Imidazolinium N-Heterocyclic Carbene Ligands for Enhanced Stability on Gold Surfaces 71
Abstract 72
Introduction 73
Results and Discussion 75
Experimental 81
References 93
Chapter 4 : Synthesis of d^{10} Perimidinium N-Heterocyclic Carbene Complexes 98
Abstract 99
Introduction 100
Results and Discussion 100
Experimental 110
References 124
Chapter 5 : Preparation of N-Heterocyclic Carbene Gold complexes for Collaborative Projects 129
Abstract 130
Manuscripts in Preparation 131
Experimental 137
References 141
Chapter 6 : Synthesis of “Click” Tagged N-Heterocyclic Carbenes for Post-synthetic Modification of Gold Nanoparticles 142
Abstract 143
Introduction 143
Results and Discussion 146
Experimental 150

References 157
Chapter 7 : Development of N-Heterocyclic Carbene Ligands for Stability and Modification on Gold Surfaces 160
Abstract 161
Introduction 162
Experimental 171
References 181
Chapter 8 : Conclusion 183
References 185
Vita 205

List of Figures

Figure 1.1: Examples of Au surface chemistry applications including A. Heterogeneous catalysis,[10] B. Environmental control,[11] C. Drug delivery[12], and D. Biosensors[13] 3
Figure 1.2: A. Schematic of N-heterocyclic carbene ligand and the stabilization through the π-donation of the neighboring nitrogens. B. NHC complexes used for the functionalization of Au surfaces. C. Methods of surface functionalization. 4
Figure 1.3: Examples of characterization techniques for Au surfaces. A. left: Scanning electron spectroscopy (SEM). right: X-ray photoelectron Spectroscopy (XPS). B. Benzimidazolium coated Au Film over nanosphere (FON) and corresponding surface-enhanced Raman spectroscopy (SERS) spectra of the various R groups. Figures were used from our groups previous publications.[28, 32] 6
Figure 1.4: N-heterocyclic carbene (NHC) ligands possess different properties depending on their heteroatoms, ring size, and conjugation. A. A variety of NHC ligands are shown, imidazolylidene (1.4a-b), benzimidazolylidene (1.4c), imidazolinylidene (1.4d), pyrrolidinylidene (CAAC, 1.4e), perimidinylidene (1.4f), versus acyclic-variant (Fisher carbene, 1.4g) and trimethylphosphene (1.4h). B. Graph showing the increase in σ-donor properties starting with PMe_3 (1.4h) then NHCs (1.4d,a,f) to Fischer carbene, 1.4g. C. Graph demonstrating the ^{13}C and ^{31}P NMR of the carbene carbon and phosphorus signals shift downfield with the increase of π-acceptor ability from NHCs (1.4b-e) and Fischer Carbene, 1.4g. Graphs were recreated from data in previously published reports[37, 38] 7
Figure 2.1: In this Letter, we investigate preferred binding of NHCs to gold surfaces: (1) surface versus tip (left), (2) the influence of side groups and their orientation (middle), and (3) which modes contribute the greatest SERS signal (right). 15
Figure 2.2: Isotopic variants of the imidazole (2.1−2.3) and benzimidazole (2.4−2.6) N-heterocyclic carbenes synthesized and spectroscopically characterized in this study. 15
Figure 2.3: Left: Raman spectrum of the CO_2 adduct (red) and the benzimidazolium iodide precursor (black) of compound 2.4 compared with the surface-enhanced Raman spectrum of 2.4-Au on the AuFON surface. Right: Raman spectrum of the CO_2 adduct (red) and the imidazolium iodide precursor (black) of compound 2.1 compared with the SERS spectrum of 2.1-Au (blue). A clear red shift of the C−N bonds moving from the CO_2 adduct to the precursor and finally to the carbene, most evident in the benzimidazolium spectra and indicated by dotted line, is attributed to the change from an electron-withdrawing group (carboxylate), to a neutral molecule, and lastly an electron-donating group (gold surface). 18
Figure 2.4: Top: Calculated SERS spectra of 2.4-Au with the NHC bound to a “surface” gold atom (black) and a “tip” gold atom (green) of a Au_{20} cluster. Optimized geometries of both tip and surface cases are presented as inset images. The strength of the Au−C bond is sufficient to pull a gold atom up from the cluster despite the known stability of the Au_{20} surface. Bottom: Calculated SERS spectra of 2.4-Au with isopropyl groups oriented up (red) and down (blue). The prominent differences between the spectra resulting from up and down isopropyl groups indicate that the SERS is very sensitive to the orientation of the side groups. 20
Figure 2.5: Experimental SERS spectra (solid) and theoretical SERS spectra (dashed), overlaid, show excellent agreement for both 2.1-Au and 2.4-Au (left and right, respectively). Theory shows that many of the most intense modes in the spectra are derived from motion on the isopropyl side groups. These modes are shown pictorially above the spectra with their energies. Red and blue coloring is used to indicate modes arising primarily from up- and down-oriented isopropyl groups, respectively. Asterisks indicate modes from polystyrene spheres below the gold film. 20
Figure 2.6: Left: Theoretical (top) and experimental (bottom) SERS spectra of 2.1-Au (black) and 2.2-Au (green). Right: Theoretical (top) and experimental (bottom) SERS spectra of 2.4-Au (black) and 2.5-Au (green). The isotope shifts upon deuteration are well reproduced by the theory, and several of the most perturbed modes are presented pictorially next to the spectra. * indicates a contribution from polystyrene spheres below the gold film. 22
Figure 2.7: X-ray crystal structure of 1,3-diisopropyl-imidazolium iodide (2.7). Purple, blue, gray, and white ellipsoids (50% probability) represent I, N, C, and H atoms, respectively. 33

Figure 2.8: X-ray crystal structure of 1,3-diisopropyl(4,5,6,7-d_4)benzimidazolium iodide (2.13). Purple, blue, gray, and white ellipsoids (50% probability) represent I, N, C, and H/D atoms, respectively. ..34
Figure 2.9: Pictorial representation of calculated vibrational modes for 2.4 which shift from 1431 cm^{-1} in the Raman spectrum of the protected carbene to 1405 cm^{-1} when bound to the surface. 63
Figure 2.10: Pictorial representation of calculated vibrational modes for 2.1 which shift from 1434 cm^{-1} in the Raman spectrum of the protected carbene to 1404 cm^{-1} when bound to the surface. 64
Figure 2.11: Experimental SERS Spectra of 2.4 (black) overlaid on the calculated SERS spectrum of 2.4 with isopropyl groups oriented upward (red), downward (blue), and a 49:51 combination of upward and downward (green). Shading in red and blue indicates primary contribution from the up and downward oriented isopropyls, respectively.....65
Figure 2.12: (*Left*) SERS spectra of 2.3-Au (black) and 2.6-Au (green). Deuteration of the isopropyl moieties causes a decoupling of the vibrational modes of the ring and isopropyl groups, causing both SERS spectra to be dominated by the ring modes. This results in a loss of sensitivity to the orientation of the isopropyl orientation. (*Right*) Pictorial representations of the ring modes for 2.3-Au and 2.6-Au in both the up (red) and down (blue) configurations illustrating the strong ring component in each case. 66
Figure 3.1: Comparison of traditional (A-B) and less-explored (C) NHC structures on gold surfaces. The imidazolium (A) and imidazolinium (C) are the focus of this work 74
Figure 3.2: Protocol for depositing NHC-CO_2 adducts onto gold substrates. While AuFONs are shown in this scheme, the same procedure is also used for flat gold mirrors. This work examines the deposition of 3.1, 3.2, and 3.3 on Au surfaces. Chechik and coworkers previously demonstrated that surfaces obtained from 3.8 are not stable.[54] The imidazolinium NHC with isopropyl side groups (bottom left) presented synthetic challenges and could not be isolated (vide infra). 76
Figure 3.3: XPS analyses of Au mirrors functionalized with ligands 3.1 (red traces) and 3.2 (green traces) along with the overall fits (black traces). (A) N1s peak is at 400.45 eV, (B) C1s peak is at 284.85 eV (C) N1s peak is at 399.92 eV, and (D) C1s peak is at 284.91 eV.....79
Figure 3.4: SERS spectra of 3.1•AuFONs (red traces) and 3.2•AuFONs (blue traces) before (top row) and after (middle row) exposure to 1 M HCl for 24 h. The bottom row is a blank SERS spectrum of the AuFONs substrate. Peaks marked with an asterisk are from the substrate. 79
Figure 3.5: Representative SEM image of gold film-over-nanospheres substrate. 89
Figure 3.6: XPS control of gold mirror, exhibiting no identifiable signal coming from N 1s prior to deposition of the N-heterocyclic carbene ligands.....90
Figure 3.7: XPS analyses of Au mirrors functionalized with ligands 3.1 (red) and 3.2 (green) along with the overall fits (black traces). (A) Au $4f_{7/2}$ peak is at 84.2 eV, and (B) Au $4f_{7/2}$ peak is at 84.5 eV. These results are consistent with previously reported binding energies for adsorbed NHC ligands on gold.[18, 27, 63] 90
Figure 3.8: SERS spectra of imidazolium and imidazolinium NHC ligands with deuterated backbones on AuFONs. Blue trace is previously published data.[25] The red trace is 3.3•AuFONs, prepared from ligand 3.3. Asterisks denote peaks from the substrate. 91
Figure 3.9: Summary of stability tests performed on 3.1•AuFONs. The NHC-coated substrates were submerged in the indicated solvent for 24 h. Each condition was performed in triplicate. 91
Figure 3.10: Summary of stability tests performed on 3.2•AuFONs. The NHC-coated substrates were submerged in the indicated solvent for 24 h. Each condition was performed in triplicate. 92
Figure 4.1: (A) Typical NHCs for five-membered and six-membered rings. (B) Examples of previously reported perimidinium metal complexes. All previous examples are on Ru, Rh, Pd (example not shown), Os, and Ir. (C) Newly reported perimidinium metal complexes in this manuscript. 101
Figure 4.2: Solid state structures of (A) ($C_{10}H_6(^iPrN)_2$)C)AuCl, 4.1, and (B) ($C_{10}H_6(^iPrN)_2$)C)AgCl, 4.2. Yellow, indigo, blue, gray, and green ellipsoids (50% probability) represent gold, silver, nitrogen, carbon, and chlorine, respectively. Hydrogen atoms are omitted for clarity unless necessary to display close interatomic interactions (dark gray spheres). Selected bond lengths (Å) and angles (°): 1 Au-C1, 2.020(3); Au-Cl, 2.3092(8); C1-Au-Cl, 179.96(8); 2 Ag-C1, 2.1312(11); Ag-Cl, 2.3628(3); C1-Ag-Cl, 170.13(3). 104

Figure 4.3: Solid state structures of (A) $[(C_{10}H_6(^iPrN)_2)C)CuCl]_2$, 4.3, and (B) $(C_{10}H_6(^iPrN)_2)C)Pt(PPh_3)_2$, 4.4. Cyan, orange, blue, gray, green, and pink ellipsoids (50% probability) represent copper, platinum, nitrogen, carbon, chlorine, and phosphorous, respectively. Hydrogen atoms are omitted for clarity unless necessary to display close interatomic interactions (dark gray spheres). Selected bond lengths (Å) and angles (°): 4.3 Cu-C1, 1.932(3); Cu-Cl, 2.263(1); Cu-Cl', 2.391(1); C1-Cu-Cl, 140.91(12); C1-Cu-Cl', 123.81(12); Cl1-Cu-Cl', 94.91(4); 4.4 Pt-C1, 2.057(3); Pt-P1, 2.2475(9); Pt-P2, 2.2581(9); C1-Pt-P1, 121.20(8); C1-Pt-P2, 124.69(8); P1-Pt-P2, 113.92(3). 105
Figure 4.4: NMR spectra of (A) $(C_{10}H_6(^iPrN)_2)C)AuCl$, 4.1 and (B) $[(C_{10}H_6(^iPrN)_2)C)CuCl]_2$, 4.3. (A) ^1H NMR of 4.1 shown with ^{13}C NMR inset. Methine proton and carbon resonances are severely broadened suggesting slow rotation about the C-N bond. (B) ^1H NMR spectra for 4.3 shown at two temperatures, 300 K (top) and 230 K (bottom). 107
Figure 6.1: Ideal example of aptamer coupling to the NHC coated surface through amide coupling (A) and click coupling (B). The aptamer bound surface would then react with a target biomolecule of choice (C). The ideal NHCs of choice would be the benzimidazolium and imidazolium ligands containing a terminal alkyne (D). Ideally, to utilize the LSPR effect of Au NPs the alkyne needs to be closer to the surface (n=0) but other lengths can be explored. 145
Figure 6.2: Raman (red) of 6.1 and SERS (blue) of 6.1-AuNPs. 149
Figure 7.1: (Top) General approach to functionalize AuNPs with NHC ligands. (Bottom) Effects of increasing concentration of NHC-Au complex in AuNPs. From left to right: 1 µL 7.1, 5 µL CH_2Cl_2, 5 µL 7.1, 25 µL 7.1, and 100 µL 7.1 solutions. All 7.1 solutions are a 1mM concentration. Image taken from our Angew. paper.[6] 163
Figure 7.2: Four examples of water-soluble NHCs used on AuNPs.[1, 2, 7, 8] 165
Figure 7.3: Examples of two NHC-Au surfaces that have been employed for chiral detection (7.15A-AuNP and 7.15B-Au)[13, 14] and our proposed chiral imidazolinium NHC on NPs (7.15C-AuNP). 168
Figure 7.4: Target chiral molecules to bind to gold surfaces. 168

List of Schemes

Scheme 2.1: Preparation of NHC AuFONs - Either with or without Air Exposure 18
Scheme 2.2: Synthesis of imidazole-CO_2 adducts (2.1-2.3). 31
Scheme 2.3: Synthesis of benzimidazole-CO_2 adducts (2.4-2.6). 32
Scheme 3.1: Synthesis of imidazolinium CO_2 adducts, including the deuterated analog (3.3). 76
Scheme 4.1: Synthesis of perimidinium complexes 4.1-4.4. 102
Scheme 4.2: Transmetalation reactions from 4.2. 109
Scheme 5.1: Target molecules previously synthesized (top). Synthesis of 5.3 from previously synthesized benzimidazolium bromide salt. 133
Scheme 5.2: Functionalization of 40nm gold nanoparticles with A. NO_2-benzimidazolium NHC and B. benzenethiol. 136
Scheme 6.1: Schemes of attempted alkyne imidazolium Au complex. 147
Scheme 6.2: Synthesis of NHC-Au complexes using the basic (top) and Ag_2O (bottom) methods. 147
Scheme 6.3: Synthetic route to the methylated alkyne imidazolium gold chloride complex, 6.1. 149
Scheme 7.1: Synthetic methods to synthesize complexes 7.6 – 7.8. 165
Scheme 7.2: Proposed synthetic route to synthesize all isomers of 7.16 and 7.17. 169

Chapter 1 : Introduction

Due to its great stability in air compared to other coinage metals, gold is at the forefront of surface chemistry despite its high cost. In the biological context, gold surfaces, as either films or nanoparticles (AuNPs), have been used for drug delivery[1, 2] and biometric sensors[3, 4] (**Figure 1.1**). Gold surfaces have also been employed in the heterogeneous catalysis[5, 6] and environmental control[7-9]. For example, AuNPs have been demonstrated to be key in catalytic hydrochlorination of alkynes[10] (**Figure 1.1A**) and the detection of mercury (Hg^{2+}) in water through colorimetric analysis[11] (**Figure 1.1B**). Examples of these applications help for the advancement in cancer detection, therapy, and treatment. The utilization of AuNPs allows for the injection of encapsulated biologically active molecules and in the specific area of treatment and upon irradiation the molecules can be released only in the targeted area (**Figure 1.1C**).[12] This advancement can prevent subjecting patients to chemotherapy over the entire body. AuNPs have also shown advancement of detecting biomarkers of a variety of cancers through modification of the surface with aptamers or RNA[13] (**Figure 1.1D**).

While elemental gold is typically unreactive, gold surfaces can be stabilized and modified using a protective coating, often called self-assembled monolayers (SAMs). SAMs on Au surfaces are often comprised of thiols[14, 15] and sometimes amines,[16] though both of their stabilities are poor. Various accounts have shown that under ambient conditions, thiols can readily oxidize or otherwise dissociate from gold surfaces. For example, Schoenfisch and Pemberton showed significant oxidation of a variety of thiols on gold surfaces in ambient conditions in as little as one hour.[17] In addition, thiols have diminished stability under heat,[18-20] UV exposure,[21-23] and in biological media such as buffer solutions and calf serum (BSA).[24, 25] The failures of the thiol-based SAMs have thus led to researchers in the chemical biology field to search for a more reliable ligand that can function under biologically relevant conditions.

In recent years, N-heterocyclic carbenes (NHCs) have proven to be a viable alternative to thiol containing SAMs. These ligands are a type of Fischer carbene consisting of a heterocycle with two nitrogen atoms and a neutral carbon in between them possessing a lone pair of electrons and an empty p-orbital. NHCs are strong σ-bond donors that are stabilized by the donation of lone pairs from the adjacent nitrogens (**Figure 1.2A**). Substituents on the NHC nitrogens can vary from alkyl to aryl groups and a variety of functional groups can be incorporated on the R group to further functionalize a surface. One caveat for using NHC ligands is the requirement for a masking group to be used for most applications (**Figure 1.2B**), as free NHCs are not stable in air. This air sensitivity prevents surfaces in aerobic and aqueous conditions from being functionalized. This problem is one of the biggest challenges for NHC incorporation onto surfaces. Fortunately, several approaches have been developed to overcome this deficiency. The synthesis of NHC-CO_2 adducts (**1.1**) or bicarbonate salts (**1.2**) allow for the functionalization of Au surfaces under aerobic conditions (**Figure 1.2C, route 1**)[26-29] while NHC Au halide complexes (**1.3**) are used for the synthesis of NHC AuNPs[30, 31] in aqueous conditions (**Figure 1.2C, route 2**). Each of these approaches will be explored in this dissertation.

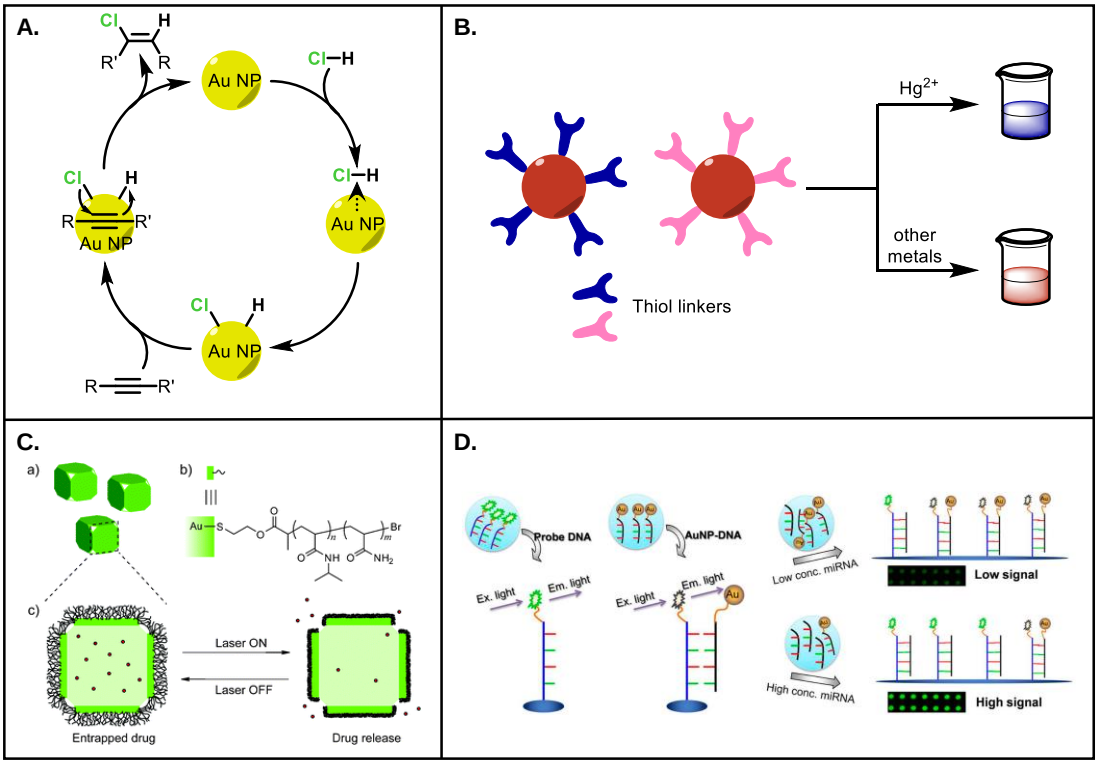


Figure 1.1: Examples of Au surface chemistry applications including **A.** Heterogeneous catalysis,[10] **B.** Environmental control,[11] **C.** Drug delivery[12], and **D.** Biosensors[13]

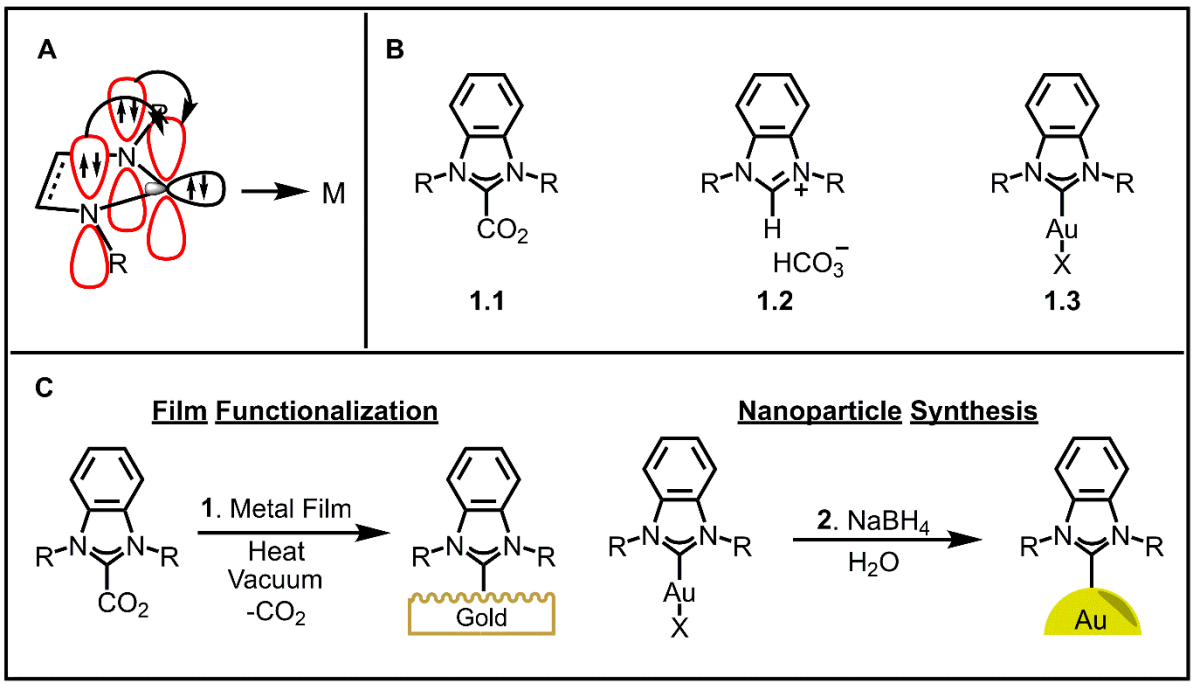


Figure 1.2: **A.** Schematic of N-heterocyclic carbene ligand and the stabilization through the π-donation of the neighboring nitrogens. **B.** NHC complexes used for the functionalization of Au surfaces. **C.** Classic methods of surface functionalization.

For gold surface chemistry, the main methods of surface characterization include X-ray photoelectron spectroscopy (XPS), scanning electron microscopy (SEM), transition electron microscopy (TEM), and atomic force microscopy (AFM), and (**Figure 1.3A**). The main concerns with these techniques are that they are destructive, expensive, binary, or they do not give exact molecular information. To combat this problem, our research group, in collaboration with the Camden group at the University of Notre Dame and, more recently, the Sharma group at the University of Tennessee, have demonstrated using surface-enhanced Raman spectroscopy (SERS) to characterize gold surfaces (**Figure 1.3B**).[28, 29, 32] SERS allows for the detection of molecules attached to the surface by utilizing the localized plasmons to significantly enhance the signal of the target molecule. Compared to previous techniques, SERS allows for the direct recognition of functional groups on the surface. As an example of how powerful this technique can be, one can examine when an R-group on an NHC ligand on a gold surface is either a proton (top) or a bromide (bottom), the spectra look similar (**Figure 1.3B**). However, the middle two spectra that corresponds to the R-group being a nitrile or ester have key peaks in the silent region, outlined in black boxes, that show the frequencies of the bonds of the key functional groups. Thus, SERS can be a powerful tool for determining most functional groups that are present on gold surfaces. SERS can also be used to show whether a reaction on the surface as occurred by monitoring the loss or shift in stretches. Therefore, we have chosen SERS as our main method of characterization of gold surfaces.

To date, the most used NHCs for surface functionalization are the imidazolium (**1.4a-b**) and benzimidazolium (**1.4c**) variants (

Figure 1.4A). These ligands have proven to be useful in the initial investigations of NHC functionalized gold surfaces, though a new set of NHC ligands have been explored as part of this dissertation. These ligands can be classified as non-standard NHCs and a few examples relevant to this dissertation are shown in **Figure 1.4A**, complexes **1.4d-f**. These ligands vary from the more traditional ones by the saturation of the backbone on an imidazolium (imidazolinium, **1.4d**), the replacement of a nitrogen in the ring (cyclic alkyl amino carbene (CAAC), **1.4e**) or the use of a six-membered heterocyclic ring (**1.4f**). The shift from the traditional imidazolium ligands to nonstandard NHCs show an increase in catalytic activity[33, 34] and has also been employed in Grubbs and Hoveyda catalysts.[35, 36] Reports by Herdtweck and Bertrand have shown that in comparison to the traditional NHC ligands, non-standard ligands possess stronger σ-donor[37] and π-accepting properties.[38]

There are two main methods of ranking the donor/acceptor properties of the various NHC ligands. The first is through the synthesis of $Rh(NHC)(CO)_2Cl$ complexes

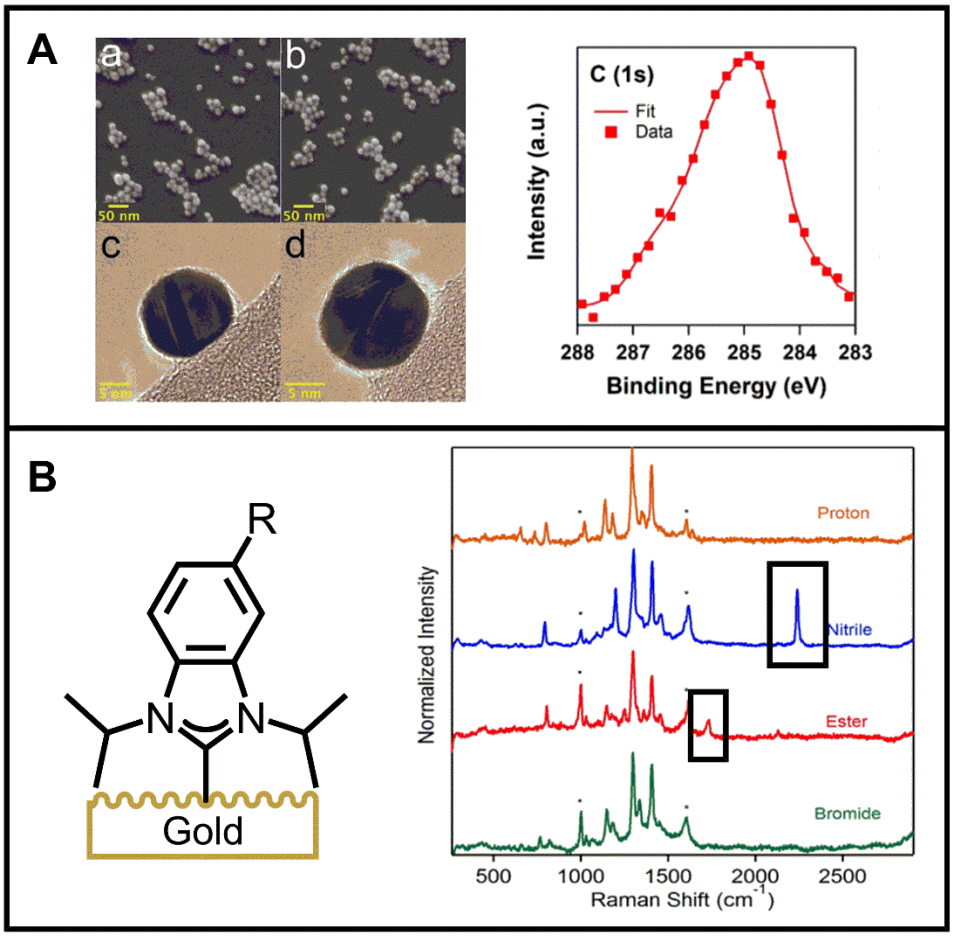


Figure 1.3: Examples of characterization techniques for Au surfaces. **A.** left: Scanning electron spectroscopy (SEM). right: X-ray photoelectron Spectroscopy (XPS). **B.** Benzimidazolium coated Au Film over nanosphere (FON) and corresponding surface-enhanced Raman spectroscopy (SERS) spectra of the various R groups. Figures were used from our groups previous publications.[28, 32]

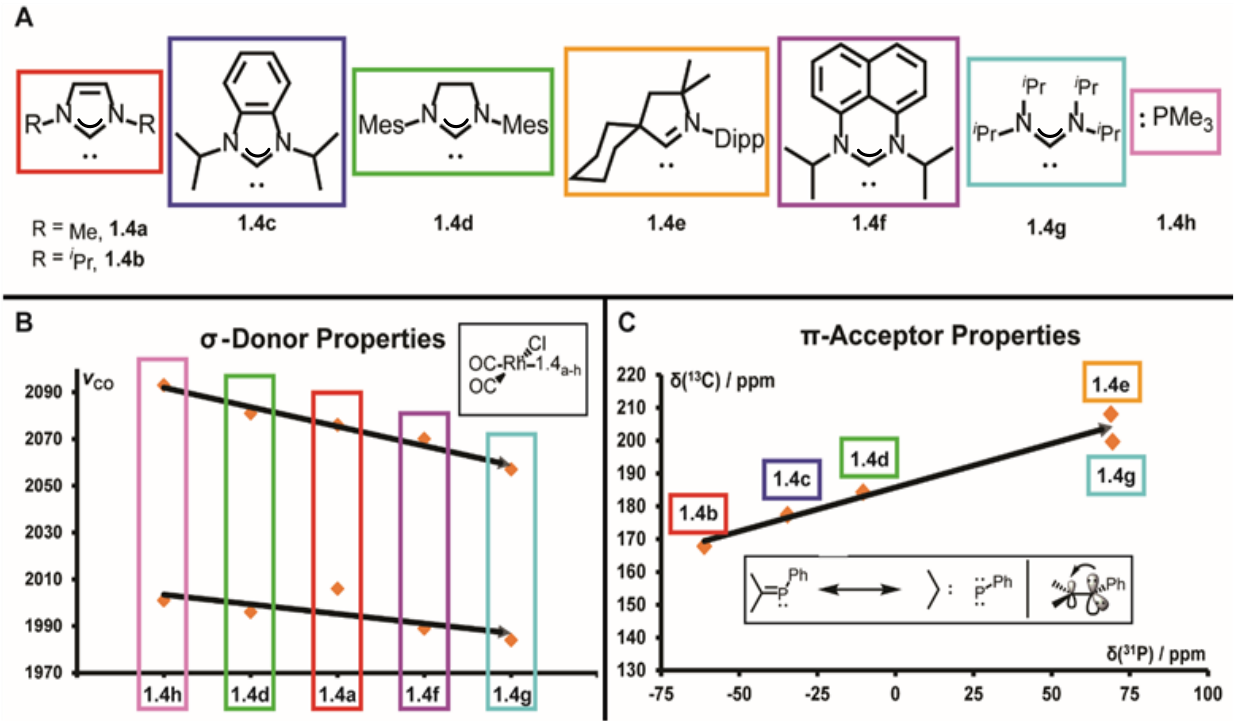


Figure 1.4: N-heterocyclic carbene (NHC) ligands possess different properties depending on their heteroatoms, ring size, and conjugation. **A.** A variety of NHC ligands are shown, imidazolylidene (**1.4a-b**), benzimidazolylidene (**1.4c**), imidazolinylidene (**1.4d**), pyrrolidinylidene (CAAC, **1.4e**), perimidinylidene (**1.4f**), versus acyclic-variant (Fisher carbene, **1.4g**) and trimethylphosphene (**1.4h**). **B.** Graph showing the increase in σ-donor properties starting with PMe_3 (**1.4h**) then NHCs (**1.4d,a,f**) to Fischer carbene, **1.4g**. **C.** Graph demonstrating the ^{13}C and ^{31}P NMR of the carbene carbon and phosphorus signals shift downfield with the increase of π-acceptor ability from NHCs (**1.4b-e**) and Fischer Carbene, **1.4g.** Graphs were recreated from data in previously published reports[37, 38]

with the different NHCs compared to a phosphine and Fischer carbene and comparing the *v*(CO) infrared data of each complexes (**Figure 1.4B**).[37]

The second is the comparison of carbene–phosphinidene adducts' ^{13}C and ^{31}P NMR shifts of the different carbene ligands (

Figure 1.4C).[38] In both cases, there is a general trend in the increase of donor/acceptor strength starting from the phosphine (**1.4h**) to the traditional imidazolium (**1.4a/b**), benzimidazolium (**1.4c**), then the following non-standard NHCs: imidazolinium (**1.4d**), CAAC (**1.4e**), and perimidinium (**1.4f**), finally the Fischer carbene (**1.4g**) being the strongest ligand. The one exception in the σ-donor trend being the imidazolinium NHC (**1.4d**), though this is not unexpected due to the lack of π-electrons to resonate in the structure compared to its unsaturated analog. However, **1.4d** does possess stronger π-acceptor properties than **1.4b** and **1.4c**. The increase in donor/acceptor properties should allow for a stronger NHC-metal bond, which is advantageous in biological applications of surface chemistry especially compared to the common thiol ligands.[18, 24] Another advantage of non-standard NHCs is the ability to introduce chirality to the surface which is important in chiral detection and heterogeneous catalysis. Specifically, ligands **1.4d** and **1.4e** possess this ability, though, to date, chiral NHC surface chemistry has not been explored with these ligands.

The research presented in this dissertation aims to show a deeper understanding of NHC ligands on metals and surfaces and will showcase three overall objectives:

1. Standard NHCs and the understanding of their binding and characterization with SERS, SESORS, LDI and DFT theory

   Chapter 2 provides insight on how NHCs bind to gold surfaces through synthesis of imidazolium and benzimidazolium CO_2-adducts and their deuterated isotopologues combined with experimental data from SERS and DFT theory[29]. The work in Chapter 2 has been published. Chapter 5 includes the synthesis of known molecules and a newly synthesized deuterated gold complex for collaborators that was necessary to develop new techniques and stability tests of NHC gold surfaces in biological media. The projects in Chapter 5 are currently manuscripts in preparation.

2. Effects of ligand modification on NHC stability on gold surfaces and synthesis of metal complexes

   Chapter 3 shows the synthesis and detection of a non-standard NHC ligand (saturated imidazolium) on a roughened Au surface through SERS while Chapter 4 demonstrates the ability to synthesize and characterize four novel 6-membered ring NHC metal complexes. Chapter 3 has been accepted into Langmuir. Chapter 4 has been submitted and is under review in Organometallics.

3. Developing functionalized NHCs for reactions on the gold surface

   Chapters 6 and 7 address the additional functions of NHC ligands including for surface modifications, water solubility, and chirality. All these synthetic modifications

will advance NHC gold surface chemistry and research in these chapters is unpublished and ongoing.

References

1. Farooq, M. U.; Novosad, V.; Rozhkova, E. A.; Wali, H.; Ali, A.; Fateh, A. A.; Neogi, P. B.; Neogi, A.; Wang, Z., Gold Nanoparticles-enabled Efficient Dual Delivery of Anticancer Therapeutics to HeLa Cells. *Scientific Reports* **2018,** *8*, 2907.
2. Xu, L.; Liu, Y.; Chen, Z.; Li, W.; Liu, Y.; Wang, L.; Liu, Y.; Wu, X.; Ji, Y.; Zhao, Y.; Ma, L.; Shao, Y.; Chen, C., Surface-Engineered Gold Nanorods: Promising DNA Vaccine Adjuvant for HIV-1 Treatment. *Nano Letters* **2012,** *12*, 2003-2012.
3. Homola, J., Present and future of surface plasmon resonance biosensors. *Anal Bioanal Chem* **2003,** *377*, 528-39.
4. Zhao, Y.; Zhou, H.; Zhang, S.; Xu, J., The synthesis of metal nanoclusters and their applications in bio-sensing and imaging. *Methods and Applications in Fluorescence* **2019,** *8*, 012001.
5. Hutchings, G. J., Vapor phase hydrochlorination of acetylene: Correlation of catalytic activity of supported metal chloride catalysts. *Journal of Catalysis* **1985,** *96*, 292-295.
6. Masatake, H.; Tetsuhiko, K.; Hiroshi, S.; Nobumasa, Y., Novel Gold Catalysts for the Oxidation of Carbon Monoxide at a Temperature far Below 0 °C. **1987,** *16*, 405-408.
7. Chen, P.-C.; Roy, P.; Chen, L.-Y.; Ravindranath, R.; Chang, H.-T., Gold and Silver Nanomaterial-Based Optical Sensing Systems. **2014,** *31*, 917-942.
8. Sener, G.; Uzun, L.; Denizli, A., Lysine-promoted colorimetric response of gold nanoparticles: a simple assay for ultrasensitive mercury(II) detection. *Analytical chemistry* **2014,** *86*, 514-20.
9. Setyawati, M. I.; Fang, W.; Chia, S. L.; Leong, D. T., Nanotoxicology of common metal oxide based nanomaterials: their ROS-y and non-ROS-y consequences. **2013,** *8*, 205-217.
10. Oliver-Meseguer, J.; Doménech-Carbó, A.; Boronat, M.; Leyva-Pérez, A.; Corma, A., Partial Reduction and Selective Transfer of Hydrogen Chloride on Catalytic Gold Nanoparticles. **2017,** *56*, 6435-6439.
11. Lee, J.-S.; Han, M. S.; Mirkin, C. A., Colorimetric Detection of Mercuric Ion (Hg^{2+}) in Aqueous Media using DNA-Functionalized Gold Nanoparticles. **2007,** *46*, 4093-4096.
12. Mout, R.; Moyano, D. F.; Rana, S.; Rotello, V. M., Surface functionalization of nanoparticles for nanomedicine. *Chemical Society Reviews* **2012,** *41*, 2539-2544.
13. Cordeiro, M.; Ferreira Carlos, F.; Pedrosa, P.; Lopez, A.; Baptista, P. V., Gold Nanoparticles for Diagnostics: Advances towards Points of Care. *Diagnostics (Basel, Switzerland)* **2016,** *6*.
14. Vericat, C.; Vela, M. E.; Benitez, G.; Carro, P.; Salvarezza, R. C., Self-assembled monolayers of thiols and dithiols on gold: new challenges for a well-known system. *Chemical Society Reviews* **2010,** *39*, 1805-1834.
15. Vericat, C.; Vela, M. E.; Corthey, G.; Pensa, E.; Cortés, E.; Fonticelli, M. H.; Ibañez, F.; Benitez, G. E.; Carro, P.; Salvarezza, R. C., Self-assembled monolayers of thiolates on metals: a review article on sulfur-metal chemistry and surface structures. *RSC Advances* **2014,** *4*, 27730-27754.

16. de la Llave, E.; Clarenc, R.; Schiffrin, D. J.; Williams, F. J., Organization of Alkane Amines on a Gold Surface: Structure, Surface Dipole, and Electron Transfer. *The Journal of Physical Chemistry C* **2014,** *118*, 468-475.
17. Schoenfisch, M. H.; Pemberton, J. E., Air Stability of Alkanethiol Self-Assembled Monolayers on Silver and Gold Surfaces. *Journal of the American Chemical Society* **1998,** *120*, 4502-4513.
18. Borzenkov, M.; Chirico, G.; D'Alfonso, L.; Sironi, L.; Collini, M.; Cabrini, E.; Dacarro, G.; Milanese, C.; Pallavicini, P.; Taglietti, A.; Bernhard, C.; Denat, F., Thermal and Chemical Stability of Thiol Bonding on Gold Nanostars. *Langmuir* **2015,** *31*, 8081-8091.
19. Delamarche, E.; Michel, B.; Kang, H.; Gerber, C., Thermal Stability of Self-Assembled Monolayers. *Langmuir* **1994,** *10*, 4103-4108.
20. Li, F.; Zhang, H.; Dever, B.; Li, X.-F.; Le, X. C., Thermal Stability of DNA Functionalized Gold Nanoparticles. *Bioconjugate Chemistry* **2013,** *24*, 1790-1797.
21. Huang, J.; Hemminger, J. C., Photooxidation of thiols in self-assembled monolayers on gold. *Journal of the American Chemical Society* **1993,** *115*, 3342-3343.
22. Hutt, D. A.; Leggett, G. J., Influence of Adsorbate Ordering on Rates of UV Photooxidation of Self-Assembled Monolayers. *The Journal of Physical Chemistry* **1996,** *100*, 6657-6662.
23. Zhang, Y.; Terrill, R. H.; Bohn, P. W., Ultraviolet Photochemistry and ex Situ Ozonolysis of Alkanethiol Self-Assembled Monolayers on Gold. *Chemistry of Materials* **1999,** *11*, 2191-2198.
24. Flynn, N. T.; Tran, T. N. T.; Cima, M. J.; Langer, R., Long-Term Stability of Self-Assembled Monolayers in Biological Media. *Langmuir* **2003,** *19*, 10909-10915.
25. Jans, K.; Bonroy, K.; De Palma, R.; Reekmans, G.; Jans, H.; Laureyn, W.; Smet, M.; Borghs, G.; Maes, G., Stability of mixed PEO-thiol SAMs for biosensing applications. *Langmuir* **2008,** *24*, 3949-54.
26. Crudden, C. M.; Horton, J. H.; Ebralidze, I. I.; Zenkina, O. V.; McLean, A. B.; Drevniok, B.; She, Z.; Kraatz, H.-B.; Mosey, N. J.; Seki, T.; Keske, E. C.; Leake, J. D.; Rousina-Webb, A.; Wu, G., Ultra stable self-assembled monolayers of N-heterocyclic carbenes on gold. *Nature Chemistry* **2014,** *6*, 409-414.
27. Crudden, C. M.; Horton, J. H.; Narouz, M. R.; Li, Z.; Smith, C. A.; Munro, K.; Baddeley, C. J.; Larrea, C. R.; Drevniok, B.; Thanabalasingam, B.; McLean, A. B.; Zenkina, O. V.; Ebralidze, I. I.; She, Z.; Kraatz, H.-B.; Mosey, N. J.; Saunders, L. N.; Yagi, A., Simple direct formation of self-assembled N-heterocyclic carbene monolayers on gold and their application in biosensing. *Nature Communications* **2016,** *7*, 12654.
28. DeJesus, J. F.; Trujillo, M. J.; Camden, J. P.; Jenkins, D. M., N-Heterocyclic Carbenes as a Robust Platform for Surface-Enhanced Raman Spectroscopy. *Journal of the American Chemical Society* **2018,** *140*, 1247-1250.
29. Trujillo, M. J.; Strausser, S. L.; Becca, J. C.; DeJesus, J. F.; Jensen, L.; Jenkins, D. M.; Camden, J. P., Using SERS To Understand the Binding of N-Heterocyclic Carbenes to Gold Surfaces. *The Journal of Physical Chemistry Letters* **2018,** *9*, 6779-6785.
30. MacLeod, M. J.; Johnson, J. A., PEGylated N-Heterocyclic Carbene Anchors Designed To Stabilize Gold Nanoparticles in Biologically Relevant Media. *Journal of the American Chemical Society* **2015,** *137*, 7974-7977.

31. Narouz, M. R.; Li, C.-H.; Nazemi, A.; Crudden, C. M., Amphiphilic N-Heterocyclic Carbene-Stabilized Gold Nanoparticles and Their Self-Assembly in Polar Solvents. *Langmuir* **2017,** *33*, 14211-14219.
32. DeJesus, J. F.; Sherman, L. M.; Yohannan, D. J.; Becca, J. C.; Strausser, S. L.; Karger, L. F. P.; Jensen, L.; Jenkins, D. M.; Camden, J. P., A Benchtop Method for Appending Protic Functional Groups to N-Heterocyclic Carbene Protected Gold Nanoparticles. **2020,** *59*, 7585-7590.
33. Marx, V. M.; Sullivan, A. H.; Melaimi, M.; Virgil, S. C.; Keitz, B. K.; Weinberger, D. S.; Bertrand, G.; Grubbs, R. H., Cyclic Alkyl Amino Carbene (CAAC) Ruthenium Complexes as Remarkably Active Catalysts for Ethenolysis. **2015,** *54*, 1919-1923.
34. Melaimi, M.; Jazzar, R.; Soleilhavoup, M.; Bertrand, G., Cyclic (Alkyl)(amino)carbenes (CAACs): Recent Developments. **2017,** *56*, 10046-10068.
35. Garber, S. B.; Kingsbury, J. S.; Gray, B. L.; Hoveyda, A. H., Efficient and Recyclable Monomeric and Dendritic Ru-Based Metathesis Catalysts. *Journal of the American Chemical Society* **2000,** *122*, 8168-8179.
36. Sanford, M. S.; Love, J. A.; Grubbs, R. H., Mechanism and Activity of Ruthenium Olefin Metathesis Catalysts. *Journal of the American Chemical Society* **2001,** *123*, 6543-6554.
37. Herrmann, W. A.; Schütz, J.; Frey, G. D.; Herdtweck, E., N-Heterocyclic Carbenes: Synthesis, Structures, and Electronic Ligand Properties. *Organometallics* **2006,** *25*, 2437-2448.
38. Back, O.; Henry-Ellinger, M.; Martin, C. D.; Martin, D.; Bertrand, G., 31P NMR Chemical Shifts of Carbene–Phosphinidene Adducts as an Indicator of the π-Accepting Properties of Carbenes. **2013,** *52*, 2939-2943.

Chapter 2 : Using SERS to Understand the Binding of N-Heterocyclic Carbenes to Gold Surfaces

A version of this chapter was originally published by Michael J. Trujillo, Shelby L. Strausser, Jeffrey C. Becca, Joseph F. DeJesus, Lasse Jensen, David M. Jenkins and Jon P. Camden as:

Trujillo Michael J.; Strausser Shelby L.; Becca Jeffrey C.; DeJesus Joseph F.; Jensen Lasse, Jenkins David M.; Camden Jon P. Using SERS to Understand the Binding of N-Heterocyclic Carbenes to Gold Surfaces. *The Journal of Physical Chemistry Letters*, **2018**, 9, 6779-6785.

The work presented in this publication was completed in a collaborative manner with groups at the University of Notre Dame (Camden lab) and Pennsylvania University (Lasse lab). My portion of the publication entails the synthesis of complexes 2.1-2.5. Joseph De Jesus at the University of Tennessee (Jenkins Lab) synthesized complex 2.6 and gave great help in the mentoring me in the synthesis of the NHC-CO_2 adducts. Michael Trujillo was responsible for the synthesis of NHC-Au FONs and obtaining their corresponding SERS spectra in both the manuscript and experimental section. Jeffrey Becca was responsible for the theoretical calculations and figures in the experimental section of the predicted SERS spectra of all the complexes on the Au substrates. The experimental section has been shortened to display the work that I have attributed to the manuscript, except where the main text refers to figures in that section.

Abstract

Surface functionalization is an essential component of most applications of noble-metal surfaces. Thiols and amines are traditionally employed to attach molecules to noble-metal surfaces, but they have limitations. A growing body of research, however, suggests that N-heterocyclic carbenes (NHCs) can be readily employed for surface functionalization with superior chemical stability compared with thiols. We demonstrate the power of surface-enhanced Raman scattering combined with theory to present a comprehensive picture of NHC binding to gold surfaces. In particular, we synthesize a library of NHC isotopologues and use surface-enhanced Raman scattering to record the vibrational spectra of these NHCs while bound to gold surfaces. Our experimental data are compared with first-principles theory, yielding numerous new insights into the binding of NHCs to gold surfaces. In addition to these insights, we expect our approach to be a general method for probing the local surface properties of NHC-functionalized surfaces for their expanding use in sensing applications.

Introduction

The role of surface functionalization cannot be underestimated when considering the myriad of applications of noble-metal surfaces. It plays a critical role in sensing,[1] drug delivery,[2] electronics,[3, 4] surface protection,[5] and synthesis of uniquely shaped nanoparticles.[6] Amines and thiols are often the first choice when functionalization of gold surfaces is required because they have relatively high affinity for noble-metal surfaces, with binding energies of 25 and 125 kJ mol^{-1} to gold, respectively.[7, 8] Whereas thiols, in particular, are used in many applications, their stability is greatly diminished in harsh chemical environments, such as oxidizing conditions, high temperature, and pH extremes.[9, 10]A viable alternative to thiols for functionalized gold surfaces has remained elusive until the recent emergence of N-heterocyclic carbenes (NHCs).[11] Although the binding of NHCs to gold surfaces is very strong, the free carbene is quite reactive[12] and their use was historically limited to carefully controlled chemical environments, which are often impractical for widespread adoption. Fortunately, progress has been made in the preparation of air-stable protected carbenes that serve as precursors to self-assembled monolayers on gold,[11, 13, 14] and NHC-functionalized gold films have been used in surface plasmon resonance[15, 16]and electrochemical[11, 17] measurements. Additionally, there is a growing body of literature reports on the preparation of NHC-functionalized nanoparticles.[18-24] After the initial reports of NHC-functionalized gold surfaces, the NHC binding, stability, and monolayer formation have been interrogated by a variety of methods.[11, 13, 25, 26] Whereas we recently demonstrated the first application of NHCs for SERS and showed that their robust binding allows post-synthetic modifications,[27] fundamental questions relating to the binding of NHCs to gold surfaces remain unexplored: (1) Where do NHCs prefer to bind on gold surfaces, (2) are the vibrational modes of surface-bound species sensitive to the NHC side moieties, and (3) which vibrational modes contribute most strongly to the SERS spectrum (**Figure 2.1**)? SERS is uniquely positioned to answer these questions because it possesses extreme sensitivity and an ability to measure the vibrational fingerprint of species in close proximity to plasmonic metal nanostructures without employing high-vacuum or complicated experimental setups. SERS can determine adsorbate orientation,[28-30] and detailed vibrational mode assignments can be made by deuteration of adsorbate molecules[31] and comparison with first-principles theory.[32, 33] Deuteration of surface-bound species alters both the molecular motions and vibrational mode energies while minimally altering other properties such as the affinity for the metal surface, a feature that was exploited when measuring single-molecule SERS spectra.[34-37] As such, it provides an excellent vehicle for exploring the detailed surface vibrational spectroscopy of NHC monolayers on noble metals.

In this Letter, we synthesize an NHC library composed of deuterated isotopologues of the imidazolium and benzimidazolium NHCs. Using this library, we prepare NHC-functionalized, SERS-active gold surfaces for spectroscopic characterization. The resulting SERS spectra show excellent agreement with first-principles theory, allowing us to extract details of the surface binding motifs. Additionally, the spectroscopy of these

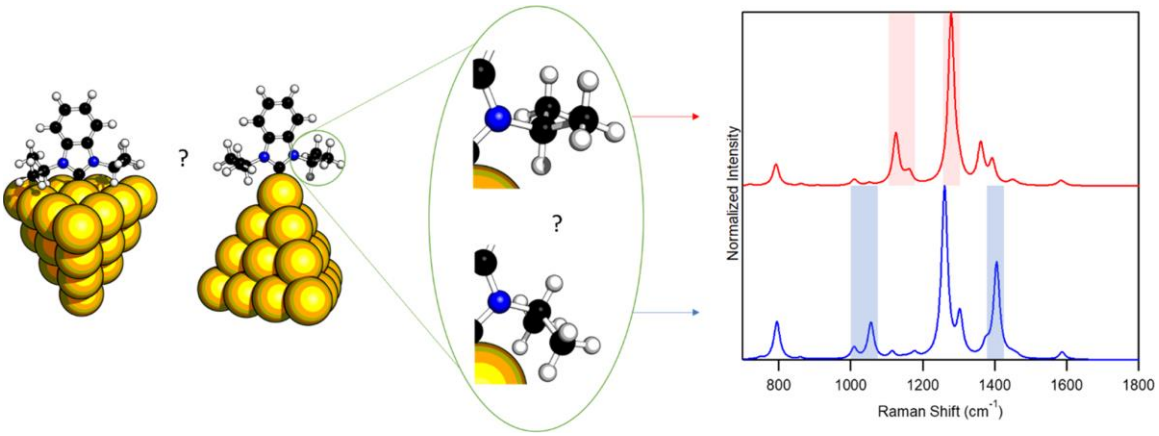


Figure 2.1: In this Letter, we investigate preferred binding of NHCs to gold surfaces: (1) surface versus tip (left), (2) the influence of side groups and their orientation (middle), and (3) which modes contribute the greatest SERS signal (right).

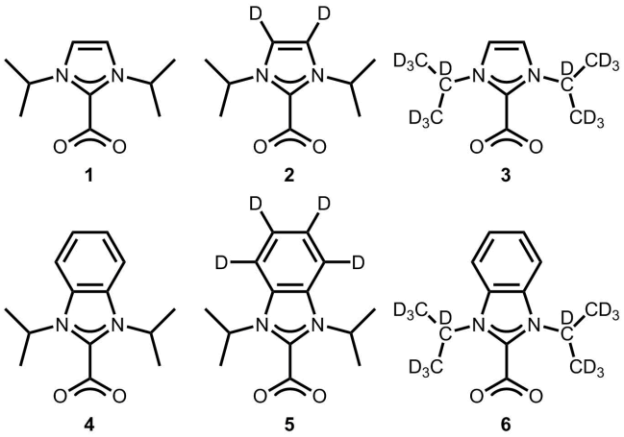


Figure 2.2: Isotopic variants of the imidazole (2.1−2.3) and benzimidazole (2.4−2.6) N-heterocyclic carbenes synthesized and spectroscopically characterized in this study.

compounds are carefully characterized with NMR, IR, Raman, and mass spectrometry. Using these data, we obtain a comprehensive picture of NHC binding to SERS-active gold substrates, and, more specifically, we obtain insight into several important open questions related to NHC films. More importantly, we demonstrate SERS to be a powerful tool when exploring as-yet unmade NHC-functionalized surfaces.

Synthesis of NHC−CO_2 Adducts and Surface Binding. In selecting the target NHCs for this study, it is notable that the N-substituent can affect the binding to the metal surface. Whereas multiple N-substituents, including methyl[20, 38, 39] and isopropyl[11] groups, have been studied, we selected isopropyls because they have been demonstrated to have excellent stability on gold.[13, 27] The six target molecules in **Figure 2.2** require a synthetic strategy that allows for deuteration, followed by the formation of the NHC−CO_2 adduct. The NHC binds to gold following the loss of CO_2 under vacuum. In addition, upon exposure to air, the NHC−CO_2 adducts yield NHC−bicarbonate salts that are equally effective for gold binding.

For the imidazoliums, 2.1−2.3, we followed the method of Louie for forming the final CO2-adducted species.[40] The general schemes for their synthesis are shown in **Scheme 2.2**. Compounds 2.2 and 2.3 required deuterium incorporation at >95% for quality SERS spectra because incomplete deuteration alters the symmetry of the molecule. In the case of 2.2, very similar imidazoliums have been previously prepared by Bartsch.[41] Compound 2.3 can be deuterated with the addition of 2-bromopropane-*d*7 (98+% d) to imidazole.

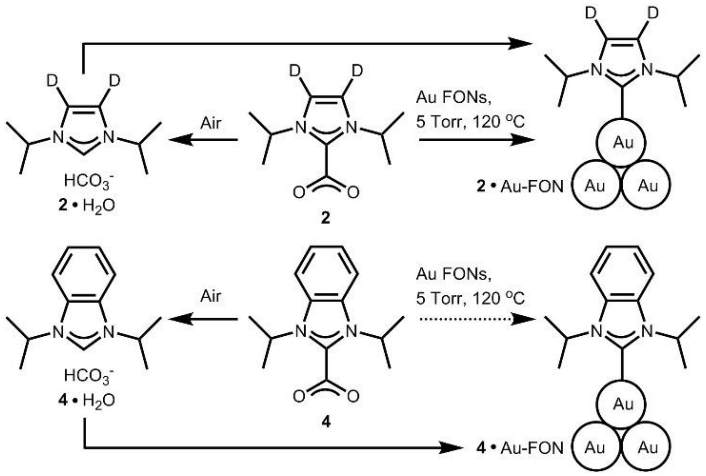
The synthesis of the benzimidazole versions of the CO_2 adducts, 2.4−2.6, proved more challenging. Despite our recent report[27] of 2.4 via a synthetic approach that we employed for 2.1−2.3, we subsequently discovered that it is a mixture of 2.4 and the bicarbonate salt (2.4·H_2O). This mixture for benzimidazole−CO_2 adduct and its associated bicarbonate salt is not uncommon because the pure CO_2 adducts of benzimidazolium are highly unstable (vide infra).[42] Fortuitously, Limbach previously prepared 2-carboxy-1,3-dimethyl-benzimidazolium, which differs only in the substituents off the nitrogen atoms.[43] Employing KO^{t}Bu as the base in THF with 2.10, followed by CO_2 gas, yields the pure product 2-carboxy-1,3-diisopropylbenzimidazolium, 2.4, based on ^{13}C NMR in CD_2Cl_2 (**Scheme 2.3** and **Spectra 2.10**), which was consistent with Limbach's report.[43] In particular, the CO_2 peak at 156.21 ppm in CD_2Cl_2 is consistent with his value for 2-carboxy-1,3-dimethyl-benzimidazolium, which comes at 154.7 ppm and is distinct from the bicarbonate salt (vide infra).

Inserting deuterium into the benzimidazole ring was not as straightforward as the equivalent imidazole, but a series of four reactions led to 2.5, which is deuterated on the aryl ring (**Scheme 2.3**). Deuteration proceeded via a modified procedure from Sajiki to give 97% total deuterium incorporation.[44] The benzimidazole, (4,5,6,7-d_4)-benzimidazole was formed through the addition of ethyl orthoformate to 2.11 under acidic conditions similar to the method of Bielawski.[45] Further reactions to form 2.5 proceeded in the same manner as for 2.4. Finally, 2-carboxy-1,3-(d_{14})-diisopropylbenzimidazolium, 2.6, was

synthesized in two steps that were analogous to the reactions for the preparation of 2.3. Deuterium incorporation for 2.6 is 99% on the isopropyl positions. The NHC−CO_2 adducts are important because they provide masked carbenes that are easily bound to the gold surface under atmospheric conditions without the need for special storage once they have been synthesized. We previously reported that 2.4 could be placed on AuFONs under solvent-free conditions by applying vacuum (5 Torr) at 120 °C.[27] However, the stability of the NHC−CO_2 adducts was tested to determine if they are effective after exposure to air. We investigated one imidazole NHC−CO_2 adduct, 2.2, and one benzimidazole NHC−CO_2 adduct, 2.4, for stability and effectiveness after air exposure (**Scheme 2.1**).

After exposure to air, the solids were dissolved in dry CD_2Cl_2 to evaluate their NMR spectra for decomposition. Compound 2.2 formed a nearly 50:50 mixture of 2.2 and its associated bicarbonate salt, 2.2·H_2O, after 1 week of exposure, which is consistent with Taton's studies on similar NHCs (**Scheme 2.1**, top; **Spectra 2.47**).[42] The key additional peaks in the ^{1}H NMR include the imidazolium peak at 10.97 ppm and the second set of peaks related to the isopropyl groups at 4.88 and 1.58 ppm. Conversely, tests with the benzimidazolium version showed that the decomposition to the bicarbonate salt was extremely rapid. The addition of air to 2.4 was tested at 4 days, 10 min, and 30 s (**Scheme 2.1**, bottom). In the first two cases, 2.4 was completely degraded to its bicarbonate salt 2.4·H_2O (**Spectra 2.48**). In the benzimidazolium case (2.4), there is a peak at 11.58 ppm and the isopropyl peaks shift upfield at 5.09 ppm, analogous to the imidazolium case. Only on the very short time of 30 s of air exposure were we able to observe both 2.4 and 2.4·H_2O (**Spectra 2.1**). We deposited the NHCs on AuFONs because they are easy to prepare and are widely used for SERS studies.[46] AuFONs are gold film over nanosphere substrates prepared by the evaporation of gold (200 nm) on polystyrene nanospheres (600 nm diameter) using a chromium (5 nm) adhesion layer (see the experimental section for details).[47] Because the AuFONs were functionalized with the NHCs by placing a 1 to 2 mg amount of solid NHC precursor directly onto the AuFON then heating the AuFONs to 120 °C under vacuum (5 Torr), this suggests that the formation of the Au−NHC bond is equally possible from both the NHC−CO_2 − and the bicarbonate salt. In practice, the imidazole variants 2.1−2.3 primarily proceed from the direct CO_2 adduct, whereas the benzimidazole versions proceed through the bicarbonate salt (**Scheme 2.1**). This result is consistent with previous reports of Au-NHCs by Crudden, who employed the bicarbonate salts, and Glorius and Johnson, who directly used the CO_2 adducts for gold films.[13, 14, 26]

Analysis of SERS Spectra. **Figure 2.3** displays a portion of the Raman spectrum of the protected carbene, the Raman spectrum of the iodide precursor, and the SERS spectrum of the carbene on an AuFON for the benzimidazolium and imidazolium families of compounds. The complete spectra can be found in the **Experimental Section**. A comparison of the Raman spectrum of the protected carbenes (2.1, 2.4) to the SERS spectrum of the carbenes on gold (2.1-Au, 2.4-Au) shows a 30 cm^{-1} red shift of the 1434 (2.1) and 1436 cm^{-1} (2.4) modes upon binding. The red shift of these bands is consistent with NHC binding to gold, which is electron-donating when compared with the electron



Scheme 2.1: Preparation of NHC AuFONs - Either with or without Air Exposure

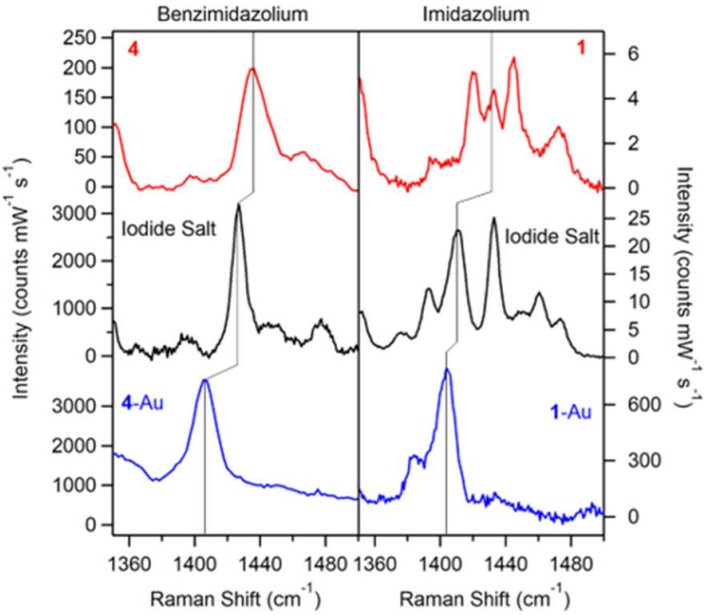


Figure 2.3: Left: Raman spectrum of the CO_2 adduct (red) and the benzimidazolium iodide precursor (black) of compound 2.4 compared with the surface-enhanced Raman spectrum of 2.4-Au on the AuFON surface. Right: Raman spectrum of the CO_2 adduct (red) and the imidazolium iodide precursor (black) of compound 2.1 compared with the SERS spectrum of 2.1-Au (blue). A clear red shift of the C−N bonds moving from the CO_2 adduct to the precursor and finally to the carbene, most evident in the benzimidazolium spectra and indicated by dotted line, is attributed to the change from an electron-withdrawing group (carboxylate), to a neutral molecule, and lastly an electron-donating group (gold surface).

withdrawing nature of the CO_2 group. This interpretation is further supported by the Raman spectrum of the iodide precursor, which is expected to be intermediate between the Au-bound and the CO_2-protected NHC. Indeed, the Raman spectra of the iodide precursors display bands in between the two extremes at 1426 and 1410 cm^{-1} for the benzimidazolium and imidazolium iodide compounds, respectively. The theoretical data also capture this effect, predicting a ~30 cm^{-1} red shift of vibrational modes upon the release of the CO_2 and binding to the AuFONs, in good agreement with experiment. Complete spectra and a pictorial representation of the vibrational modes of 2.4 and 2.1 are given in **Figure 2.9** and **Figure 2.10,** respectively.

Figure 2.4 displays the optimized geometry of compound 2.4 bound to the "tip" or the "surface" of a Au_{20} cluster. This cluster was chosen because it is known to be a good model for the calculation of SERS spectra.[48, 49] The computational data suggest that both the tip and surface configurations are remarkably similar because the surface Au is distorted by the carbene, creating its own "tip," resembling an adatom. The theoretical calculations further demonstrate sensitivity to the geometry of the R groups attached to the N, particularly for compound 2.4 (**Figure 2.4**, bottom). The best agreement between theory and experiment was obtained from an equal combination of upward and downward orientation of the isopropyl groups, as determined by creating a series of spectra ranging from 100% upward to 100% downward and calculating the correlation with the experimental data. A maximum correlation was obtained at 49% upward- and 51% downward-oriented isopropyl groups (**Figure 2.11**). The difference in energy between the two configurations is negligible for the level of theory used (4.59 and 3.75 kcal/mol difference for 2.4-Au and 2.1-Au, respectively), further supporting this view. The simulated Raman cross-sections for both the upward and downward configurations are also within the same order of magnitude, justifying the comparison between the individually normalized configurations. The theoretical data also show that a surface gold atom is pulled up from the surface, which is remarkable given the inherent stability of the Au_{20} cluster used in the modeling.[50] This finding is in agreement with Glorius and Fuchs and coworkers' previously published scanning tunneling microscopy (STM) studies indicating that the carbene draws a gold atom from the surface, taking an adatom configuration, which can then move across the surface in this configuration by a "ballbot" type motion.[26] Taking these results together, the following discussion relies on calculations with the NHCs bound to the tip of a Au_{20} cluster with equal contribution from both the up and down isopropyl configurations.

Comparisons of experiment and theory for 2.1-Au and 2.4-Au indicate that the most intense modes in the SERS spectra are due to the movement of the hydrogen atoms of the isopropyl groups bound to the NHC nitrogens, particularly the hydrogen bound to the central carbon of the isopropyl group. Modes listed in red and blue correspond to those that are primarily attributed to the up and down configured isopropyl groups, respectively. The high intensity of the modes centered on the isopropyl groups is logical because the isopropyl groups are closest to the surface, therefore benefiting from the greatest surface enhancement. Even though this interpretation appears sound, it is

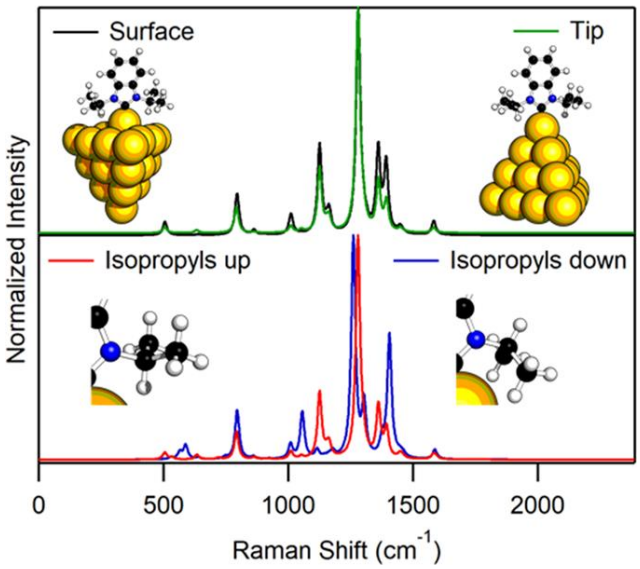


Figure 2.4: Top: Calculated SERS spectra of 2.4-Au with the NHC bound to a “surface” gold atom (black) and a “tip” gold atom (green) of a Au_{20} cluster. Optimized geometries of both tip and surface cases are presented as inset images. The strength of the Au−C bond is sufficient to pull a gold atom up from the cluster despite the known stability of the Au_{20} surface. Bottom: Calculated SERS spectra of 2.4-Au with isopropyl groups oriented up (red) and down (blue). The prominent differences between the spectra resulting from up and down isopropyl groups indicate that the SERS is very sensitive to the orientation of the side groups.

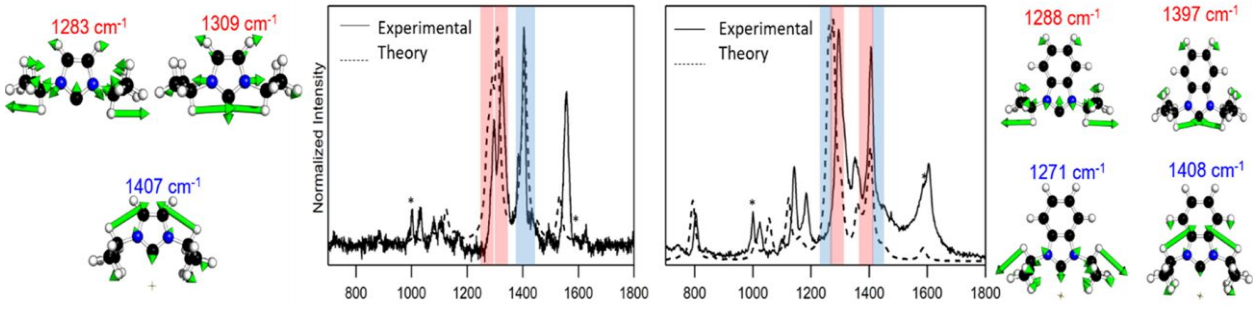


Figure 2.5: Experimental SERS spectra (solid) and theoretical SERS spectra (dashed), overlaid, show excellent agreement for both 2.1-Au and 2.4-Au (left and right, respectively). Theory shows that many of the most intense modes in the spectra are derived from motion on the isopropyl side groups. These modes are shown pictorially above the spectra with their energies. Red and blue coloring is used to indicate modes arising primarily from up- and down-oriented isopropyl groups, respectively. Asterisks indicate modes from polystyrene spheres below the gold film.

somewhat counterintuitive because in previous SERS spectra of aromatic molecules the most intense bands are dominated by modes centered on the ring.[51] The excellent agreement also elucidates another key point. The experimental data are very accurately simulated with just two configurations averaged together in a near-1:1 ratio, showing that the distribution on the surface must contain primarily upward and downward isopropyl configurations. If other configurations were present in significant numbers on the surface, then the theory would need to include all possible configurations, considering the large effect the isopropyl groups have on the SERS spectra.

Figure 2.6 compares the experimental and predicted SERS spectra of NHCs where the hydrogens of the heterocycles have been substituted with deuterium, which allows us to further confirm our vibrational assignments. In this case, we additionally see modes that correspond to motion of the atoms in the heterocycle, although they are not the most intense bands in the spectrum. There is an obvious shift and change of intensity of the 1532 cm^{-1} mode in the SERS spectrum of 2.1-Au after deuteration (2.2-Au), which is expected because that mode is dominated almost entirely by the motion of the ring hydrogens (**Figure 2.6**, left). A similar change is observed in the SERS spectra of 2.4-Au and 2.5-Au, notably from 807, 1129, and 1589 cm^{-1} to 817, 1123, and 1562 cm^{-1}, respectively (**Figure 2.6**, right). The sensitivity of the isopropyl vibrations to the local geometry can be explored by deuterating the isopropyl wing groups instead of the ring protons. This change in weight is expected to greatly alter the resulting SERS spectra because the most intense modes of the protonated NHCs exhibit motion of the isopropyl group hydrogens, as discussed previously. **Figure 2.12** displays the experimental SERS spectra of the NHCs with deuterated isopropyl groups (2.3-Au and 2.6-Au). Surprisingly, the SERS spectra of the imidazolium and benzimidazolium carbenes with deuterated isopropyl wing groups become very similar to each other and are dominated by bands at 1352 or 1367 cm^{-1} in 2.3-Au and 2.6-Au, respectively. Clearly, deuteration of the isopropyl groups decouples the motion on the ring from the alkyl groups, which greatly increases the contribution of the imidazolium ring in the SERS spectra. Because both NHCs contain the imidazole ring, the resulting SERS spectra appear very similar. Additionally, two bands near 1000−1030 cm^{-1} are also present in both spectra and arise from motion on the isopropyl groups. The previously discussed ring modes near 1330−1340 cm^{-1} in the deuterated samples are visualized with vector representations in **Figure 2.12**.

Vector overlap of normal modes was calculated to elucidate the effect of deuteration on the isopropyl groups. This was done by calculating the difference in 3-N normal mode vectors between two pairs, the benzimidazolium (2.4-Au and 2.6-Au) and the imidazolium (2.1-Au and 2.3-Au). If the normal modes are mostly the same after deuteration, then a high vector overlap of normal modes would be expected. Results showed that for the 2.1-Au to 2.3-Au deuteration a significant decoupling occurred, with most of the intense modes for 2.1-Au being heavily altered. The largest normal mode

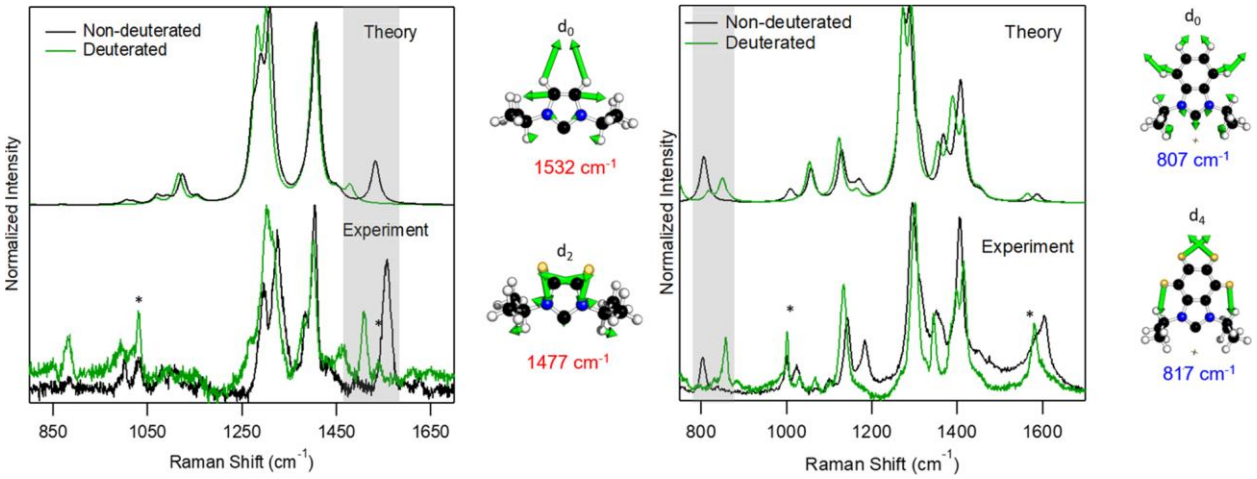


Figure 2.6: Left: Theoretical (top) and experimental (bottom) SERS spectra of 2.1-Au (black) and 2.2-Au (green). Right: Theoretical (top) and experimental (bottom) SERS spectra of 2.4-Au (black) and 2.5-Au (green). The isotope shifts upon deuteration are well reproduced by the theory, and several of the most perturbed modes are presented pictorially next to the spectra. * indicates a contribution from polystyrene spheres below the gold film.

overlap for the 1407 cm^{-1} mode in 2.3-Au was very small (~39% overlap). For the 2.4-Au modes around 1408 cm^{-1}, a similar result was found but with slightly higher overlap (~53%). Modes that were not heavily related to the isopropyl groups, such as the 1532 cm^{-1} mode for 2.1-Au, were found to have high mode overlaps (87%). This large difference in vector overlap for normal modes with isopropyl contribution further emphasizes how important the N-substituents are to the SERS spectra. Deuteration of the side groups largely decoupled ring and side group vibrations, which resulted in very different spectra.

In summary, in this manuscript, we presented a comprehensive experimental and theoretical investigation of the Raman and SERS spectra of benzimidazolium and imidazolium NHC-functionalized gold films by comparison of deuterated isotopologues of 2.1 and 2.4. The NHC−Au films can be facilely formed from either the NHC−CO_2 adducts or the NHC−bicarbonate salt, which is a degradation product of the NHC−CO_2 adduct from exposure to air. The fidelity of the match between the theoretical and the experimental SERS spectra of the NHCs on the gold surfaces yields three major findings. First, the NHCs binds to tips and adatoms on the film and not a purely flat surface. Second, the isopropyl moieties on the NHCs point to a mixture of solely up and down toward the gold surface, and it is impossible to replicate the experimental spectra with only one isopropyl position. Finally, the vibrational modes in the spectra are dominated by the hydrogens on the isopropyl moieties and not the ring modes of the NHC. Whereas this is due to the close proximity of these hydrogen atoms to the surface plasmon, this phenomenon is not typically observed with other typical binding ligands, such as amines or thiols, because their modes cannot be easily separated from a ring mode itself. Our method provides a general method for understanding the surface structure of NHCs films, which is critical when targeting NHCs with specific properties on gold surfaces.

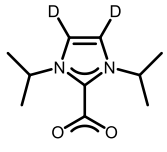
Experimental

General Considerations for Synthesis. All glassware for air and water sensitive reactions were dried at 170 °C overnight before use. All reactions were stirred vigorously with magnetic stirrers. A glovebox with a dinitrogen atmosphere was used for formation of the free carbenes for NHC-CO_2 adduct synthesis. Tetrahydrofuran used in NHC-CO_2 adduct reactions was dried on an Innovative Technologies (Newburyport, MA) Pure Solv MD-7 Solvent Purification System, degassed by three freeze-pump-thaw cycles on a Schlenk line to remove dioxygen and stored under activated 4 Å molecular sieves prior to use. Carbon dioxide gas was ultra pure grade from Airgas. Celite was dried at 240 °C under vacuum overnight and stored in a dinitrogen glovebox. The compounds 1,3-diisopropylimidazolium iodide (2.7),[52] and 2- carboxy-1,3-diisopropylimidazolium (2.1) [40] and 1,3-diisopropylbenzimidazolium iodide (2.10)[53] were prepared from previous literature procedures. All other compounds were purchased from commercial vendors at highest available purity and used without any further purification. All deuterium labeling sources were purchased from Cambridge Isotope at a minimum of 98% deuteration. Solution ^{1}H NMR and ^{13}C NMR were performed on a Varian VNMRS 500 MHz narrow-bore broadband system and Varian VNMRS 600 MHz narrow-bore broadband system at 298 K. All ^{1}H and ^{13}C shifts were referenced to the residual solvent. All mass spectrometry analyses were conducted at the Mass Spectrometry Center located in the Department of Chemistry at the University of Tennessee. The DART analyses on neutral organic molecules were performed using a JEOL AccuTOF-D time-of-flight (TOF) mass spectrometer with a DART (direct analysis in real time) ionization source from JEOL USA, Inc. (Peabody, MA). The ESI/MS analyses on charged organic molecules were performed using a QSTAR Elite quadrupole time-of-flight (QTOF) mass spectrometer with an electrospray ionization source from AB Sciex (Concord, Ontario, Canada). Solutions for mass spectrometry were prepared in acetonitrile. Infrared spectra were collected on a Thermo Scientific Nicolet iS10 with a Smart iTR accessory for attenuated total reflectance (ATR) using the neat molecules. Gold pellets and chromium pieces (Kurt J Lesker), polystyrene spheres (Sigma-Aldrich), Hydrogen Peroxide (35%) and sulfuric acid (VWR), were all purchased and used as received. Gold film-over-nanosphere substrates (AuFONs) were prepared utilizing a varied previously reported procedure.[46] Briefly, glass slides were cleaned using piranha solution and rinsed thoroughly. Polystyrene spheres were floated in water by dropping a 1:1 polystyrene sphere suspension in water to methanol, dropping slowly onto a slide partially immersed in ultrapure water. The floated polystyrene layer was then deposited onto the cleaned glass slides. After drying of the polystyrene films, a 5 nm adhesion layer of chromium, and a gold layer (200 nm) was evaporated over the spheres, using a physical vapor deposition system (Nano36, Kurt J Lesker).

AuFONs were functionalized with the NHCs by placing a 1-5 mg amount of solid NHC precursor directly onto the AuFON then heating the AuFONs to 120 °C under vacuum (5 torr). The functionalized AuFONs were rinsed thoroughly with acetone, methanol, and

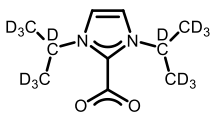
water to remove excess unbound product. Samples are then ready for analysis by SERS. SERS spectra were acquired using a custom-built system composed of a 633 nm HeNe laser (Thorlabs) aligned into an inverted microscope (Nikon, 20X, NA = 0.5), with backscattered light collected through the same objective, passed through a Rayleigh rejection filter (Semrock), and detected using a dispersive spectrometer (Princeton Instruments, Acton SP2300, 1200 grooves mm^{-1}). Laser power of 50 μW measured at the objective was used throughout SERS data collection; 7 mW was used for acquisition of Raman spectra. Theory: All geometry optimizations, frequency, normal mode analysis, and static polarizability calculations were carried out with a local version of the Amsterdam Density Functional (ADF)[54] package. A triple-ζ basis set (TZP) from the ADF basis set library was used, with the 1s-4d gold orbitals and 1s carbon and nitrogen orbitals kept frozen. The Zeroth Order Relativistic Approximation (ZORA)[55, 56] was used to account for relativistic effects. The Becke-Perdew (BP86)[57, 58] functional was used since it has been shown to yield harmonic frequencies close to that of experiment.10 A few optimized imid-Au_{20} were found to have small negative frequencies (largest of -5.2 cm^{-1}) due to instabilities in the numerical grid. The imaginary vibrations were not found to affect resulting spectra. The SERS spectra for the 2.4-Au on the surface in **Figure 2.4** was calculated without dispersion corrections. This is not believed to impact the SERS spectra significantly. X-ray Structure Determinations. X-ray diffraction measurements were performed on single crystals coated with Paratone oil and mounted on glass fibers. Each crystal was frozen under a stream of N_2 while data were collected on a Bruker APEX diffractometer. Reflections were merged and corrected for Lorenz and polarization effects, scan speed, and background using SAINT 4.05. Absorption corrections, including odd and even ordered spherical harmonics, were performed using SADABS. Space group assignments were based upon systematic absences, E statistics, and successful refinement of the structure. The structures were solved by a combination of intrinsic phasing method and were refined using the SHELXTL 5.0 software package and Olex2 software package.

Synthesis of 2-carboxy-1,3-diisopropyl(4,5-d_2)imidazolium, 2.2.



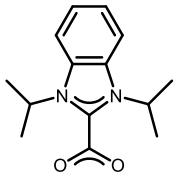
The NHC-CO_2 adduct of 1,3-diisopropyl(1,4,5-d_3)imidazolium iodide, 2.8, (0.2611 g, 0.9221 mmol) was prepared following the method of Louie[40] by addition of solid potassium bis(trimethylsilyl)amide (0.1839 g, 0.9221 mmol) and toluene (15 mL), followed by excess CO_2 gas. DART HR-MS shows no decrease of deuterium content from 2.8 to 2.2. Yield: 0.144 g, 78.6%. ^{1}H NMR (CD_2Cl_2, 499.74 MHz): δ 7.11 (s, 0.07H), 5.57 (septet, *J* = 6.1 Hz, 2H), 1.49 (d, *J* = 6.9 Hz, 12H). ^{13}C NMR (CD_2Cl_2, 125.66 MHz): δ 155.44, 144.07, 116.27 (t, *J* = 30.2 Hz), 51.56, 23.33. IR: 2973, 2934, 2677, 2290, 1663, 1612, 1538, 1503, 1465, 1397, 1383, 1371, 1357, 1325, 1277, 1212, 1182, 1138, 1116, 1081, 1065, 1001, 942, 877, 839, 796, 745, 689, 668, 639 cm^{-1}. DART HR-MS (m/z): $[M\text{-}CO_2+H]^+$: 155.1520, $[C_9H_{15}D_2N_2]^+$: 155.1512 (calc).

Synthesis of 2-carboxy-1,3-(d_{14})diisopropylimidazolium, 2.3.



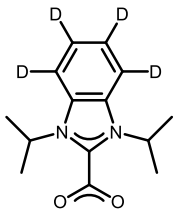
The NHC-CO_2 adduct of 1,3-(d_{14})-diisopropylimidazolium bromide, 2.9, (0.1046 g, 0.3555 mmol) was prepared following the method of Louie[40] by addition of solid potassium bis(trimethylsilyl)amide (0.0709 g, 0.3554 mmol) and toluene (15 mL), followed by excess CO_2 gas. DART HR-MS shows no decrease of deuterium content from 2.9 to 2.3. Yield: 0.0572 g, 76.5%. ^{1}H NMR (CD_2Cl_2, 499.74 MHz): δ 7.09 (s, 2H). ^{13}C NMR (CD_2Cl_2, 125.66 MHz): δ 155.43, 144.17, 116.57, 50.98 (t, J = 23.7), 22.31 (pentet observed, J = 18.6). IR: 3091, 2231, 1661, 1634, 1617, 1564, 1545, 1484, 1406, 1328, 1301, 1222, 1205, 1191, 1173, 1143, 1083, 1051, 1004, 909, 867, 840, 790, 764, 726, 691, 658 cm^{-1}. DART HR-MS (m/z): $[M\text{-}CO_2+H]^+$: 167.2273 (found), $[C_9H_3D_{14}N_2]^+$: 167.2265 (calc).

Synthesis of 2-carboxy-1,3-diisopropyl-benzimidazolium, 2.4.



The NHC-CO_2 adduct of 1,3-diisopropyl-benzimidazolium iodide, 2.10, (0.3122 g, 0.9454 mmol) was prepared following the method of Limbach[43] by addition of solid potassium tert-butoxide (0.1273 g, 1.134 mmol) and tetrahydrofuran (1 mL), followed by excess CO_2 gas. After the addition of CO_2 gas, the solution was triturated with diethyl ether (20 mL). The solid was then filtered over a fine porosity frit and washed with additional diethyl ether (15 mL) and dried under vacuum to give a white powder. Yield: 0.0899 g, 38.6%. ^{1}H NMR (CD_2Cl_2, 499.74 MHz): δ 7.79 (m, J = 3.2 Hz, 2H), 7.52 (m, J = 3.2 Hz, 2H), 5.28, (sept, J = 7.2 Hz, 2H), 1.73 (d, J = 7.0 Hz, 12H). ^{13}C NMR (CD_2Cl_2, 125.66 MHz): δ 156.21, 150.34, 130.29, 125.99, 115.29, 52.57, 21.37. IR: 2974, 1669, 1626, 1555, 1458, 1441, 1371, 1302, 1248, 1176, 1143, 1096, 982, 887, 837, 754, 687, 645 cm^{-1}. DART HR-MS (m/z): $[M\text{-}CO_2+H]^+$: 203.1553 (found), $[C_{13}H_{19}N_2]^+$: 203.1543 (calc).

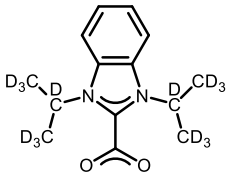
Synthesis of 2-carboxy-1,3-diisopropyl(4,5,6,7-d_4)benzimidazolium, 2.5.



The NHC-CO_2 adduct of 1,3-diisopropyl(4,5,6,7-d_4)benzimidazolium iodide, 2.13, (0.0741 g, 0.222 mmol) was prepared following the method of Limbach[43] by addition of solid potassium tert-butoxide (0.0299 g, 0.266 mmol) and tetrahydrofuran (1 mL), followed by excess CO_2 gas. After the addition of CO_2 gas, the solution was triturated with diethyl ether (30 mL). The solid was then filtered over a fine porosity frit and washed with additional diethyl ether (15 mL) and dried under vacuum to give a white powder. DART HR-MS shows no decrease of deuterium content from 2.13 to 2.5. Yield: 0.0107g, 19.3%. ^{1}H NMR (CD_2Cl_2, 499.74 MHz): δ 7.80 (s, 0.09H), 7.53 (s, 0.09H), 5.30 (sept, J = 7.7 Hz, 2H), 1.75 (d, J = 7.0 Hz, 12H) ^{13}C NMR (CD_2Cl_2, 125.66 MHz): δ 156.20, 150.31, 130.20, 125.50 (t, J = 24.9 Hz), 114.93 (t, J = 24.7). IR: 2973, 2269, 1668, 1625, 1553, 1445, 1370, 1303, 1259, 1212, 1174, 1139, 1010, 992, 963, 885, 868, 836, 812, 733, 688, 670,

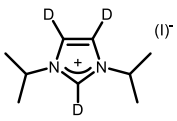
645 cm-1. DART HR-MS (m/z): $[M\text{-}CO_2+H]^+$: 207.1803 (found), $[C_{13}H_{15}D_4N_2]^+$: 207.1794 (calc).

Synthesis of 2-carboxy-1,3-(d_{14})-diisopropylbenzimidazolium, 2.6.



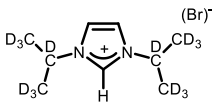
The NHC-CO_2 adduct of 1,3-(d_{14})-diisopropylbenzimidazolium bromide, 14, (0.106 g, 0.357 mmol) was prepared following the method of Limbach[43] by addition of, solid potassium tert-butoxide (0.0480 g, 0.428 mmol) and tetrahydrofuran (1 mL) followed by excess CO_2 gas. After the addition of CO_2 gas, the solution was triturated with diethyl ether (20 mL). The solid was then filtered over a fine porosity frit and washed with additional diethyl ether (10 mL) and dried under vacuum to give a white powder. DART HR-MS shows no decrease of deuterium content from 2.14 to 2.6. Yield: 0.0220 g, 23.7%. ^{1}H NMR (CD_2Cl_2, 499.74 MHz): δ 7.80 (m, J = 3.1 Hz, 2H), 7.54 (m, J = 3.1 Hz, 2H). ^{13}C NMR (CD_2Cl_2, 125.66 MHz): δ 156.21, 150.29, 130.31, 125.99, 115.25, 51.90 (t, J = 21.6 Hz), 20.36 (pentet observed, J = 21.3 Hz). IR: 2969, 2233, 1666, 1628, 1548, 1458, 1378, 1306, 1207, 1162, 1081, 1050, 1017, 1005, 937, 922, 890, 861, 837, 812, 772, 749, 687 cm^{-1}. DART HR-MS (m/z): $[M - CO_2 + H]^+$: 217.24189 (found), $[C_{13}H_5D_{14}N_2]^+$: 217.2427 (calc).

Synthesis of 1,3-diisopropyl(1,4,5-d_3)imidazolium iodide, 2.8.



1,3-diisopropylimidazolium iodide (2.7) (1.022 g, 3.647 mmol) was deuterated with D_2O and cesium carbonate by the method of Bartsch[41] with the only difference being the protonated isopropyl substituents. Yield: 0.892 g, 86.6%. ^{1}H NMR ($CDCl_3$, 499.74 MHz): δ 9.93 (s, 0.14H), 7.51 (s, 0.03H), 4.79 (sept, J = 6.7 Hz, 2H), 1.48 (d, J = 6.8 Hz, 12H). ^{13}C NMR ($CDCl_3$, 125.66 MHz): δ 133.26 (t, J = 35.6 Hz), 119.89 (t, J = 30.3 Hz), 52.96, 22.90. IR: 3146, 2974, 2933, 2879, 2337, 2294, 1548, 1517, 1503, 1465, 1423, 1396, 1375, 1325, 1291, 1275, 1205, 1177, 1134, 1122, 1097, 1011, 974, 940, 910, 887, 852, 805, 731, 650 cm^{-1}. ESI HR-MS (m/z): $[M]^+$: 156.1569 (found), $[C_9H_{14}D_3N_2]^+$: 156.1575 (calc).

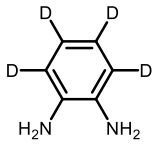
Synthesis of 1,3-(d_{14})-diisopropylimidazolium bromide, 2.9.



Imidazole (1.0015 g, 14.71 mmol) was added to a 35 mL thick-walled glass pressure flask. Cesium carbonate (4.790 g, 14.70 mmol), 2-bromopropane-d_7 (7.651 g, 58.84 mmol) and acetonitrile (15 mL) were then added to the flask. The flask was sealed with a teflon screw cap and stirred at 80 °C for 96 hours. The solution was then filtered over a medium porosity frit and washed with additional acetonitrile (30 mL). The filtrate was then concentrated to a waxy solid, and then dissolved in dichloromethane (30 mL) and filtered over a Celite plug to remove

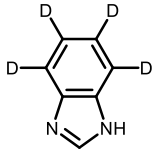
residual salt. The Celite plug was washed with additional dichloromethane (60 mL). This dichloromethane filtrate was then concentrated to a waxy solid and was dissolved in acetonitrile (10 mL) and triturated with diethyl ether (100 mL). The yellow solid was collected on a fine frit and washed with additional ether (30 mL). This process was repeated again to produce a light tan hygroscopic solid. Yield: 2.93 g, 67.7%. ^{1}H NMR (CD_2Cl_2, 499.74 MHz): δ 10.66 (s, 1H), 7.48 (s, 2H), 4.86 (sept, 0.01H), 1.60 (d, J = 6.6 Hz, 0.01H). ^{13}C NMR (CD_2Cl_2, 125.66 MHz): δ 135.86, 120.29, 53.05 (t, J = 22.2 Hz), 22.38 (t observed, J = 19.6 Hz). IR: 3131, 3081, 3047, 2230, 2071, 1639, 1551, 1365, 1304, 1204, 1184, 1133, 1118, 1062, 1005, 912, 872, 816, 765, 697, 639 cm^{-1}. ESI HRMS (m/z): $[M]^+$: 167.2259 (found), $[C_9H_3D_{14}N_2]^+$: 167.2265 (calc).

Synthesis of 1,2-diamino(3,4,5,6-d$_4$)benzene, 2.11.



1,2-diamino(3,4,5,6-d$_4$)benzene was synthesized with a minor modification of a previous literature procedure.[44] 1,2-diaminobenzene (1.009 g, 9.255 mmol) and a magnetic stir bar were added to a 110 mL Fischer Porter bottle. 5% Platinum on activated carbon (0.2000 g, 20% wt.) and then deuterium oxide (34 mL) were added to the bottle. The bottle was sealed and then pressurized with hydrogen (15 psi). The mixture was stirred at 170 °C for 24 hours. The reaction was then cooled and filtered over a short Celite plug and washed with dichloromethane. The two layers were then separated, and the aqueous layer was extracted three times with dichloromethane (3 x 50 mL). The organic layers were combined and then dried with anhydrous magnesium sulfate and then filtered over a medium porosity frit and concentrated to dryness under vacuum to give an off-white crystalline solid. Yield: 0.600 g, 57.3%. The ^{1}H NMR spectra was identical to the reported values.[44] Additional characterization is provided here. ^{13}C NMR ($CDCl_3$, 150.81 MHz): δ 134.72, 119.90 (t, J = 24.3 Hz), 116.42 (t, J = 23.7 Hz). IR: 3385, 3369, 3350, 3277, 2527, 2511, 2490, 2370, 2270, 1627, 1566, 1430, 1374, 1301, 1241, 1190, 1135, 1064, 932, 882, 754, 639 cm^{-1}. DART HR-MS (m/z): $[M+H]^+$: 113.1016 (found), $[C_6H_5D_4N_2]^+$: 113.1011 (calc). 12.4% d$_3$, 87.6% d$_4$ based on DART HR-MS.

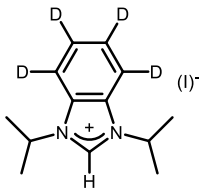
Synthesis of (4,5,6,7-d$_4$)-benzimidazole, 2.12.



(4,5,6,7-d$_4$)-benzimidazole was synthesized based on previous literature procedures with a minor modification.[45] 1,2-diamino(3,4,5,6-d$_4$)benzene, 2.11, (0.1200 g, 1.070 mmol) was added to a 20 mL scintillation vial. Triethyl orthoformate (3.00 mL, 18.0 mmol) and concentrated hydrochloric acid (0.0524 ml, 4.33 mmol) were added to the vial and stirred at ambient temperature for 24 hours. The volatiles were then removed in vacuo until solid started to precipitate out. The solid was then collected via filtration over a fine porosity frit and washed with diethyl ether to give a light brown powder. Yield: 0.323 g, 63.3%. ^{1}H NMR (C_2D_6SO, 499.74 MHz): δ

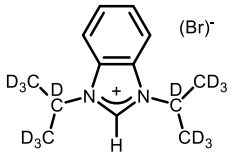
9.6 (br s, 1H), 7.86 (s, 0.06H), 7.57 (s, 0.06H). ^{13}C NMR (C_2D_6SO, 150.81 MHz): δ 140.25, 130.52, 125.44 (t, *J* = 24.2 Hz), 114.06 (t, *J* = 25.0 Hz). IR: 3486, 3077, 3003, 2960, 2867, 2754, 2614, 2506, 2232, 1866, 1640, 1602, 1562, 1527, 1486, 1452, 1386, 1343, 1299, 1225, 1020, 947, 817, 760, 715, 655, 642 cm^{-1}. DART HR-MS (m/z): $[M+H]^+$: 123.0863 (found), $[C_7H_3D_4N_2]^+$: 123.0860 (calc). 12.4% d_3, 87.6% d_4 based on DART HR-MS.

Synthesis of 1,3-diisopropyl(4,5,6,7-d$_4$)benzimidazolium iodide, 2.13.



(4,5,6,7-d$_4$)benzimidazole, 2.12, (0.2605 g, 2.132 mmol) was added to a 48 mL thick-walled glass pressure flask. Cesium carbonate (1.75 g, 5.37 mmol) and neat 2-iodopropane (4 mL, 41.0 mmol) were then added to the flask. The flask was sealed with a teflon screw cap and stirred at 90 °C for 72 hours. The flask was then cooled to room temperature the solids formed were filtered over a medium porosity frit washing the flask and solids with acetonitrile (30 mL). The filtrate was then concentrated to dryness under vacuum. The solid was then dissolved in dichloromethane (40 mL) and then filtered over a short Celite plug to remove residual salts. The filtrate was then concentrated to dryness under vacuum. The resulting solid was then dissolved in 20 mL acetonitrile and 150 mL of diethyl ether was then added to the solution and stirred until precipitation ceased. The solid was then collected via filtration over a fine porosity frit and washed with additional diethyl ether and dried under vacuum to give a tan crystalline solid. NMR shows no decrease of deuterium content from 2.12. Single crystals for X-ray diffraction were grown by vapor diffusing diethyl ether into a methanol solution of 2.13. Yield: 0.293 g, 41.1%. ^{1}H NMR (CD_2Cl_2, 499.74 MHz): δ 10.74 (s, 1H), 7.83 (s, 0.07H), 7.67 (s, 0.07H), 5.16 (sept, *J* = 6.7 Hz, 2H), 1.84 (d, *J* = 6.9 Hz, 12H). ^{13}C NMR ($CDCl_3$, 125.66 MHz): δ 139.87, 131.37, 127.02 (t, *J* = 25.0 Hz) 114.01 (t, *J* = 25.6 Hz), 52.84, 22.57. IR: 3176, 2985, 2936, 2257, 1648, 1599, 1553, 1467, 1442, 1411, 1392, 1379, 1367, 1343, 1327, 1257, 1199, 1171, 1140, 1118, 1073, 1032, 964, 947, 880, 846, 824, 765, 729, 658, 634 cm^{-1} . ESI HR-MS (m/z): $[M]^+$: 207.1795 (found), $[C_{13}H_{15}D_4N_2]^+$: 207.1794 (calc).

Synthesis of 1,3-(d$_{14}$)-diisopropylbenzimidazolium bromide, 2.14.



Benzimidazole (0.5002 g, 4.232 mmol) and cesium carbonate (1.779 g, 4.232 mmol) were added to a 35 mL thick-walled glass pressure flask. Acetonitrile (10 mL) was then added to the flask, followed by the addition of 2-bromopropane-d$_7$ (98% d-content) (2.201 g, 16.93 mmol). The flask was sealed with a Teflon screw cap and stirred at 82 °C for 36 hours. The solution was then filtered over a medium porosity frit and washed with additional acetonitrile (20 mL). The filtrate was then concentrated to a waxy solid, and then dissolved in dichloromethane (50 mL) and filtered over a Celite plug to remove residual salt. The Celite plug was washed with additional dichloromethane (15 mL). This dichloromethane filtrate was then concentrated to an oil solid and was dissolved in acetonitrile (25 mL) and

triturated with diethyl ether (125 mL). The white solid was collected on a fine frit and washed with additional ether (60 mL). This process was repeated again to produce a white solid. Yield: 0.194 g, 15.4%. ^{1}H NMR (C_2D_6OS, 499.74 MHz): δ 9.81 (s, 1H), 8.15 (dd, *J* = 3.2 Hz, *J* = 6.33 Hz, 2H), 7.69 (dd, *J* = 3.0 Hz, *J* = 6.2, 2H). ^{13}C NMR (C_2D_6OS, 125.66 MHz): δ 139.01, 130.62, 126.44, 114.04, 50.05 (t, *J* = 21.2 Hz), 20.50 (pentet observed, *J* = 19.1 Hz). IR: 3142, 3064, 3024, 2233, 1611, 1545, 1474, 1399, 1331, 1272, 1219, 1206, 1160, 1052, 1020, 961, 946, 900, 862, 833, 784, 756, 695 cm^{-1}. ESI HR-MS (m/z): $[M]^+$ 217.2431 (found), $[C_{13}H_5D_{14}N_2]^+$: 217.2427 (calc).

Decay of CO_2 adduct, 2.2, to bicarbonate salt.

Pure 2.2 was subjected to the atmosphere for one week as a solid to show the decomposition of the NHC-CO_2 adduct to the bicarbonate salt version of this complex (2.2•H_2O). After exposure for one week, 2.2 decomposed to an approximately 1:1 mixture of the starting NHC-CO_2 adduct and its associated bicarbonate salt. See **Spectra 2.47**.

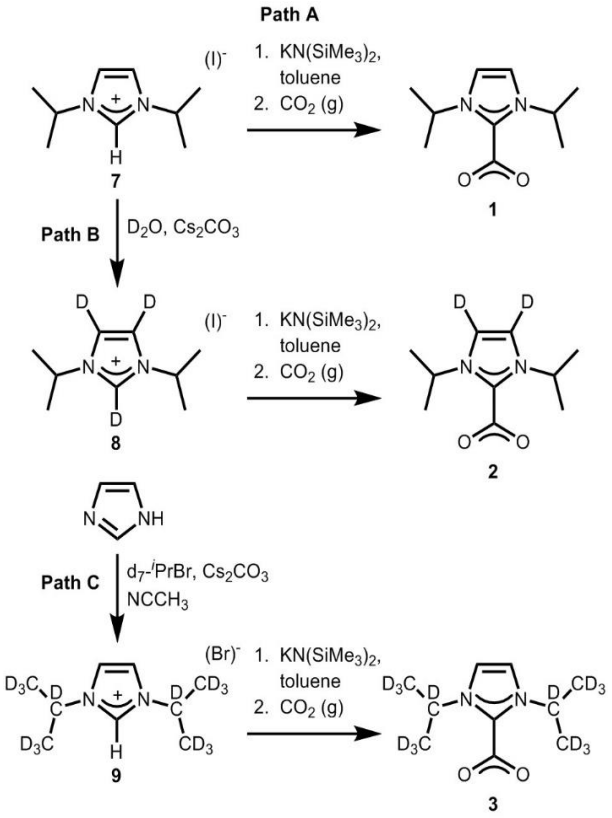
Decay of CO_2 adduct, 2.4, to bicarbonate salt.

Pure 2.4 was subjected to the atmosphere for four days as a solid to show the decomposition of the NHC-CO_2 adduct to the bicarbonate salt version of this complex (2.4•H_2O). After exposure for four days, 2.4 decomposed completely to its associated bicarbonate salt. See **Spectra 2.48**.

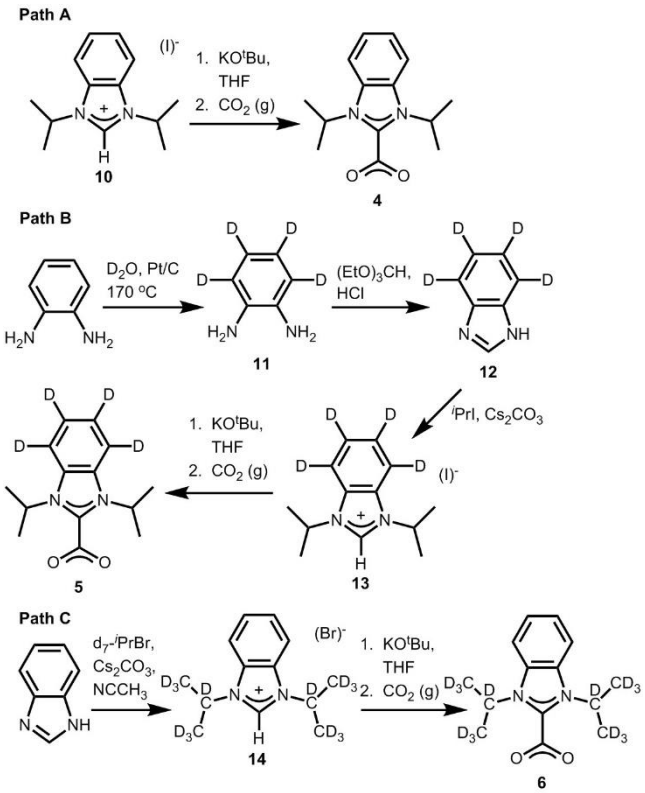
Pure 2.4 was subjected to the atmosphere for 10 minutes as a solid to show the decomposition of the NHC-CO_2 adduct to the bicarbonate salt version of this complex (2.4•H_2O). After exposure for 10 minutes, 2.4 decomposed almost completely to its associated bicarbonate salt. Only a trace of 2.4 could be seen in NMR. See **Spectra 2.49**.

Pure 2.4 was subjected to the atmosphere for 30 seconds as a solid to show the decomposition of the NHC-CO_2 adduct to the bicarbonate salt version of this complex (2.4•H_2O). After exposure for 30 seconds, 2.4 decomposed to an approximately 1:1 mixture of the starting NHC-CO_2 adduct and its associated bicarbonate salt. See **Spectra 2.50**.

Synthetic Schemes



Scheme 2.2: Synthesis of imidazole-CO_2 adducts (2.1-2.3).



Scheme 2.3: Synthesis of benzimidazole-CO_2 adducts (2.4-2.6).

Single Crystal X-ray Structures

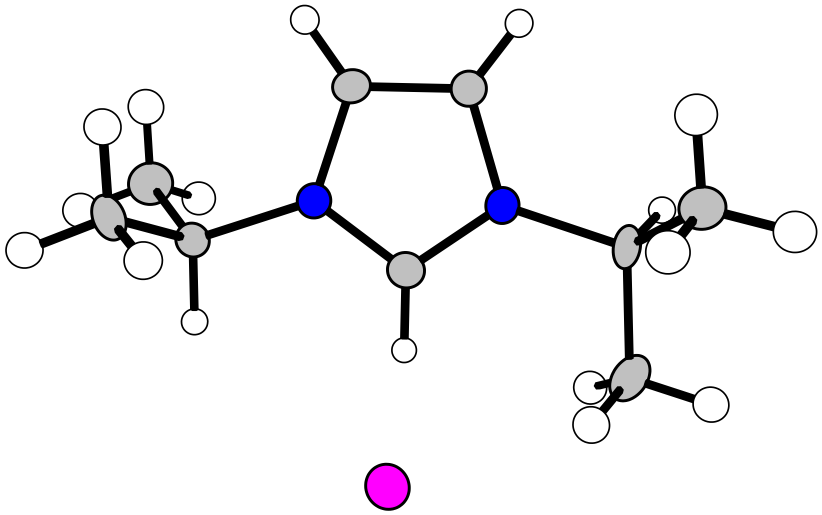


Figure 2.7: X-ray crystal structure of 1,3-diisopropyl-imidazolium iodide (2.7). Purple, blue, gray, and white ellipsoids (50% probability) represent I, N, C, and H atoms, respectively.

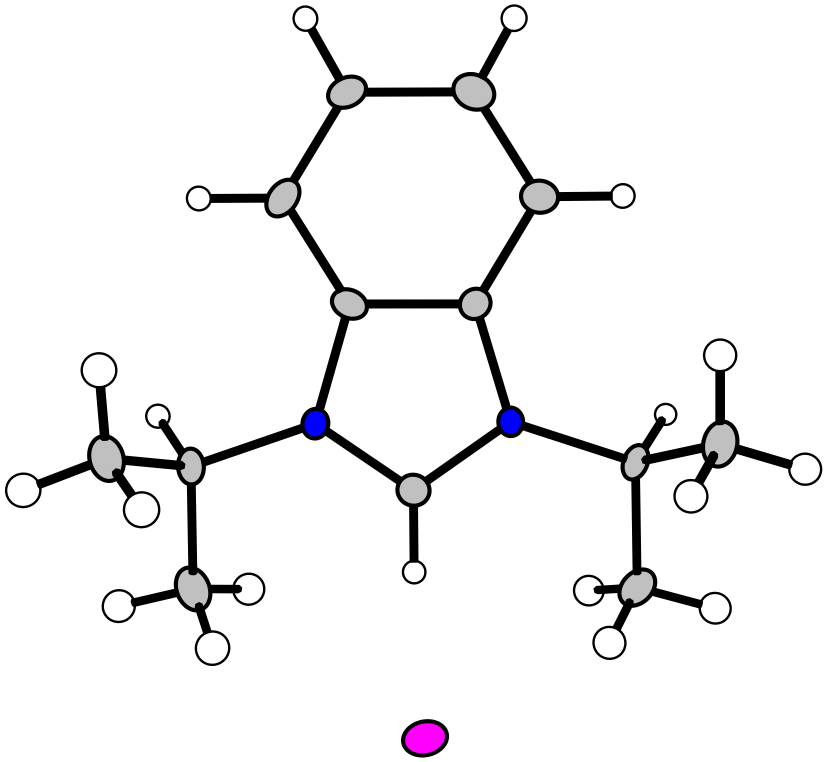
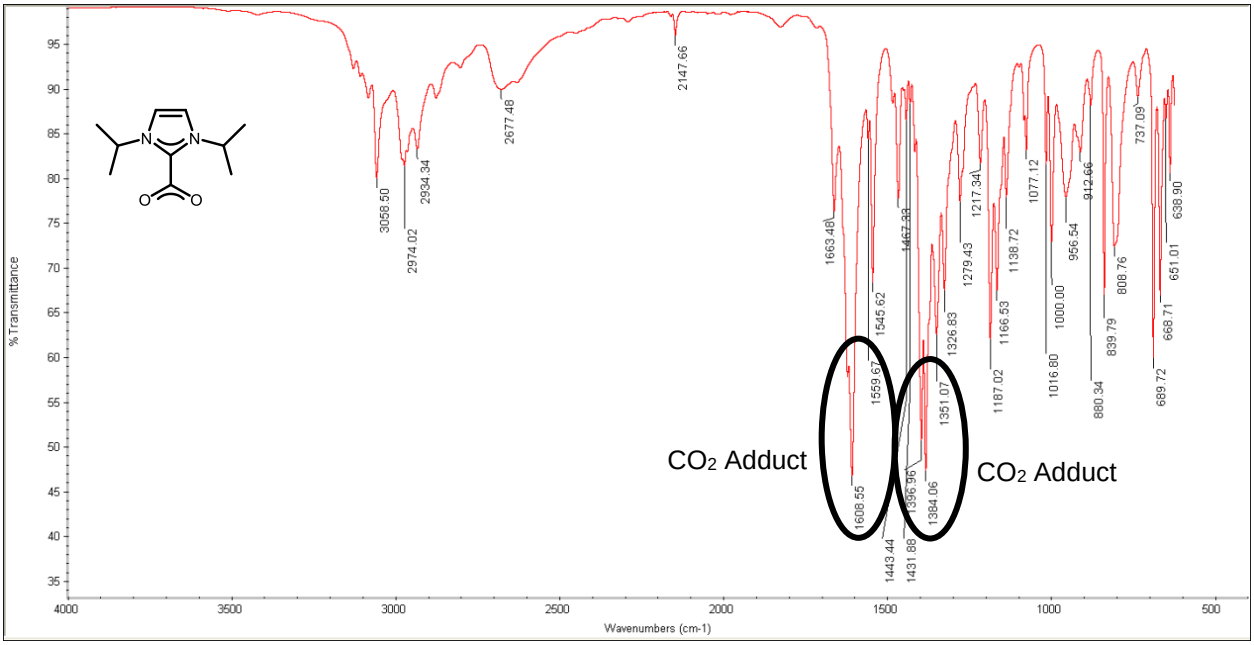
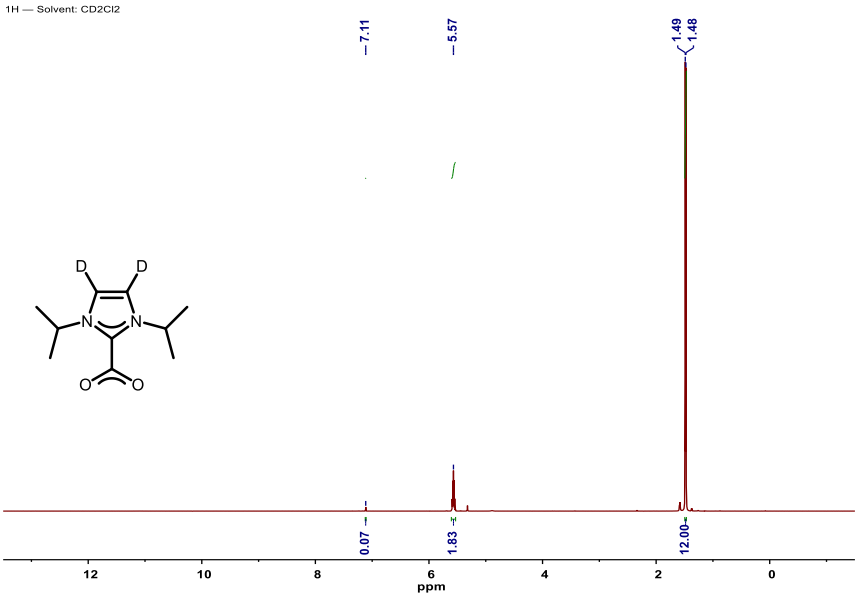


Figure 2.8: X-ray crystal structure of 1,3-diisopropyl(4,5,6,7-d_4)benzimidazolium iodide (2.13). Purple, blue, gray, and white ellipsoids (50% probability) represent I, N, C, and H/D atoms, respectively.

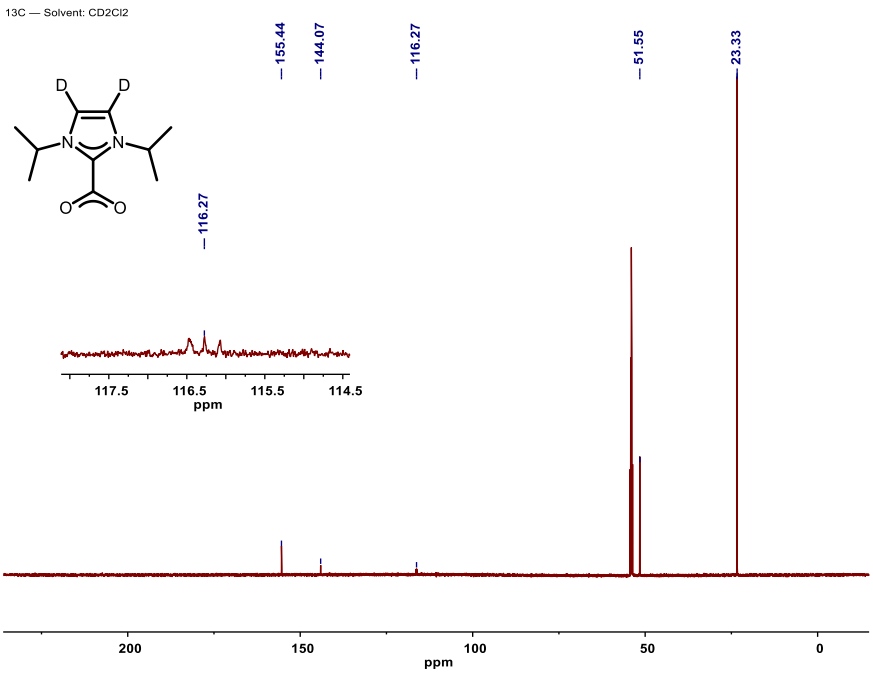
Annotated NMRs, IRs, MS for 2.1-2.14.



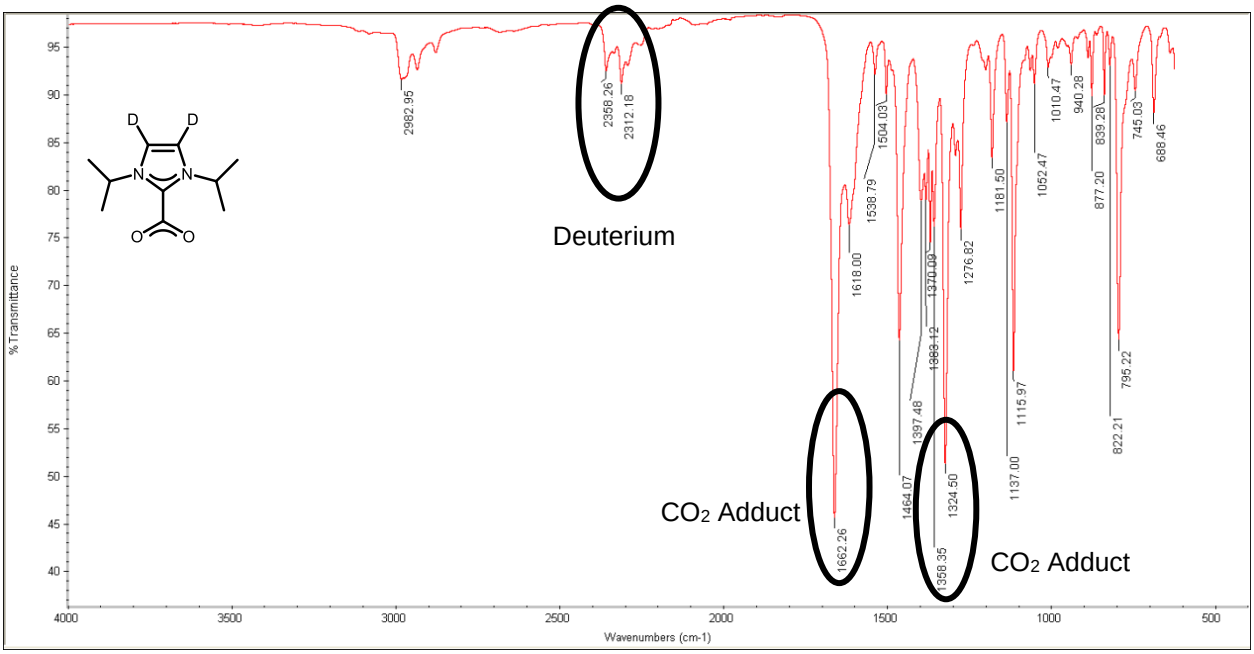
Spectra 2.1: ATR-IR of 2.1. Signature NHC-CO_2 adduct peaks are denoted by stretches at 1609 and 1384 cm^{-1}.



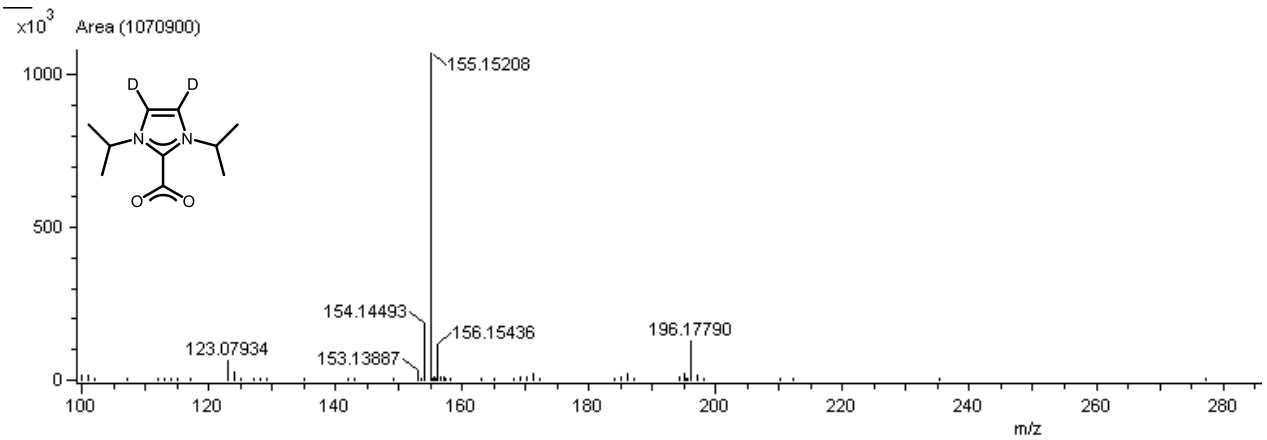
Spectra 2.2: ^{1}H NMR of **2.2** in CD_2Cl_2.



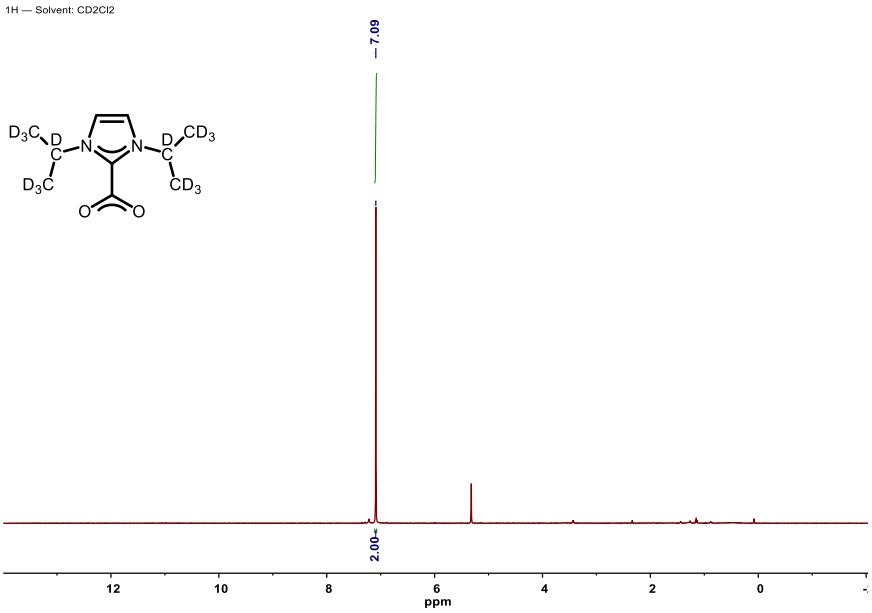
Spectra 2.3: ^{13}C NMR of **2.2** in CD_2Cl_2.



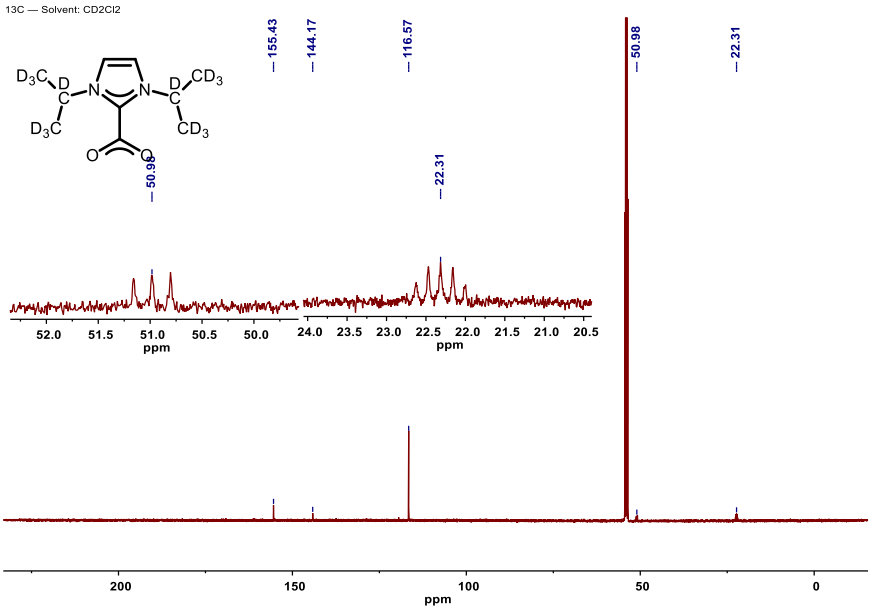
Spectra 2.4: ATR-IR of **2.2**. Signature NHC-CO_2 adduct peaks are denoted by stretches at 1662 and 1358 cm^{-1} and carbon deuterium peaks are denoted by stretches at 2358 and 2312 cm^{-1}.



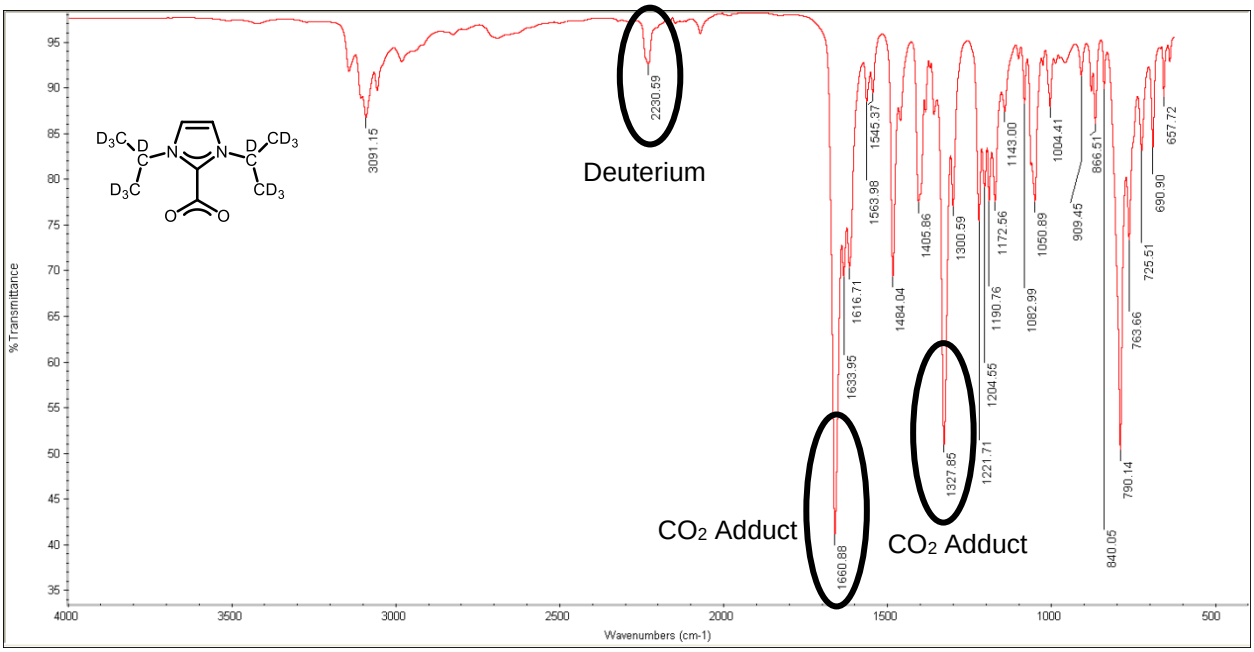
Spectra 2.5: DART HR-MS (m/z): $[M+H]^+$ of **2.2**.



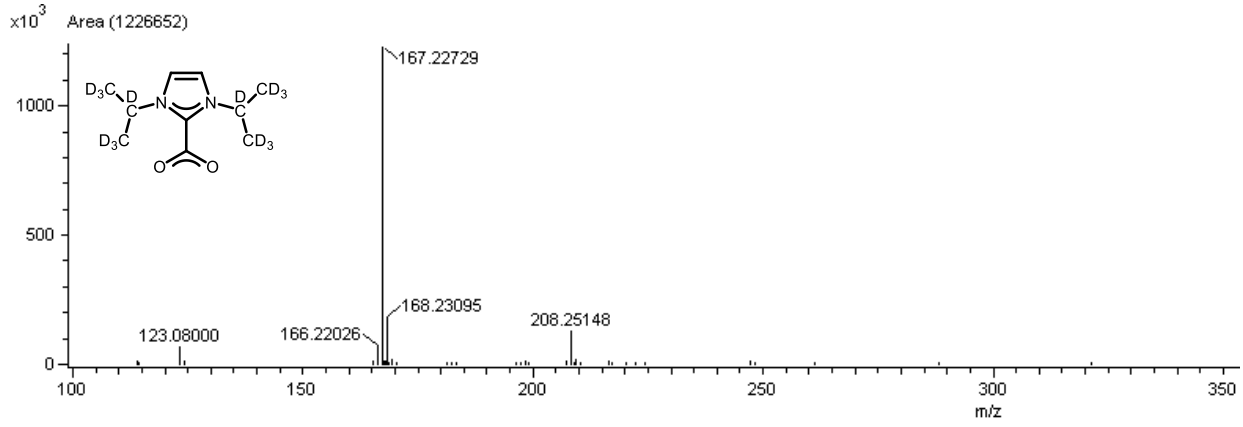
Spectra 2.6: ^{1}H NMR of **2.3** in CD_2Cl_2.



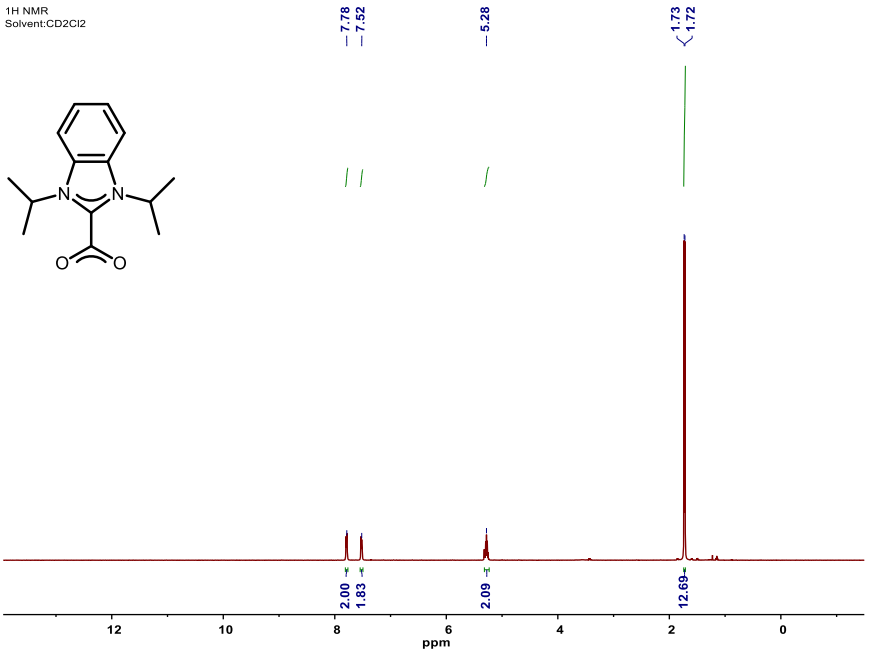
Spectra 2.7: ^{13}C NMR of **2.3** in CD_2Cl_2.



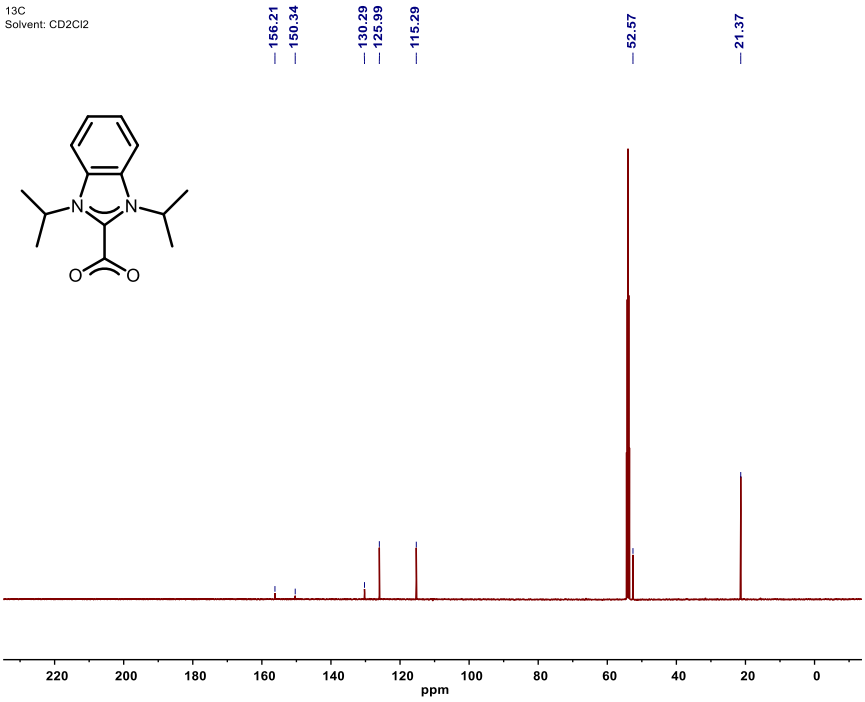
Spectra 2.8: ATR-IR of **2.3**. Signature NHC-CO_2 adduct peaks are denoted by stretches at 1661 and 1328 cm^{-1} and carbon deuterium peaks are denoted by stretch at 2230 cm^{-1}.



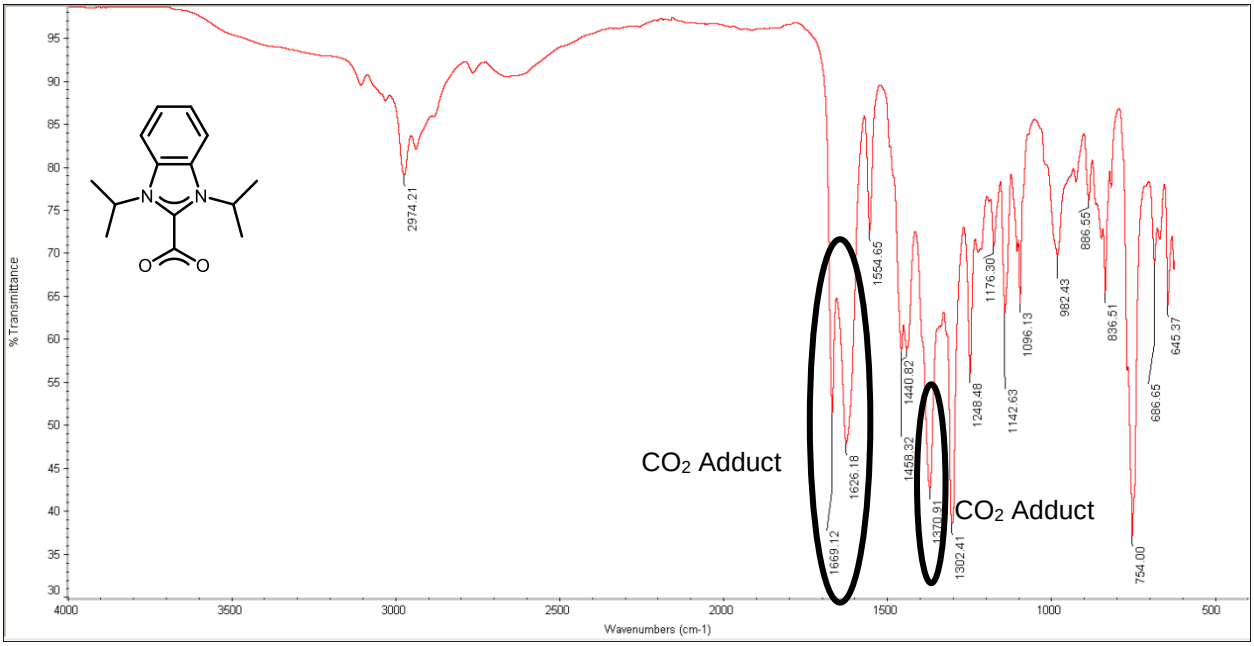
Spectra 2.9: DART HR-MS (m/z): $[M+H]^+$ of **2.3**.



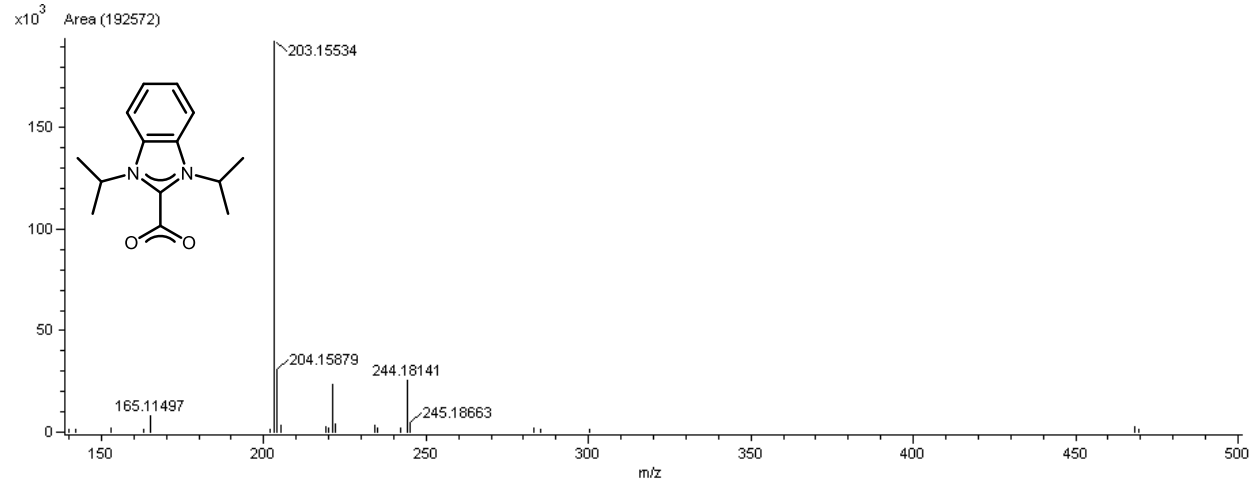
Spectra 2.10: ^{1}H NMR of **2.4** in CD_2Cl_2.



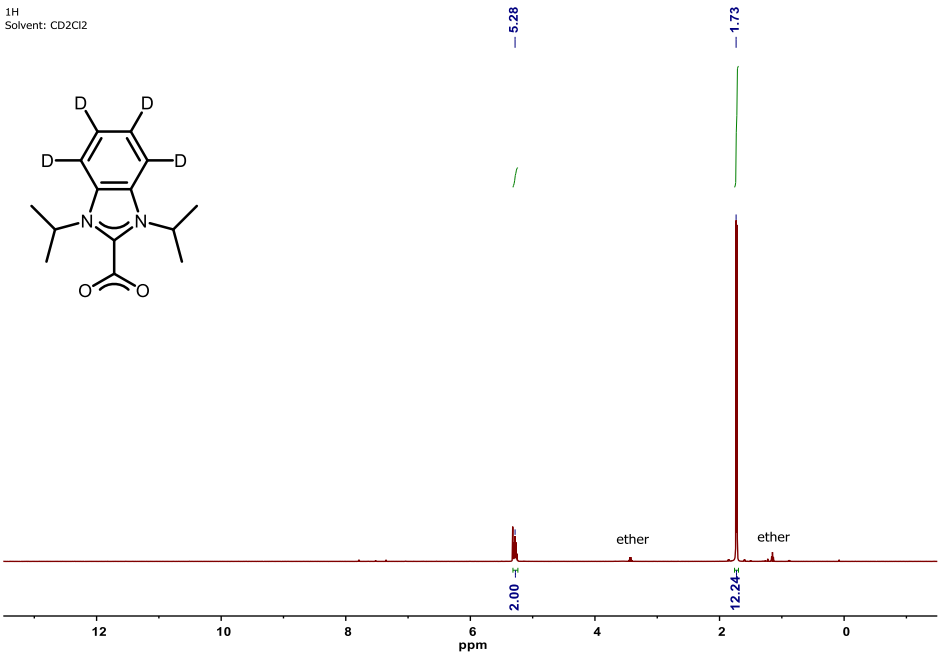
Spectra 2.11: ^{13}C NMR of **2.4** in CD_2Cl_2.



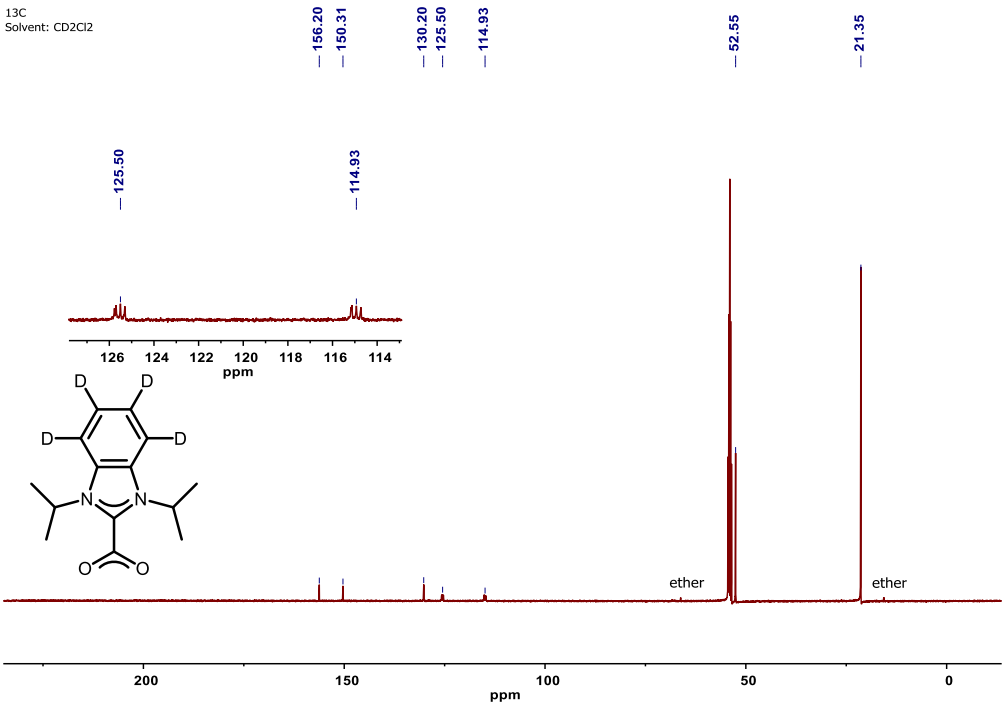
Spectra 2.12: ATR-IR of **2.4**. Signature NHC-CO_2 adduct peaks are denoted by stretches at 1669, 1626 and 1371 cm^{-1}.



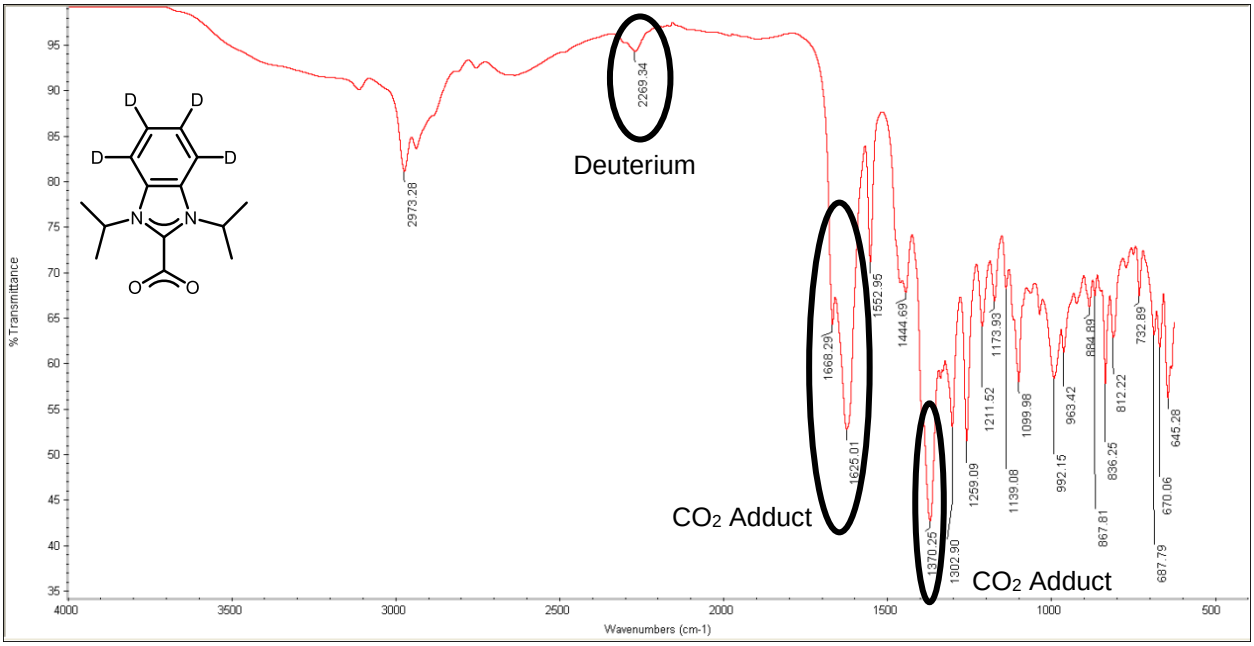
Spectra 2.13: DART HR-MS (m/z): $[M+H]^+$ of **2.4**.



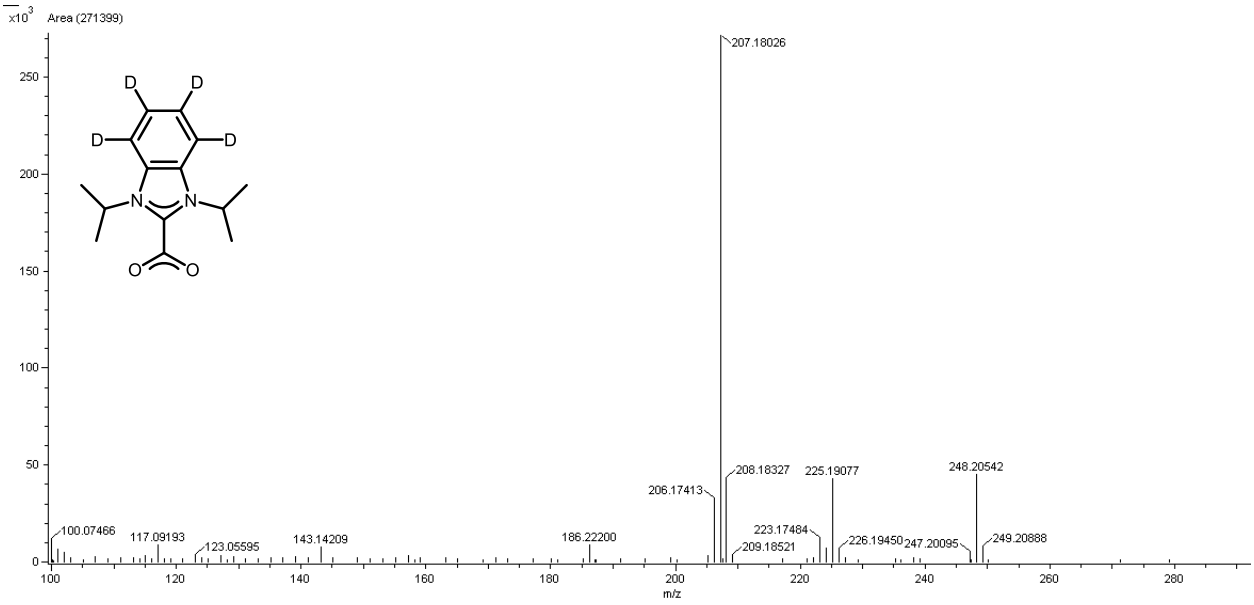
Spectra 2.14: ^{1}H NMR of **2.5** in CD_2Cl_2.



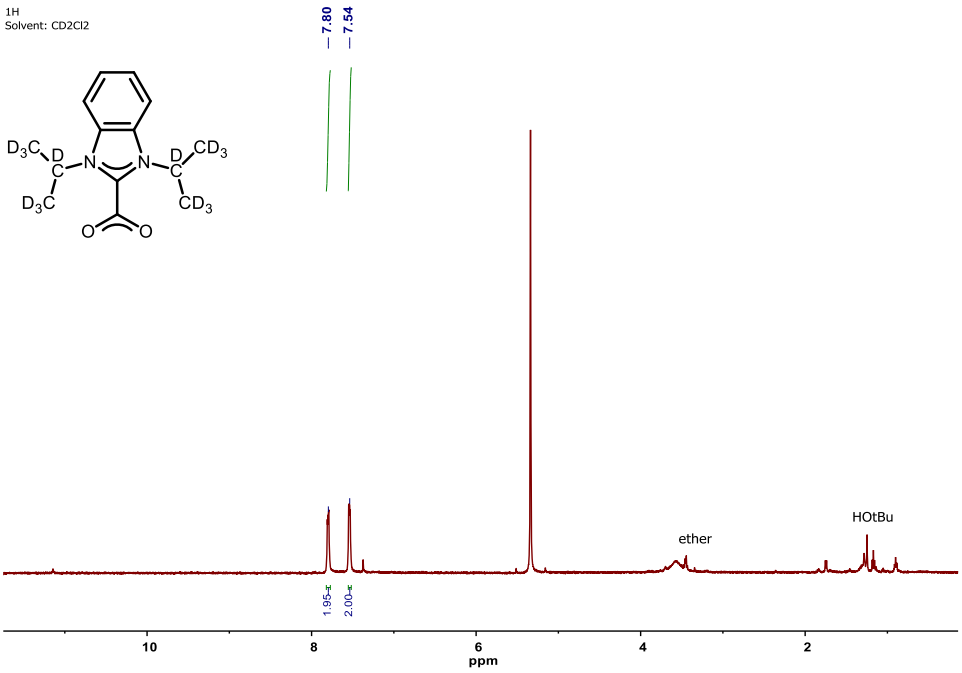
Spectra 2.15: ^{13}C NMR of **2.5** in CD_2Cl_2.



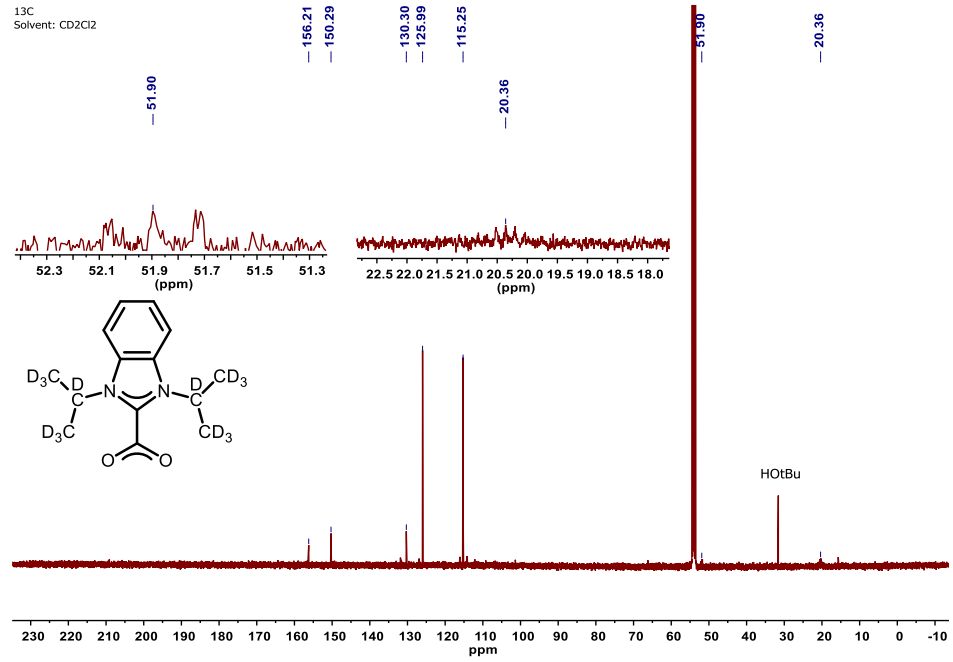
Spectra 2.16: ATR-IR of **2.5**. Signature NHC-CO_2 adduct peaks are denoted by stretches at 1625 and 1370 cm^{-1} and carbon deuterium peaks are denoted by stretch at 2269 cm^{-1}.



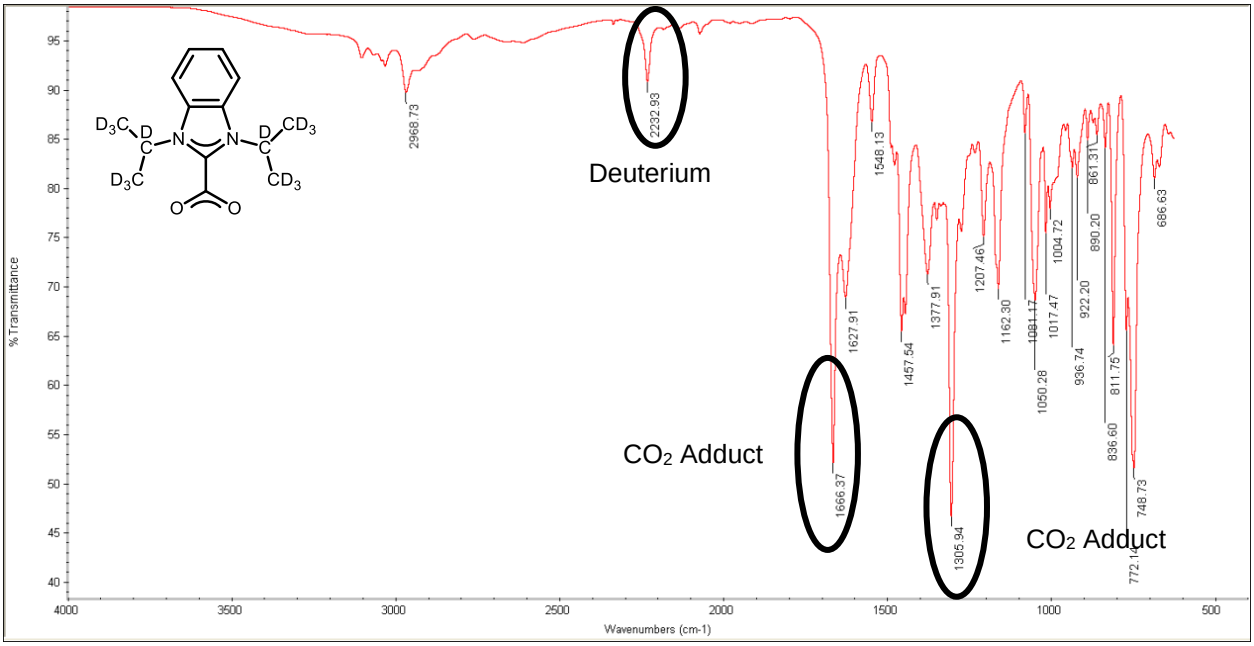
Spectra 2.17: DART HR-MS (m/z): $[M+H]^+$ of **2.5**.



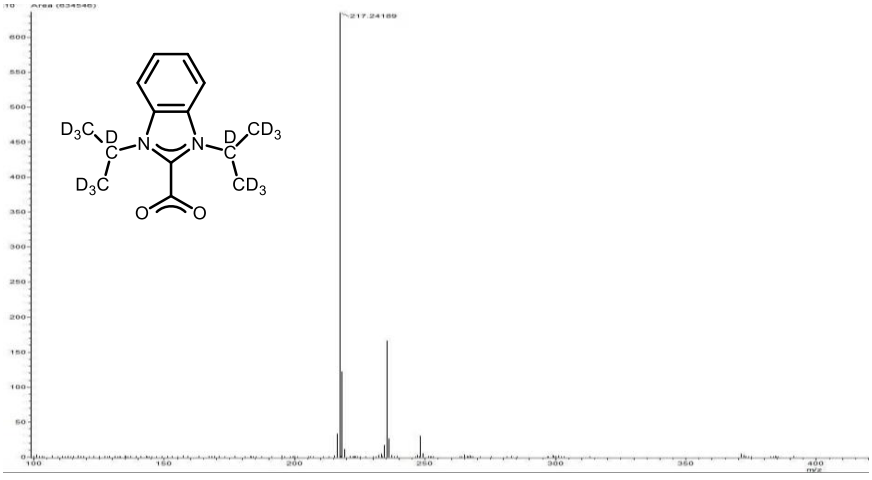
Spectra 2.18: ^{1}H NMR of **2.6** in CD_2Cl_2.



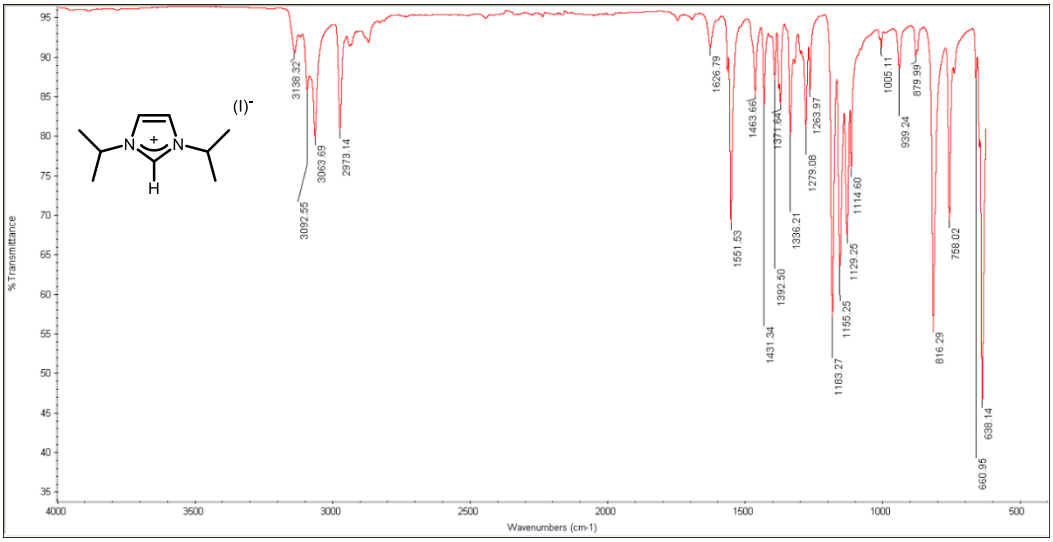
Spectra 2.19: ^{13}C NMR of **2.6** in CD_2Cl_2.



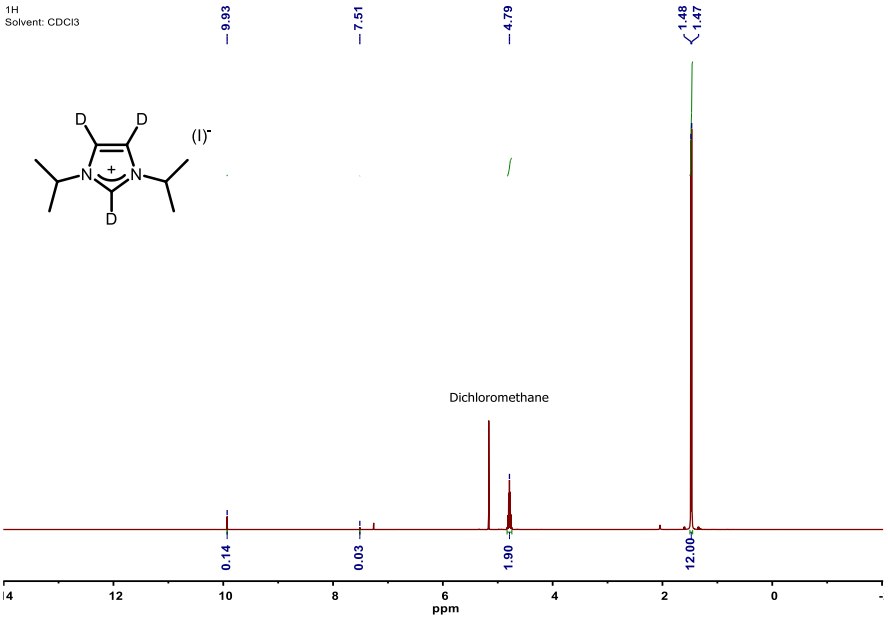
Spectra 2.20: ATR-IR of **2.6**. Signature NHC-CO_2 adduct peaks are denoted by stretches at 1666 and 1306 cm^{-1} and carbon deuterium peaks are denoted by stretch at 2233 cm^{-1}.



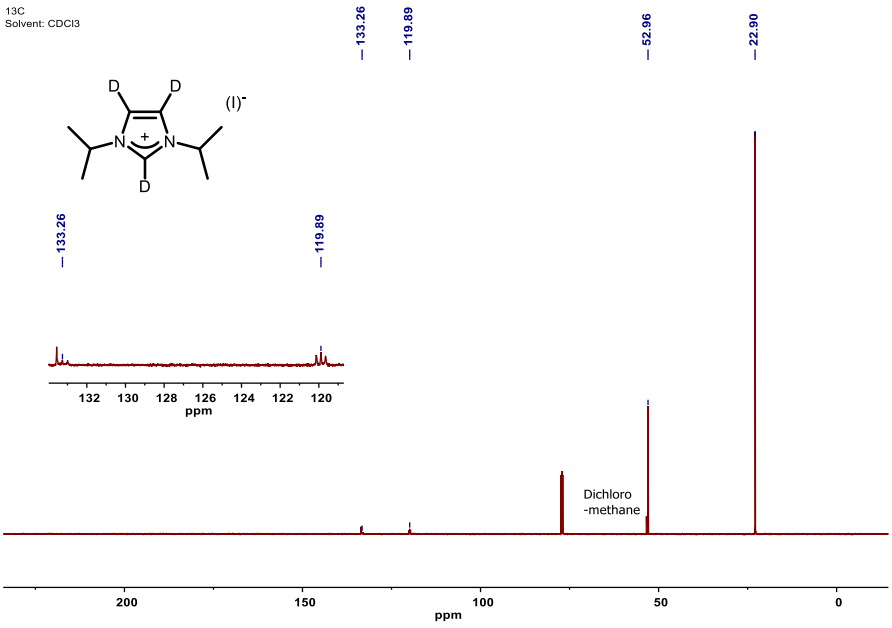
Spectra 2.21: DART HR MS (m/z): $[M+H]^+$ of **2.6**.



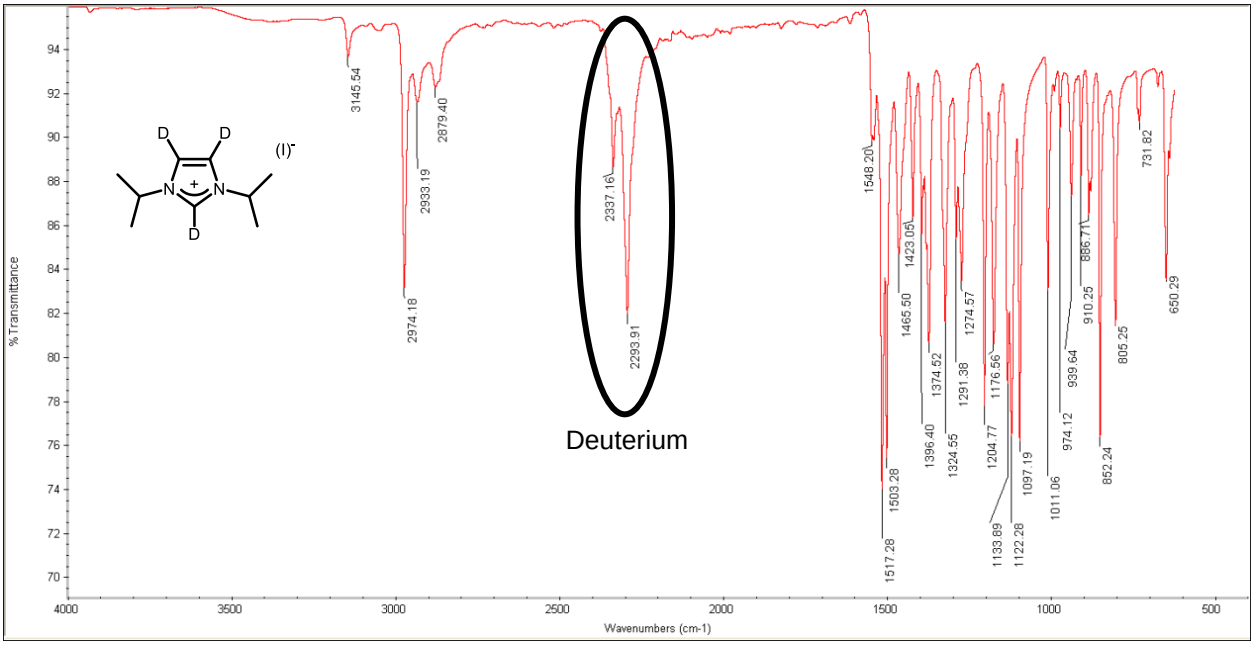
Spectra 2.22: ATR-IR of **2.7**.



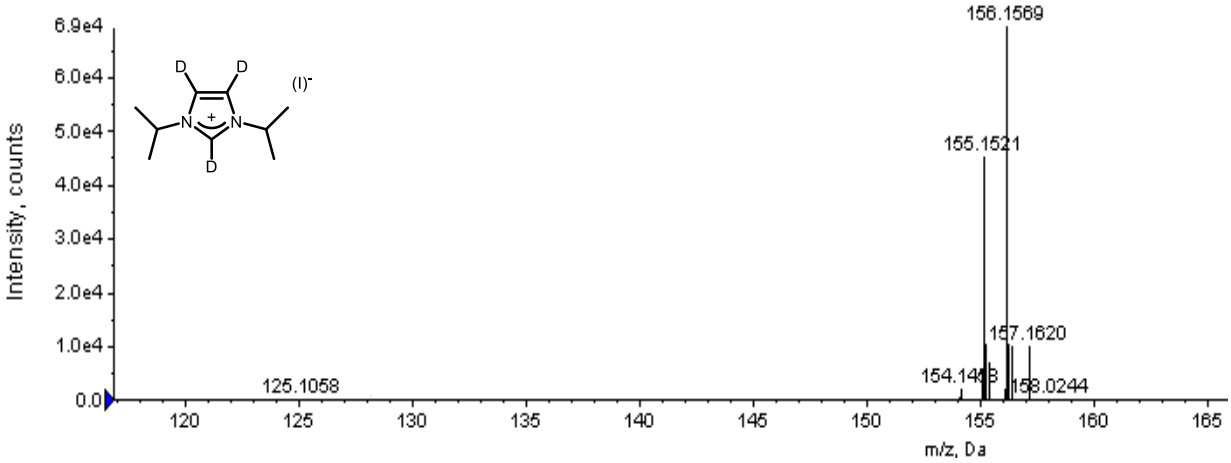
Spectra 2.23: ^{1}H NMR of **2.8** in $CDCl_3$.



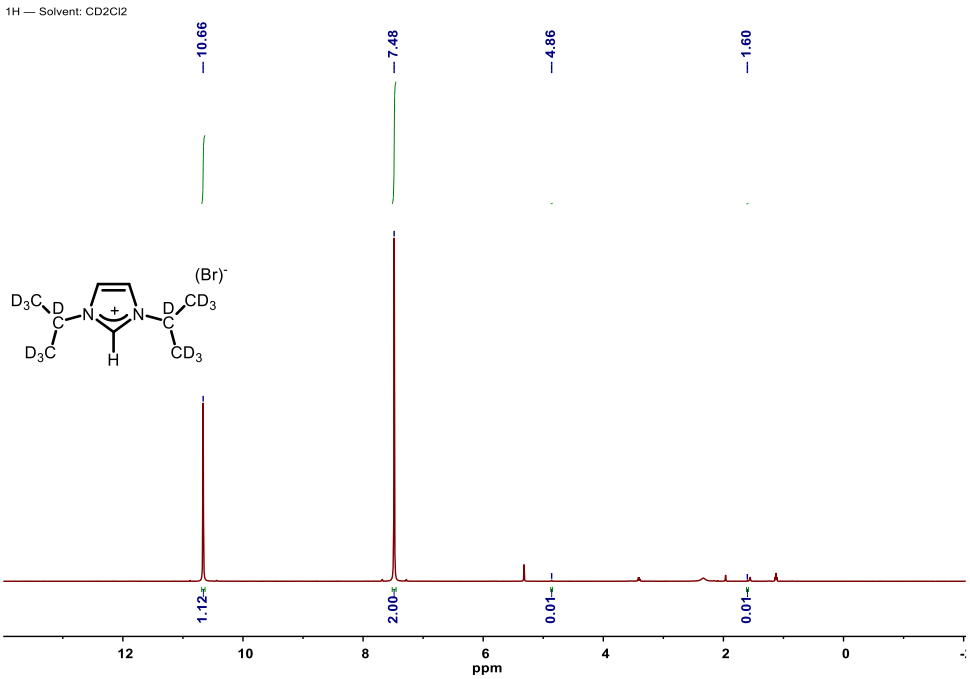
Spectra 2.24: ^{13}C NMR of **2.8** in $CDCl_3$.



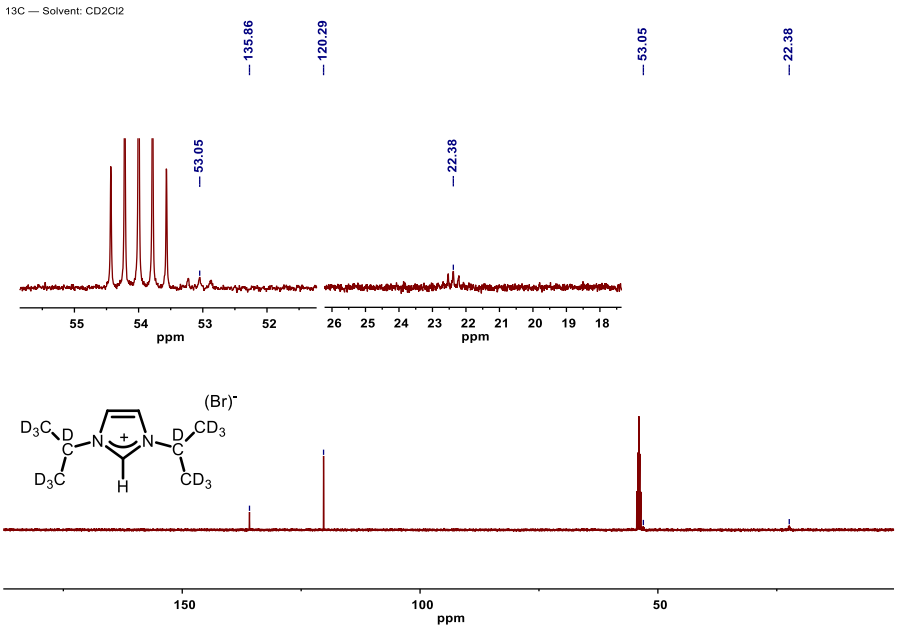
Spectra 2.25: ATR-IR of **2.8**. Signature carbon deuterium peaks are denoted by stretches at 2337 and 2294 cm^{-1}.



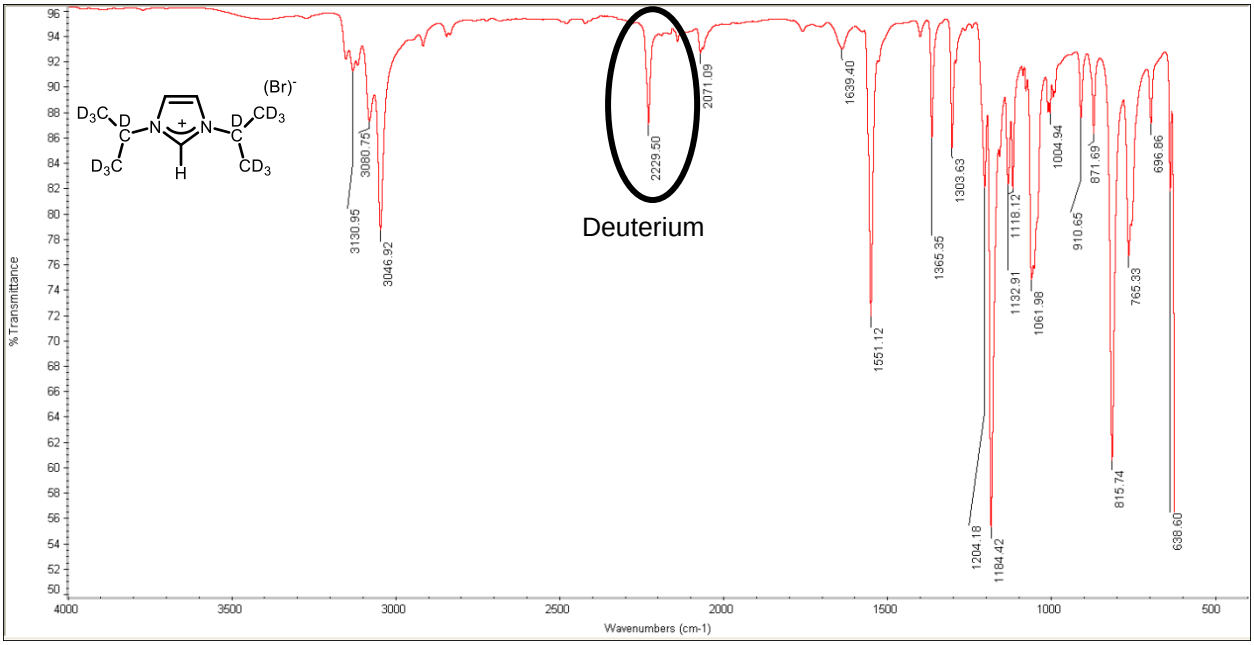
Spectra 2.26: ESI HR-MS (m/z): $[M]^+$ of **2.8**.



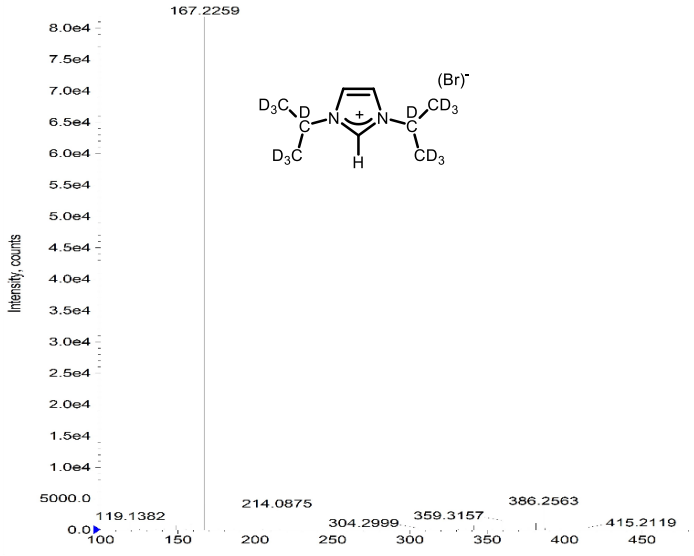
Spectra 2.27: ^{1}H NMR of **2.9** in CD_2Cl_2.



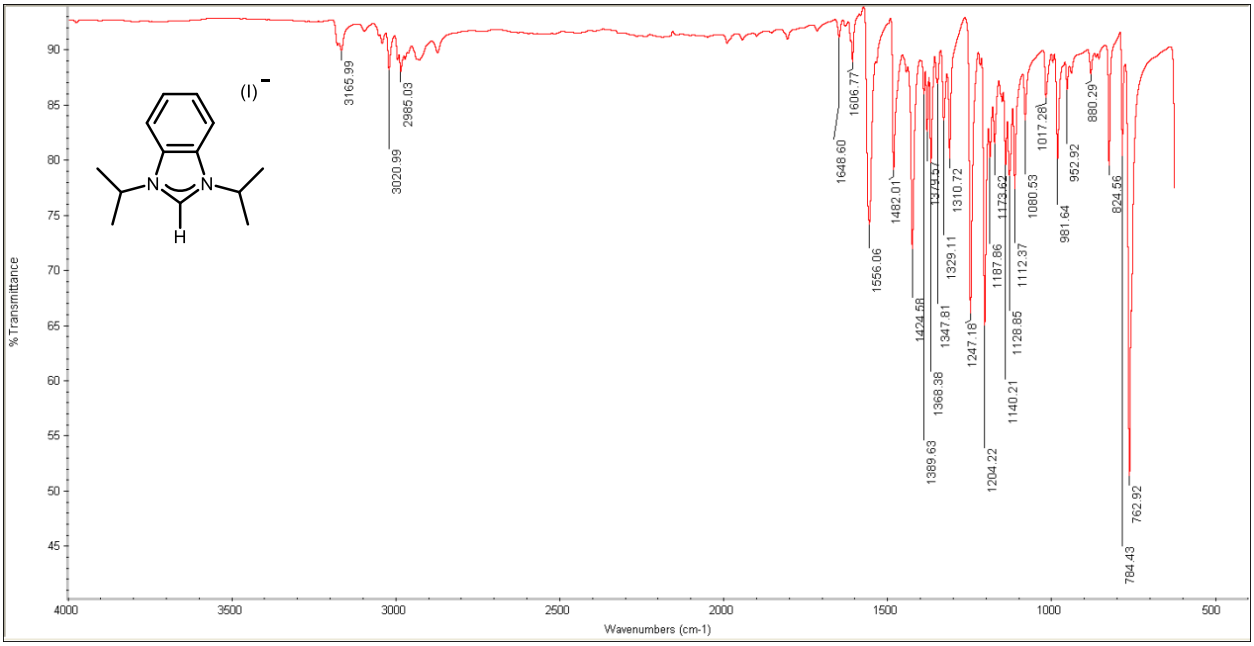
Spectra 2.28: ^{13}C NMR of **2.9** in CD_2Cl_2.



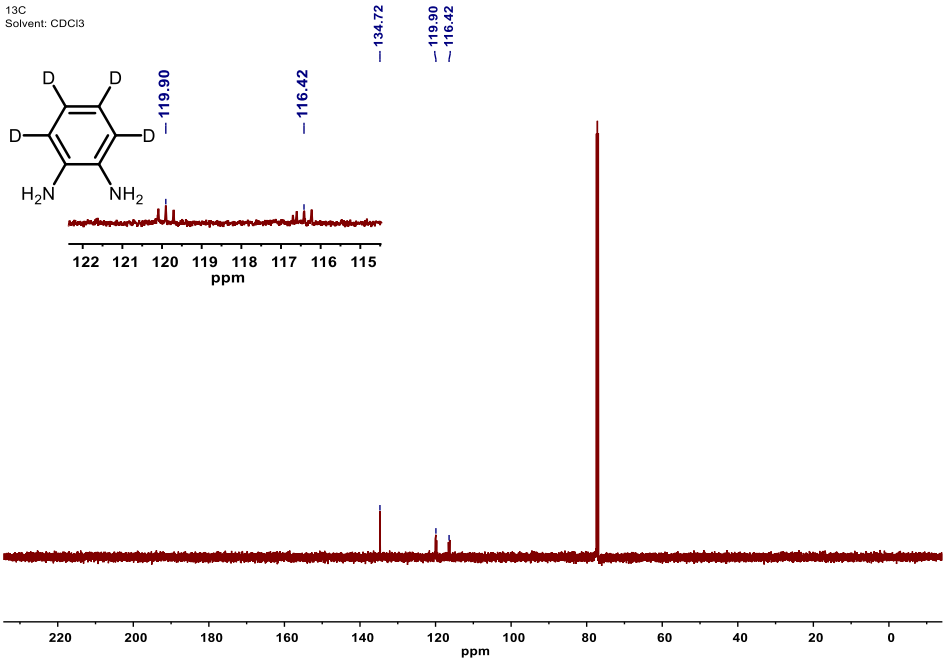
Spectra 2.29: ATR-IR of **2.9**. Signature carbon deuterium peaks are denoted by stretches at 2230 cm^{-1}.



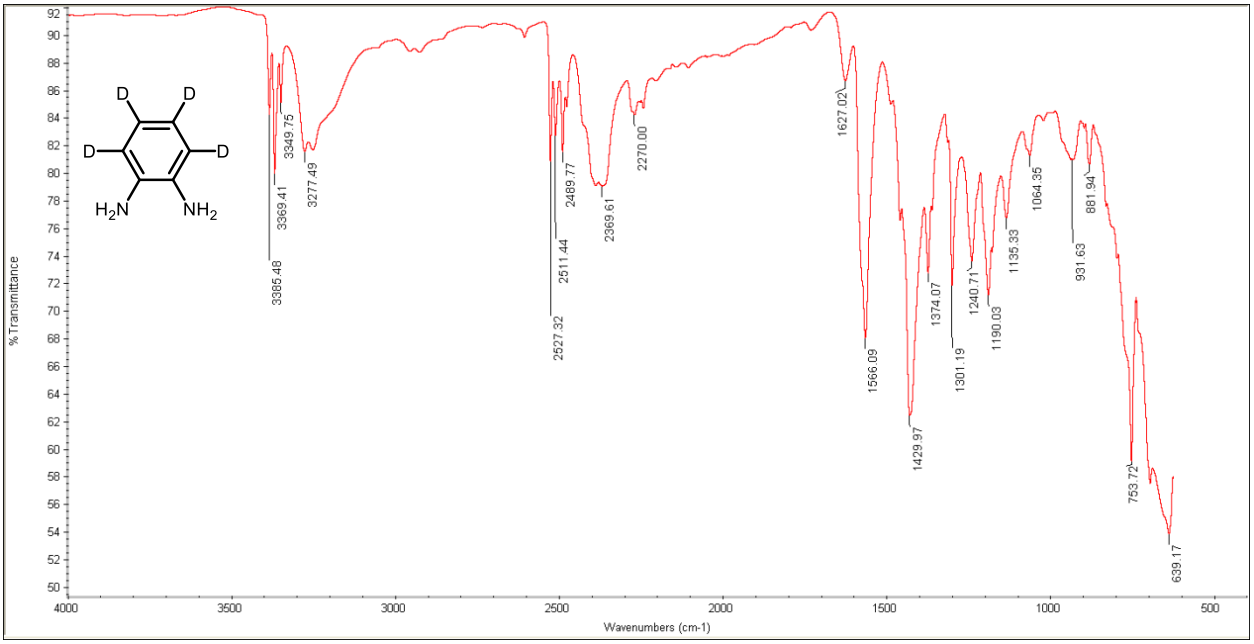
Spectra 2.30: ESI HR-MS (m/z): $[M]^+$ of **2.9**.



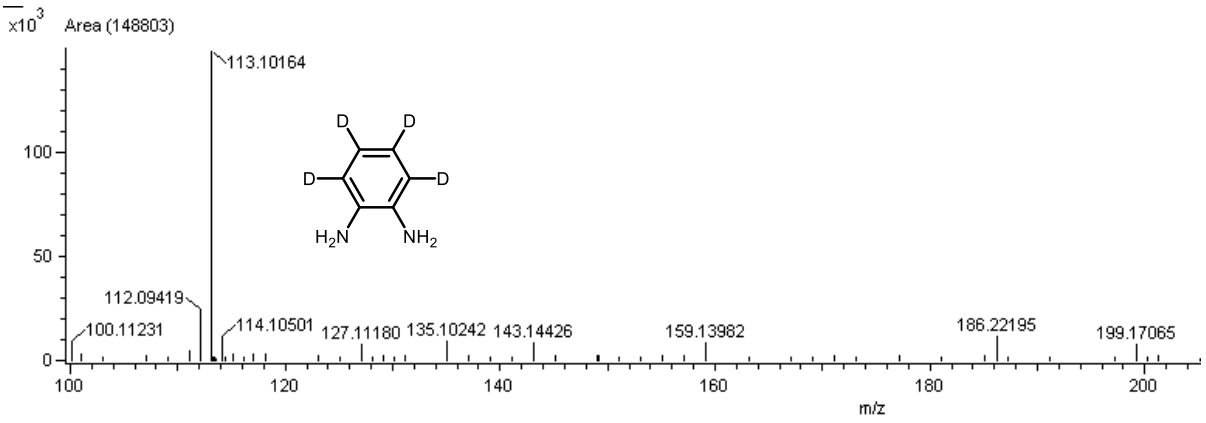
Spectra 2.31: ATR-IR of **2.10**.



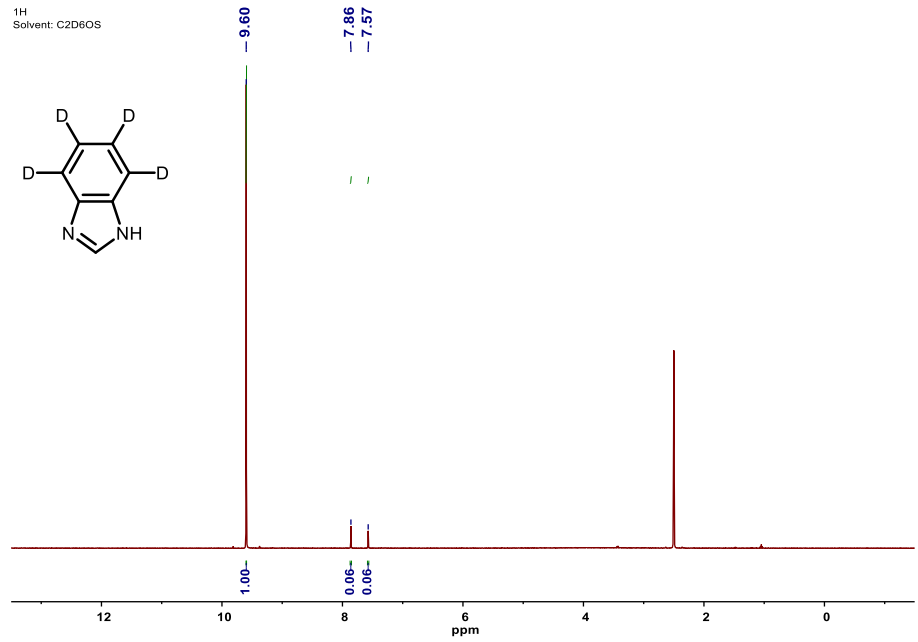
Spectra 2.32: ^{13}C NMR of **2.11** in $CDCl_3$.



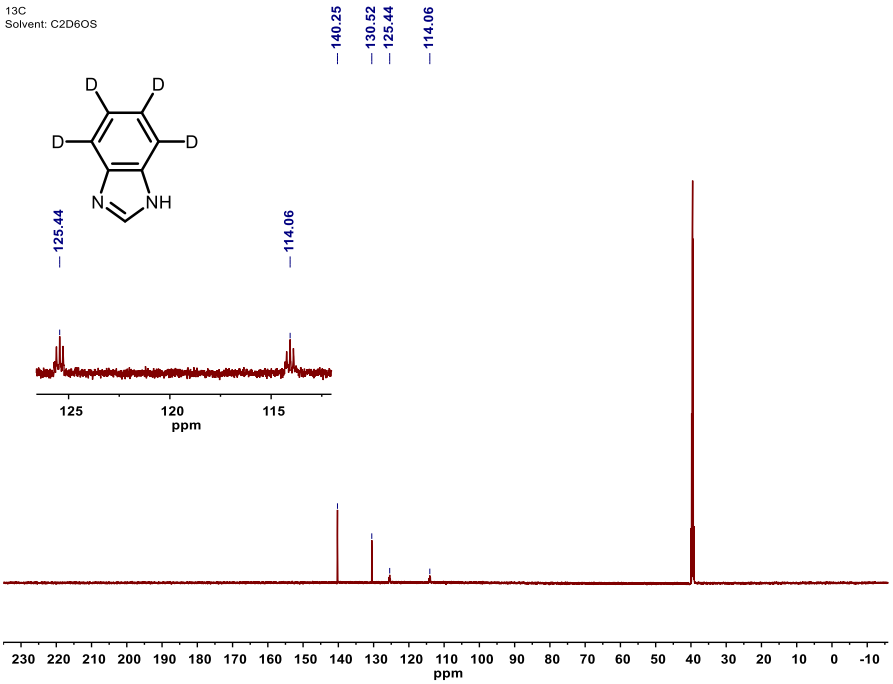
Spectra 2.33: ATR-IR of **2.11**.



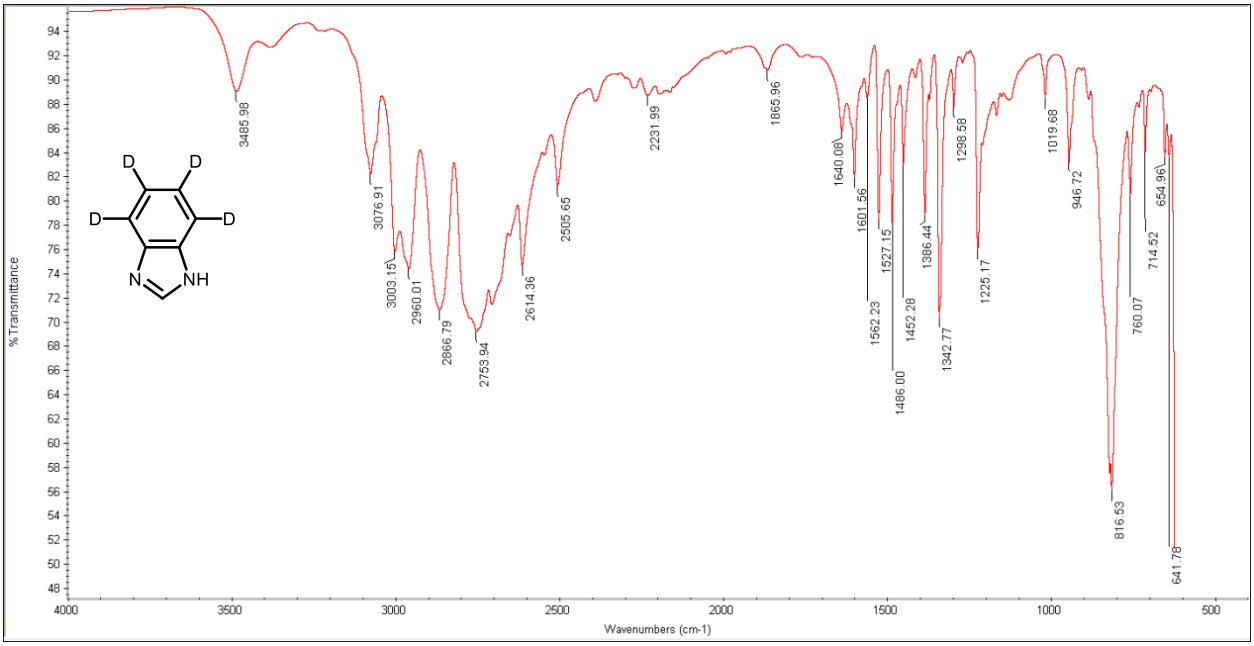
Spectra 2.34: DART HR-MS (m/z): $[M+H]^+$ of **2.11**.



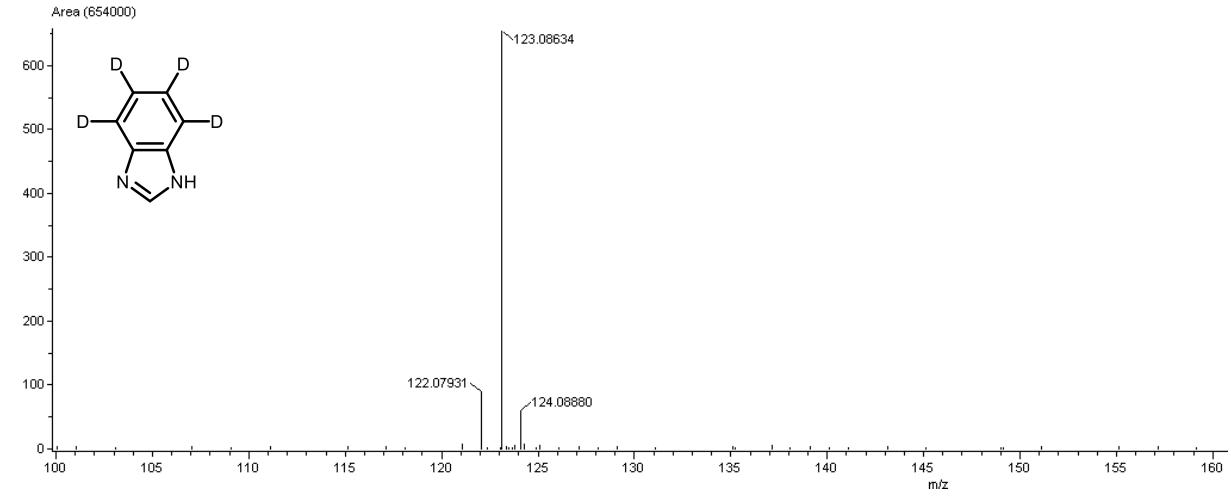
Spectra 2.35: ^{1}H NMR of **2.12** in C_2D_6OS.



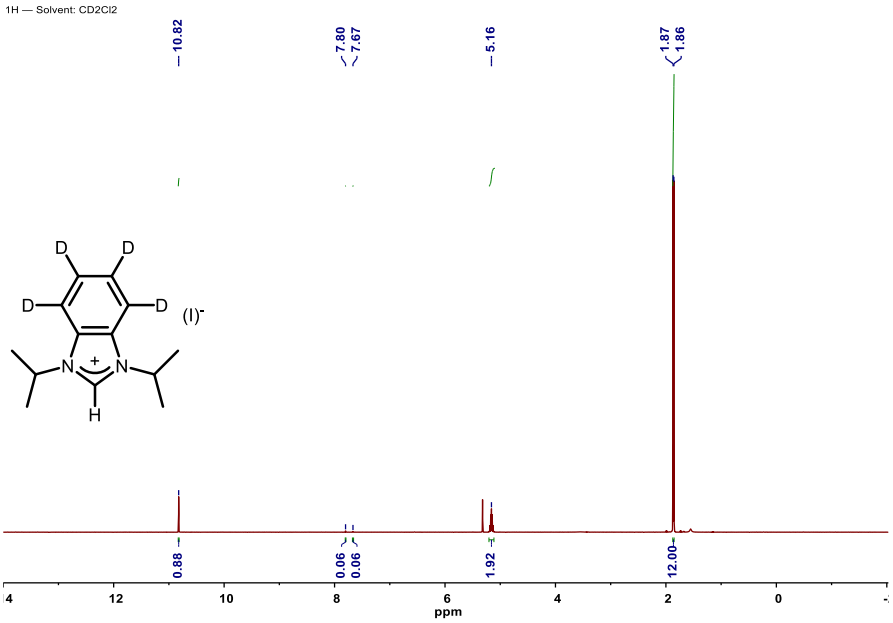
Spectra 2.36: ^{13}C NMR of **2.12** in C_2D_6OS.



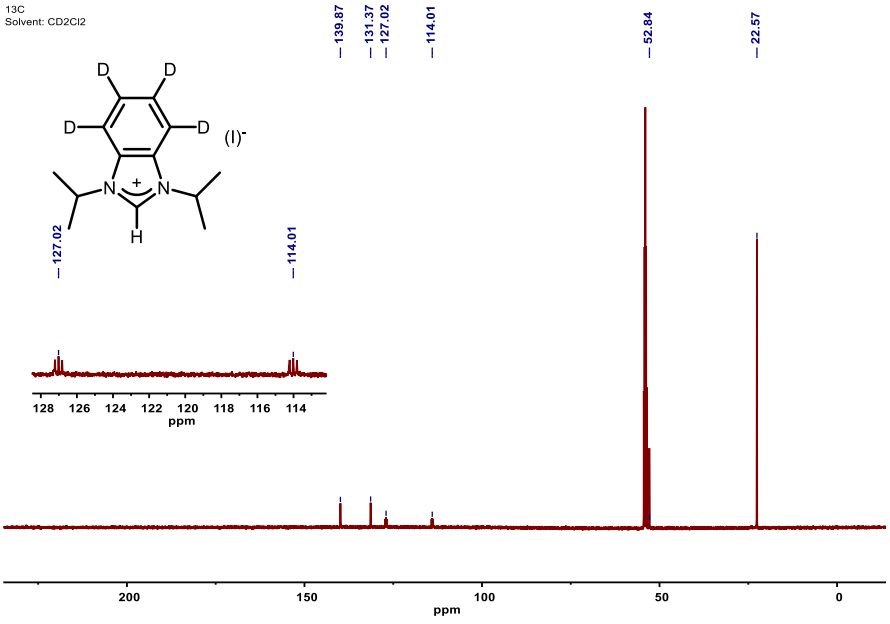
Spectra 2.37: ATR-IR of **2.12**.



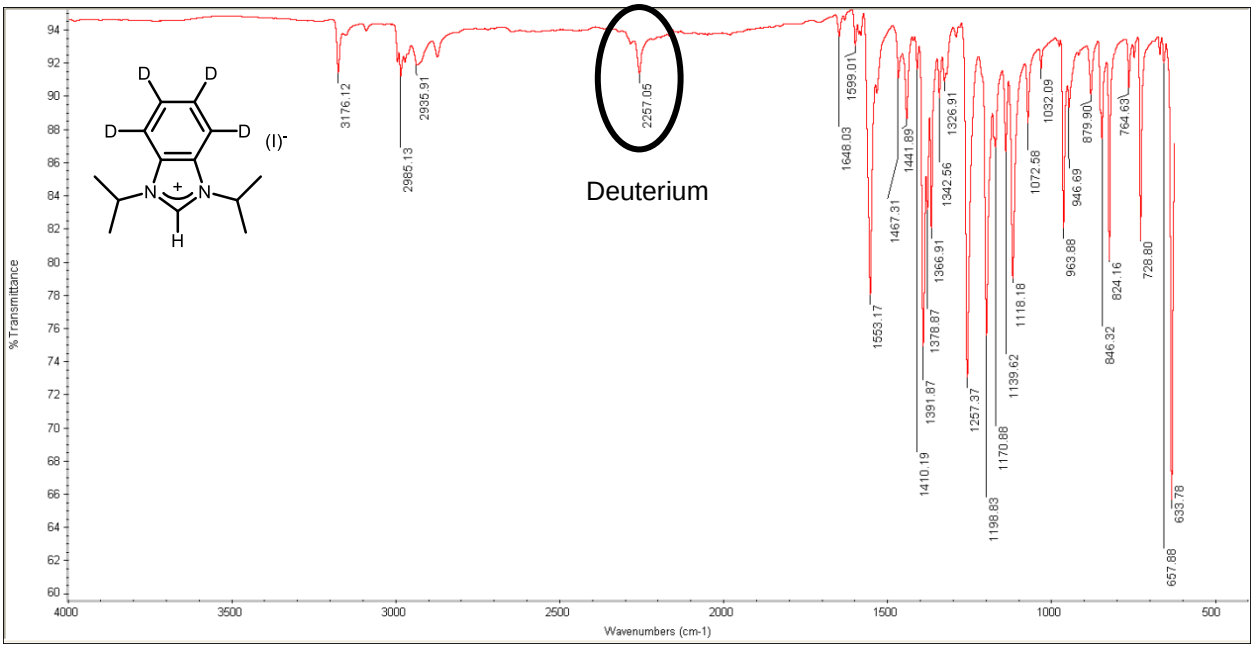
Spectra 2.38: DART HR-MS (m/z): $[M+H]^+$ of **2.12**.



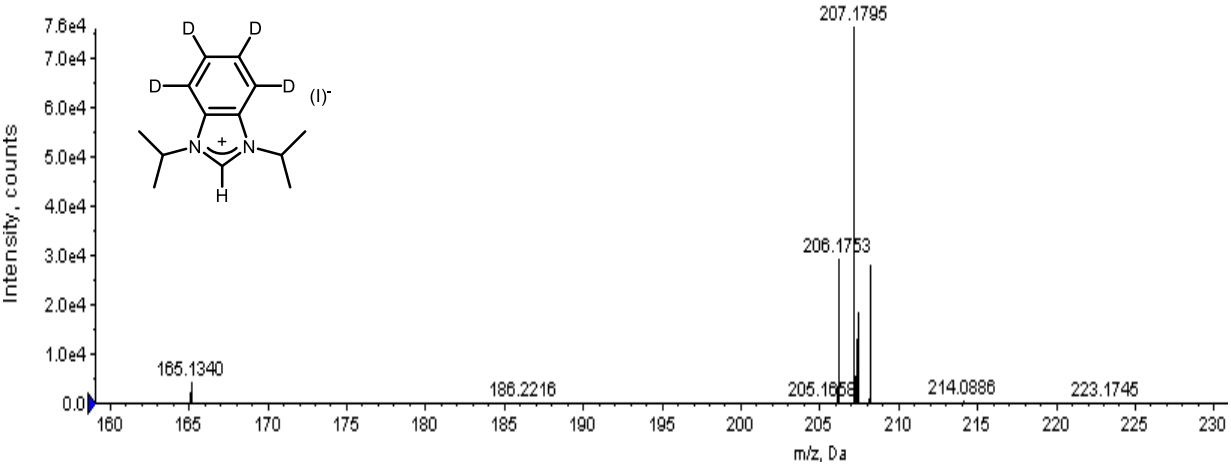
Spectra 2.39: ^{1}H NMR of **2.13** in CD_2Cl_2.



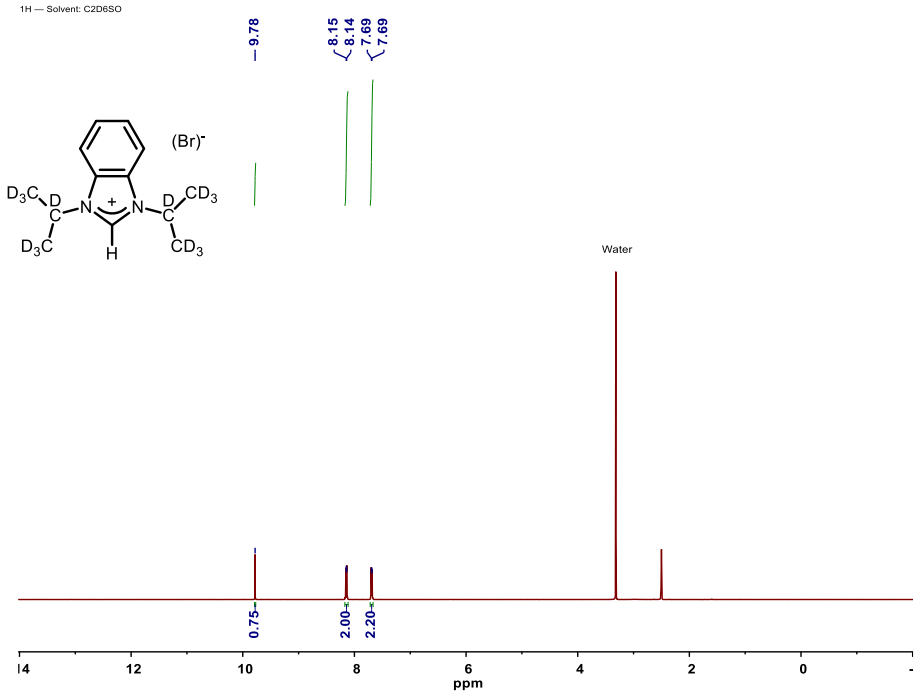
Spectra 2.40: ^{13}C NMR of **2.13** in CD_2Cl_2.



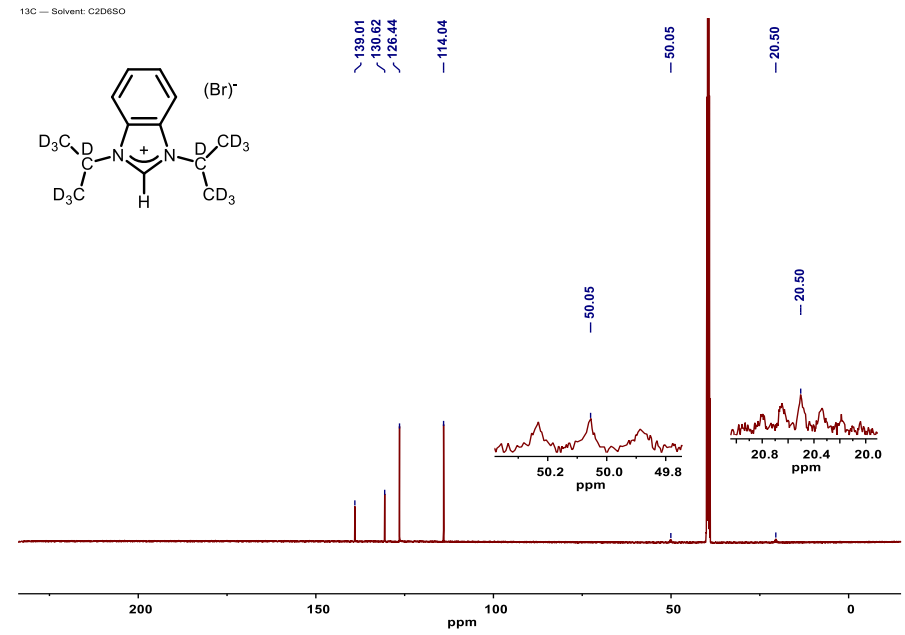
Spectra 2.41: ATR-IR of **2.13**. Signature carbon deuterium peaks are denoted by stretches at 2257cm^{-1}.



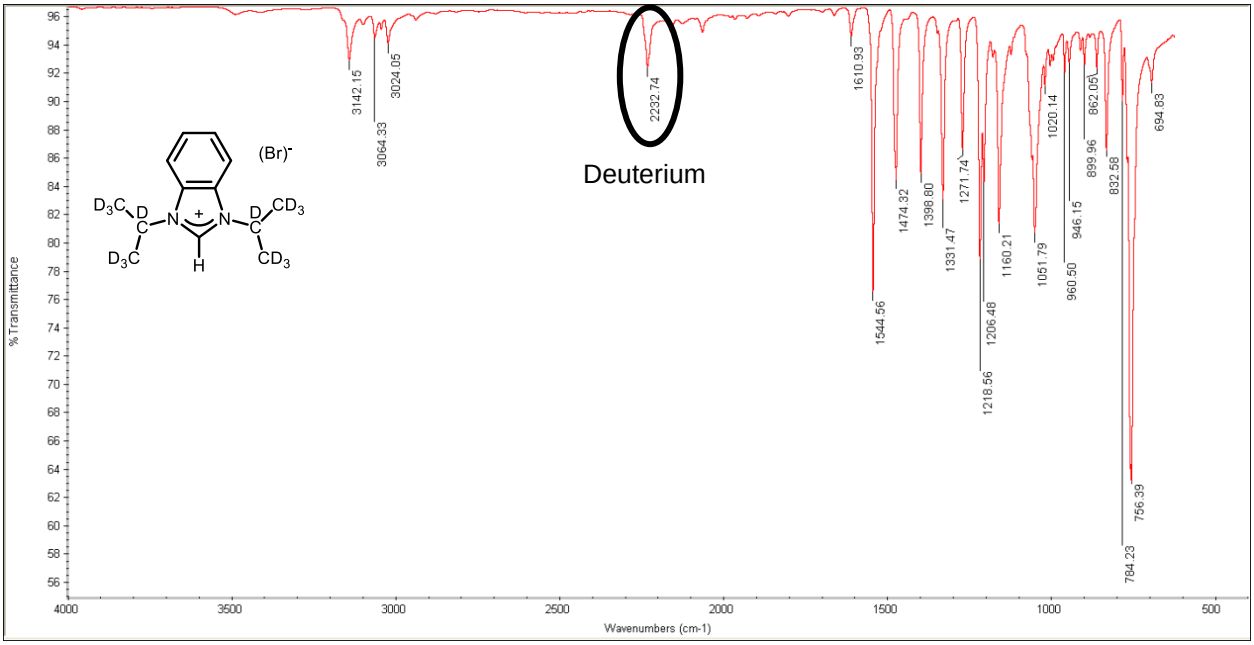
Spectra 2.42: ESI HR-MS (m/z): $[M]^+$ of **2.13**.



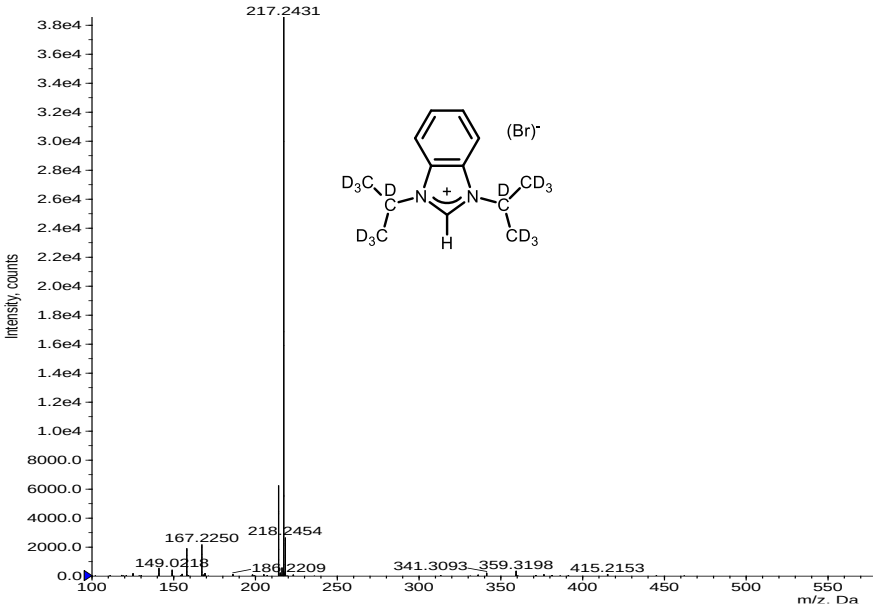
Spectra 2.43: ^{1}H NMR of **2.14** in C_2D_6OS.



Spectra 2.44: ^{13}C NMR of **2.14** in C_2D_6OS.

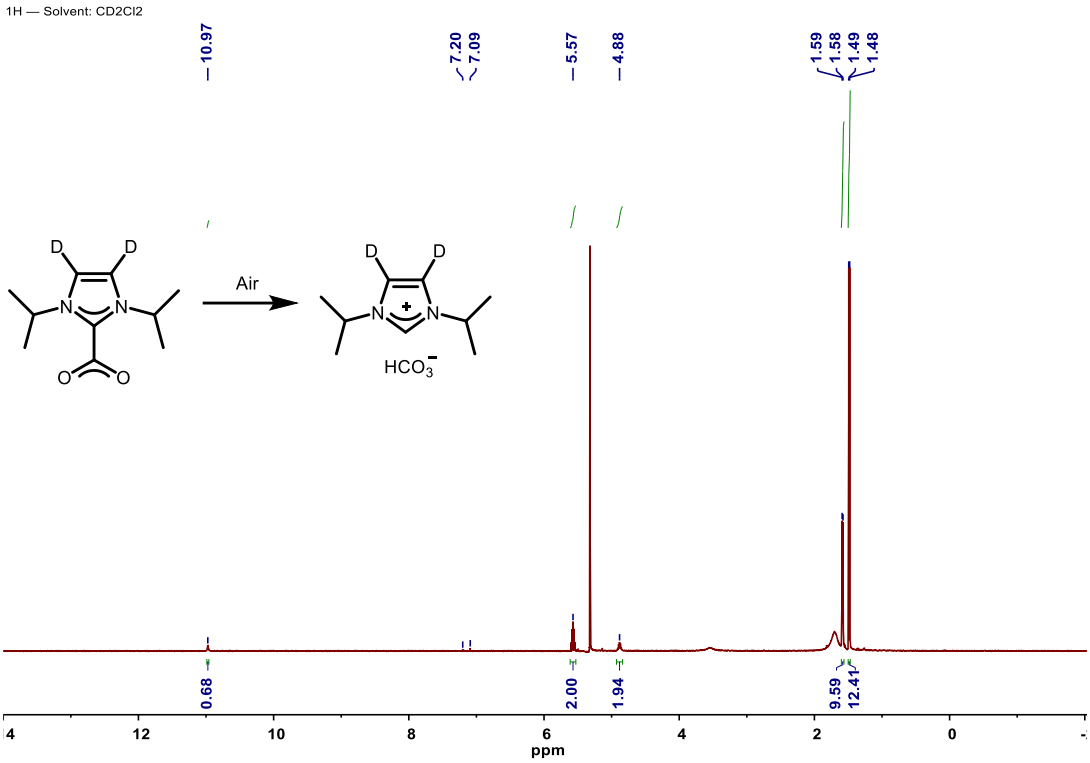


Spectra 2.45: ATR-IR of **2.14**. Signature carbon deuterium peaks are denoted by stretches at 2233 cm^{-1}.

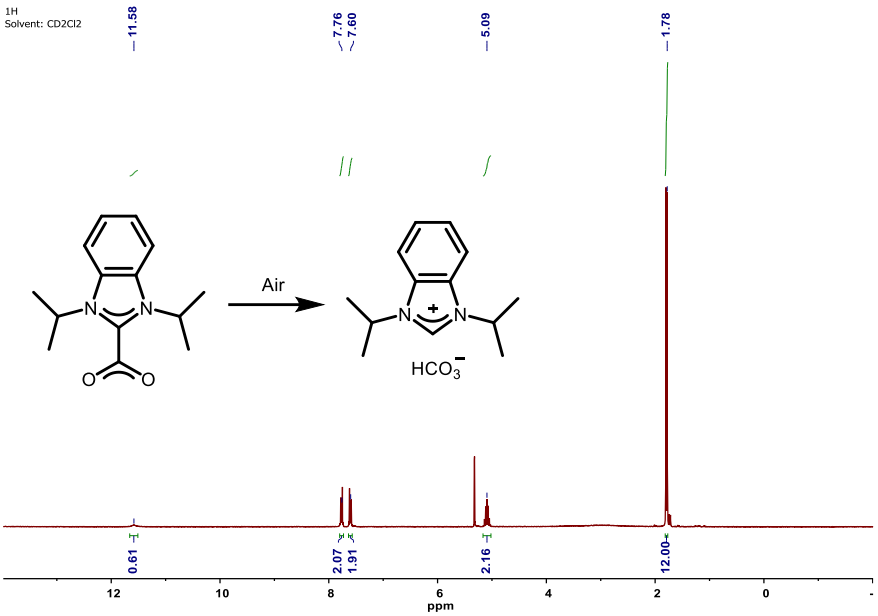


Spectra 2.46: ESI HR-MS (m/z): $[M]^+$ of **2.14**.

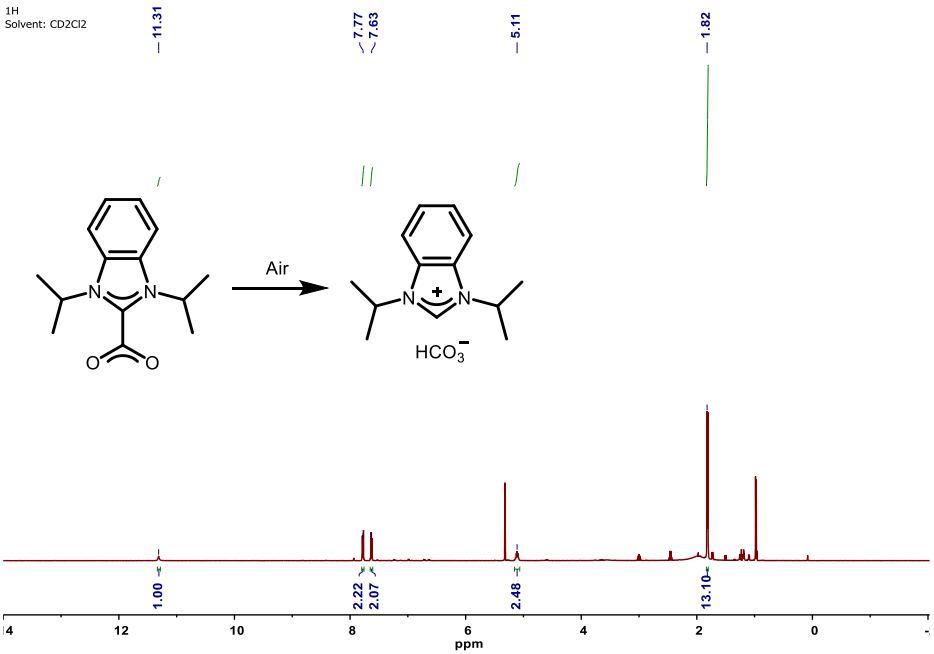
NMRs for decomposition of CO_2 adducts to hydrated bicarbonate salts.



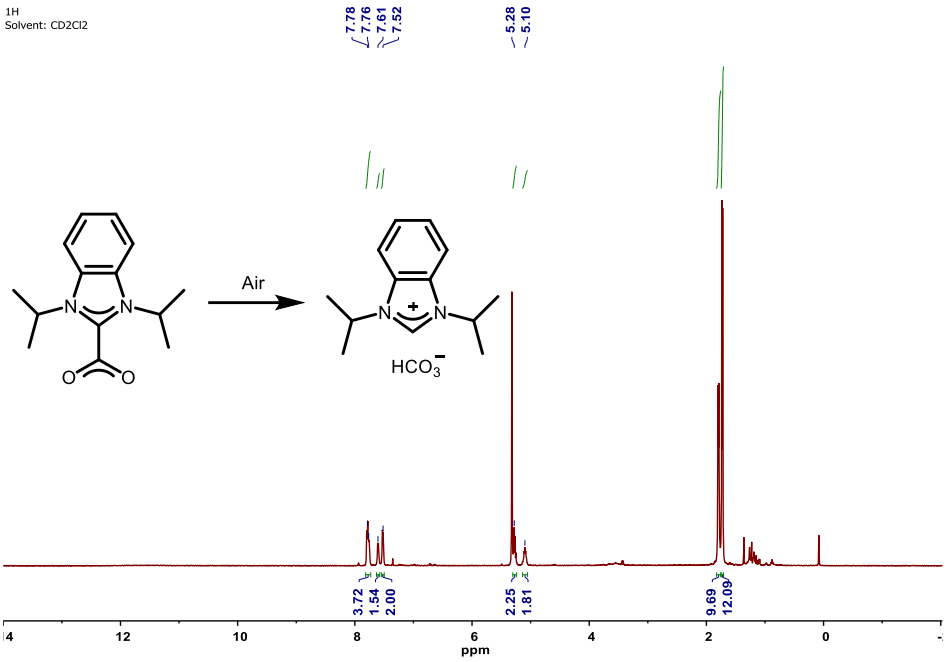
Spectra 2.47: Decay of NHC-CO_2 adduct **2.2** to the corresponding bicarbonate salt (**2.2**•H_2O) with exposure to air. **2.2** had been left in air for seven days as a solid.



Spectra 2.48: Decay of NHC-CO_2 adduct **2.4** to the corresponding bicarbonate salt (**2.4**•H_2O) with exposure to air. **2.4** had been left in air for four days as a solid.



Spectra 2.49: Decay of NHC-CO_2 adduct **2.4** to the corresponding bicarbonate salt (**2.4**•H_2O) with exposure to air. **2.4** had been left in air for 10 minutes as a solid.



Spectra 2.50: Decay of NHC-CO_2 adduct **2.4** to the corresponding bicarbonate salt (**2.4**•H_2O) with exposure to air. **2.4** had been left in air for 30 seconds as a solid.

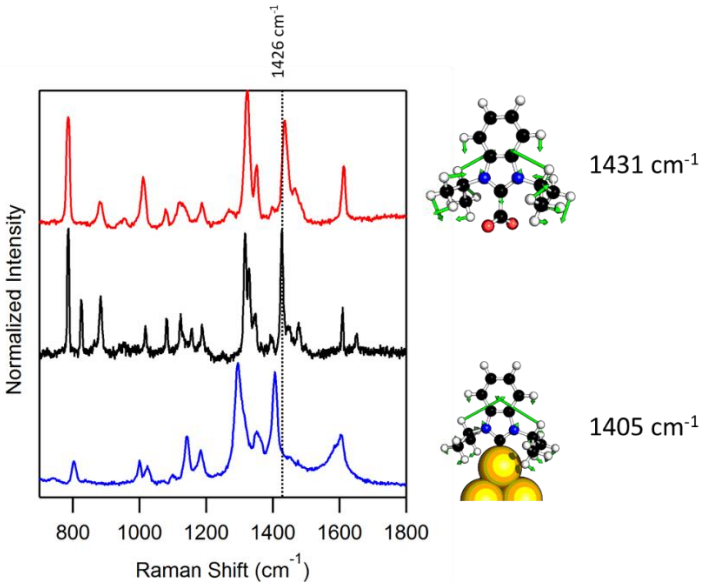


Figure 2.9: Pictorial representation of calculated vibrational modes for **2.4** which shift from 1431 cm^{-1} in the Raman spectrum of the protected carbene to 1405 cm^{-1} when bound to the surface.

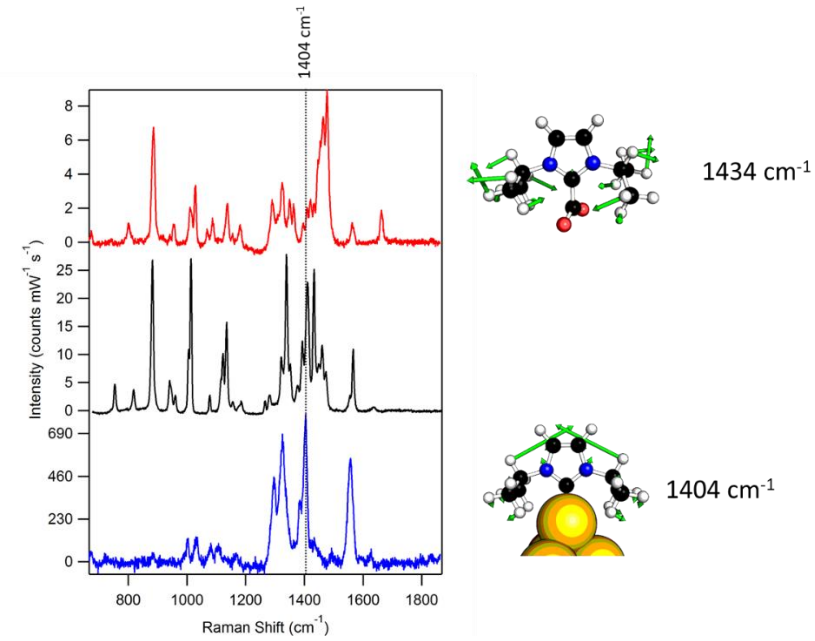


Figure 2.10: Pictorial representation of calculated vibrational modes for **2.1** which shift from 1434 cm^{-1} in the Raman spectrum of the protected carbene to 1404 cm^{-1} when bound to the surface.

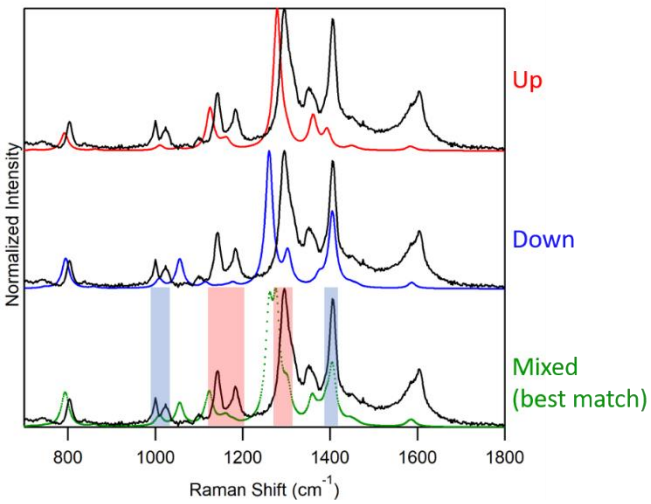


Figure 2.11: Experimental SERS Spectra of **2.4** (black) overlaid on the calculated SERS spectrum of **2.4** with isopropyl groups oriented upward (red), downward (blue), and a 49:51 combination of upward and downward (green). Shading in red and blue indicates primary contribution from the up and downward oriented isopropyls, respectively.

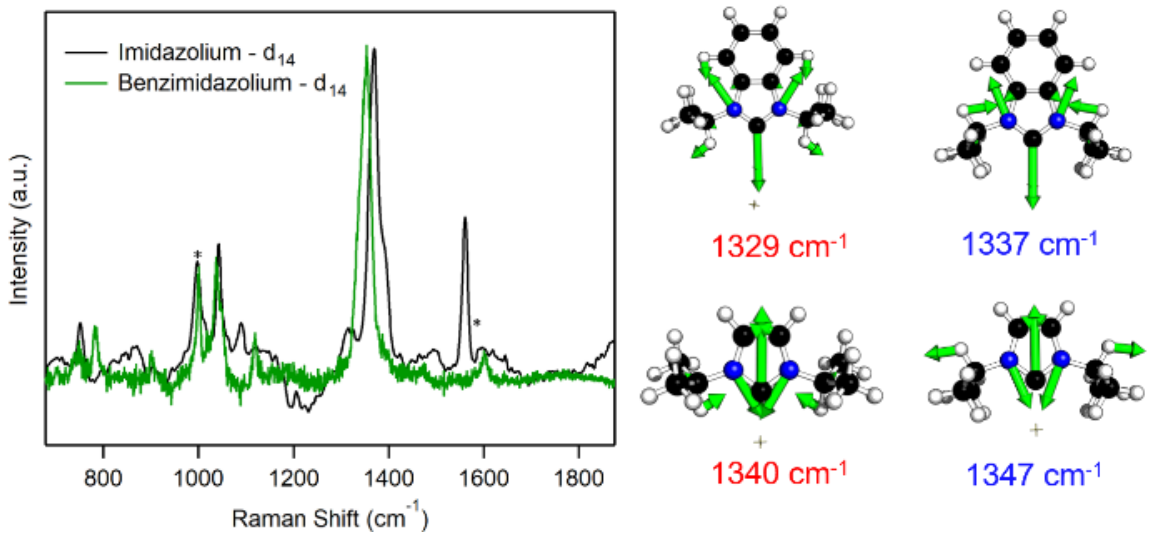


Figure 2.12: (*Left*) SERS spectra of **2.3-Au** (black) and **2.6-Au** (green). Deuteration of the isopropyl moieties causes a decoupling of the vibrational modes of the ring and isopropyl groups, causing both SERS spectra to be dominated by the ring modes. This results in a loss of sensitivity to the orientation of the isopropyl orientation. (*Right*) Pictorial representations of the ring modes for **2.3-Au** and **2.6-Au** in both the up (red) and down (blue) configurations illustrating the strong ring component in each case.

References

1. Homola, J., Present and future of surface plasmon resonance biosensors. *Analytical and Bioanalytical Chemistry* **2003,** *377*, 528-539.
2. Han, G.; Ghosh, P.; Rotello, V. M., Functionalized gold nanoparticles for drug delivery. *Nanomedicine* **2007,** *2*, 113-123.
3. DiBenedetto, S. A.; Facchetti, A.; Ratner, M. A.; Marks, T. J., Molecular Self-Assembled Monolayers and Multilayers for Organic and Unconventional Inorganic Thin-Film Transistor Applications. *Advanced Materials* **2009,** *21*, 1407-1433.
4. Lv, A.; Freitag, M.; Chepiga, K. M.; Schäfer, A. H.; Glorius, F.; Chi, L., N-Heterocyclic-Carbene-Treated Gold Surfaces in Pentacene Organic Field-Effect Transistors: Improved Stability and Contact at the Interface. *Angewandte Chemie International Edition* **2018,** *57*, 4792-4796.
5. Zamborini, F. P.; Crooks, R. M., Corrosion Passivation of Gold by n-Alkanethiol Self-Assembled Monolayers: Effect of Chain Length and End Group. *Langmuir* **1998,** *14*, 3279-3286.
6. Grzelczak, M.; Pérez-Juste, J.; Mulvaney, P.; Liz-Marzán, L. M., Shape control in gold nanoparticle synthesis. *Chemical Society Reviews* **2008,** *37*, 1783-1791.
7. Hoft, R. C.; Ford, M. J.; McDonagh, A. M.; Cortie, M. B., Adsorption of Amine Compounds on the Au(111) Surface: A Density Functional Study. *The Journal of Physical Chemistry C* **2007,** *111*, 13886-13891.
8. Lavrich, D. J.; Wetterer, S. M.; Bernasek, S. L.; Scoles, G., Physisorption and Chemisorption of Alkanethiols and Alkyl Sulfides on Au(111). *The Journal of Physical Chemistry B* **1998,** *102*, 3456-3465.
9. Srisombat, L.; Jamison, A. C.; Lee, T. R., Stability: A key issue for self-assembled monolayers on gold as thin-film coatings and nanoparticle protectants. *Colloids and Surfaces A: Physicochemical and Engineering Aspects* **2011,** *390*, 1-19.
10. Vericat, C.; Vela, M. E.; Benitez, G.; Carro, P.; Salvarezza, R. C., Self-assembled monolayers of thiols and dithiols on gold: new challenges for a well-known system. *Chemical Society Reviews* **2010,** *39*, 1805-1834.
11. Crudden, C. M.; Horton, J. H.; Ebralidze, I. I.; Zenkina, O. V.; McLean, A. B.; Drevniok, B.; She, Z.; Kraatz, H.-B.; Mosey, N. J.; Seki, T.; Keske, E. C.; Leake, J. D.; Rousina-Webb, A.; Wu, G., Ultra stable self-assembled monolayers of N-heterocyclic carbenes on gold. *Nature Chemistry* **2014,** *6*, 409-414.
12. Hopkinson, M. N.; Richter, C.; Schedler, M.; Glorius, F., An overview of N-heterocyclic carbenes. *Nature* **2014,** *510*, 485-496.
13. Crudden, C. M.; Horton, J. H.; Narouz, M. R.; Li, Z.; Smith, C. A.; Munro, K.; Baddeley, C. J.; Larrea, C. R.; Drevniok, B.; Thanabalasingam, B.; McLean, A. B.; Zenkina, O. V.; Ebralidze, I. I.; She, Z.; Kraatz, H.-B.; Mosey, N. J.; Saunders, L. N.; Yagi, A., Simple direct formation of self-assembled N-heterocyclic carbene monolayers on gold and their application in biosensing. *Nature Communications* **2016,** *7*, 12654.
14. Zhukhovitskiy, A. V.; Mavros, M. G.; Van Voorhis, T.; Johnson, J. A., Addressable Carbene Anchors for Gold Surfaces. *Journal of the American Chemical Society* **2013,** *135*, 7418-7421.

15. Li, Z.; Munro, K.; Ebralize, I. I.; Narouz, M. R.; Padmos, J. D.; Hao, H.; Crudden, C. M.; Horton, J. H., N-Heterocyclic Carbene Self-Assembled Monolayers on Gold as Surface Plasmon Resonance Biosensors. *Langmuir* **2017,** *33*, 13936-13944.
16. Li, Z.; Narouz, M. R.; Munro, K.; Hao, B.; Crudden, C. M.; Horton, J. H.; Hao, H., Carboxymethylated Dextran-Modified N-Heterocyclic Carbene Self-Assembled Monolayers on Gold for Use in Surface Plasmon Resonance Biosensing. *ACS Applied Materials & Interfaces* **2017,** *9*, 39223-39234.
17. Cao, Z.; Derrick, J. S.; Xu, J.; Gao, R.; Gong, M.; Nichols, E. M.; Smith, P. T.; Liu, X.; Wen, X.; Copéret, C.; Chang, C. J., Chelating N-Heterocyclic Carbene Ligands Enable Tuning of Electrocatalytic CO2 Reduction to Formate and Carbon Monoxide: Surface Organometallic Chemistry. *Angewandte Chemie International Edition* **2018,** *57*, 4981-4985.
18. Baquero, E. A.; Tricard, S.; Coppel, Y.; Flores, J. C.; Chaudret, B.; de Jesús, E., Water-soluble platinum nanoparticles stabilized by sulfonated N-heterocyclic carbenes: influence of the synthetic approach. *Dalton Transactions* **2018,** *47*, 4093-4104.
19. Bridonneau, N.; Hippolyte, L.; Mercier, D.; Portehault, D.; Desage-El Murr, M.; Marcus, P.; Fensterbank, L.; Chanéac, C.; Ribot, F., N-Heterocyclic carbene-stabilized gold nanoparticles with tunable sizes. *Dalton Transactions* **2018,** *47*, 6850-6859.
20. MacLeod, M. J.; Johnson, J. A., PEGylated N-Heterocyclic Carbene Anchors Designed To Stabilize Gold Nanoparticles in Biologically Relevant Media. *Journal of the American Chemical Society* **2015,** *137*, 7974-7977.
21. Man, R. W. Y.; Li, C.-H.; MacLean, M. W. A.; Zenkina, O. V.; Zamora, M. T.; Saunders, L. N.; Rousina-Webb, A.; Nambo, M.; Crudden, C. M., Ultrastable Gold Nanoparticles Modified by Bidentate N-Heterocyclic Carbene Ligands. *Journal of the American Chemical Society* **2018,** *140*, 1576-1579.
22. Narouz, M. R.; Li, C.-H.; Nazemi, A.; Crudden, C. M., Amphiphilic N-Heterocyclic Carbene-Stabilized Gold Nanoparticles and Their Self-Assembly in Polar Solvents. *Langmuir* **2017,** *33*, 14211-14219.
23. Salorinne, K.; Man, R. W. Y.; Li, C.-H.; Taki, M.; Nambo, M.; Crudden, C. M., Water-Soluble N-Heterocyclic Carbene-Protected Gold Nanoparticles: Size-Controlled Synthesis, Stability, and Optical Properties. *Angewandte Chemie International Edition* **2017,** *56*, 6198-6202.
24. Vignolle, J.; Tilley, T. D., N-Heterocyclic carbene-stabilized gold nanoparticles and their assembly into 3D superlattices. *Chemical Communications* **2009**, 7230-7232.
25. Larrea, C. R.; Baddeley, C. J.; Narouz, M. R.; Mosey, N. J.; Horton, J. H.; Crudden, C. M., N-Heterocyclic Carbene Self-assembled Monolayers on Copper and Gold: Dramatic Effect of Wingtip Groups on Binding, Orientation and Assembly. *ChemPhysChem* **2017,** *18*, 3536-3539.
26. Wang, G.; Rühling, A.; Amirjalayer, S.; Knor, M.; Ernst, J. B.; Richter, C.; Gao, H.-J.; Timmer, A.; Gao, H.-Y.; Doltsinis, N. L.; Glorius, F.; Fuchs, H., Ballbot-type motion of N-heterocyclic carbenes on gold surfaces. *Nature Chemistry* **2016,** *9*, 152.
27. DeJesus, J. F.; Trujillo, M. J.; Camden, J. P.; Jenkins, D. M., N-Heterocyclic Carbenes as a Robust Platform for Surface-Enhanced Raman Spectroscopy. *Journal of the American Chemical Society* **2018,** *140*, 1247-1250.
28. Allen, C. S.; Van Duyne, R. P., Orientational specificity of Raman scattering from molecules adsorbed on silver electrodes. *Chemical Physics Letters* **1979,** *63*, 455-459.

29. Golab, J. T.; Sprague, J. R.; Carron, K. T.; Schatz, G. C.; Van Duyne, R. P., A surface enhanced hyper-Raman scattering study of pyridine adsorbed onto silver: Experiment and theory. *The Journal of Chemical Physics* **1988,** *88*, 7942-7951.
30. Turley, H. K.; Hu, Z.; Jensen, L.; Camden, J. P., Surface-Enhanced Resonance Hyper-Raman Scattering Elucidates the Molecular Orientation of Rhodamine 6G on Silver Colloids. *The Journal of Physical Chemistry Letters* **2017,** *8*, 1819-1823.
31. Giese, B.; McNaughton, D., Surface-Enhanced Raman Spectroscopic and Density Functional Theory Study of Adenine Adsorption to Silver Surfaces. *The Journal of Physical Chemistry B* **2002,** *106*, 101-112.
32. Chiang, N.; Jiang, N.; Madison, L. R.; Pozzi, E. A.; Wasielewski, M. R.; Ratner, M. A.; Hersam, M. C.; Seideman, T.; Schatz, G. C.; Van Duyne, R. P., Probing Intermolecular Vibrational Symmetry Breaking in Self-Assembled Monolayers with Ultrahigh Vacuum Tip-Enhanced Raman Spectroscopy. *Journal of the American Chemical Society* **2017,** *139*, 18664-18669.
33. Lee, J.; Tallarida, N.; Chen, X.; Jensen, L.; Apkarian, V. A., Microscopy with a single-molecule scanning electrometer. *Science Advances* **2018,** *4*.
34. Blackie, E.; Le Ru, E. C.; Meyer, M.; Timmer, M.; Burkett, B.; Northcote, P.; Etchegoin, P. G., Bi-analyte SERS with isotopically edited dyes. *Physical Chemistry Chemical Physics* **2008,** *10*, 4147-4153.
35. Camden, J. P.; Dieringer, J. A.; Wang, Y.; Masiello, D. J.; Marks, L. D.; Schatz, G. C.; Van Duyne, R. P., Probing the Structure of Single-Molecule Surface-Enhanced Raman Scattering Hot Spots. *Journal of the American Chemical Society* **2008,** *130*, 12616-12617.
36. Kleinman, S. L.; Ringe, E.; Valley, N.; Wustholz, K. L.; Phillips, E.; Scheidt, K. A.; Schatz, G. C.; Van Duyne, R. P., Single-Molecule Surface-Enhanced Raman Spectroscopy of Crystal Violet Isotopologues: Theory and Experiment. *Journal of the American Chemical Society* **2011,** *133*, 4115-4122.
37. Titus, E. J.; Weber, M. L.; Stranahan, S. M.; Willets, K. A., Super-Resolution SERS Imaging beyond the Single-Molecule Limit: An Isotope-Edited Approach. *Nano Letters* **2012,** *12*, 5103-5110.
38. Campos, J.; Sharninghausen, L. S.; Crabtree, R. H.; Balcells, D., A Carbene-Rich but Carbonyl-Poor $[Ir^6(IMe)^8(CO)^2H^{14}]^{2+}$ Polyhydride Cluster as a Deactivation Product from Catalytic Glycerol Dehydrogenation. *Angewandte Chemie International Edition* **2014,** *53*, 12808-12811.
39. Voutchkova, A. M.; Appelhans, L. N.; Chianese, A. R.; Crabtree, R. H., Disubstituted Imidazolium-2-Carboxylates as Efficient Precursors to N-Heterocyclic Carbene Complexes of Rh, Ru, Ir, and Pd. *Journal of the American Chemical Society* **2005,** *127*, 17624-17625.
40. Van Ausdall, B. R.; Glass, J. L.; Wiggins, K. M.; Aarif, A. M.; Louie, J., A Systematic Investigation of Factors Influencing the Decarboxylation of Imidazolium Carboxylates. *The Journal of Organic Chemistry* **2009,** *74*, 7935-7942.
41. Dzyuba, S. V.; Li, S.; Bartsch, R. A., Convenient syntheses of perdeuterated ionic liquids. *Journal of Heterocyclic Chemistry* **2007,** *44*, 223-225.
42. Fèvre, M.; Pinaud, J.; Leteneur, A.; Gnanou, Y.; Vignolle, J.; Taton, D.; Miqueu, K.; Sotiropoulos, J.-M., Imidazol(in)ium Hydrogen Carbonates as a Genuine Source of N-Heterocyclic Carbenes (NHCs): Applications to the Facile Preparation of NHC Metal

Complexes and to NHC-Organocatalyzed Molecular and Macromolecular Syntheses. *Journal of the American Chemical Society* **2012,** *134*, 6776-6784.
43. Lindner, R.; Lejkowski, M. L.; Lavy, S.; Deglmann, P.; Wiss, K. T.; Zarbakhsh, S.; Meyer, L.; Limbach, M., Ring-Opening Polymerization and Copolymerization of Propylene Oxide Catalyzed by N-Heterocyclic Carbenes. *ChemCatChem* **2014,** *6*, 618-625.
44. Ito, N.; Esaki, H.; Maesawa, T.; Imamiya, E.; Maegawa, T.; Sajiki, H., Efficient and Selective Pt/C-Catalyzed H–D Exchange Reaction of Aromatic Rings. *Bulletin of the Chemical Society of Japan* **2008,** *81*, 278-286.
45. Khramov, D. M.; Bielawski, C. W., Donor−Acceptor Triazenes: Synthesis, Characterization, and Study of Their Electronic and Thermal Properties. *The Journal of Organic Chemistry* **2007,** *72*, 9407-9417.
46. Farcau, C.; Astilean, S., Mapping the SERS Efficiency and Hot-Spots Localization on Gold Film over Nanospheres Substrates. *The Journal of Physical Chemistry C* **2010,** *114*, 11717-11722.
47. Péron, O.; Rinnert, E.; Toury, T.; Lamy de la Chapelle, M.; Compère, C., Quantitative SERS sensors for environmental analysis of naphthalene. *Analyst* **2011,** *136*, 1018-1022.
48. Aikens, C. M.; Schatz, G. C., TDDFT Studies of Absorption and SERS Spectra of Pyridine Interacting with Au20. *The Journal of Physical Chemistry A* **2006,** *110*, 13317-13324.
49. Zhao, L.; Jensen, L.; Schatz, G. C., Pyridine−Ag_{20} Cluster: A Model System for Studying Surface-Enhanced Raman Scattering. *Journal of the American Chemical Society* **2006,** *128*, 2911-2919.
50. Li, J.; Li, X.; Zhai, H.-J.; Wang, L.-S., Au_{20}: A Tetrahedral Cluster. *Science* **2003,** *299*, 864-867.
51. Watanabe, H.; Hayazawa, N.; Inouye, Y.; Kawata, S., DFT Vibrational Calculations of Rhodamine 6G Adsorbed on Silver: Analysis of Tip-Enhanced Raman Spectroscopy. *The Journal of Physical Chemistry B* **2005,** *109*, 5012-5020.
52. Gardner, S.; Kawamoto, T.; Curran, D. P., Synthesis of 1,3-Dialkylimidazol-2-ylidene Boranes from 1,3-Dialkylimidazolium Iodides and Sodium Borohydride. *The Journal of Organic Chemistry* **2015,** *80*, 9794-9797.
53. Chen, W.-C.; Lai, Y.-C.; Shih, W.-C.; Yu, M.-S.; Yap, G. P. A.; Ong, T.-G., Mechanistic Study of a Switch in the Regioselectivity of Hydroheteroarylation of Styrene Catalyzed by Bimetallic Ni–Al through C-H Activation. **2014,** *20*, 8099-8105.
54. te Velde, G.; Bickelhaupt, F. M.; Baerends, E. J.; Fonseca Guerra, C.; van Gisbergen, S. J. A.; Snijders, J. G.; Ziegler, T., Chemistry with ADF. **2001,** *22*, 931-967.
55. Lenthe, E. V.; Baerends, E. J.; Snijders, J. G., Relativistic regular two-component Hamiltonians. **1993,** *99*, 4597-4610.
56. Lenthe, E. v.; Ehlers, A.; Baerends, E.-J., Geometry optimizations in the zero order regular approximation for relativistic effects. **1999,** *110*, 8943-8953.
57. Becke, A. D., Density-functional exchange-energy approximation with correct asymptotic behavior. *Physical Review A* **1988,** *38*, 3098-3100.
58. Perdew, J. P., Density-functional approximation for the correlation energy of the inhomogeneous electron gas. *Physical Review B* **1986,** *33*, 8822-8824.

Chapter 3 : Imidazolinium N-Heterocyclic Carbene Ligands for Enhanced Stability on Gold Surfaces

A version of this chapter was accepted to Langmuir by Lindy M. Sherman, Shelby L. Strausser, Rowan K. Borsari, David M. Jenkins, and Jon P. Camden.

The work presented in this publication was completed in a collaborative manner with the Camden lab at the University of Notre Dame. My portion of the publication entails the synthesis of complexes 3.1-3.7. Rowan Borsari at the University of Tennessee (Jenkins Lab but was working at the Camden Lab for a summer exchange) was responsible for developing the method and depositing the CO_2 adducts for the imidazolinium onto Au FONs. Lindy Sherman was responsible for the synthesis of NHC-Au FONs that remained and obtaining their corresponding SERS spectra in both the manuscript and experimental section. The experimental section has been shortened to display the work that I have attributed to the manuscript, except where the main text refers to figures in that section.

Abstract

N-heterocyclic carbenes (NHCs) have emerged as versatile and robust ligands for noble metal surface modifications due to their ability to form compact, self-assembled monolayers. Despite a growing body of research, previous NHC surface modification schemes have employed just two structural motifs: the benzimidazolium NHC and the imidazolium NHC. However, different NHC moieties, including saturated NHCs, are often more effective in homogenous catalysis chemistry than these aforementioned motifs and may impart numerous advantages to NHC surfaces, such as increased stability and access to chiral groups. This work explores the preparation and stability of NHC-coated gold surfaces using imidazolium and imidazolinium NHC ligands. X-ray photoelectron spectroscopy (XPS) and surface-enhanced Raman spectroscopy (SERS) demonstrate the attachment of NHC ligands to the gold surface and show enhanced stability of imidazolinium compared to the traditional imidazolium under harsh acidic conditions.

Introduction

Controlling the surface environment on metal substrates via ligand chemistry is essential for applications ranging from catalysis to sensing and therapeutics.[1-6] Despite the well-documented challenges associated with thiol ligands, such as oxidation and degradation in ambient conditions,[7-11] they remain the most common molecule class for functionalizing noble metal surfaces due to their high affinity for gold and silver.[5] For example, recent reports have employed thiol-based ligands to develop patterned molecular films for site-specific immobilization of biomolecules,[12, 13] to investigate host-guest complexation for surface detection of polycyclic aromatic hydrocarbons,[14] and to tether aptamers on implantable electrochemical devices for *in vivo* diagnostics.[15, 16] In 2014, Crudden and coworkers[17] reported that N-heterocyclic carbene (NHC) ligands form stable, well-ordered, self-assembled monolayers on crystalline gold that can, in many situations, exceed the performance of thiols. Since their initial work, multiple research groups have explored the capabilities of NHC-coated surfaces towards a variety of applications.[18-24]

Despite the increasing popularity of NHCs for noble metal surface modification, previous investigations of NHCs on gold have focused almost exclusively on the traditional NHC motifs: imidazolium (**Figure 3.1A**) and benzimidazolium (**Figure 3.1B**). These two designs are widely employed because their precursor salts are synthesized via straightforward protocols with commercially-available imidazole or benzimidazole as starting materials.[17, 25] The NHC-CO_2 adducts employed for surface deposition can then be synthesized via a deprotonation reaction in strong base.[19, 26] The presence of the NHC ligand on the substrate surface has been monitored using a variety of techniques, particularly scanning tunneling microscopy (STM),[27] atomic force microscopy (AFM),[28] X-ray photoelectron spectroscopy (XPS),[17] and surface-enhanced Raman spectroscopy (SERS).[19] Among these techniques, SERS is a particularly powerful method because it is highly surface specific, can be performed in ambient conditions, and exploits a molecule's unique vibrational fingerprint to determine the structure of the surface-bound molecules.[29, 30] The SERS spectral features for imidazolium and benzimidazolium NHCs on gold film-over-nanospheres (AuFONs) substrates have been well-characterized previously by our groups through a dual experimental and theoretical approach.[25]

This paucity of NHC motifs is unfortunate since synthetic NHC chemistry has achieved extraordinary range in structure and application beyond these two basic designs.[31] In the field of organometallic homogenous catalysis, NHC ligands have noticeably shifted from imidazolium NHCs to include a wider array of NHC motifs which often lead to improvements in catalytic activity.[32-34] A similar shift to different NHC structures on gold surfaces may significantly improve nanosystem stability as well as introduce an array of new applications to carbene-functionalized surfaces (**Figure 3.1**).

Less-explored NHCs offer two promising advantages over imidazolium and benzimidazolium NHC ligands. First, they exhibit stronger metal-ligand bonds due to either increased σ-donor strength or π-backbonding.[35] Stronger bonds could yield a more stable ligand surface and minimize the potential for desorption into the supernatant, which is particularly important for applications involving tethered catalysts[36, 37]

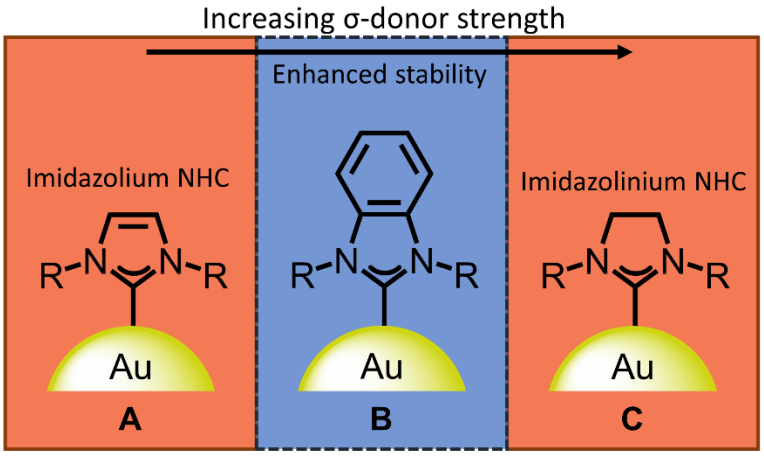


Figure 3.1: Comparison of traditional (**A-B**) and less-explored (**C**) NHC structures on gold surfaces. The imidazolium (**A**) and imidazolinium (**C**) are the focus of this work

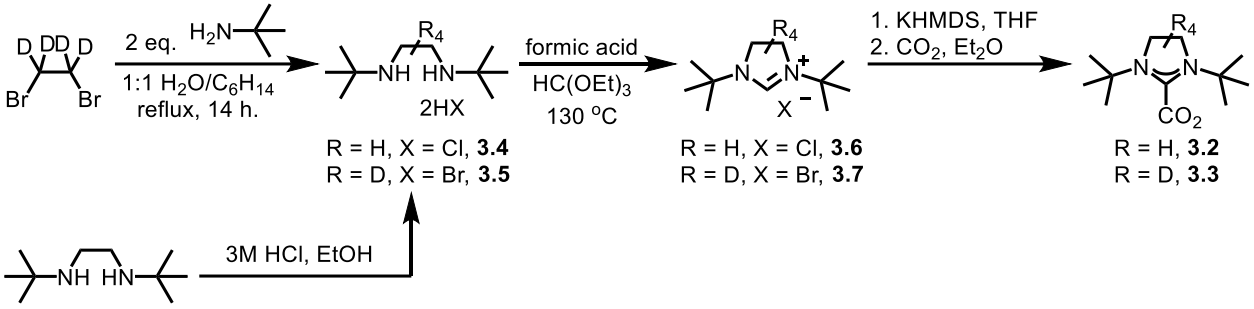
or biological media.[38, 39] Second, these different carbene ligands, specifically imidazolinium NHCs, offer the synthetic possibility for appending two different functionalities in C_2-symmetry onto the carbene backbone. Thus, a host of chiral NHC ligands may be achievable, yielding novel enantiomeric surfaces. Although chiral NHCs have been synthesized for many homogenous reactions,[40-42] very few examples of such NHC surfaces exist, and the ones that do often involve complex monolayers or surfaces where the chiral group is distanced considerably from the surface.[21, 43, 44] For example, chiral molecule detection schemes sometimes rely on thiol binding ligands that are limited by the thiol linker's stability.[45-47] In addition to the potentially increased stability, C_2-symmetric imidazolinium NHC coatings may allow for the chiral moiety to be closer to the surface, which is integral for techniques relying on the signal enhancement offered by surface plasmon resonances.[48-50] Despite these potential advantages, to date, only one additional carbene motif has been reported on a gold surface, 1,3-dimesityl-imidazolinium; however, this surface was only characterized by XPS.[17]

In this manuscript, we prepare NHC-coated gold surfaces with either a standard (i.e., imidazolium) or less-explored (i.e., imidazolinium) NHC ligand via a CO_2 adduct deposition method, showcasing the first successful deposition of a NHC ligand that does not include imidazolium or benzimidazolium moieties on a SERS-active substrate. Comparing the stability of these surface-bound molecules under extreme pH conditions, we find a clear stability enhancement in acidic conditions for the imidazolinium NHC. More generally, this research highlights the deposition, characterization, and stability of imidazolinium, and points to a promising future for different NHC ligands on metal surfaces.

Results and Discussion

Synthesis of the imidazolinium CO_2 adduct (**Scheme 3.1**, **3.2**) and imidazolium CO_2 adduct (**Figure 3.2**, **3.1**) were completed following previous literature procedures.[25, 51] Synthesis of the deuterated imidazolinium CO_2 adduct (**Scheme 3.1**, **3.3**) was completed by modifying previous protocols. First, following the method of Jiao with slight modifications, d_4-dibromoethylenediamine was reacted with *tert*-butylamine at reflux.[52] The resulting solid was collected and washed with hexanes and dried to give N,N'-di-*tert*-butyl-(d_4)-ethylenediamine dihydrobromic acid, **3.5**. Compound **3.5** was then reacted with triethyl orthoformate and a catalytic amount of formic acid at reflux following the method of Barry.[53] Upon cooling, the solution was titrated with diethyl ether and the resulting precipitate was filtered and washed with additional ether and dried to give 1,3-di-*tert*-butyl-4,5-tetradeuteroimidazolinium bromide, **3.7**. The deuterated CO_2 adduct, **3.3**, was synthesized following the method of Buchmeiser.[51] The imidazolinium salt, **3.7**, was deprotonated with KHMDS. The solution was then dried and the free carbene of **3.7** was extracted with diethyl ether and placed into a Schlenk flask. CO_2 gas was then added to the flask under an N_2 atmosphere, resulting in the immediate formation of a precipitate. The reaction flask was brought into the glovebox and filtered. The solid was then washed with diethyl ether and dried under vacuum for no longer than five minutes to prevent the loss of CO_2, to give pure **3.3** in a 71% yield.

Scheme 3.1: Synthesis of imidazolinium CO_2 adducts, including the deuterated analog (**3.3**).



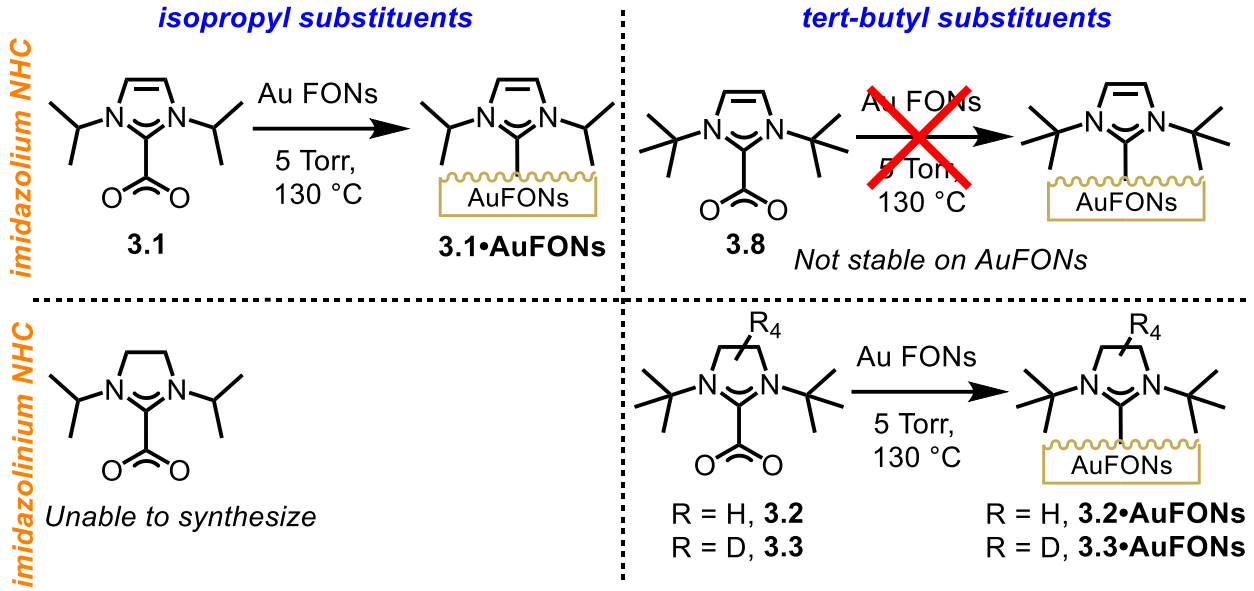


Figure 3.2: Protocol for depositing NHC-CO_2 adducts onto gold substrates. While AuFONs are shown in this scheme, the same procedure is also used for flat gold mirrors. This work examines the deposition of **3.1**, **3.2**, and **3.3** on Au surfaces. Chechik and coworkers previously demonstrated that surfaces obtained from **3.8** are not stable.[54] The imidazolinium NHC with isopropyl side groups (bottom left) presented synthetic challenges and could not be isolated (vide infra).

The CO_2 adducts, **3.1-3.3**, were characterized with ^1H and ^{13}C NMR spectroscopy. A successful adduct formation is indicated by the disappearance of the C2 C-H signal between 8 and 10 ppm in the ^1H NMR, as well as the appearance of a CO_2 carbon peak around 155 and 163 ppm in the ^{13}C NMR for the imidazolium, **3.1**, and imidazoliniums, **3.2-3.3**, respectively (**Spectra 3.1-3.10**). The ^1H NMR of **3.3** shows no loss of deuteration content in the synthesis of the final CO_2 adduct.

Metal film-over-nanospheres (FONs) were employed as SERS substrates due to their relatively straightforward preparation, high stability, and uniform intensity enhancement.[55, 56] Scanning electron microscopy (SEM) images of prepared AuFONs display a compact layer of gold-coated polystyrene spheres (**Figure 3.5**). Air-stable, NHC-CO_2 adducts are optimal for this study because they offer a facile approach for depositing NHC ligands onto solid surfaces, particularly gold.[19] With CO_2 as a leaving group, the NHC directly attaches to the surface without needing additional reagents, which reduces the potential for fouling.[19] For this approach to be successful, both the NHC-CO_2 adduct must be able to be synthesized and it needs to react with AuFONs to form a stable surface.

We began by pursuing isopropyl substituents since these have shown great stability with benzimidazolium NHCs on solid surfaces and nanoparticles (**Figure 3.1B**).[17-19] Compound **3.1**, the imidazolium NHC-CO_2 adduct powder, was placed directly on top of the gold surface and was heated to 130° C *in vacuo* (**Figure 3.2**, top left) resulting in **3.1•AuFONs**.[19] While we attempted the synthesis of the imidazolinium NHC-CO_2 adduct with isopropyl groups as the N-substituents (**Figure 3.2**, bottom left), the product could not be isolated due to high solubility in all tested solvents. The closest match to an isopropyl group that affords stable NHC-CO_2 adducts are NHCs with *tert*-butyl substituents. The imidazolinium NHC-CO_2 adduct, **3.2**, was previously synthesized,[51] and we appended it to AuFONs in the same manner as **3.1**, yielding **2•AuFONs** (**Figure 3.2**, bottom right). Its deuterated analog, **3.3**, was also successfully deposited. We also synthesized the di-*tert*-butyl imidazolium CO_2 adduct, **3.8**,[57] starting from commercially available di-*tert*-butyl imidazolium chloride as a direct comparison to the imidazolinium (**Figure 3.2**, top right). Unfortunately, the reaction to append **3.8** to the AuFONs surface was not successful, which is not unexpected as Chechik and coworkers previously reported that **3.8** was not stable on gold nanoparticles and leached into solution in less than 12 hours.[54]

Given that both the NHCs' nitrogen substituents and the electronics of the NHC are distinct, it is important to determine whether the differences in stability are due to electronic or steric effects. Fortunately, the steric parameters for NHCs are well-known and often described in terms of buried volume, which is analogous to cone angle for phosphines.[58, 59] NHC **3.1** has a buried volume of 27.4% and its benzimidazolium variant which we previously reported on AuFONs (**3.1** in Ref 19) has a buried volume of 27.9%.[59] Switching to the tert-butyl substituents increases the buried volume significantly (36.2% for **3.2** and 35.5% for **3.8)**.[60] Note that in both cases, changing the electronic structure of the NHC (i.e., saturated versus unsaturated) does not change the steric parameters of buried volume significantly.

We also synthesized **3.1** and **3.2** Au NHC surfaces on gold mirrors, and they were characterized with XPS. Flat gold mirrors were used to avoid any residual signal from polystyrene. A control spectrum of the gold mirror before NHC deposition exhibits no observable N1s signal (**Figure 3.6**). High-resolution N1s spectra for imidazolinium and imidazolium presents one symmetric peak at 399.92 eV and 400.45 eV, respectively (**Figure 3.3**). This slight variance in peak position suggests the presence of unique chemical environments for two different molecular species. Hamers and coworkers,[61] for example, observed that nitrogen-containing moieties on Si(001) surfaces exhibited a 1 eV shift in the N1s peak between aromatic pyrrole and its completely saturated analog pyrrolidine, claiming that the higher binding energy is a direct result of the retained aromaticity of pyrrole on the surface. Therefore, the ~0.5 eV shift to a higher binding energy may be due to the higher degree of aromaticity in the imidazolium moiety. High-resolution C1s spectra for imidazolinium and imidazolium both yield peaks around 285 eV (**Figure 3.3**). However, the broadness of the peaks indicate multiple chemical states which cannot be easily differentiated as the complex carbon-carbon and carbon-nitrogen environments give rise to multiple peaks between 284-285 eV and 285-288 eV, respectively.[62] Most importantly for the current work, these N, C, and Au (**Figure 3.7**) peak values are all consistent with literature reports for NHC ligands bonded directly to the gold surface.[17, 18, 27, 63] Therefore, XPS indicates the presence of intact carbene molecules on the gold surface.

Figure 3.4 (top row) presents SERS spectra of **3.1•AuFONs** and **3.2•AuFONs** directly following CO_2 adduction deposition. **3.1•AuFONs** exhibits characteristic, dominant peaks at 1325 cm^{-1} and 1405 cm^{-1} which are primarily attributed to the isopropyl side groups interacting strongly with the NHC nitrogens.[25] Due to the nuanced vibrational modes that SERS can reveal, we can be confident that our resulting spectra for **3.1•AuFONs** is, in fact, distinct from **3.2•AuFONs** which has two dominating peaks at 1297 cm^{-1} and 1402 cm^{-1}. This deposition protocol and corresponding SERS signature for **3.2•AuFONs** is found to be highly reproducible.

As an additional test, the deuterated analog of the imidazolinium NHC ligand was affixed to AuFONs, forming **3.3•AuFONs**. By substituting the hydrogens on the NHC backbone with deuterium, the vibrational signature changes significantly (**Figure 3.8**). Previously reported d_2-imidazolium spectra has dominant peaks at 1303 cm^{-1} and 1401 cm^{-1},[25] whereas **3.3•AuFONs** exhibits a dominant peak at 1350 cm^{-1}. The deposition and SERS analysis were performed in triplicate to ensure the spectrum was consistent.

While benzimidazolium NHCs adhere to Au surfaces very well,[17, 19, 64] similar tests have not been as extensively conducted for imidazolium NHCs and no tests of imidazolinium have been undertaken. We postulated that the imidazolinium NHC ligand, **3.2**, would exhibit enhanced stability in acid due to increased σ-donation and because it would not be prone to electrophilic attack in the 4 and 5 positions on the ring in the same manner as imidazole NHC, **3.1**.[65] Indeed, a few unsaturated imidazoliums have been converted to saturated imidazoliniums by addition of strong acid.[66, 67] Upon submerging the respective NHC-coated AuFONs in hydrochloric acid (1 M) for 24 h, we observed a complete degradation of the imidazolium NHC signal (**Figure 3.4**, right), whereas the imidazolinium variant is unchanged (**Figure 3.4**, left). These results demonstrate a

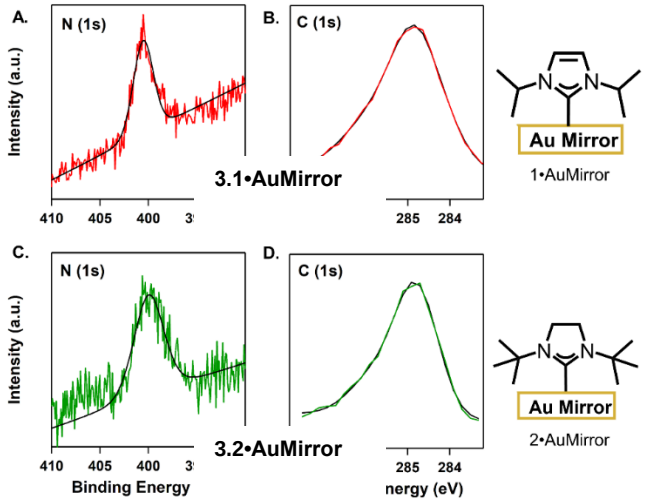


Figure 3.3: XPS analyses of Au mirrors functionalized with ligands **3.1** (red traces) and **3.2** (green traces) along with the overall fits (black traces). (A) N1s peak is at 400.45 eV, (B) C1s peak is at 284.85 eV (C) N1s peak is at 399.92 eV, and (D) C1s peak is at 284.91 eV.

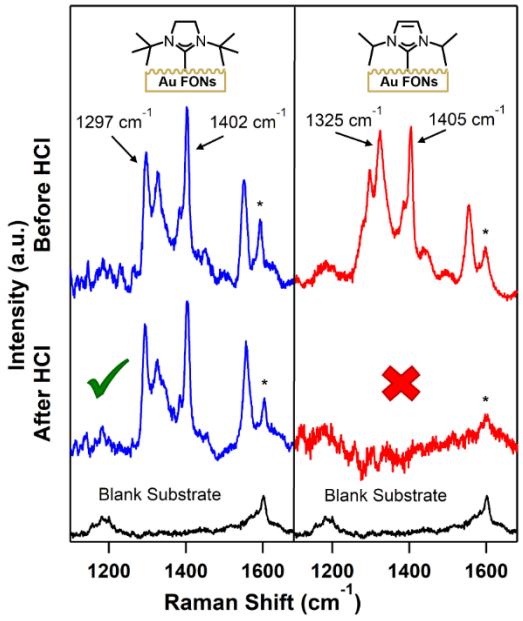


Figure 3.4: SERS spectra of **3.1•AuFONs** (red traces) and **3.2•AuFONs** (blue traces) before (top row) and after (middle row) exposure to 1 M HCl for 24 h. The bottom row is a blank SERS spectrum of the AuFONs substrate. Peaks marked with an asterisk are from the substrate.

limitation for one of the two most commonly used NHC ligands on gold surfaces: stability towards strong acid. It should be noted that while the tert-butyl group provides additional steric stability to the ligand, we believe that the primary degradation mechanism is via electrophilic attack on the imidazolium ring as described above. The rationale behind this is that the buried volumes for the imidazolium and previously studied benzimidazolium NHCs are almost identical (see above), but the benzimidazolium, which is not susceptible to electrophilic attack, is stable to acid.[19] In addition, we find that both the imidazolium and imidazolinium are stable when exposed to strongly basic conditions (1 M KOH, 24 h) or water as a control (**Figure 3.9** and **Figure 3.10**). All stability tests were performed in triplicate.

We report the first detailed exploration of imidazolinium NHCs, including deposition from the CO_2 adduct, demonstrating enhanced stability in acidic conditions compared to traditional imidazolium. In addition to SERS and XPS characterization of the imidazolinium surfaces, a deuterated isotopologue of imidazolinium was synthesized for the first time. We envision this work promoting the broader use of different carbene motifs on gold surfaces and future investigations could include synthesizing chiral moieties on the imidazolinium backbone for surface detection and depositing these carbenes on aqueous nanoparticles via gold complexes.

Experimental

A. Materials and General Considerations

All glassware for air and water sensitive reactions were dried at 170 ˚C overnight before use. All reactions were stirred vigorously with magnetic stirrers. Syntheses of the NHC-CO_2 adducts were performed under a dry dinitrogen atmosphere with use of either a glovebox or standard Schlenk techniques. Solvents used under N_2 atmosphere were dried on an Innovative Technologies (Newburyport, MA) Pure Solv MD-7 Solvent Purification System, degassed by three freeze-pump-thaw cycles on a Schlenk line to remove dioxygen and stored over activated 4 Å molecular sieves prior to use. Celite was dried at 240 ˚C under vacuum overnight and stored in a dinitrogen glovebox. Compounds **3.1**,[25] **3.2**,[51] **3.4**,[68] and **3.6**[68] were prepared from previous literature procedures. All other compounds were purchased from commercial vendors at highest available purity and used without any further purification.

Glass slides were purchased from VWR International. Polystyrene spheres (d = 600 nm) were purchased from Sigma-Aldrich. Gold (99.99% pure) and chromium (99.95% pure) pieces were purchased from the Kurt J. Lesker Company. Chemicals were used as received without further purification.

B. AuNHC Substrate Preparation

First, gold mirrors and gold film-over-nanospheres (AuFONs) were prepared for the XPS and SERS measurements, respectively. Glass slides were thoroughly cleaned using a Plasma Prepp II SPI O_2 Plasma Instrument. Following a previously reported synthesis procedure for AuFONs,[55] a compact monolayer of polystyrene spheres (d = 600 nm) was deposited onto a glass slide. Then, polystyrene-coated slides and bare glass slides were inserted into a physical vapor deposition chamber (Nano 36, Kurt J. Lesker) whereby a chromium adhesion layer (~ 5 nm) was evaporated onto the slides followed by a thick gold layer (~ 200 nm), yielding AuFONs and gold mirrors, respectively.

To prepare the NHC-coated substrates, a previously reported protocol was followed.[19] First, the substrate (e.g., mirror or AuFONs) was placed in an Erlenmeyer flask with the gold layer facing up. The NHC-CO_2 adduct powder was carefully placed on top of the exposed gold surface. The flask was connected to a vacuum line achieving a base pressure of 5 torr before immersion in a 130˚C oil bath. Upon heating, the CO_2 group leaves, exposing the free carbene to readily react with the gold surface. After approximately 10 min, the reaction is completed with no visible powder remaining on the surface.

C. Instrumentation

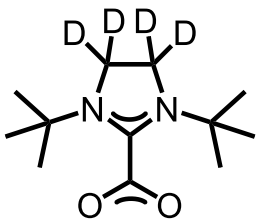
Solution ^{1}H nuclear magnetic resonance (NMR) spectroscopy and ^{13}C NMR spectroscopy were performed on a Varian VNMRS 500 MHz narrow-bore broadband system and Varian VNMRS 600 MHz narrow-bore broadband system at 298 K. All ^{1}H and ^{13}C shifts were referenced to the residual solvent. Infrared spectra were collected on a Thermo Scientific Nicolet iS10 with a Smart iTR accessory for attenuated total reflectance (ATR) using the neat compounds.

XPS measurements were obtained with a PHI VersaProbe II surface analysis instrument (Physical Electronics). The instrument operates under ultra-high vacuum with a monochromatic Al Kα X-ray source (photon energy = 1486.6 eV). High resolution

spectra were obtained using a 23.50 eV pass energy. All resulting spectra were calibrated versus the binding energy of sp^3 hybridized carbon (C1s = 284.8 eV) and background subtracted according to the Shirley algorithm.[69]

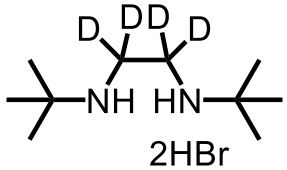
SERS spectra were recorded using a custom-built Raman spectrometer equipped with a 633 nm HeNe laser (Thor Labs). The laser beam was aligned into an inverted microscope objective (Nikon, 20x, NA = 0.5) with approximately 600 μW of power at the sample. Acquisitions were approximately 3 min. The resulting backscattered photons were passed through a Rayleigh rejection filter (Semrock) prior to detection in a dispersive spectrometer (Acton SP2300, Princeton Instruments, 1200 g mm^{-1}) equipped with a back-illuminated deep depletion CCD (PIXIS, Spec-10, Princeton Instruments). The resulting scans were recorded with Winspec 32 software (Princeton Instruments). For each sample, scans were taken at three different positions on the substrate to ensure signal reproducibility. The acquired spectra were background subtracted (Multipeak Fitting 2.0 Package) and graphed in IGOR Pro (Wavemetrics).

D. Synthesis of Compound 3.3.



The NHC-CO_2 adduct of 1,3-di-*tert*-butyl-4,5-tetradeuteroimidazolinium bromide, **3.7**, was prepared following a slightly modified method of Buchmeiser.[51] Solid potassium bis(trimethylsilyl)amide (0.3560 g, 1.785 mmol) and tetrahydrofuran (12 mL) were added to a vial containing **3.7** (0.4774 g, 1.786 mmol), and was stirred overnight at RT in a glovebox. The solvent was then removed under vacuum. The residue was then extracted with diethyl ether (15 mL) and filtered into a Schlenk flask over a short Celite plug to remove solid KBr formed during the reaction. The Schlenk flask containing the free carbene in diethyl ether was removed from the glovebox and CO_2 gas was added to the flask under an air free setup and stirred for 15 min. After addition of CO_2, a white solid immediately formed. The reaction vessel was placed under a vacuum and returned to the glove box. The suspension was filtered over a fine porosity frit and washed with 10 mL of diethyl ether. The solid was dried under vacuum for no more than 5 minutes to give a white powder. Yield: 0.292 g, 71.0%. ^{1}H NMR (CD_2Cl_2, 499.74 MHz): δ 1.46 (s, 18H). ^{13}C NMR (CD_2Cl_2, 125.66 MHz): δ 164.63, 159.38, 58.45, 44.28 (pent, J = 22.54 Hz), 28.25. IR: 2973, 2238, 1669, 1571, 1484, 1407, 1390, 1377, 1366, 1322, 1262, 1230, 1194, 1137, 1088, 1051, 991, 978, 946, 930, 909, 892, 816, 770, 725 cm^{-1}.

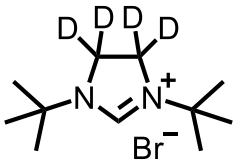
E. Synthesis of Compound 3.5.



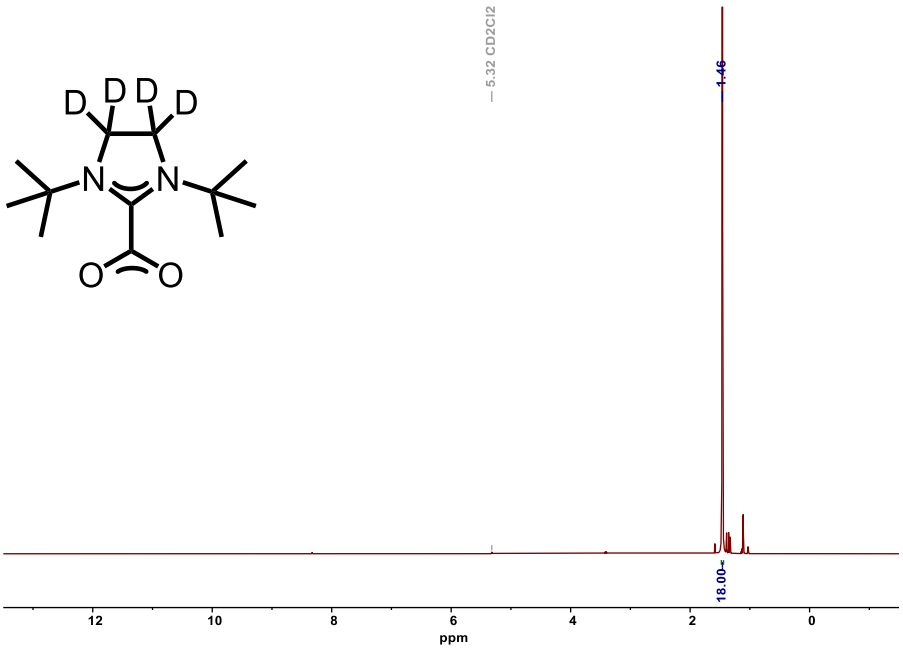
N,N'-di-*tert*-butyl-(d_4)-ethylenediamine dihydrobromic acid, **3.5**, was prepared using a modification of a previously reported literature method.[52] A 20 mL scintillation vial was charged with a stir bar, d_4-dibromoethylenediamine (1.312 g, 6.837 mmol), *tert*-butylamine (3.952 mL, 37.61 mmol), 2 mL of hexanes, and 2 mL of DI water and capped with a Teflon screw cap. The solution was stirred overnight at 110 °C. The reaction was cooled to RT and, upon cooling, a white precipitate formed. The supernatant was decanted off and the solid was washed with 10 mL of hexanes and dried under vacuum, to give a white tacky solid. Yield: 1.95 g, 84.4%. ^{1}H NMR ($CDCl_3$, 499.74 MHz): δ 5.58 (s, 4H), 1.41 (s, 9H), 1.29 (s, 9H) ^{13}C NMR ($CDCl_3$, 125.66 MHz): δ 54.46, 52.33, 39.71 (pent, J = 21.06), 29.06, 27.74. IR: 3380, 3217, 2966,

2891, 2838, 2770, 2678, 2584, 2485, 2409, 2222, 2091, 2033, 1621, 1501, 1479, 1451, 1400, 1377, 1363, 1298, 1246, 1210, 1136, 1108, 1062, 1042, 986, 968, 936, 880, 762, 730 cm^{-1}.

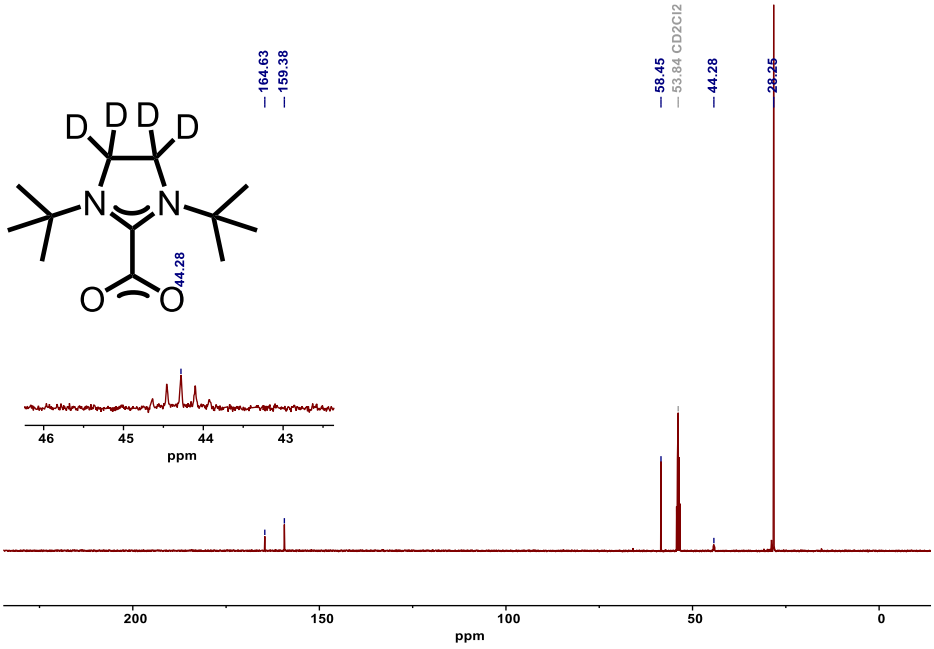
F. Synthesis of Compound 3.7.



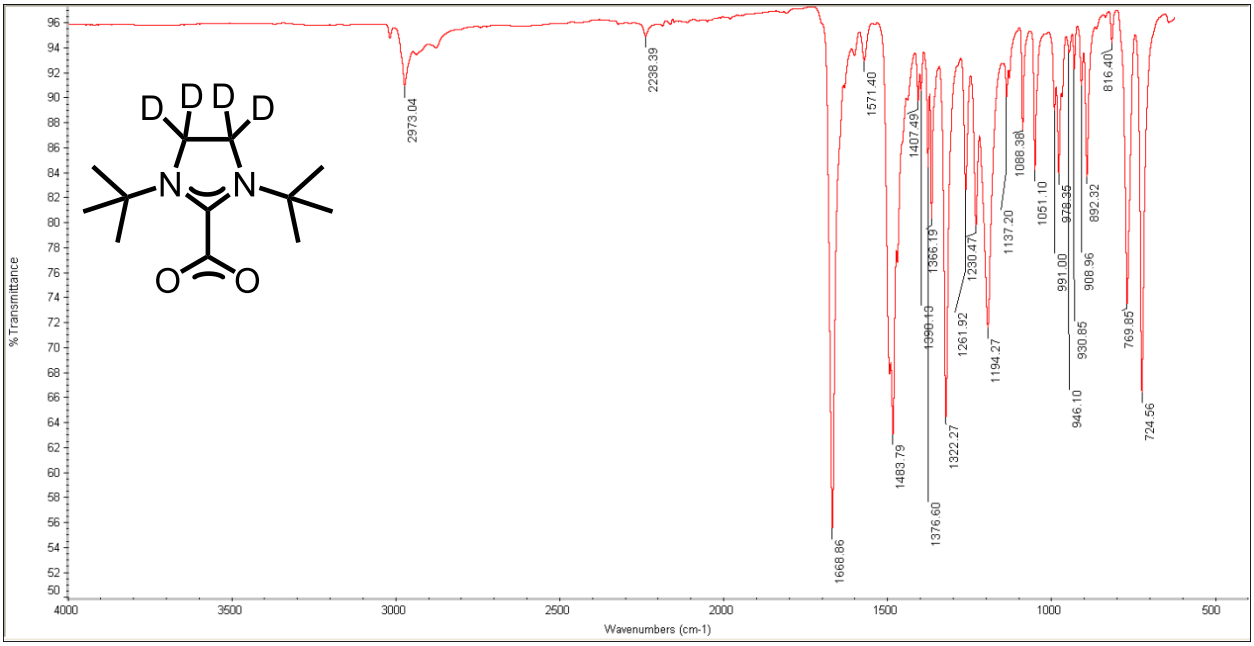
Compound **3.7** was prepared following the method of Barry.[70] A 100 mL round bottom flask was charged with a stir bar, compound **5** (1.073 g, 3.173 mmol), triethyl orthoformate (18 mL, 0.1082 mol), and seven drops of formic acid and was stirred for 24 hours at 130 °C. The reaction was then cooled to RT and 40 mL of diethyl ether was added. The resulting suspension was filtered over a medium porosity frit and washed with an additional 30 mL of ether. The solid was dried under vacuum to give a white powder. Yield: 0.481 g, 56.8%. ^{1}H NMR (CD_2Cl_2, 499.74 MHz): δ 8.53 (s, 1H), 1.49 (s, 18H). ^{13}C NMR (CD_2Cl_2, 150.81 MHz): δ 153.78, 57.31, 44.99 (pent, J = 22.80 Hz), 28.26. IR: 2971, 2917, 2875, 2236, 2128, 1613, 1472, 1459, 1402, 1376, 1368, 1314, 1280, 1233, 1205, 1140, 1120, 1082, 1044, 981, 920, 887, 861, 825, 789 cm^{-1}.



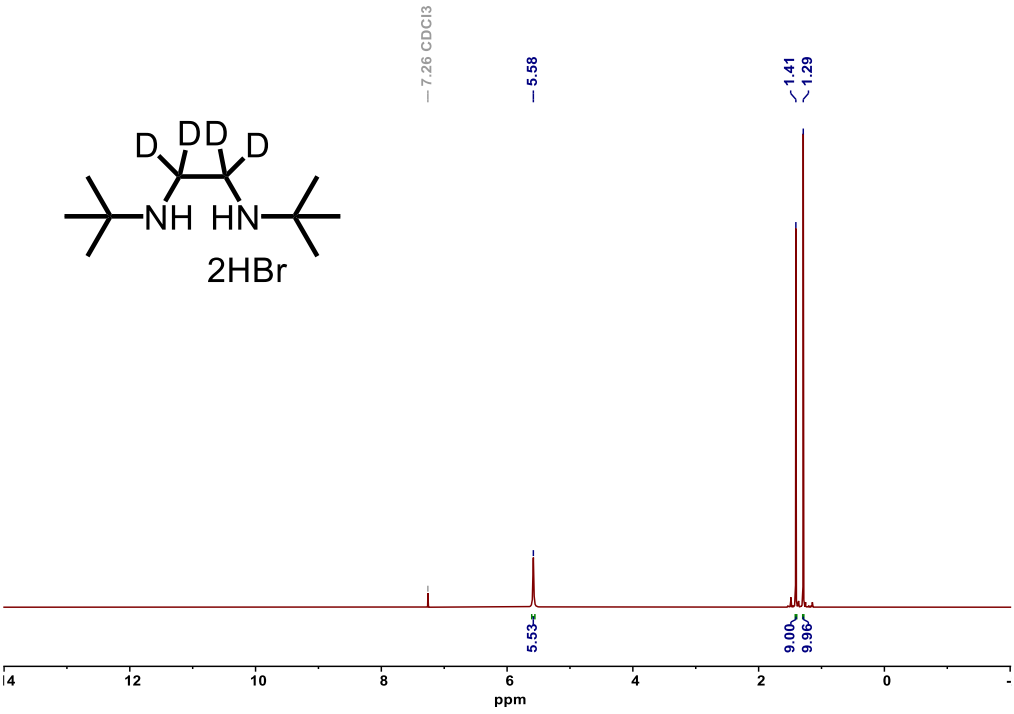
Spectra 3.1: ^{1}H NMR of **3.3** in CD_2Cl_2.



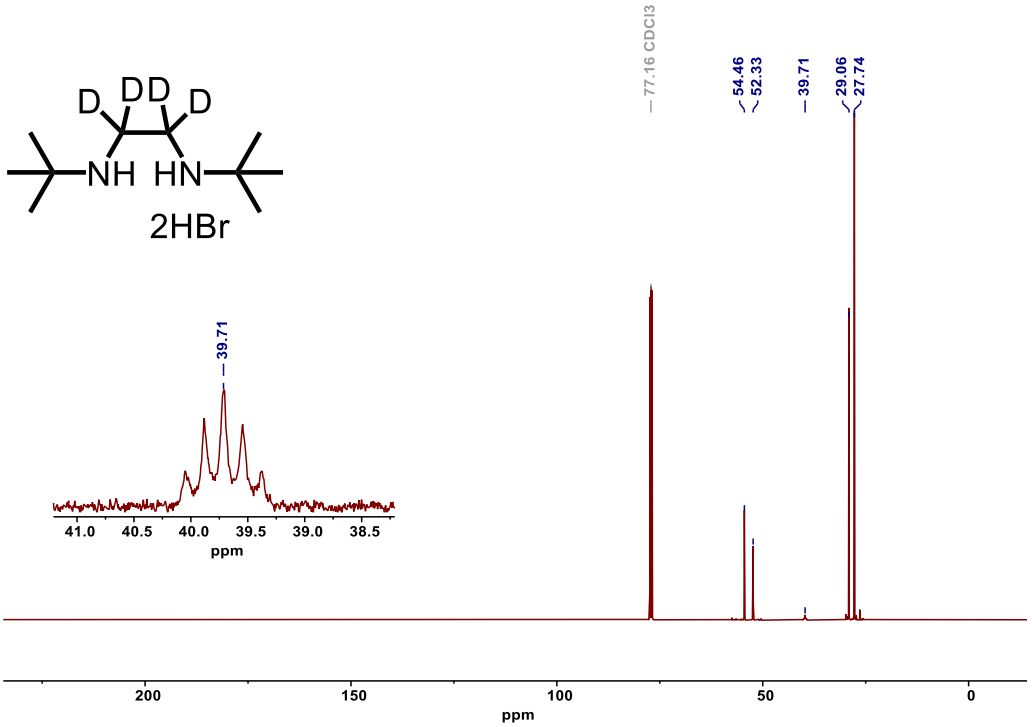
Spectra 3.2: ^{13}C NMR of **3.3** in CD_2Cl_2.



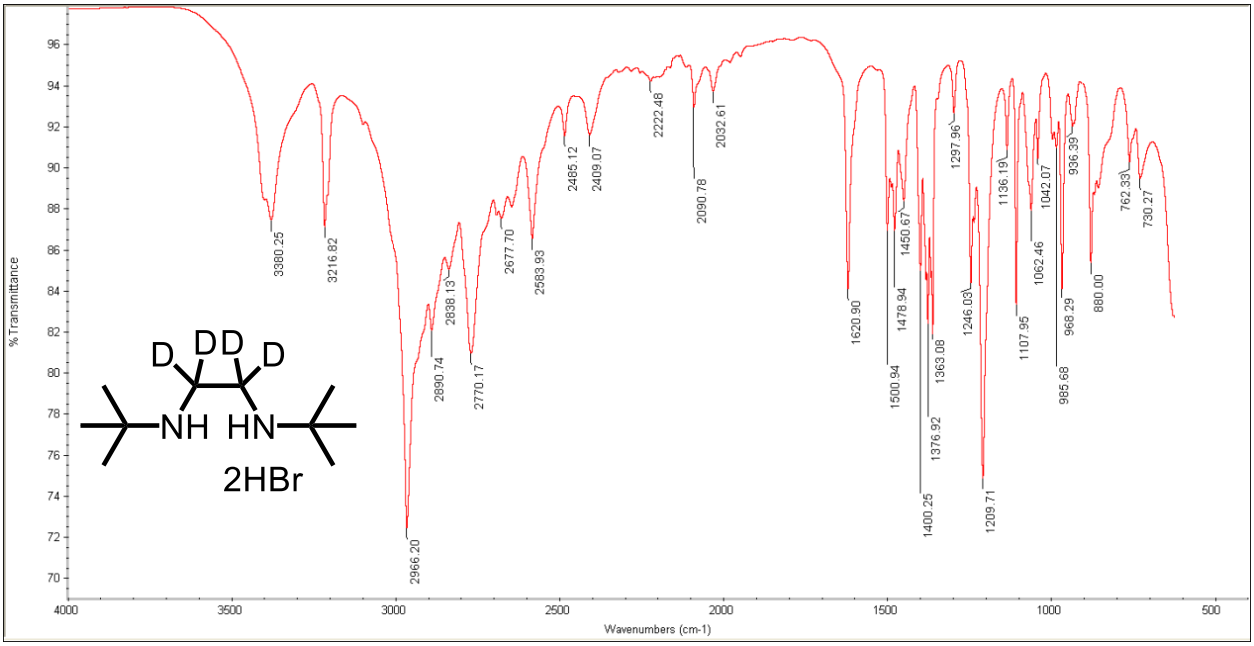
Spectra 3.3: ATR-IR of **3.3**. Deuterium stretch at 2238 cm^{-1}.



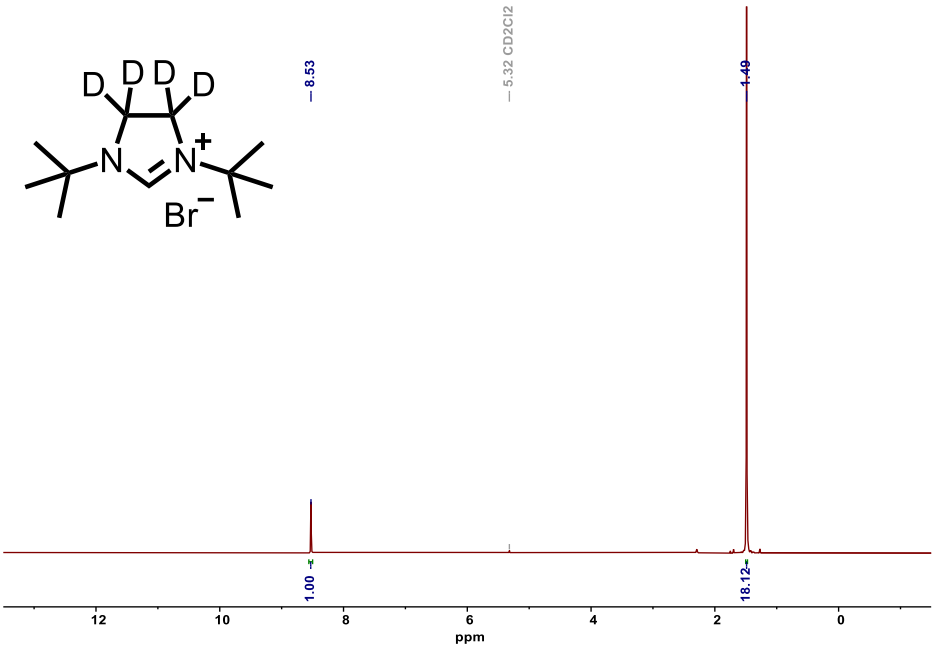
Spectra 3.4: ^{1}H NMR of **3.5** in $CDCl_3$.



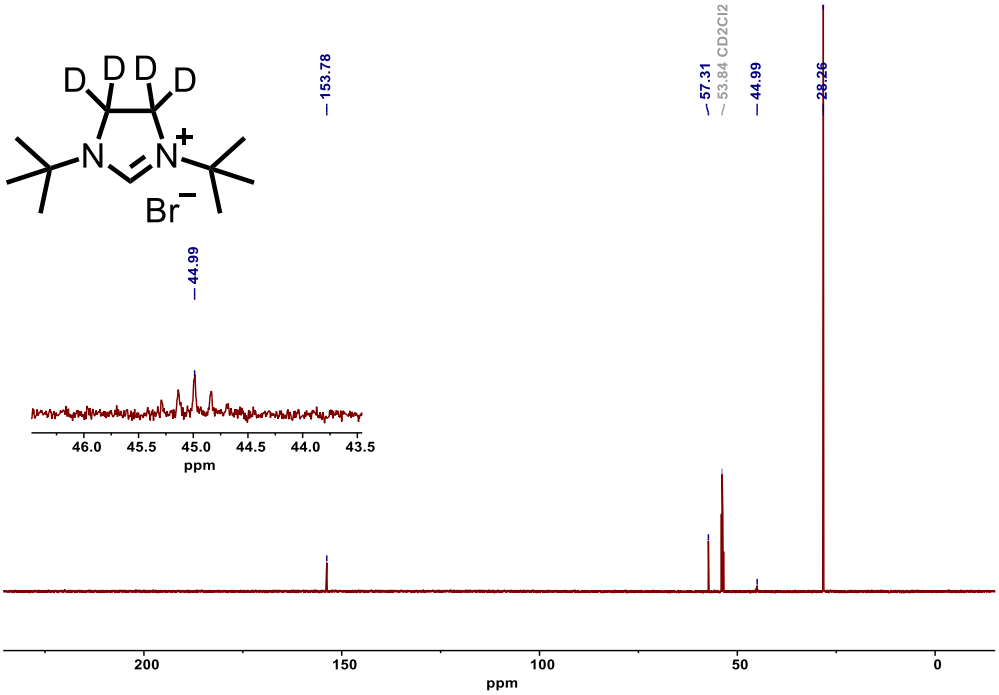
Spectra 3.5: ^{13}C NMR of **3.5** in $CDCl_3$.



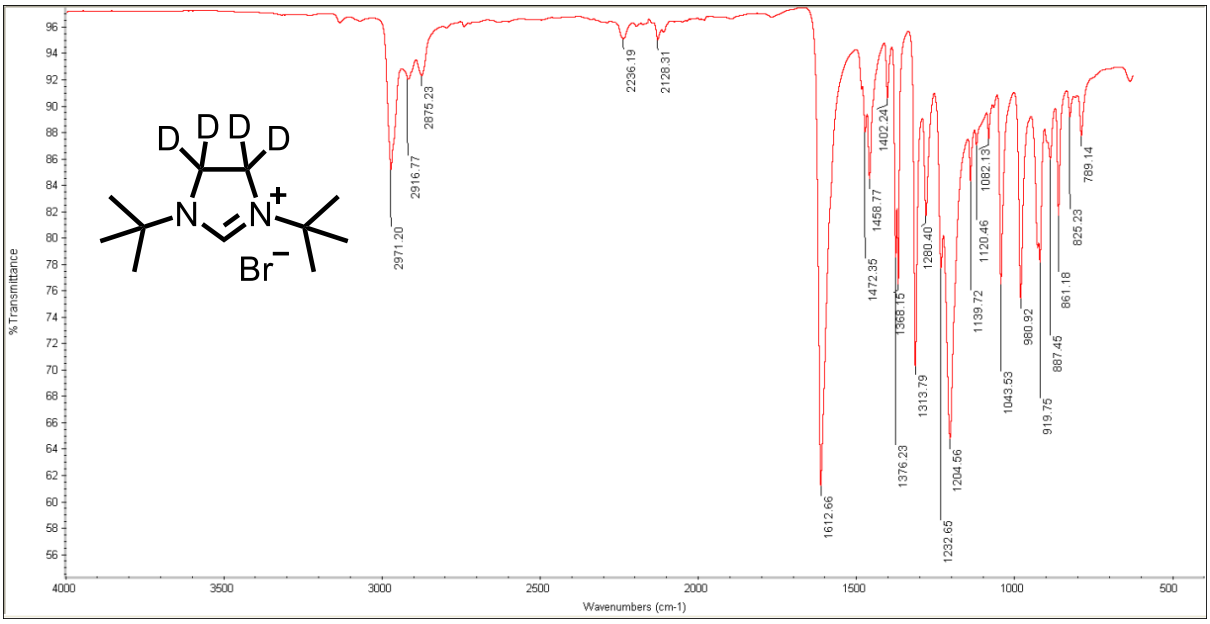
Spectra 3.6: ATR-IR of **3.5**.



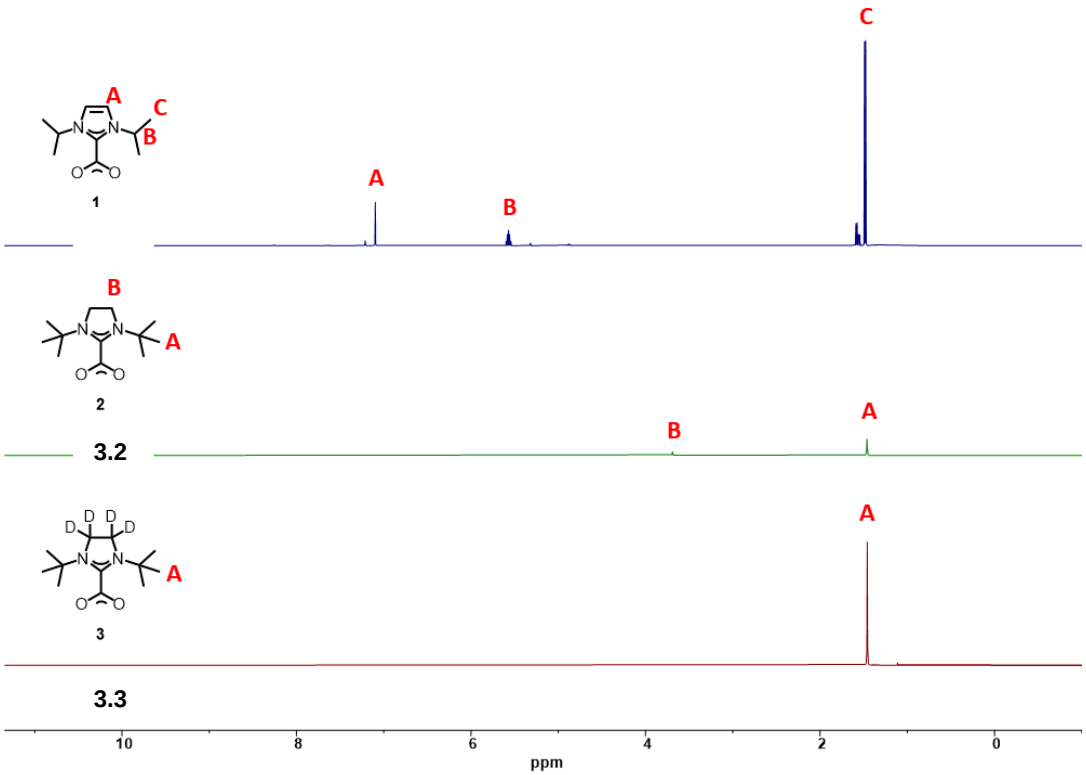
Spectra 3.7: ^{1}H NMR of **3.7** in CD_2Cl_2.



Spectra 3.8: ^{13}C NMR of **3.7** in CD_2Cl_2.



Spectra 3.9: ATR-IR of **3.7**. Deuterium stretches at 2236 and 2128 cm^{-1}.



Spectra 3.10: Stacked ^{1}H NMRs of **3.1-3.3**.

SEM Image:

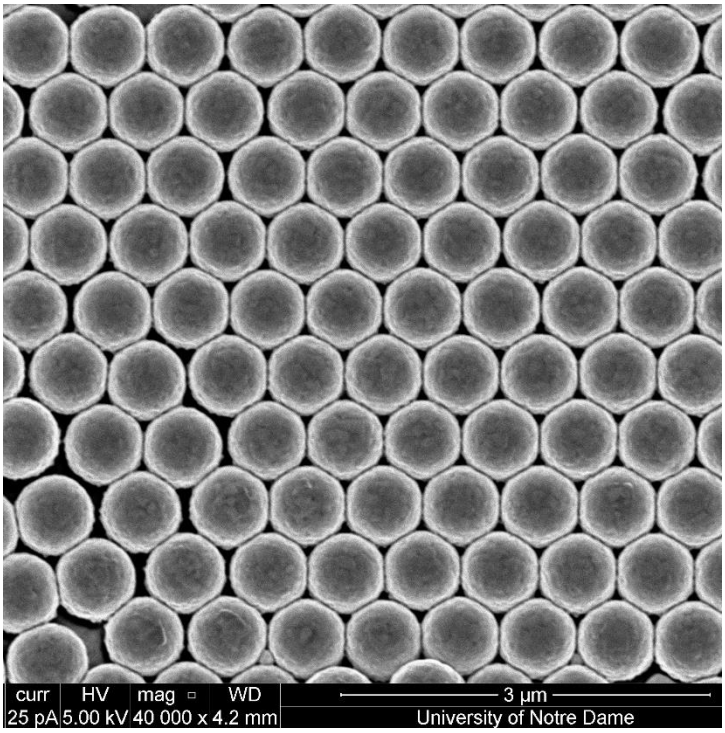


Figure 3.5: Representative SEM image of gold film-over-nanospheres substrate.

XPS Analyses:

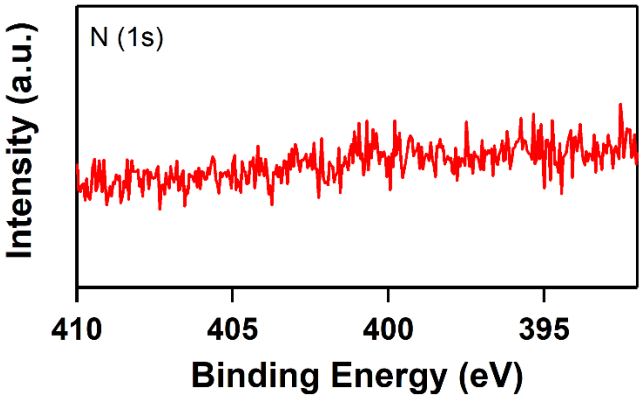


Figure 3.6: XPS control of gold mirror, exhibiting no identifiable signal coming from N 1s prior to deposition of the N-heterocyclic carbene ligands.

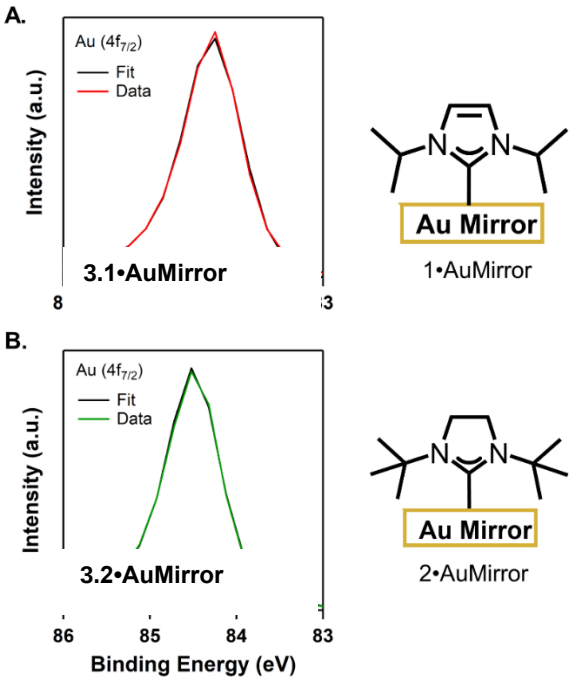


Figure 3.7: XPS analyses of Au mirrors functionalized with ligands **3.1** (red) and **3.2** (green) along with the overall fits (black traces). (A) Au $4f_{7/2}$ peak is at 84.2 eV, and (B) Au $4f_{7/2}$ peak is at 84.5 eV. These results are consistent with previously reported binding energies for adsorbed NHC ligands on gold.[18, 27, 63]

SERS Spectra:

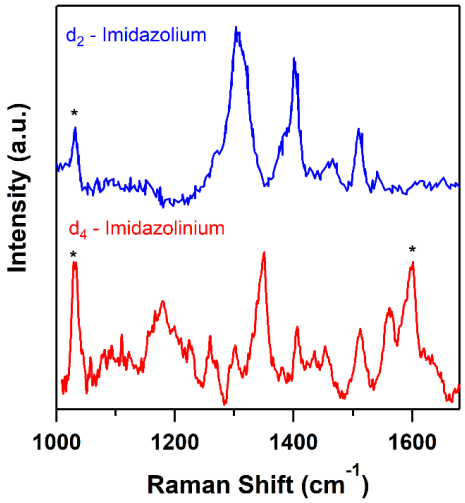


Figure 3.8: SERS spectra of imidazolium and imidazolinium NHC ligands with deuterated backbones on AuFONs. Blue trace is previously published data.[25] The red trace is **3.3•AuFONs**, prepared from ligand **3.3**. Asterisks denote peaks from the substrate.

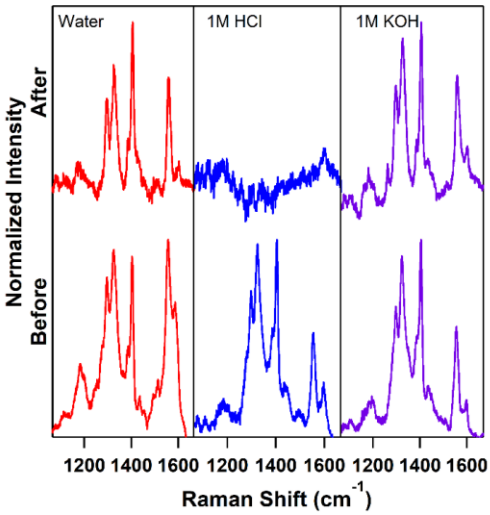


Figure 3.9: Summary of stability tests performed on **3.1•AuFONs**. The NHC-coated substrates were submerged in the indicated solvent for 24 h. Each condition was performed in triplicate.

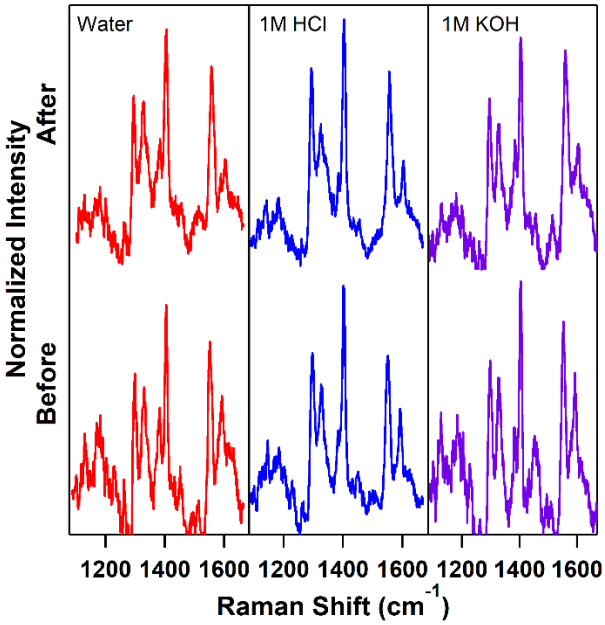


Figure 3.10: Summary of stability tests performed on **3.2•AuFONs**. The NHC-coated substrates were submerged in the indicated solvent for 24 h. Each condition was performed in triplicate.

References

1. Engel, S.; Fritz, E.-C.; Ravoo, B. J., New trends in the functionalization of metallic gold: from organosulfur ligands to N-heterocyclic carbenes. *Chemical Society Reviews* **2017,** *46*, 2057-2075.
2. Goddard, Z. R.; Marín, M. J.; Russell, D. A.; Searcey, M., Active targeting of gold nanoparticles as cancer therapeutics. *Chemical Society Reviews* **2020,** *49*, 8774-8789.
3. Heuer-Jungemann, A.; Feliu, N.; Bakaimi, I.; Hamaly, M.; Alkilany, A.; Chakraborty, I.; Masood, A.; Casula, M. F.; Kostopoulou, A.; Oh, E.; Susumu, K.; Stewart, M. H.; Medintz, I. L.; Stratakis, E.; Parak, W. J.; Kanaras, A. G., The Role of Ligands in the Chemical Synthesis and Applications of Inorganic Nanoparticles. *Chemical Reviews* **2019,** *119*, 4819-4880.
4. Smith, C. A.; Narouz, M. R.; Lummis, P. A.; Singh, I.; Nazemi, A.; Li, C.-H.; Crudden, C. M., N-Heterocyclic Carbenes in Materials Chemistry. *Chemical Reviews* **2019,** *119*, 4986-5056.
5. Sun, F.; Galvan, D. D.; Jain, P.; Yu, Q., Multi-functional, thiophenol-based surface chemistry for surface-enhanced Raman spectroscopy. *Chemical Communications* **2017,** *53*, 4550-4561.
6. Zhukhovitskiy, A. V.; MacLeod, M. J.; Johnson, J. A., Carbene Ligands in Surface Chemistry: From Stabilization of Discrete Elemental Allotropes to Modification of Nanoscale and Bulk Substrates. *Chemical Reviews* **2015,** *115*, 11503-11532.
7. Li, Y.; Huang, J.; McIver, R. T.; Hemminger, J. C., Characterization of thiol self-assembled films by laser desorption Fourier transform mass spectrometry. *Journal of the American Chemical Society* **1992,** *114*, 2428-2432.
8. Schoenfisch, M. H.; Pemberton, J. E., Air Stability of Alkanethiol Self-Assembled Monolayers on Silver and Gold Surfaces. *Journal of the American Chemical Society* **1998,** *120*, 4502-4513.
9. Willey, T. M.; Vance, A. L.; van Buuren, T.; Bostedt, C.; Terminello, L. J.; Fadley, C. S., Rapid degradation of alkanethiol-based self-assembled monolayers on gold in ambient laboratory conditions. *Surface Science* **2005,** *576*, 188-196.
10. Andrieux-Ledier, A.; Tremblay, B.; Courty, A., Stability of Self-Ordered Thiol-Coated Silver Nanoparticles: Oxidative Environment Effects. *Langmuir* **2013,** *29*, 13140-13145.
11. Bhatt, N.; Huang, P.-J. J.; Dave, N.; Liu, J., Dissociation and Degradation of Thiol-Modified DNA on Gold Nanoparticles in Aqueous and Organic Solvents. *Langmuir* **2011,** *27*, 6132-6137.
12. Wu, Y.; Lian, J.; Gonçales, V. R.; Pardehkhorram, R.; Tang, W.; Tilley, R. D.; Gooding, J. J., Patterned Molecular Films of Alkanethiol and PLL-PEG on Gold–Silicate Interfaces: How to Add Functionalities while Retaining Effective Antifouling. *Langmuir* **2020,** *36*, 5243-5250.
13. Zhang, J.; Léonard, D.; Yeromonahos, C.; Mazurczyk, R.; Géhin, T.; Monfray, S.; Chevolot, Y.; Cloarec, J.-P., Orthogonal Chemical Functionalization of Au/SiO_2/TiW Patterned Substrates. *Langmuir* **2020,** *36*, 14960-14966.
14. Zhang, D.; Hao, R.; Zhang, L.; You, H.; Fang, J., Ratiometric Sensing of Polycyclic Aromatic Hydrocarbons Using Capturing Ligand Functionalized Mesoporous Au Nanoparticles as a Surface-Enhanced Raman Scattering Substrate. *Langmuir* **2020,** *36*, 11366-11373.

15. Arroyo-Currás, N.; Somerson, J.; Vieira, P. A.; Ploense, K. L.; Kippin, T. E.; Plaxco, K. W., Real-time measurement of small molecules directly in awake, ambulatory animals. *Proceedings of the National Academy of Sciences* **2017,** *114*, 645.
16. Li, H.; Dauphin-Ducharme, P.; Arroyo-Currás, N.; Tran, C. H.; Vieira, P. A.; Li, S.; Shin, C.; Somerson, J.; Kippin, T. E.; Plaxco, K. W., A Biomimetic Phosphatidylcholine-Terminated Monolayer Greatly Improves the In Vivo Performance of Electrochemical Aptamer-Based Sensors. *Angewandte Chemie International Edition* **2017,** *56*, 7492-7495.
17. Crudden, C. M.; Horton, J. H.; Ebralidze, I. I.; Zenkina, O. V.; McLean, A. B.; Drevniok, B.; She, Z.; Kraatz, H.-B.; Mosey, N. J.; Seki, T.; Keske, E. C.; Leake, J. D.; Rousina-Webb, A.; Wu, G., Ultra stable self-assembled monolayers of N-heterocyclic carbenes on gold. *Nature Chemistry* **2014,** *6*, 409.
18. DeJesus, J. F.; Sherman, L. M.; Yohannan, D. J.; Becca, J. C.; Strausser, S. L.; Karger, L. F. P.; Jensen, L.; Jenkins, D. M.; Camden, J. P., A Benchtop Method for Appending Protic Functional Groups to N-Heterocyclic Carbene Protected Gold Nanoparticles. *Angewandte Chemie International Edition* **2020,** *59*, 7585-7590.
19. DeJesus, J. F.; Trujillo, M. J.; Camden, J. P.; Jenkins, D. M., N-Heterocyclic Carbenes as a Robust Platform for Surface-Enhanced Raman Spectroscopy. *Journal of the American Chemical Society* **2018,** *140*, 1247-1250.
20. MacLeod, M. J.; Johnson, J. A., PEGylated N-Heterocyclic Carbene Anchors Designed To Stabilize Gold Nanoparticles in Biologically Relevant Media. *Journal of the American Chemical Society* **2015,** *137*, 7974-7977.
21. Nguyen, D. T.; Freitag, M.; Gutheil, C.; Sotthewes, K.; Tyler, B. J.; Böckmann, M.; Das, M.; Schlüter, F.; Doltsinis, N. L.; Arlinghaus, H. F.; Ravoo, B. J.; Glorius, F., An Arylazopyrazole-Based N-Heterocyclic Carbene as a Photoswitch on Gold Surfaces: Light-Switchable Wettability, Work Function, and Conductance. *Angewandte Chemie International Edition* **2020,** *59*, 13651-13656.
22. Li, Z.; Munro, K.; Ebralize, I. I.; Narouz, M. R.; Padmos, J. D.; Hao, H.; Crudden, C. M.; Horton, J. H., N-Heterocyclic Carbene Self-Assembled Monolayers on Gold as Surface Plasmon Resonance Biosensors. *Langmuir* **2017,** *33*, 13936-13944.
23. Mayall, R. M.; Smith, C. A.; Hyla, A. S.; Lee, D. S.; Crudden, C. M.; Birss, V. I., Ultrasensitive and Label-Free Detection of the Measles Virus Using an N-Heterocyclic Carbene-Based Electrochemical Biosensor. *ACS Sensors* **2020,** *5*, 2747-2752.
24. Roland, S.; Ling, X.; Pileni, M.-P., N-Heterocyclic Carbene Ligands for Au Nanocrystal Stabilization and Three-Dimensional Self-Assembly. *Langmuir* **2016,** *32*, 7683-7696.
25. Trujillo, M. J.; Strausser, S. L.; Becca, J. C.; DeJesus, J. F.; Jensen, L.; Jenkins, D. M.; Camden, J. P., Using SERS To Understand the Binding of N-Heterocyclic Carbenes to Gold Surfaces. *The Journal of Physical Chemistry Letters* **2018,** *9*, 6779-6785.
26. Voutchkova, A. M.; Feliz, M.; Clot, E.; Eisenstein, O.; Crabtree, R. H., Imidazolium Carboxylates as Versatile and Selective N-Heterocyclic Carbene Transfer Agents: Synthesis, Mechanism, and Applications. *Journal of the American Chemical Society* **2007,** *129*, 12834-12846.
27. Wang, G.; Rühling, A.; Amirjalayer, S.; Knor, M.; Ernst, J. B.; Richter, C.; Gao, H.-J.; Timmer, A.; Gao, H.-Y.; Doltsinis, N. L.; Glorius, F.; Fuchs, H., Ballbot-type

motion of N-heterocyclic carbenes on gold surfaces. *Nature Chemistry* **2017,** *9*, 152-156.
28. Nguyen, D. T.; Freitag, M.; Körsgen, M.; Lamping, S.; Rühling, A.; Schäfer, A. H.; Siekman, M. H.; Arlinghaus, H. F.; van der Wiel, W. G.; Glorius, F.; Ravoo, B. J., Versatile Micropatterns of N-Heterocyclic Carbenes on Gold Surfaces: Increased Thermal and Pattern Stability with Enhanced Conductivity. *Angewandte Chemie International Edition* **2018,** *57*, 11465-11469.
29. Haynes, C. L.; McFarland, A. D.; Van Duyne, R. P., Surface-Enhanced Raman Spectroscopy. *Analytical Chemistry* **2005,** *77*, 338 A-346 A.
30. Schlücker, S., Surface-Enhanced Raman Spectroscopy: Concepts and Chemical Applications. *Angewandte Chemie International Edition* **2014,** *53*, 4756-4795.
31. Hopkinson, M. N.; Richter, C.; Schedler, M.; Glorius, F., An overview of N-heterocyclic carbenes. *Nature* **2014,** *510*, 485-496.
32. Bakker, A.; Freitag, M.; Kolodzeiski, E.; Bellotti, P.; Timmer, A.; Ren, J.; Schulze Lammers, B.; Moock, D.; Roesky, H. W.; Mönig, H.; Amirjalayer, S.; Fuchs, H.; Glorius, F., An Electron-Rich Cyclic (Alkyl)(Amino)Carbene on Au(111), Ag(111), and Cu(111) Surfaces. *Angewandte Chemie International Edition* **2020,** *59*, 13643-13646.
33. Marx, V. M.; Sullivan, A. H.; Melaimi, M.; Virgil, S. C.; Keitz, B. K.; Weinberger, D. S.; Bertrand, G.; Grubbs, R. H., Cyclic Alkyl Amino Carbene (CAAC) Ruthenium Complexes as Remarkably Active Catalysts for Ethenolysis. *Angewandte Chemie International Edition* **2015,** *54*, 1919-1923.
34. Melaimi, M.; Jazzar, R.; Soleilhavoup, M.; Bertrand, G., Cyclic (Alkyl)(amino)carbenes (CAACs): Recent Developments. *Angewandte Chemie International Edition* **2017,** *56*, 10046-10068.
35. Back, O.; Henry-Ellinger, M.; Martin, C. D.; Martin, D.; Bertrand, G., ^{31}P NMR Chemical Shifts of Carbene–Phosphinidene Adducts as an Indicator of the π-Accepting Properties of Carbenes. *Angewandte Chemie International Edition* **2013,** *52*, 2939-2943.
36. Murakami, K.; Tanaka, Y.; Sakai, R.; Hisai, Y.; Hayashi, S.; Mizutani, Y.; Higo, T.; Ogo, S.; Seo, J. G.; Tsuneki, H.; Sekine, Y., Key factor for the anti-Arrhenius low-temperature heterogeneous catalysis induced by H^+ migration: H^+ coverage over support. *Chemical Communications* **2020,** *56*, 3365-3368.
37. Zhao, F.; Bhanage, B. M.; Shirai, M.; Arai, M., Heck Reactions of Iodobenzene and Methyl Acrylate with Conventional Supported Palladium Catalysts in the Presence of Organic and/and Inorganic Bases without Ligands. *Chemistry – A European Journal* **2000,** *6*, 843-848.
38. Borzenkov, M.; Chirico, G.; D'Alfonso, L.; Sironi, L.; Collini, M.; Cabrini, E.; Dacarro, G.; Milanese, C.; Pallavicini, P.; Taglietti, A.; Bernhard, C.; Denat, F., Thermal and Chemical Stability of Thiol Bonding on Gold Nanostars. *Langmuir* **2015,** *31*, 8081-8091.
39. Flynn, N. T.; Tran, T. N. T.; Cima, M. J.; Langer, R., Long-Term Stability of Self-Assembled Monolayers in Biological Media. *Langmuir* **2003,** *19*, 10909-10915.
40. Ma, J.-T.; Cheng, Y., Construction of enantiopure imine bridged benzo[c]azepinones by a silver(I) and chiral N-heterocyclic carbene multicatalytic reaction sequence of N′-(2-alkynylbenzylidene)hydrazides and cyclopropanecarbaldehydes. *Organic Chemistry Frontiers* **2020,** *7*, 3459-3467.

41. Singha, S.; Patra, T.; Daniliuc, C. G.; Glorius, F., Highly Enantioselective [5 + 2] Annulations through Cooperative N-Heterocyclic Carbene (NHC) Organocatalysis and Palladium Catalysis. *Journal of the American Chemical Society* **2018,** *140*, 3551-3554.
42. Thongpaen, J.; E. Schmid, T.; Toupet, L.; Dorcet, V.; Mauduit, M.; Baslé, O., Directed ortho C–H borylation catalyzed using Cp*Rh(III)–NHC complexes. *Chemical Communications* **2018,** *54*, 8202-8205.
43. Chang, L.-M.; An, Y.-Y.; Li, Q.-H.; Gu, Z.-G.; Han, Y.-F.; Zhang, J., N-Heterocyclic Carbene as a Surface Platform for Assembly of Homochiral Metal–Organic Framework Thin Films in Chiral Sensing. *ACS Applied Materials & Interfaces* **2020,** *12*, 38357-38364.
44. Young, A. J.; Sauer, M.; Rubio, G. M. D. M.; Sato, A.; Foelske, A.; Serpell, C. J.; Chin, J. M.; Reithofer, M. R., One-step synthesis and XPS investigations of chiral NHC–Au(0)/Au(I) nanoparticles. *Nanoscale* **2019,** *11*, 8327-8333.
45. Lim, I. I. S.; Mott, D.; Engelhard, M. H.; Pan, Y.; Kamodia, S.; Luo, J.; Njoki, P. N.; Zhou, S.; Wang, L.; Zhong, C. J., Interparticle Chiral Recognition of Enantiomers: A Nanoparticle-Based Regulation Strategy. *Analytical Chemistry* **2009,** *81*, 689-698.
46. Wang, Y.; Yu, Z.; Han, X.; Su, H.; Ji, W.; Cong, Q.; Zhao, B.; Ozaki, Y., Charge-Transfer-Induced Enantiomer Selective Discrimination of Chiral Alcohols by SERS. *The Journal of Physical Chemistry C* **2016,** *120*, 29374-29381.
47. Wang, Y.; Zhao, X.; Yu, Z.; Xu, Z.; Zhao, B.; Ozaki, Y., A Chiral-Label-Free SERS Strategy for the Synchronous Chiral Discrimination and Identification of Small Aromatic Molecules. *Angewandte Chemie International Edition* **2020,** *59*, 19079-19086.
48. Gu, X.; Trujillo, M. J.; Olson, J. E.; Camden, J. P., SERS Sensors: Recent Developments and a Generalized Classification Scheme Based on the Signal Origin. *Annual Review of Analytical Chemistry* **2018,** *11*, 147-169.
49. Willets, K. A.; Van Duyne, R. P., Localized Surface Plasmon Resonance Spectroscopy and Sensing. *Annual Review of Physical Chemistry* **2007,** *58*, 267-297.
50. Zeng, Y.; Hu, R.; Wang, L.; Gu, D.; He, J.; Wu, S.-Y.; Ho, H.-P.; Li, X.; Qu, J.; Gao, B. Z.; Shao, Y., Recent advances in surface plasmon resonance imaging: detection speed, sensitivity, and portability. *Nanophotonics* **2017,** *6*, 1017-1030.
51. Naumann, S.; Schmidt, F. G.; Schowner, R.; Frey, W.; Buchmeiser, M. R., Polymerization of methyl methacrylate by latent pre-catalysts based on CO_2-protected N-heterocyclic carbenes. *Polymer Chemistry* **2013,** *4*, 2731-2740.
52. Zhang, L.; Yang, H.; Jiao, L., Revisiting the Radical Initiation Mechanism of the Diamine-Promoted Transition-Metal-Free Cross-Coupling Reaction. *Journal of the American Chemical Society* **2016,** *138*, 7151-7160.
53. Barry, S. C., T. J.; Coyle, J.; Hastie, J. J. M. Group 11 Mono-Metallic Precursor Compounds and use Thereof in Metal Deposition. 2012.
54. Farcau, C.; Astilean, S., Mapping the SERS Efficiency and Hot-Spots Localization on Gold Film over Nanospheres Substrates. *The Journal of Physical Chemistry C* **2010,** *114*, 11717-11722.
55. Litorja, M.; Haynes, C. L.; Haes, A. J.; Jensen, T. R.; Van Duyne, R. P., Surface-Enhanced Raman Scattering Detected Temperature Programmed Desorption: Optical Properties, Nanostructure, and Stability of Silver Film over SiO2 Nanosphere Surfaces. *The Journal of Physical Chemistry B* **2001,** *105*, 6907-6915.

56. Cao, X.; Coulter, S. K.; Ellison, M. D.; Liu, H.; Liu, J.; Hamers, R. J., Bonding of Nitrogen-Containing Organic Molecules to the Silicon(001) Surface: The Role of Aromaticity. *The Journal of Physical Chemistry B* **2001,** *105*, 3759-3768.
57. Moulder, J. F.; Stickle, W. F.; Sobol, P. E.; Bomben, K. D., *Handbook of X-ray Photoelectron Spectroscopy*. Perkin-Elmer Corporation: 1992.
58. Bridonneau, N.; Hippolyte, L.; Mercier, D.; Portehault, D.; Desage-El Murr, M.; Marcus, P.; Fensterbank, L.; Chanéac, C.; Ribot, F., N-Heterocyclic carbene-stabilized gold nanoparticles with tunable sizes. *Dalton Transactions* **2018,** *47*, 6850-6859.
59. Crudden, C. M.; Horton, J. H.; Narouz, M. R.; Li, Z.; Smith, C. A.; Munro, K.; Baddeley, C. J.; Larrea, C. R.; Drevniok, B.; Thanabalasingam, B.; McLean, A. B.; Zenkina, O. V.; Ebralidze, I. I.; She, Z.; Kraatz, H.-B.; Mosey, N. J.; Saunders, L. N.; Yagi, A., Simple direct formation of self-assembled N-heterocyclic carbene monolayers on gold and their application in biosensing. *Nature Communications* **2016,** *7*, 12654.
60. Shirley, D. A., High-Resolution X-Ray Photoemission Spectrum of the Valence Bands of Gold. *Physical Review B* **1972,** *5*, 4709-4714.
61. Barry, S.; Clark, T. J.; Coyle, J.; Hastie, J. J. M. Group 11 Mono-Metallic Precursor Compounds and use Thereof in Metal Deposition. WO2012155264A1, November 22, 2012.

Chapter 4 : Synthesis of d^{10} Perimidinium N-Heterocyclic Carbene Complexes

A version of this chapter has been submitted Organometallics by Shelby L. Strausser and David M. Jenkins as:

Shelby L. Strausser and David M. Jenkins. Synthesis of d^{10} Perimidinium N-Heterocyclic Carbene Complexes

Abstract

N-heterocyclic carbenes (NHCs) are vital auxiliary ligands for organometallic chemistry and although many variants have been synthesized, by far the most common are based on five-membered rings, such as imidazolium or benzimidazolium. Unlike NHC complexes built on five-membered rings, which are typically conjugated, exploration of six-membered ring NHC variants has focused on non-conjugated versions, such as N,N′-diamidocarbenes. Reports of conjugated six-membered ring NHCs are limited to perimidinium metal complexes that are in a narrow range of between six and eight d-electrons (on metals from groups 8-10). This manuscript showcases the synthesis of the first d^{10} perimidinium complexes on four different metals. The gold and silver complexes have a linear geometry while the copper and platinum complexes are three-coordinate. All complexes were characterized by single crystal X-ray crystallography, multi-nuclear NMR, and additional spectroscopic methods.

Introduction

N-heterocyclic carbenes (NHCs) are critical auxiliary ligands for transition metals, with applications ranging from homogenous catalysis to surface functionalization.[1-5] While unsaturated examples, such as imidazolium and benzimidazolium NHCs, dominate the literature (**Figure 4.1A**),[6] there has been a shift to non-standard NHCs in recent years that have shown greater effectiveness for catalysis.[7-13] In particular, saturated NHCs (imidazoliniums) have proven a popular choice due to their increased σ-donor strength, despite saturated NHCs being more challenging to synthesize than imidazole variants. Notable examples where saturated NHCs are highly effective include Grubbs second generation catalyst for olefin metathesis and reactions that induce chirality.[11, 14-16]

Remarkably, the case for six-membered ringed NHCs is reversed. The saturated variants have dominated the literature and conjugated examples based on a perimidinium scaffold are rare (**Figure 4.1A**).[17-21] To date, perimidinium complexes that have been characterized are restricted to group 8-10 transition metals with d-electron counts of 6 or 8. (**Figure 4.1B**). Richeson first reported perimidinium NHCs and prepared complexes on Rh and Pd.[22-24] Mashima and coworkers later developed iridium complexes for C-H bond activation and catalysis,[25, 26] while Hill[27-30] and others[31-33] have developed perimidinium NHC pincer complexes for catalytic applications. Lastly, a few scattered examples have been synthesized for drug development[34] or fluorescent applications.[35]

In this manuscript, we present the synthesis and characterization of four new perimidinium NHC metal complexes. All four complexes are d^{10}, and include the first group 11 perimidinium NHC compounds. All complexes are characterized by single crystal X-ray diffraction and multinuclear NMR. Finally, we demonstrate that these late transition metal complexes can act as perimidinium NHC transfer reagents, which will open up this class of NHC across more of the periodic table.

Results and discussion

The synthesis of 1,3-diisopropylperimidinium bromide ($(C_{10}H_6(^{i}PrN)_2CH)(Br)$) was originally reported by Richeson[24, 36] who also isolated the free carbene 1,3-$(^{i}Pr)_2$-perimidin-2-ylidene, $(C_{10}H_6(^{i}PrN)_2C)$.[23] We employed $(C_{10}H_6(^{i}PrN)_2CH)(Br)$ due to its ease of synthesis from commercial reagents in five steps. The gold complex, $(C_{10}H_6(^{i}PrN)_2C)AuCl$ (**4.1**), was synthesized through a two-step approach (**Scheme 4.1**). In an inert atmosphere, $KN(SiMe_3)_2$ was dissolved in THF and was added to a stirring suspension of the $(C_{10}H_6(^{i}PrN)_2CH)(Br)$ in THF. The reaction mixture was stirred for two hours, after which it was filtered over a short Celite plug to remove KBr. The solution was added to a vial containing $Au(SMe_2)Cl$ and the reaction was stirred for one day. The solvent was removed, the resulting residue was extracted with methylene chloride which was passed over a short Celite plug. The filtrate was then dried and the crude solid was purified through column chromatography to yield **4.1** as a yellow solid. Notably, pincer style perimidinium NHCs do not yield gold complexes since the gold only binds to the phosphine arms, and thus we were excited to prepare the first perimidinium gold complex.[28, 37] Single crystals for X-ray crystallography were grown by layering hexanes over a solution of **4.1** in methylene chloride.

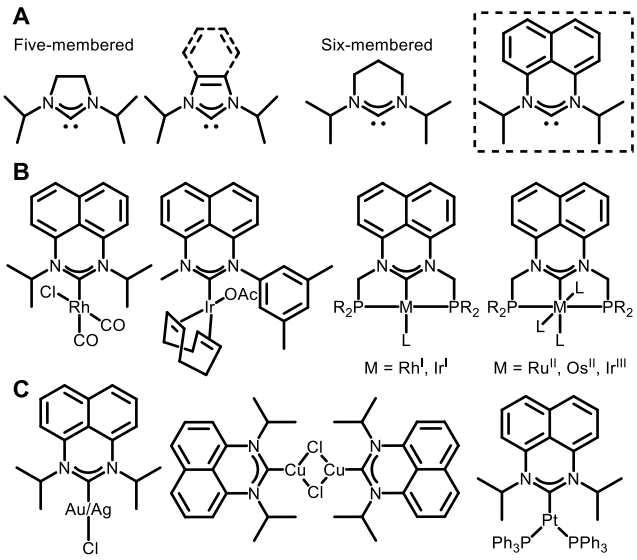
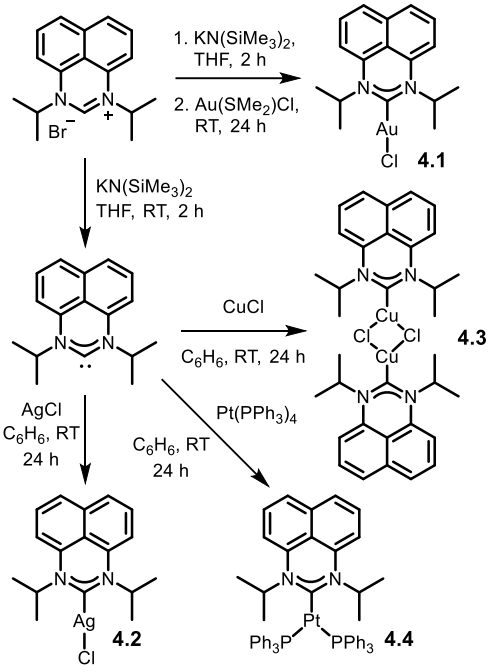


Figure 4.1: (A) Typical NHCs for five-membered and six-membered rings. (B) Examples of previously reported perimidinium metal complexes. All previous examples are on Ru, Rh, Pd (example not shown), Os, and Ir. (C) Newly reported perimidinium metal complexes in this manuscript.

Scheme 4.1: Synthesis of perimidinium complexes **4.1-4.4**.



For the synthesis of the Pt, Ag, and Cu complexes, we followed one general approach with slight differences for each metal. The free carbene ligand, ($C_{10}H_6(^iPrN)_2C$), was synthesized through deprotonation with $KN(SiMe_3)_2$ in THF, and was isolated and confirmed per Richeson's prior account.[23] The ligand (2 eq. twice for Pt and 1 eq. for the Ag and Cu complexes) was dissolved in benzene, added to the appropriate metal salts, and the reactions were stirred for 24 hours (**Scheme 4.1**). The platinum complex required excess ligand to drive the reaction to completion since both the NHC and phosphines are similar neutral Lewis bases. The reaction mixtures were filtered over Celite and the filtrate volume was concentrated to 2 mL. Hexanes was then layered over the concentrated benzene solutions yielding ($C_{10}H_6(^iPrN)_2C$)AgCl, **4.2**, [($C_{10}H_6(^iPrN)_2C$)CuCl]$_2$, **4.3**, and ($C_{10}H_6(^iPrN)_2C$)Pt(PPh_3)$_2$, **4.4** as yellow single crystals for X-ray crystallography. Unlike **4.1**, which is stable in air, these complexes are highly sensitive to oxygen and water.

Since so few perimidinium NHC complexes have been structurally characterized, the solid-state structures of these d^{10} complexes are particularly noteworthy. Indeed, all previous published examples, with the exception of a few iridium complexes that are five-coordinate,[26] have given square planar[22-27, 29, 35, 38, 39] or octahedral complexes.[25-29, 33, 40] The solid-state structure for complex **4.1** shows a two-coordinate linear complex with a Au-C distance of 2.020(3) Å and a C-Au-Cl bond angle of 179.96(8)° (**Figure 4.2A**). The Au-C bond distance is slightly longer than isostructural gold complexes with five-membered ringed NHCs,[41-43] but shorter than the one example with a saturated six-membered ring.[44] The other notable feature in the crystal structure is the close contacts between the methine protons (which were located in the difference map) and the gold (H12…Au, 2.34 Å, H14…Au, 2.33 Å). These distances are well within the combined van der Walls radii for these atoms and is consistent with Richeson's observation that the isopropyl groups may not be able to rotate freely for perimidinium NHCs.[22, 23]

The solid-state structure for the silver complex, ($C_{10}H_6(^iPrN)_2C$)AgCl, **4.2**, also revealed a two coordinate geometry at the metal center. In this case, the Ag-C1 bond (2.1312(11) Å) was significantly elongated versus **4.1**. Notably, direct NHC isostructural analogs (i.e. with isopropyl groups off the nitrogen) with either five-membered or six-membered rings have not been synthesized on silver. Isopropyl analogs form dimers,[45, 46] but switching to more sterically encumbering R-groups can lead to similar two-coordinate complexes.[47-49] However, in both cases the C-Ag bond distances are shorter than **4.2**. The C1-Ag-Cl angle is also slightly bent at 170.13(3)°. This bend away from linearity may be due to interactions with hydrogen atoms on the NHC ligand. Unlike complex **4.1**, for **4.2** the interactions are asymmetric, with one coming from an alpha-carbon (H12…Ag, 2.43 Å) and the second coming from a beta-carbon (H17…Ag, 2.34 Å).

The final group eleven complex that we synthesized, [($C_{10}H_6(^iPrN)_2C$)CuCl]$_2$, **4.3**, yielded a three-coordinate dimer in the solid-state (**Figure 4.3A**) with two bridging chlorides. Complex **3** has the third shortest M-C1 bond distance of any reported perimidinium NHC complex at 1.932(3) Å.[27, 35] The bridging chloride ligands are highly asymmetric with bond distances of Cu-Cl, 2.263(1); Cu-Cl', 2.391(1), and there are few reported examples of similar copper(I) NHC complexes with bridging chlorides.[50, 51] Like

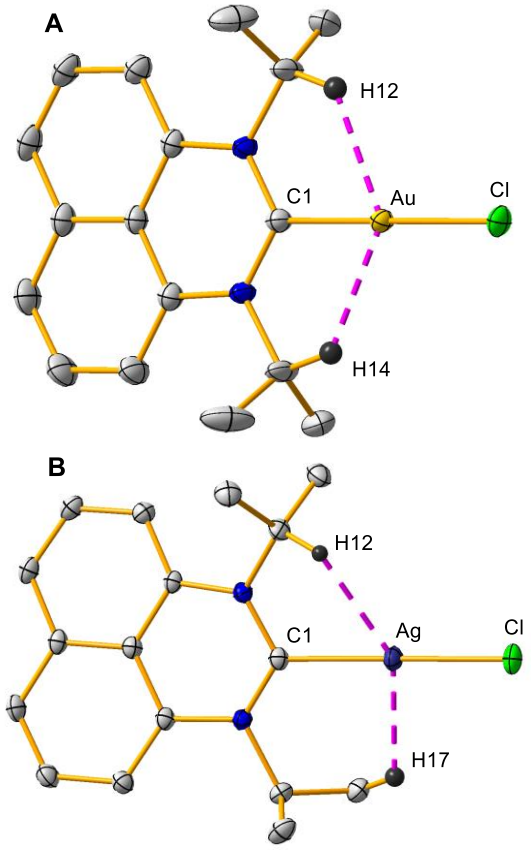


Figure 4.2: Solid state structures of (A) ($C_{10}H_6(^{i}PrN)_2$)C)AuCl, **4.1**, and (B) ($C_{10}H_6(^{i}PrN)_2$)C)AgCl, **4.2**. Yellow, indigo, blue, gray, and green ellipsoids (50% probability) represent gold, silver, nitrogen, carbon, and chlorine, respectively. Hydrogen atoms are omitted for clarity unless necessary to display close interatomic interactions (dark gray spheres). Selected bond lengths (Å) and angles (°): 1 Au-C1, 2.020(3); Au-Cl, 2.3092(8); C1-Au-Cl, 179.96(8); 2 Ag-C1, 2.1312(11); Ag-Cl, 2.3628(3); C1-Ag-Cl, 170.13(3).

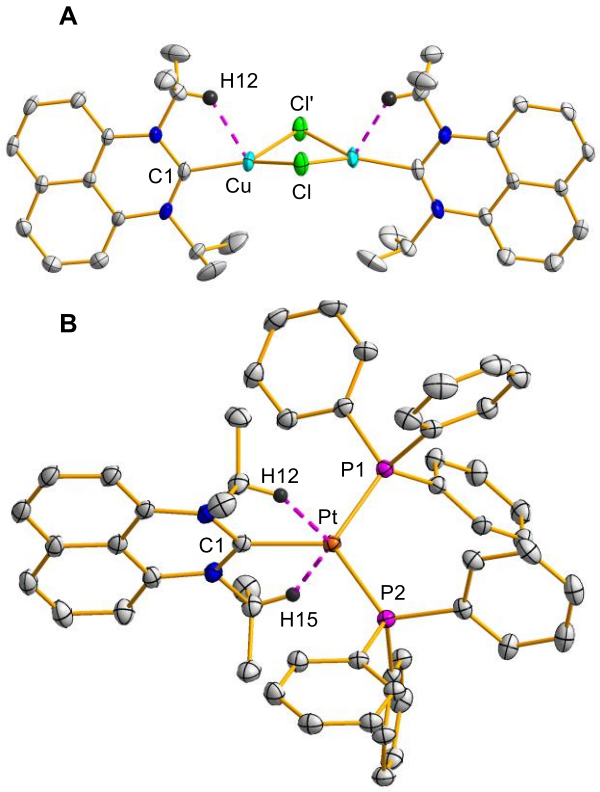


Figure 4.3: Solid state structures of (A) $[(C_{10}H_6(^{i}PrN)_2)C)CuCl]_2$, **4.3**, and (B) $(C_{10}H_6(^{i}PrN)_2)C)Pt(PPh_3)_2$, **4.4**. Cyan, orange, blue, gray, green, and pink ellipsoids (50% probability) represent copper, platinum, nitrogen, carbon, chlorine, and phosphorous, respectively. Hydrogen atoms are omitted for clarity unless necessary to display close interatomic interactions (dark gray spheres). Selected bond lengths (Å) and angles (°): **4.3** Cu-C1, 1.932(3); Cu-Cl, 2.263(1); Cu-Cl', 2.391(1); C1-Cu-Cl, 140.91(12); C1-Cu-Cl', 123.81(12); Cl1-Cu-Cl', 94.91(4); **4.4** Pt-C1, 2.057(3); Pt-P1, 2.2475(9); Pt-P2, 2.2581(9); C1-Pt-P1, 121.20(8); C1-Pt-P2, 124.69(8); P1-Pt-P2, 113.92(3).

4.1 and **4.2**, the copper complex **4.3** has a close contact with a methine proton (H12…Cu, 2.20 Å), but in this case there is only one contact. The asymmetry of the isopropyl groups in the crystal structure stimulated our investigation of this in solution via NMR (*vide supra*).

Our final d^{10} complex, $(C_{10}H_6(^{i}PrN)_2C)Pt(PPh_3)_2$, **4.4**, has a trigonal planar geometry in the solid-state. The Pt-C1 bond distance is 2.057(3) Å which is in between the distances for **4.1** and **4.2**. NHC complexes with Pt(0) are quite rare and a few three-coordinate species have been reported;[52, 53] most Pt(0) complexes are two coordinate.[54-59] All of these Pt(0) complexes display shorter Pt-C bond distances than **4.4** and notably all feature 5-atom ringed NHCs. The three ligands on **4.4** form a plane where the Pt is in the center, but the steric bulk from the isopropyl groups on the NHC push the phosphines close together, which reduces the P1-Pt-P2 bond angle to 113.92(3)°. Like the group 11 complexes discussed earlier, complex **4.4** has close contacts between the metal center and the methine protons (H12…Pt, 2.39Å; H15…Pt, 2.31 Å).

Since the solid-state structures demonstrated that there are close contacts between the protons on the perimidinium NHCs and the metal, we were particularly interested in the ^{1}H NMR spectra. Evaluation of the ^{1}H NMR for $(C_{10}H_6(^{i}PrN)_2C)AuCl$ shows the influence of the metal center (**Figure 4.4A**). In particular, the methine protons are shifted downfield (6.17 ppm) and broadened significantly to where the expected splitting is not observed. In fact, the methine carbons in the ^{13}C NMR for **4.1** are also significantly broadened to where they are barely visible above the baseline at 64.24 ppm (**Figure 4.4A**, inset). The carbene resonance is visible at 192.89 ppm (**Spectra 4.2**). These observations are consistent with reports of the NMRs of complexes that employed the same perimidinium NHC.[22-24] The silver complex, **4.2**, shows a less pronounced downfield shift (4.81 ppm) for the methine protons that is also significantly broadened (**Spectra 4.5**). Notably, neither the methine carbons nor the carbene carbon were observed in the ^{13}C NMR (**Spectra 4.6**). Their absence is due to the splitting of the two spin active isotopes of silver which often make observation of carbons near the metal challenging.[60] HSQC measurements for **4.2** also could not resolve the methine carbon resonance.

The isopropyl groups on the solid-state structure for $[(C_{10}H_6(^{i}PrN)_2C)CuCl]_2$, **4.3**, are in different conformations. If this is true in solution, then there would be separate resonances for their protons. However, a ^{1}H NMR at room temperature revealed a spectrum similar to **4.2** (**Figure 4.4B**), with broad singlets at 4.64 and 1.40 ppm. Cooling the solution to 230 K in d_8-toluene revealed the resonances for the isopropyl diverge to two distinct sets of peaks eliminating the coalescence (**Figure 4.4B**, **Spectra 4.11** for COSY). As the temperature is reduced, there is not sufficient energy for rotation about the bond and the isopropyl groups are locked into two distinct positions, matching the observation in the X-ray structure. Finally, the carbene resonance for **4.3** is observed in the ^{13}C NMR at 197.68 ppm (**Spectra 4.9**).

The NMR for the platinum complex, **4.4**, was distinct from the group 11 complexes (**4.1**-**4.3**) due to the additional phosphine ligands. A single phosphorus resonance with Pt satellites was observed at 45.6 ppm in the ^{31}P NMR (**Spectra 4.17**). More notably, complex **4** was the only perimidinium complex that was synthesized that showed the expected septet coupling on the methine proton at 6.84 ppm in the ^{1}H NMR

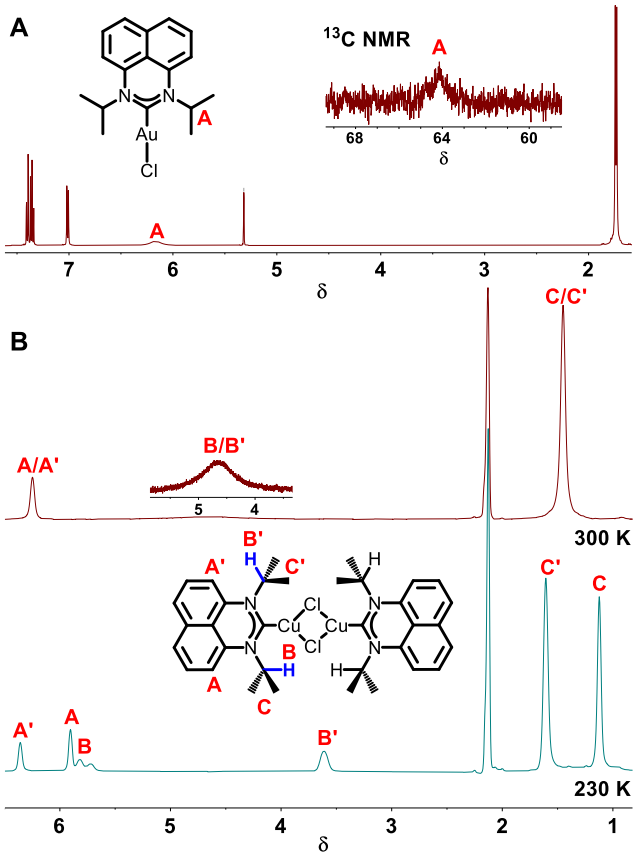


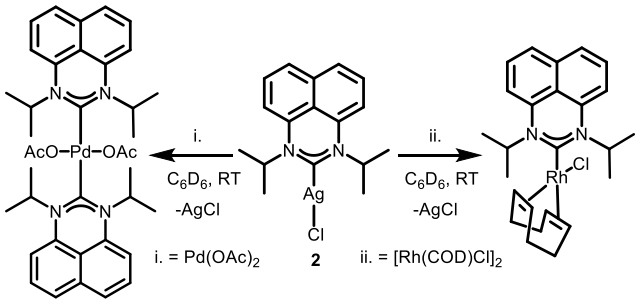
Figure 4.4: NMR spectra of (A) $(C_{10}H_6(^iPrN)_2)C)AuCl$, **4.1** and (B) $[(C_{10}H_6(^iPrN)_2)C)CuCl]_2$, **4.3**. (A) ^{1}H NMR of **4.1** shown with ^{13}C NMR inset. Methine proton and carbon resonances are severely broadened suggesting slow rotation about the C-N bond. (B) ^{1}H NMR spectra for **4.3** shown at two temperatures, 300 K (top) and 230 K (bottom).

(**Spectra 4.14**). The sharp peaks on the isopropyl resonances demonstrate that the isopropyl groups rotate freely at room temperature even though there are close contacts observed in the solid-state structure. Finally, all expected carbon resonances were observed in the ^{13}C NMR (or HSQC) except the perimidinium carbene resonance. We attribute the lack of observable signal for the carbene due to additional splitting from the phosphines and platinum which divides an already typically weak signal.

Although the free carbene, ($C_{10}H_6(^{i}PrN)_2C$), can be prepared under air free conditions, it is often more convenient to employ silver NHC transmetalation reagents.[61-64] To our knowledge, there have been no reported transmetalation reactions with this NHC. We tested the ability of **4.2** to transmetalate the NHC to form known perimidinium complexes (**Scheme 4.2**). Reacting ($C_{10}H_6(^{i}PrN)_2C$)AgCl, **4.2**, in deuterated benzene with $Pd(OAc)_2$ immediately led to the formation of a gray solid (AgCl). After two hours, ^1H NMR confirmed the formation of previously reported ($C_{10}H_6(^{i}PrN)_2C)_2Pd(OAc)_2$ in 55% yield versus an internal standard, which is similar to the yield achieved from the free carbene method.[24] An analogous reaction with $[Rh(COD)Cl]_2$ and **4.2** yielded the product ($C_{10}H_6(^{i}PrN)_2C$)Rh(COD)Cl in 62% yield in only one hour based on integration versus an internal standard.[23]

In conclusion, we have synthesized the first perimidinium NHC d^{10} complexes, including the first noble metal examples. The copper complex is also the first perimidinium complex on a first-row transition metal. All four complexes were characterized by single crystal X-ray diffraction and the gold and silver complexes yielded linear geometries, while the platinum complex is trigonal planar. The copper complex forms a dimer with bridging chlorides in the solid-state. All four complexes showed close contacts with methine protons in the solid-state and these interactions were confirmed in solution by ^1H NMR which revealed downfield resonances, a lack of splitting, and severe broadening. Low temperature NMR confirmed that for the copper complex, the isopropyl moieties can be prevented from rotating freely. Finally, the silver complex is an effective transmetalation reagent to transfer the perimidinium NHC to palladium and rhodium. Transmetalation is an effective strategy for forming NHC complexes, so this outcome can expand the breadth of perimidinium NHC chemistry beyond the few metals on the periodic table studied to date.

Scheme 4.2: Transmetalation reactions from 4.2.



Experimental

General Considerations for Synthesis.

All glassware for air and water sensitive reactions were dried at 160 ˚C overnight before use. All reactions were stirred vigorously with magnetic stirrers. Syntheses of the NHC-metal complexes were performed under a dry dinitrogen atmosphere using a glovebox. Solvents used under N_2 atmosphere were dried on an Innovative Technologies (Newburyport, MA) Pure Solv MD-7 Solvent Purification System, degassed by three freeze-pump-thaw cycles on a Schlenk line to remove dioxygen and stored over activated 4 Å molecular sieves prior to use. Celite was dried at 240 ˚C under vacuum overnight and stored in a dinitrogen glovebox. The compounds 1,3-diisopropylperimidinium bromide ($C_{10}H_6(^iPrN)_2CH)(Br)$[24, 65] and 1,3-(^{i}Pr)$_2$-perimidin-2-ylidene ($C_{10}H_6(^iPrN)_2C$)[23] were prepared from previous literature procedures. All other compounds were purchased from commercial vendors at the highest available purity and used without any further purification.

Solution ^{1}H NMR, ^{13}C{^{1}H}, and ^{31}P{^{1}H} NMR were performed on a Bruker Avance 500 MHz narrow-bore broadband system at 298 K. All ^{1}H and ^{13}C shifts were referenced to the residual solvent. ^{31}P{^{1}H} shift was referenced to H_3PO_4. Infrared spectra were collected on a Thermo Scientific Nicolet iS10 with a Smart iTR accessory for attenuated total reflectance (ATR) using the neat compounds. UV-vis measurements were obtained inside a dry glovebox on an Ocean Optics USB4000 UV-vis system with a 1 cm path length quartz crystal cell. All UV-vis sample measurements were collected in benzene.

All mass spectrometry analyses were conducted at the Biological and Small Molecule Mass Spectrometry Core Facility located in the Department of Chemistry at the University of Tennessee. The analysis of **4.1** and **4.4** were performed using a Waters Synapt G2-S*i* qTOF instrument with ESI ion source. The reflector was set to positive mode and data were collected from 100-1000 Daltons. The analysis of **4.3** was performed using a JEOL AccuTOF-D time-of-flight (TOF) mass spectrometer with a DART (direct analysis in real time) ionization source from JEOL USA, Inc. (Peabody, MA). Solutions for mass spectrometry were prepared in methanol for **4.1**, C_6D_6 for **4.3**, and acetonitrile for **4.4**.

X-ray data for all metal complexes were collected with a Mo micro source on a Bruker Kappa DUO with a Photon 100 detector. Crystals were placed in Paratone oil, mounted on a Mitegen loop, and placed in a 100 K cold stream provided by an Oxford Cryostream low-temperature apparatus. All data sets were reduced with Bruker SAINT and were corrected for absorption using SADABS. Structures were solved and refined using SHELXT.

Synthesis of ($C_{10}H_6(^iPrN)_2C$)AuCl, 4.1.

1,3-diisopropylperimidinium bromide (0.4123 g, 1.237 mmol), KHMDS (0.3118 g, 1.563 mmol), and 10 mL of THF were added to a 20 mL vial and the reaction was stirred for two

hours at RT in a glovebox. The reaction mixture was then filtered over a short Celite plug to remove solid KBr and the solution was added to a second 20 mL vial containing $Au(SMe_2)Cl$ (0.3049 g, 1.035 mmol). The reaction was allowed to stir at RT overnight, at which point the reaction was removed from the glovebox and the solvent was removed under reduced pressure. The brown solid residue was extracted with CH_2Cl_2 (40 mL) and filtered over a Celite plug. The filtrate was then concentrated to approximately 2 mL and pipetted into a 100 mL Erlenmeyer flask containing 50 mL hexanes and a stir bar with vigorous stirring. The resulting precipitate was collected and dried under vacuum to give a yellow solid. The crude material was purified with flash chromatography (R_f = 0.45, 100% CH_2Cl_2) on silica, yielding **4.1** as a yellow powder (0.0913 g, 18.2%). Single crystals for X-ray diffraction were grown by layering hexanes over a CH_2Cl_2 solution of **4.1**. ^{1}H NMR (CD_2Cl_2, 499.74 MHz): □ 7.40 (d, *J* = 8.20 Hz, 2H), 7.36 (t, *J* = 7.99, 2H), 7.02 (d, *J* = 7.64 Hz, 2H), 6.17 (bs, 2H), 1.73 (d, *J* = 7.20 Hz, 12H). ^{1}H NMR (C_6D_6, 499.74 MHz): □ 6.99 (s, 2H), 6.83 (s, 2H), 6.38 (s, 2H), 6.03 (bs, 2H), 1.15 (s, 12H). $^{13}C\{^1H\}$ NMR (CD_2Cl_2, 125.66 MHz): □□192.89, 135.49, 132.37, 127.56, 123.20, 122.20, 109.27, 64.12, 19.49. IR: 2969, 2930, 1633, 1601, 1581, 1527, 1447, 1421, 1410, 1368, 1329, 1261, 1233, 1211, 1186, 1166, 1147, 1097, 1081, 945, 878, 811, 763, 748, 658 cm^{-1}. ESI HR-MS (*m*/*z*): $[LMCl+Na]^+$: 507.0860 (found), $[LMCl+Na]^+$: 507.0873 (calc). UV-Vis (C_6H_6): □$_{max}$ 335 nm (15,000 L/mol*cm).

Synthesis of ($C_{10}H_6$(^{i}PrN)$_2$C)AgCl, 4.2.

1,3-(^{i}Pr)$_2$-perimidin-2-ylidene ($C_{10}H_6$(^{i}PrN)$_2$C) (0.1115 g, 0.4418 mmol) was dissolved in 10 mL of benzene and added to a vial containing AgCl (0.0633 g, 0.4416 mmol) in the dark. The reaction mixture was stirred for 24 hours at RT, at which point a yellow solid precipitated. The reaction mixture was filtered over a short Celite pad and the solvent was removed under reduced pressure giving a yellow solid. The solid was crystallized by dissolving in CH_2Cl_2 and then layering with hexanes to give yellow crystals (0.0401 g, 22.9%). ^{1}H NMR (C_6D_6, 499.74 MHz): □ 7.00 (s, 2H), 6.86 (s, 2H), 6.28 (s, 2H), 4.81 (bs, 2H), 1.25 (s, 12H). $^{13}C\{^1H\}$ NMR (C_6D_6, 125.66 MHz): □□135.56, 132.55, 127.22, 123.23, 121.54, 107.41, 19.86. IR: 2975, 2917, 2849, 1628, 1578, 1524, 1463, 1440, 1427, 1410, 1395,1370, 1333, 1306, 1212, 1164, 1153, 1138, 1096, 1039, 976, 939, 883, 857, 814, 773, 751, 700, 652 cm^{-1}. UV-VIS (C_6H_6): □$_{max}$ 332 nm (30,000 L/mol*cm). Note: ESI HR MS and DART HR MS only showed ($C_{10}H_6$(^{i}PrN)$_2$CH)$^+$ and no silver containing peaks.

Synthesis of $[(C_{10}H_6(^iPrN)_2C)CuCl]_2$, 4.3.

1,3-(^{i}Pr)$_2$-perimidin-2-ylidene ($C_{10}H_6(^iPrN)_2C$) (0.0555 g, 0.2199 mmol) was dissolved in 10 mL of benzene and added to a vial containing CuCl (0.0230 g, 0.232 mmol). The reaction was stirred for 24 hours at RT at which point a yellow solid precipitated. The reaction mixture was filtered over a short Celite pad and the filtrate was reduced to 2 mL under reduced pressure. Hexanes was layered over the solution to give yellow crystals (0.0420 g, 54.5%). ^{1}H NMR (C_6D_6, 499.74 MHz): □ 7.01 (d, *J* = 8.20, 2H), 6.89 (t, *J* = 7.99, 2H), 6.19 (s, 2H), 4.64 (bs, 2H), 1.40 (s, 12H). ^{13}C{^{1}H} NMR (C_6D_6, 125.66 MHz): □□197.28, 135.16, 133.04, 127.22, 122.29, 121.07, 106.07, 20.58. IR: 2972, 1627, 1579, 1478, 1439, 1409, 1396, 1368, 1327, 1225, 1181, 1161, 1096, 1035, 963, 888, 860, 817, 776, 753, 698, 655 cm^{-1}. DART HR-MS (m/z): [LMCl]$^+$: 350.0604 (found), $[C_{17}H_{20}ClCuN_2]^+$: 350.0611 (calc). UV-VIS (C_6H_6): □$_{max}$ 277 nm (300,000 L/mol*cm).

Synthesis of $(C_{10}H_6(^iPrN)_2C)Pt(PPh_3)_2$, 4.4.

1,3-(^{i}Pr)$_2$-perimidin-2-ylidene ($C_{10}H_6(^iPrN)_2C$) (0.1047 g, 0.4149 mmol) was dissolved in 10 mL of benzene and added to a vial containing $Pt(PPh_3)_4$ (0.2581 g, 0.2074 mmol) in 3 mL of benzene. The reaction was stirred for two hours at RT. The reaction was placed into a -34 °C freezer and the solid benzene was lyophilized. The resulting powder was extracted with hexanes (10 mL) and the supernatant was removed. The entire process was repeated on the solid with a second round of ($C_{10}H_6(^iPrN)_2C$) (0.1032 g, 0.4089 mmol). After the second extraction with hexanes, the solid was recrystallized by layering hexanes over a benzene solution (Yield: 0.132 g, 66.5%). ^{1}H NMR (C_6D_6, 499.74 MHz): □ 7.53 (s, 12H), 7.13 (m, *J* = 7.83 Hz 4H), 6.97 (s, 18H), 6.84 (sept, *J* = 7.18 Hz, 2H), 6.79 (d, *J* = 7.51 Hz, 2H), 1.35 (d, *J* = 7.18 Hz, 12H). ^{13}C{^{1}H} NMR (C_6D_6, 125.66 MHz): □. 141.08 (*J* = 18.2 Hz), 136.60, 134.18, 133.97 (t, *J* = 8.30 Hz), 128.0 (2 peaks seen by HSQC), 127.42, 122.08, 118.81, 106.13, 59.35, 18.21. ^{31}P{^{1}H} NMR (C_6D_6, 202.49 MHz): □□45.63 (t, *J* = 1970 Hz) IR: 3050, 2794, 1625, 1577, 1477, 1433, 1417, 1372, 1301, 1284, 1228, 1188, 1162, 1132, 1082, 1026, 998, 848, 814, 792, 770, 741, 693, 647 cm^{-1}. ESI HR-MS (m/z): [LM(PPh$_3$)$_2$+H]$^+$: 972.3210 (found), $[C_{53}H_{51}N_2P_2Pt]^+$: 972.3170 (calc). UV-VIS (C_6H_6): □$_{max}$ 330 nm (23,000 L/mol*cm).

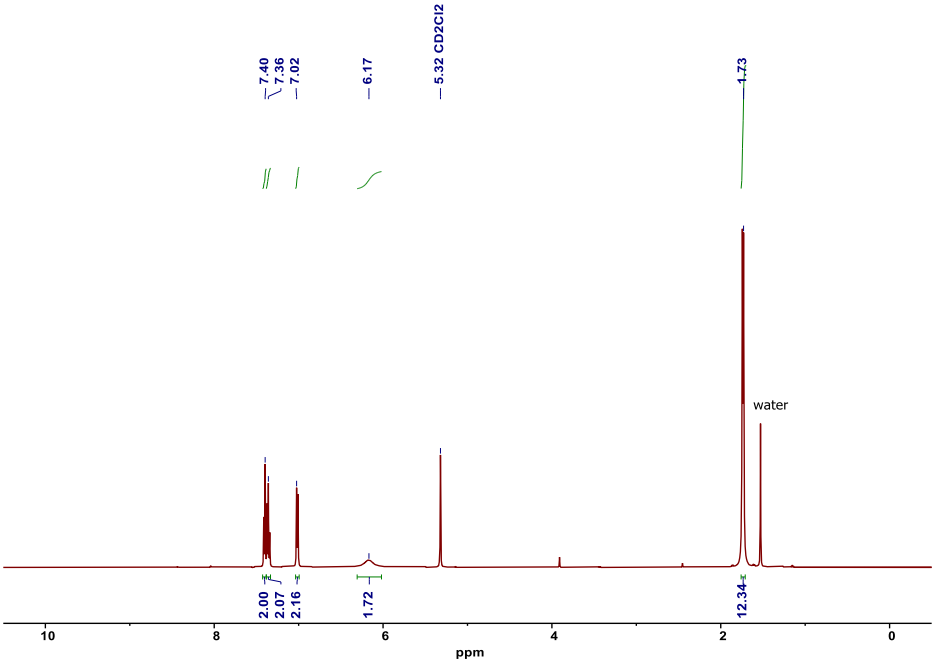
Reaction of 4.2 with $Pd(OAc)_2$ to form $(C_{10}H_6(^iPrN)_2C)_2Pd(OAc)_2$.

Complex **4.2** (0.0216 g, 0.0544 mmol) was added to a vial with 5 mL C_6D_6. $Pd(OAc)_2$ (0.0060 g, 0.0267 mmol) and 30 µL of mesitylene were added and the reaction was stirred for two hours in a N_2 glovebox. A gray solid (AgCl) immediately formed when the reaction started. After two hours, a ^{1}H NMR was collected and the product, $(C_{10}H_6(^iPrN)_2C)_2Pd(OAc)_2$, was confirmed[1] and integrated versus the internal standard of mesitylene showing an *in situ* NMR yield of 55%.

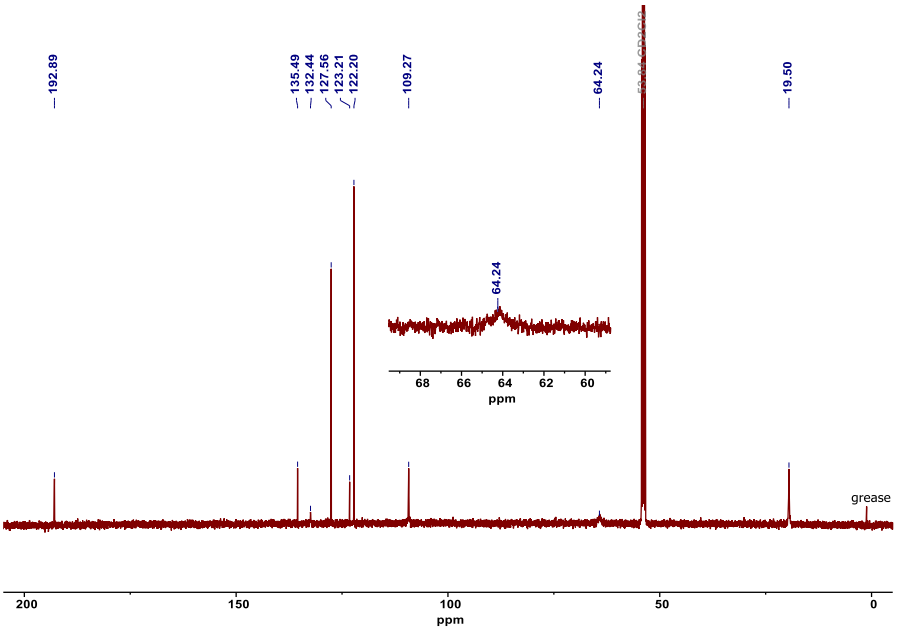
Reaction of 4.2 with [(COD)RhCl]$_2$ to form ($C_{10}H_6$(^{i}PrN)$_2$C)Rh(COD)Cl.

In a 20 mL scintillation vial, 1 mL of a 0.005 M (0.005 mmol) solution of complex **4.2** in C_6D_6, 0.25 mL of a 0.01 M (0.0025 mmol) solution of [Rh(COD)Cl]$_2$ in C_6D_6, and 30 µL of a 30% by vol. solution of mesitylene were added and stirred for one hour in a N_2 glovebox. A gray solid (AgCl) immediately formed when the reaction started. After one hour, a ^{1}H NMR was collected and the product, ($C_{10}H_6$(^{i}PrN)$_2$C)Rh(COD)Cl, was confirmed[3] and integrated versus the internal standard of mesitylene showing an *in situ* NMR yield of 62%.

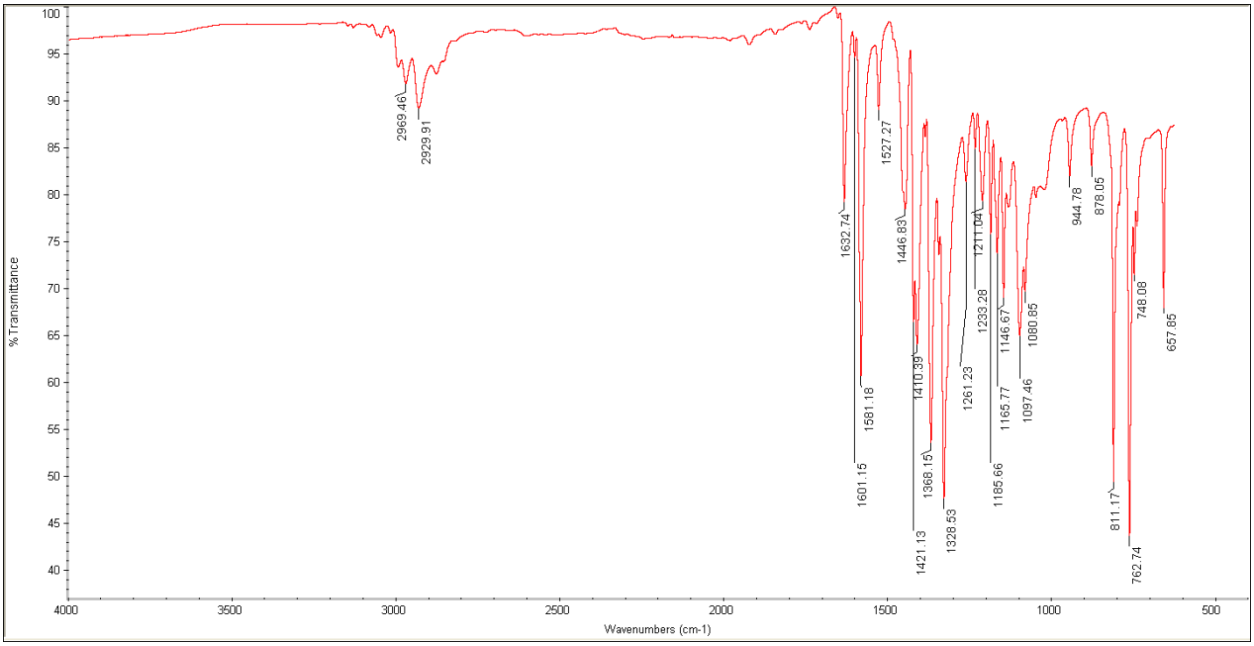
Annotated NMRs, IRs, MS for 4.1-4.4.



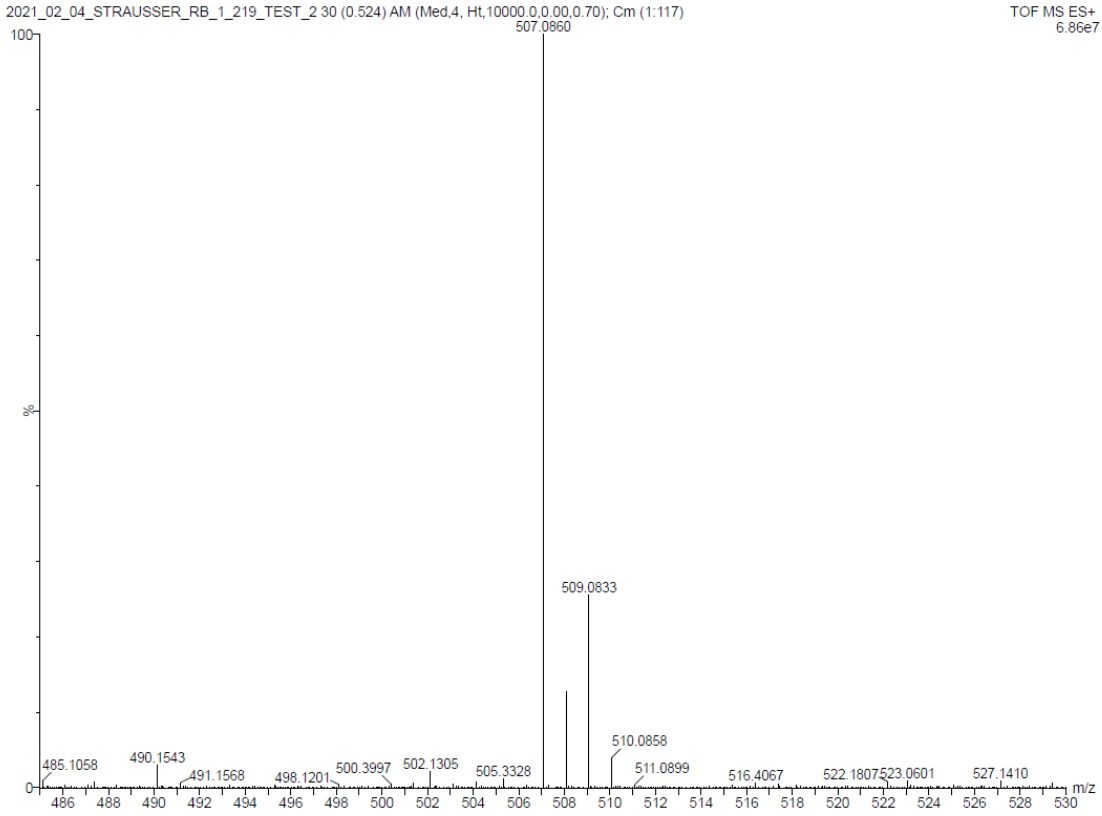
Spectra 4.1. ^{1}H NMR of ($C_{10}H_6(^{i}PrN)_2C$)AuCl (**4.1**) in CD_2Cl_2.



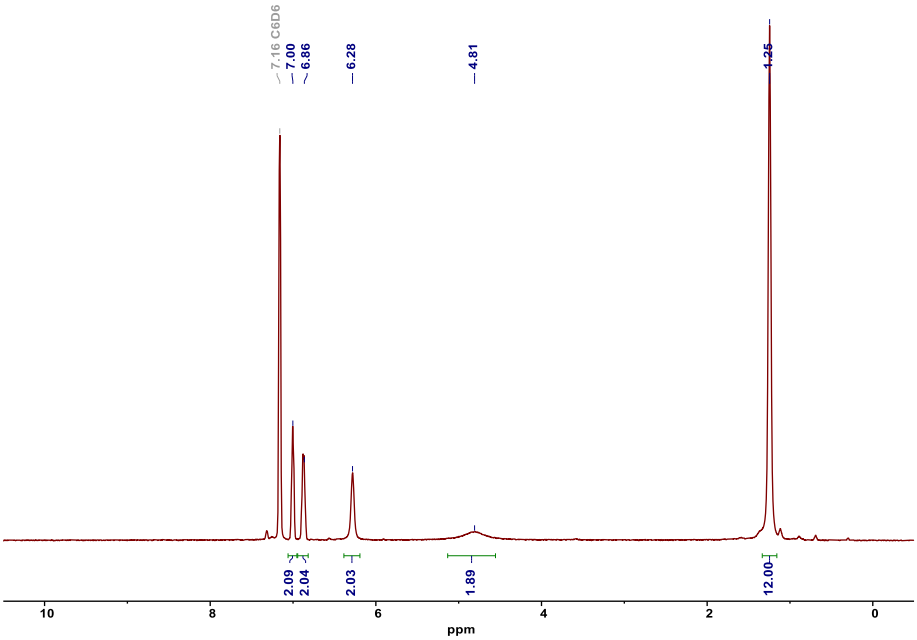
Spectra 4.2. ^{13}C NMR of ($C_{10}H_6(^{i}PrN)_2C$)AuCl (**4.1**) in CD_2Cl_2. Inset shows broad peak near 64 ppm.



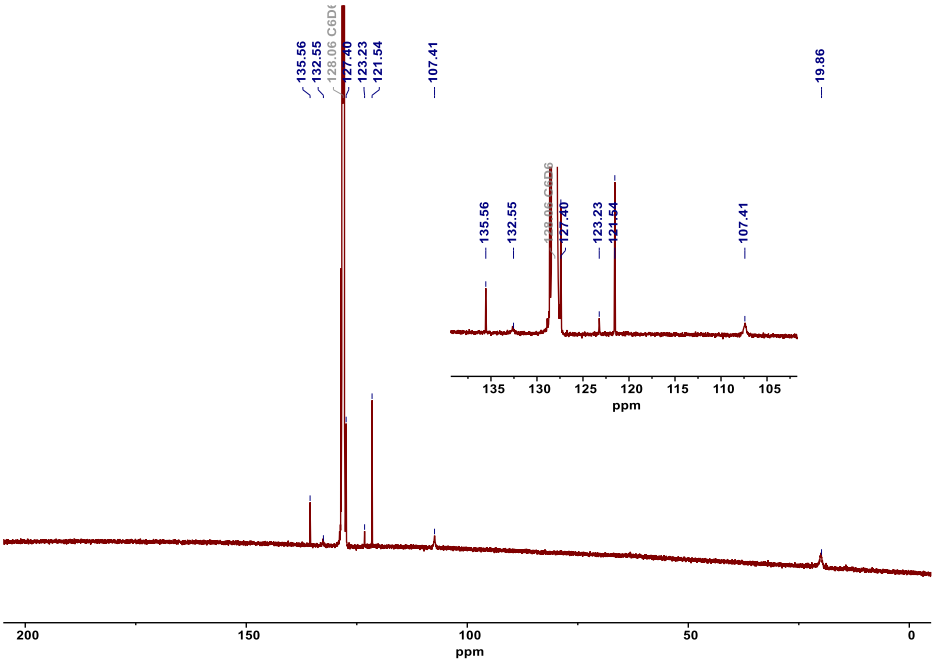
Spectra 4.3. ATR IR of ($C_{10}H_6(^{i}PrN)_2C$)AuCl (**4.1**).



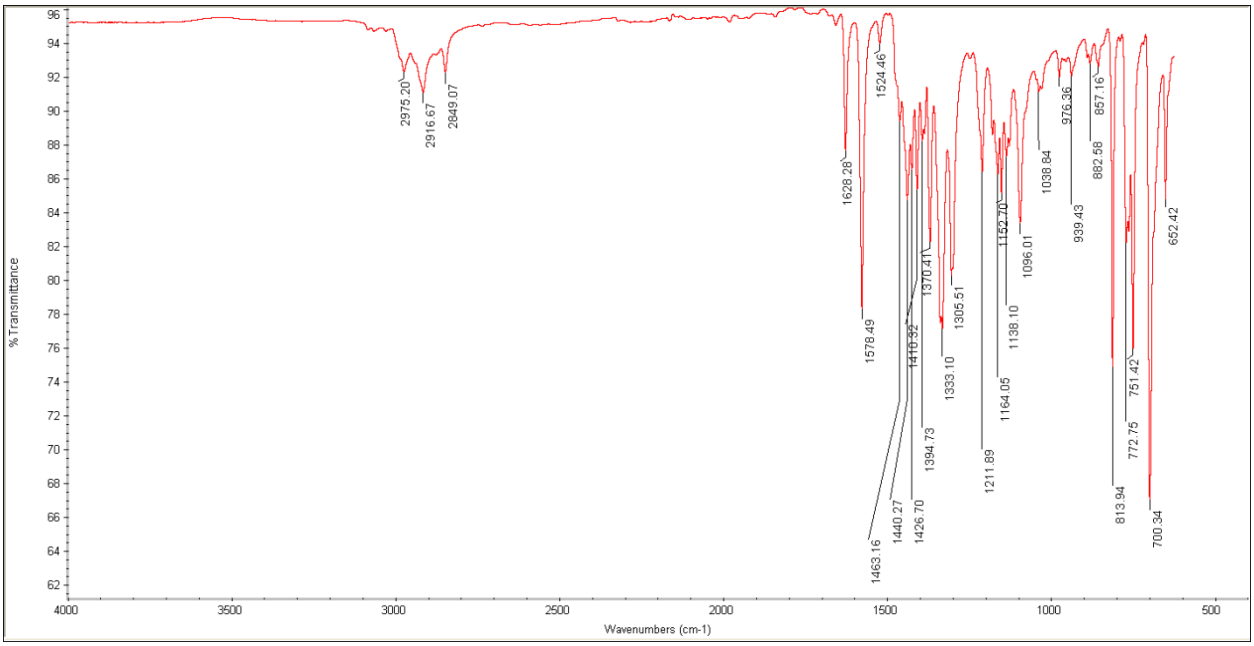
Spectra 4.4. HR ESI-MS of ($C_{10}H_6(^{i}PrN)_2C$)AuCl (**4.1**). $[LAuClNa]^+$ is observed in MS.



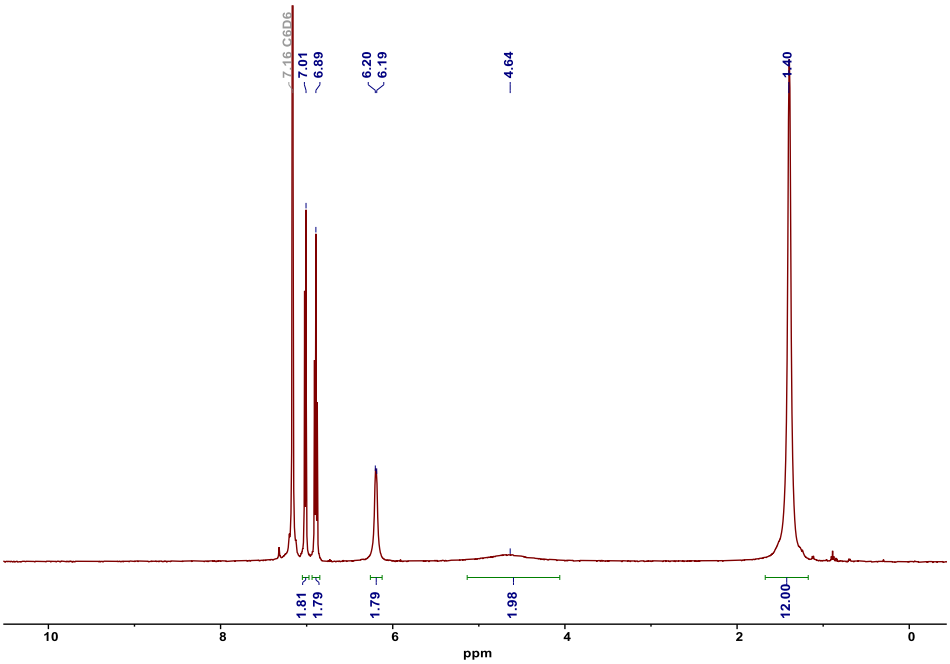
Spectra 4.5. ^{1}H NMR of $(C_{10}H_6(^{i}PrN)_2C)AgCl$ (**4.2**) in C_6D_6.



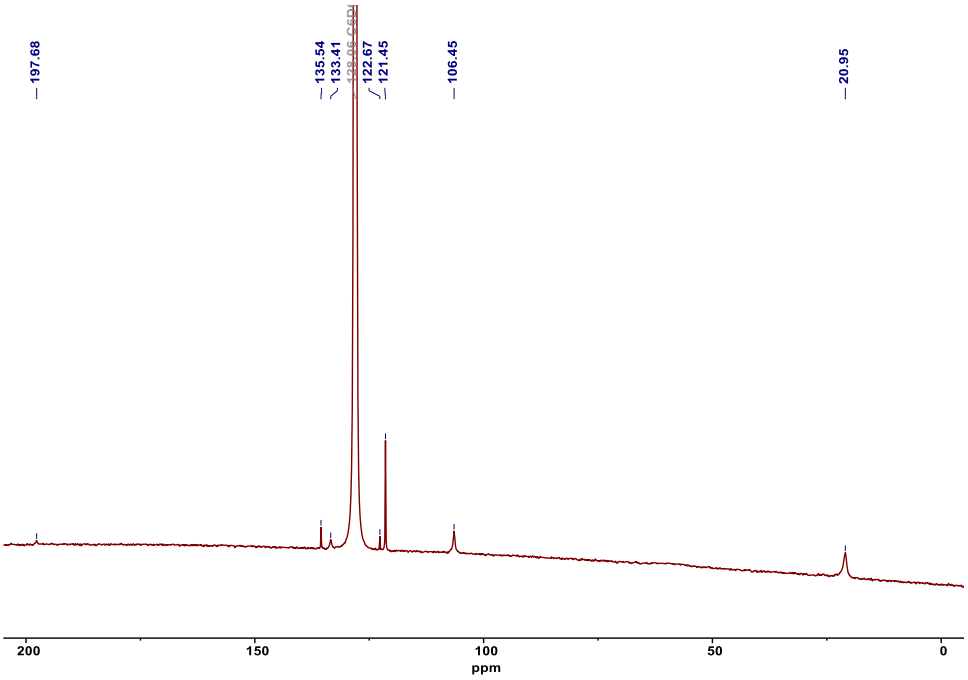
Spectra 4.6. ^{13}C NMR of $(C_{10}H_6(^{i}PrN)_2C)AgCl$ (**4.2**) in C_6D_6.



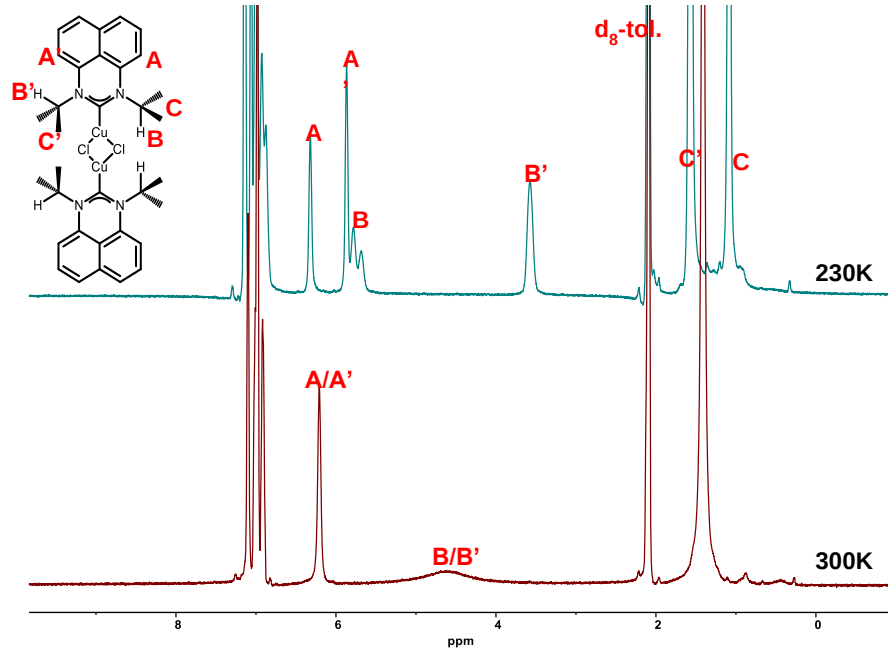
Spectra 4.7. IR of ($C_{10}H_6(^{i}PrN)_2C$)AgCl (**4.2**).



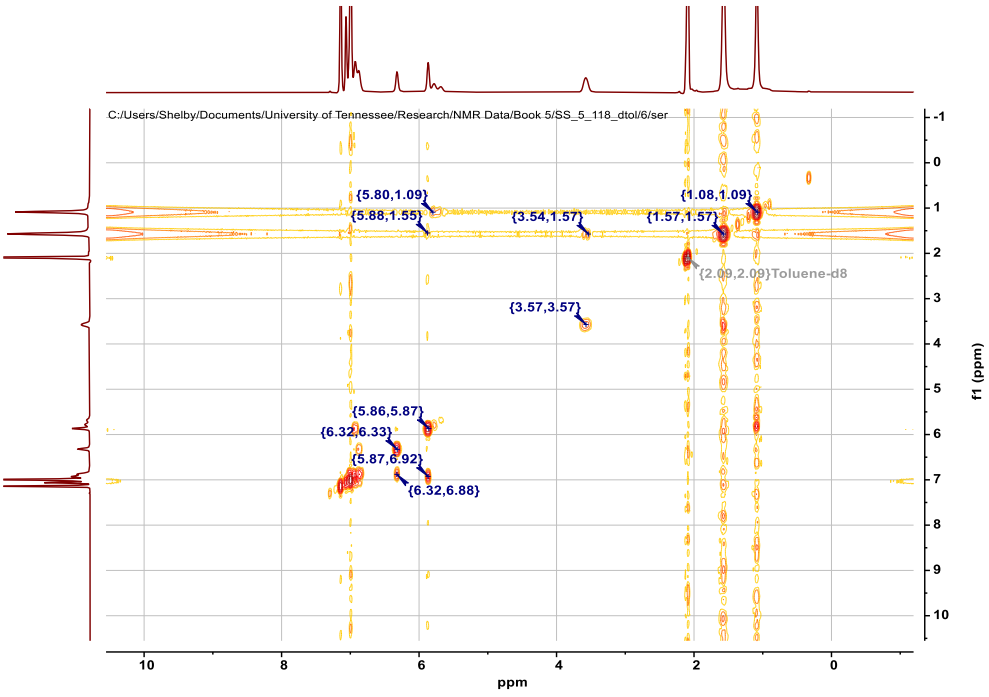
Spectra 4.8. ^{1}H NMR of $[(C_{10}H_6(^{i}PrN)_2C)CuCl]_2$ (**4.3**) in C_6D_6.



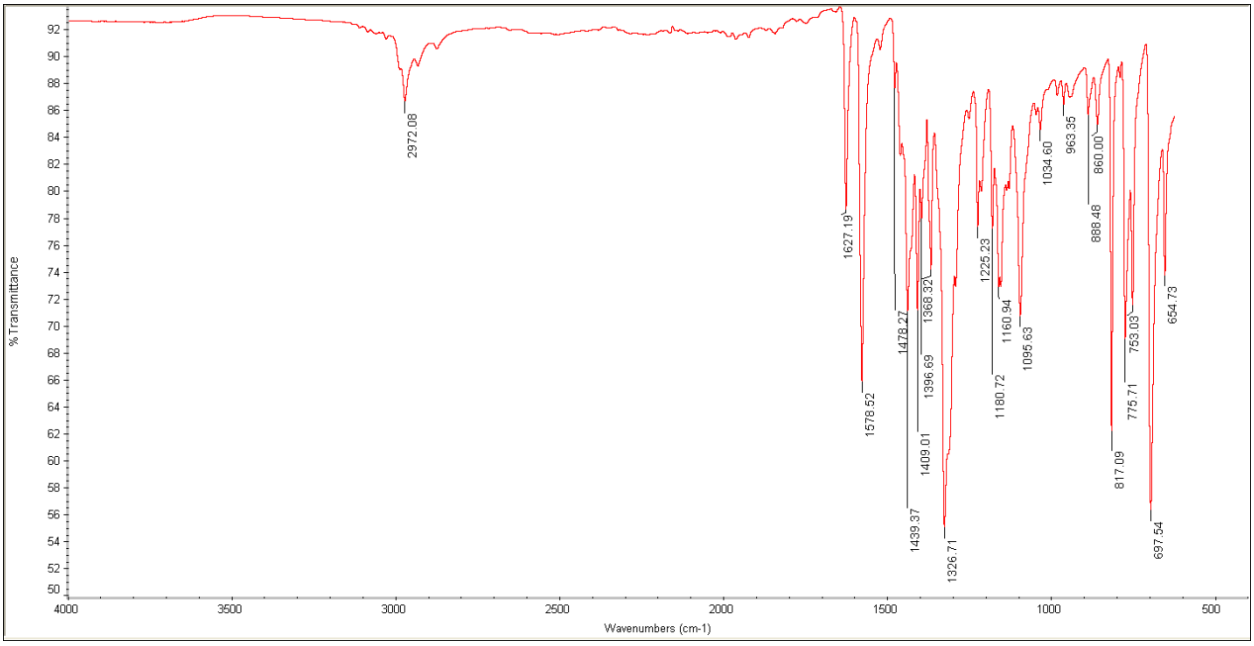
Spectra 4.9. ^{13}C NMR of $[(C_{10}H_6(^{i}PrN)_2C)CuCl]_2$ (**4.3**) in C_6D_6.



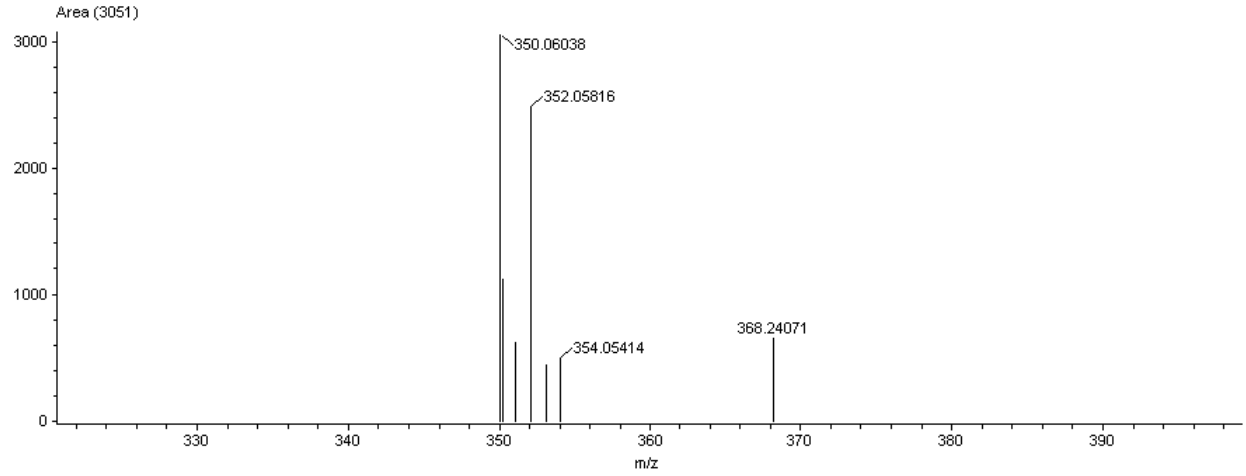
Spectra 4.10. ^{1}H NMR of [($C_{10}H_6$(^{i}PrN)$_2$C)CuCl]$_2$ (**4.3**) at 230 K (top) and 300 K (bottom) in C_7D_8.



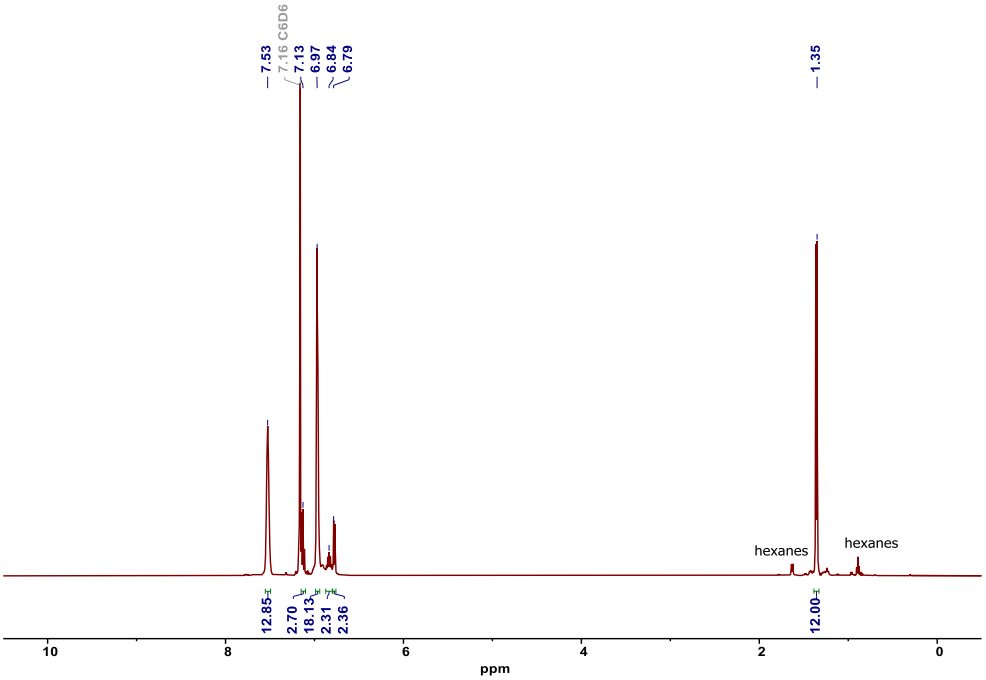
Spectra 4.11. COSY of [($C_{10}H_6$(^{i}PrN)$_2$C)CuCl]$_2$ (**4.3**) at 230 K in C_7D_8.



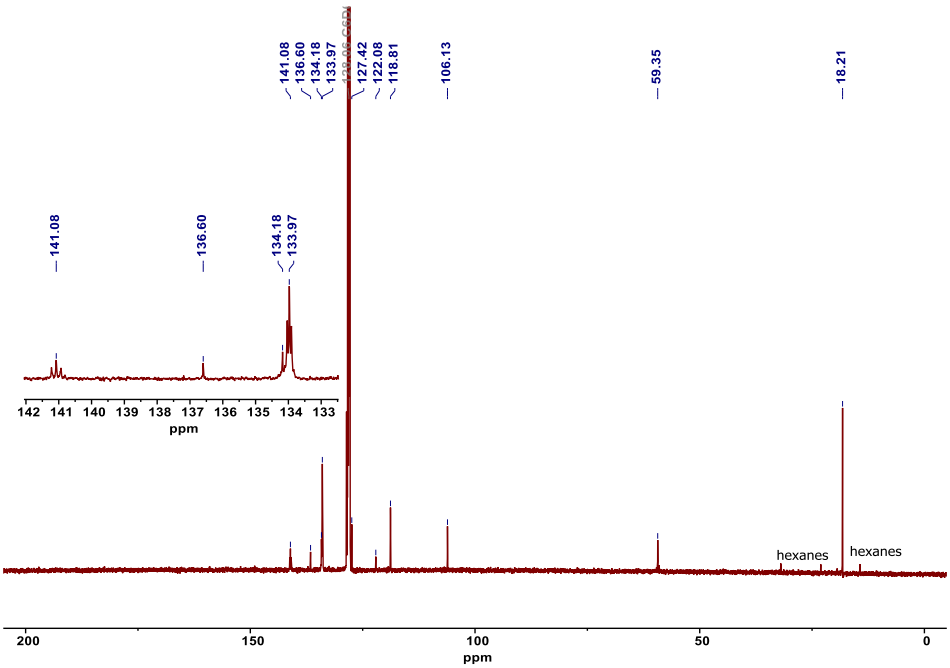
Spectra 4.12. ATR IR of $[(C_{10}H_6(^{i}PrN)_2C)CuCl]_2$ (**4.3**).



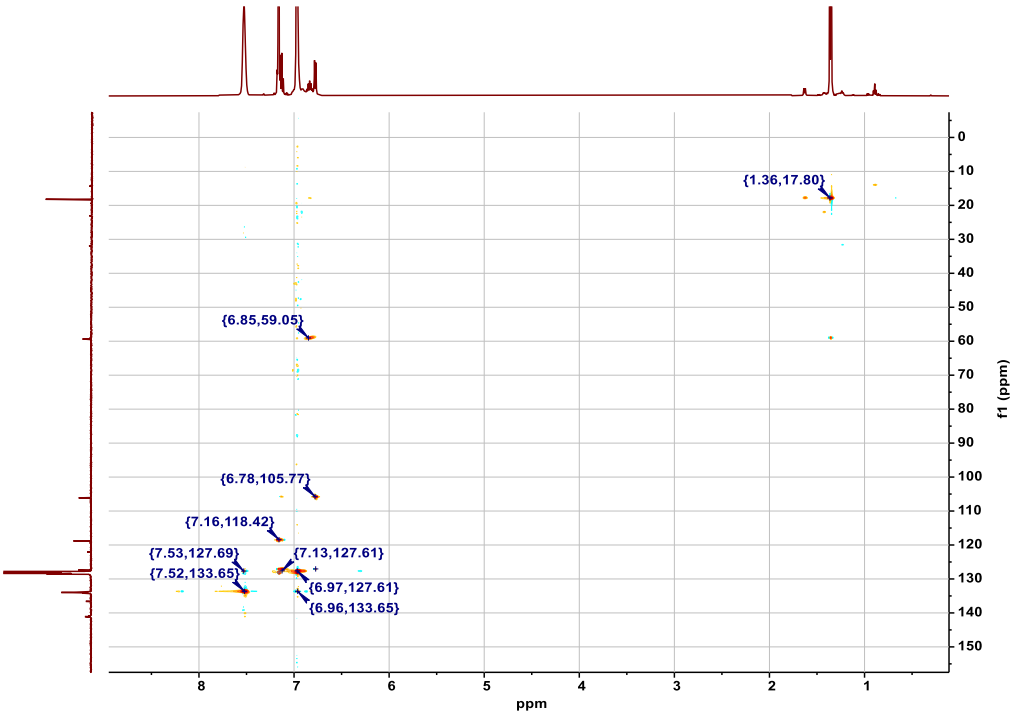
Spectra 4.13. MS of $[(C_{10}H_6(^{i}PrN)_2C)CuCl]_2$ (**4.3**).



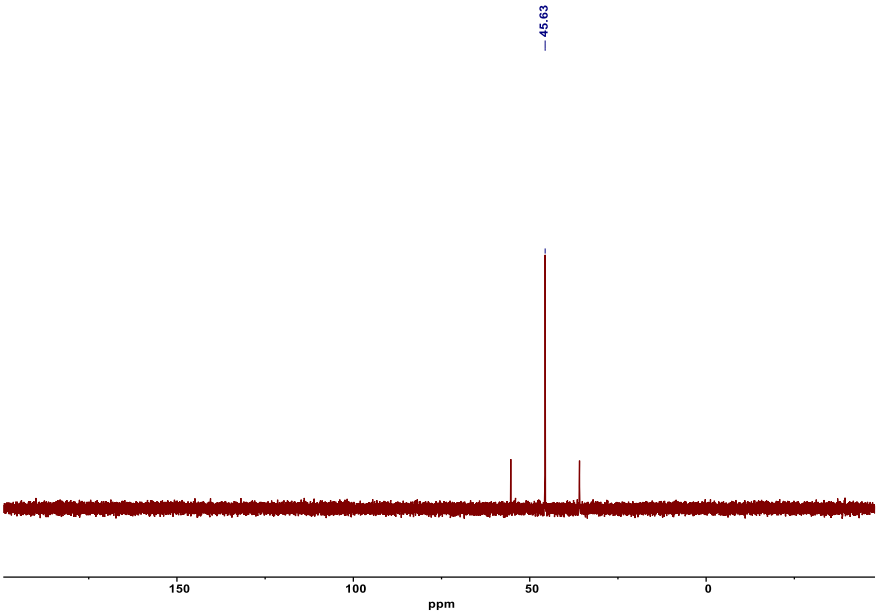
Spectra 4.14. ^{1}H NMR of ($C_{10}H_6(^{i}PrN)_2C$)Pt(PPh_3)$_2$ (**4.4**) in C_6D_6.



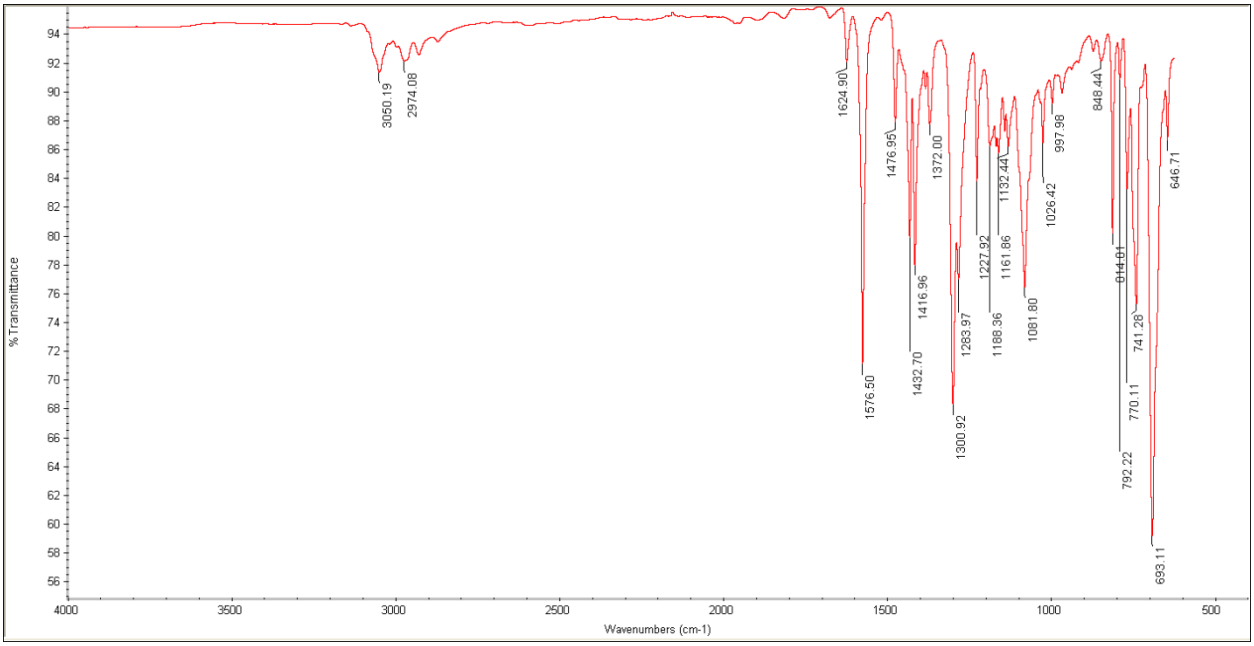
Spectra 4.15. ^{13}C NMR of ($C_{10}H_6(^{i}PrN)_2C$)Pt(PPh_3)$_2$ (**4.4**) in C_6D_6.



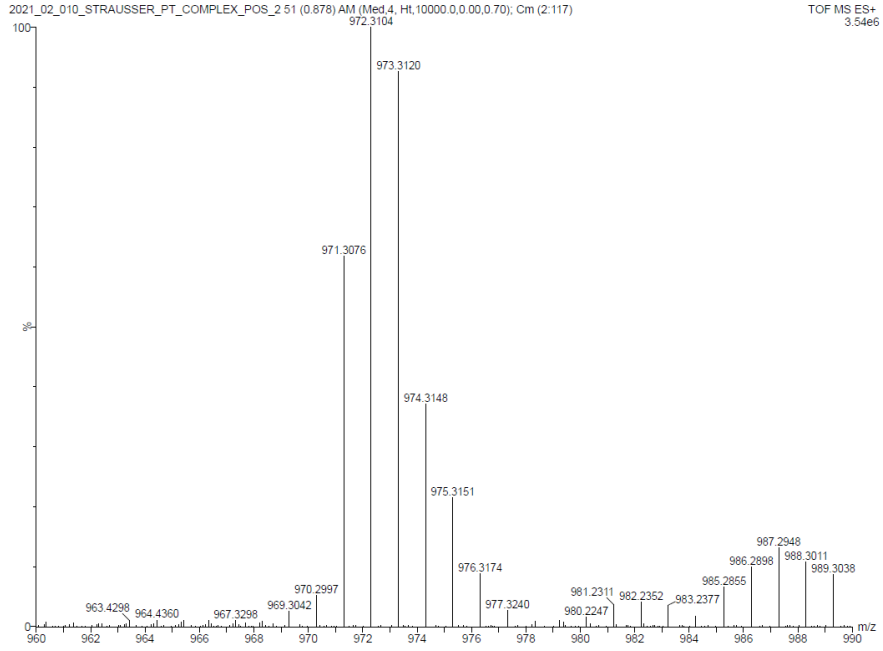
Spectra 4.16. HSQC of ($C_{10}H_6(^{i}PrN)_2C$)Pt(PPh_3)$_2$ (**4.4**) in C_6D_6.



Spectra 4.17. ^{31}P NMR of ($C_{10}H_6(^{i}PrN)_2C$)Pt(PPh_3)$_2$ (**4.4**) in C_6D_6.



Spectra 4.18. IR of $(C_{10}H_6(^{i}PrN)_2C)Pt(PPh_3)_2$ (**4.4**).



Spectra 4.19. MS of $(C_{10}H_6(^{i}PrN)_2C)Pt(PPh_3)_2$ (**4.4**).

References

1. Crudden, C. M.; Allen, D. P., Stability and reactivity of N-heterocyclic carbene complexes. *Coordination Chemistry Reviews* **2004,** *248*, 2247-2273.
2. Díez-González, S.; Marion, N.; Nolan, S. P., N-Heterocyclic Carbenes in Late Transition Metal Catalysis. *Chemical Reviews* **2009,** *109*, 3612-3676.
3. Mercs, L.; Albrecht, M., Beyond catalysis: N-heterocyclic carbene complexes as components for medicinal, luminescent, and functional materials applications. *Chemical Society Reviews* **2010,** *39*, 1903-1912.
4. Smith, C. A.; Narouz, M. R.; Lummis, P. A.; Singh, I.; Nazemi, A.; Li, C.-H.; Crudden, C. M., N-Heterocyclic Carbenes in Materials Chemistry. *Chemical Reviews* **2019,** *119*, 4986-5056.
5. De Jesus, J. F.; Sherman, L. M.; Yohannan, D. J.; Becca, J. C.; Strausser, S. L.; Karger, L. F. P.; Jensen, L.; Jenkins, D. M.; Camden, J. P., A Benchtop Method for Appending Protic Functional Groups to N-Heterocyclic Carbene Protected Gold Nanoparticles. *Angew. Chem., Int. Ed.* **2020,** *59*, 7585-7590.
6. Benhamou, L.; Chardon, E.; Lavigne, G.; Bellemin-Laponnaz, S.; César, V., Synthetic Routes to N-Heterocyclic Carbene Precursors. *Chemical Reviews* **2011,** *111*, 2705-2733.
7. Garber, S. B.; Kingsbury, J. S.; Gray, B. L.; Hoveyda, A. H., Efficient and Recyclable Monomeric and Dendritic Ru-Based Metathesis Catalysts. *Journal of the American Chemical Society* **2000,** *122*, 8168-8179.
8. Sanford, M. S.; Love, J. A.; Grubbs, R. H., Mechanism and Activity of Ruthenium Olefin Metathesis Catalysts. *Journal of the American Chemical Society* **2001,** *123*, 6543-6554.
9. Lavallo, V.; Canac, Y.; Präsang, C.; Donnadieu, B.; Bertrand, G., Stable Cyclic (Alkyl)(Amino)Carbenes as Rigid or Flexible, Bulky, Electron-Rich Ligands for Transition-Metal Catalysts: A Quaternary Carbon Atom Makes the Difference. *Angewandte Chemie International Edition* **2005,** *44*, 5705-5709.
10. Schuster, O.; Yang, L.; Raubenheimer, H. G.; Albrecht, M., Beyond Conventional N-Heterocyclic Carbenes: Abnormal, Remote, and Other Classes of NHC Ligands with Reduced Heteroatom Stabilization. *Chemical Reviews* **2009,** *109*, 3445-3478.
11. Wang, F.; Liu, L.-j.; Wang, W.; Li, S.; Shi, M., Chiral NHC–metal-based asymmetric catalysis. *Coordination Chemistry Reviews* **2012,** *256*, 804-853.
12. Marx, V. M.; Sullivan, A. H.; Melaimi, M.; Virgil, S. C.; Keitz, B. K.; Weinberger, D. S.; Bertrand, G.; Grubbs, R. H., Cyclic Alkyl Amino Carbene (CAAC) Ruthenium Complexes as Remarkably Active Catalysts for Ethenolysis. **2015,** *54*, 1919-1923.
13. Melaimi, M.; Jazzar, R.; Soleilhavoup, M.; Bertrand, G., Cyclic (Alkyl)(amino)carbenes (CAACs): Recent Developments. **2017,** *56*, 10046-10068.
14. Ranganath, K. V. S.; Kloesges, J.; Schäfer, A. H.; Glorius, F., Asymmetric Nanocatalysis: N-Heterocyclic Carbenes as Chiral Modifiers of Fe_3O_4/Pd nanoparticles. *Angewandte Chemie International Edition* **2010,** *49*, 7786-7789.
15. Vougioukalakis, G. C.; Grubbs, R. H., Ruthenium-Based Heterocyclic Carbene-Coordinated Olefin Metathesis Catalysts. *Chemical Reviews* **2010,** *110*, 1746-1787.
16. Endo, K.; Grubbs, R. H., Chelated Ruthenium Catalysts for Z-Selective Olefin Metathesis. *Journal of the American Chemical Society* **2011,** *133*, 8525-8527.

17. Moerdyk, J. P.; Schilter, D.; Bielawski, C. W., N,N′-Diamidocarbenes: Isolable Divalent Carbons with Bona Fide Carbene Reactivity. *Accounts of Chemical Research* **2016,** *49*, 1458-1468.
18. Takebayashi, S.; Fayzullin, R. R., [Co(NHC)$(CO)_3$]: Isolation and Reactivity Study of a Model 17-Electron Species in the Oxo Process. *Organometallics* **2021,** *40*, 500-507.
19. Horsley Downie, T. M.; Hall, J. W.; Collier Finn, T. P.; Liptrot, D. J.; Lowe, J. P.; Mahon, M. F.; McMullin, C. L.; Whittlesey, M. K., The first ring-expanded NHC–copper(i) phosphides as catalysts in the highly selective hydrophosphination of isocyanates. *Chemical Communications* **2020,** *56*, 13359-13362.
20. Bermesheva, E. V.; Wozniak, A. I.; Andreyanov, F. A.; Karpov, G. O.; Nechaev, M. S.; Asachenko, A. F.; Topchiy, M. A.; Melnikova, E. K.; Nelyubina, Y. V.; Gribanov, P. S.; Bermeshev, M. V., Polymerization of 5-Alkylidene-2-norbornenes with Highly Active Pd–N-Heterocyclic Carbene Complex Catalysts: Catalyst Structure–Activity Relationships. *ACS Catalysis* **2020,** *10*, 1663-1678.
21. Benedikter, M. J.; Musso, J. V.; Frey, W.; Schowner, R.; Buchmeiser, M. R., Cationic Group VI Metal Imido Alkylidene N-Heterocyclic Carbene Nitrile Complexes: Bench-Stable, Functional-Group-Tolerant Olefin Metathesis Catalysts. *Angewandte Chemie International Edition* **2021,** *60*, 1374-1382.
22. Bazinet, P.; Yap, G. P. A.; Richeson, D. S., Constructing a Stable Carbene with a Novel Topology and Electronic Framework. *Journal of the American Chemical Society* **2003,** *125*, 13314-13315.
23. Bazinet, P.; Ong, T.-G.; O'Brien, J. S.; Lavoie, N.; Bell, E.; Yap, G. P. A.; Korobkov, I.; Richeson, D. S., Design of Sterically Demanding, Electron-Rich Carbene Ligands with the Perimidine Scaffold. *Organometallics* **2007,** *26*, 2885-2895.
24. Lee, S.; Gabidullin, B.; Richeson, D., Distinct Palladium(II) Carbene Complexes Supported by Six-Membered 1,3-Disubstituted Permidin-2-ylidene, Six-Membered N-Heterocyclic Carbenes. *ACS Omega* **2018,** *3*, 6587-6594.
25. Tsurugi, H.; Fujita, S.; Choi, G.; Yamagata, T.; Ito, S.; Miyasaka, H.; Mashima, K., Carboxylate Ligand-Induced Intramolecular C−H Bond Activation of Iridium Complexes with N-Phenylperimidine-Based Carbene Ligands. *Organometallics* **2010,** *29*, 4120-4129.
26. Choi, G.; Tsurugi, H.; Mashima, K., Hemilabile N-Xylyl-N′-methylperimidine Carbene Iridium Complexes as Catalysts for C–H Activation and Dehydrogenative Silylation: Dual Role of N-Xylyl Moiety for ortho-C–H Bond Activation and Reductive Bond Cleavage. *Journal of the American Chemical Society* **2013,** *135*, 13149-13161.
27. Hill, A. F.; McQueen, C. M. A., Dihydroperimidine-Derived N-Heterocyclic Pincer Carbene Complexes via Double C–H Activation. *Organometallics* **2012,** *31*, 8051-8054.
28. McQueen, C. M. A.; Hill, A. F.; Ma, C.; Ward, J. S., Ruthenium and osmium complexes of dihydroperimidine-based N-heterocyclic carbene pincer ligands. *Dalton Transactions* **2015,** *44*, 20376-20385.
29. Hill, A. F.; Ma, C.; McQueen, C. M. A.; Ward, J. S., Iridium complexes of perimidine-based N-heterocyclic carbene pincer ligands via aminal C–H activation. *Dalton Transactions* **2018,** *47*, 1577-1587.
30. Lam, R. H.; McQueen, C. M. A.; Pernik, I.; McBurney, R. T.; Hill, A. F.; Messerle, B. A., Selective formylation or methylation of amines using carbon dioxide catalysed by a rhodium perimidine-based NHC complex. *Green Chemistry* **2019,** *21*, 538-549.

31. Özdemir, İ.; Alıcı, B.; Gürbüz, N.; Çetinkaya, E.; Çetinkaya, B., In situ generated palladium catalysts bearing 1,3-dialkylperimidin-2-yline ligands for Suzuki reactions of aryl chlorides. *Journal of Molecular Catalysis A: Chemical* **2004,** *217*, 37-40.
32. Tu, T.; Malineni, J.; Bao, X.; Dötz, K. H., A Lutidine-Bridged Bis-Perimidinium Salt: Synthesis and Application as a Precursor in Palladium-Catalyzed Cross-Coupling Reactions. *Advanced Synthesis & Catalysis* **2009,** *351*, 1029-1034.
33. Toda, T.; Kuwata, S., Central N-heterocyclic carbene moieties in protic pincer-type bis(pyrazole) ligands: Perturbation on steric and electronic properties of ruthenium center. *Journal of Organometallic Chemistry* **2020,** *917*, 121270.
34. Oehninger, L.; Küster, L. N.; Schmidt, C.; Muñoz-Castro, A.; Prokop, A.; Ott, I., A Chemical–Biological Evaluation of Rhodium(I) N-Heterocyclic Carbene Complexes as Prospective Anticancer Drugs. *Chemistry – A European Journal* **2013,** *19*, 17871-17880.
35. Langbein, S.; Wadepohl, H.; Gade, L. H., Ditopic N-Heterocyclic Pincer Carbene Complexes Containing a Perylene Backbone. *Organometallics* **2016,** *35*, 809-815.
36. Richeson, D. S.; Bazinet, P. R. Preparation of carbene ligands and their transition metal complexes useful as catalysts for organic synthesis. 2005.
37. Krieck, S.; Schulze, D.; Görls, H.; Westerhausen, M., Coordination Chemistry of N,N′-Bis(diphenylphosphanylmethyl)- 2,3-dihydro-1H-perimidine – Lewis Acid-Base Complexes with the d10-Metals Nickel(0) and Gold(I). *Zeitschrift für Naturforschung B* **2014,** *69*, 1299-1305.
38. Akıncı, P. A.; Gülcemal, S.; Kazheva, O. N.; Alexandrov, G. G.; Dyachenko, O. A.; Çetinkaya, E.; Çetinkaya, B., Perimidin-2-ylidene rhodium(I) complexes; unexpected halogen exchange and catalytic activities in transfer hydrogenation reaction. *Journal of Organometallic Chemistry* **2014,** *765*, 23-30.
39. Verlinden, K.; Ganter, C., Converting a perimidine derivative to a cationic N-heterocyclic carbene. *Journal of Organometallic Chemistry* **2014,** *750*, 23-29.
40. Hill, A. F.; McQueen, C. M. A., Dihydroperimidine-Derived PNP Pincer Complexes as Intermediates en Route to N-Heterocyclic Carbene Pincer Complexes. *Organometallics* **2014,** *33*, 1909-1912.
41. Baker, M. V.; Barnard, P. J.; Berners-Price, S. J.; Brayshaw, S. K.; Hickey, J. L.; Skelton, B. W.; White, A. H., Synthesis and structural characterisation of linear Au(I) N-heterocyclic carbene complexes: New analogues of the Au(I) phosphine drug Auranofin. *Journal of Organometallic Chemistry* **2005,** *690*, 5625-5635.
42. Griffiths, M. B. E.; Koponen, S. E.; Mandia, D. J.; McLeod, J. F.; Coyle, J. P.; Sims, J. J.; Giorgi, J. B.; Sirianni, E. R.; Yap, G. P. A.; Barry, S. T., Surfactant Directed Growth of Gold Metal Nanoplates by Chemical Vapor Deposition. *Chemistry of Materials* **2015,** *27*, 6116-6124.
43. Ray, L.; Katiyar, V.; Barman, S.; Raihan, M. J.; Nanavati, H.; Shaikh, M. M.; Ghosh, P., Gold(I) N-heterocyclic carbene based initiators for bulk ring-opening polymerization of l-lactide. *Journal of Organometallic Chemistry* **2007,** *692*, 4259-4269.
44. Sampford, K. R.; Carden, J. L.; Kidner, E. B.; Berry, A.; Cavell, K. J.; Murphy, D. M.; Kariuki, B. M.; Newman, P. D., Twisting the arm: structural constraints in bicyclic expanded-ring N-heterocyclic carbenes. *Dalton Transactions* **2019,** *48*, 1850-1858.
45. Okayama, T.; Watanabe, T.; Hatayama, Y.; Ishihara, S.; Yamaguchi, Y., Transformation of NHC·BEt_3 into AgCl·NHC: Efficiently preparative method for early–

late heterobimetallic complexes using indenyl-functionalized N-heterocyclic carbene as a bridging ligand. *Inorganica Chimica Acta* **2016,** *448*, 1-6.
46. Doud, E. A.; Inkpen, M. S.; Lovat, G.; Montes, E.; Paley, D. W.; Steigerwald, M. L.; Vázquez, H.; Venkataraman, L.; Roy, X., In Situ Formation of N-Heterocyclic Carbene-Bound Single-Molecule Junctions. *Journal of the American Chemical Society* **2018,** *140*, 8944-8949.
47. de Frémont, P.; Scott, N. M.; Stevens, E. D.; Ramnial, T.; Lightbody, O. C.; Macdonald, C. L. B.; Clyburne, J. A. C.; Abernethy, C. D.; Nolan, S. P., Synthesis of Well-Defined N-Heterocyclic Carbene Silver(I) Complexes. *Organometallics* **2005,** *24*, 6301-6309.
48. Ogle, J. W.; Zhang, J.; Reibenspies, J. H.; Abboud, K. A.; Miller, S. A., Synthesis of Electronically Diverse Tetraarylimidazolylidene Carbenes via Catalytic Aldimine Coupling. *Organic Letters* **2008,** *10*, 3677-3680.
49. Herrmann, W. A.; Schneider, S. K.; Öfele, K.; Sakamoto, M.; Herdtweck, E., First silver complexes of tetrahydropyrimid-2-ylidenes. *Journal of Organometallic Chemistry* **2004,** *689*, 2441-2449.
50. Humenny, W. J.; Mitzinger, S.; Khadka, C. B.; Najafabadi, B. K.; Vieira, I.; Corrigan, J. F., N-heterocyclic carbene stabilized copper- and silver-phenylchalcogenolate ring complexes. *Dalton Transactions* **2012,** *41*, 4413-4422.
51. Collins, L. R.; Lowe, J. P.; Mahon, M. F.; Poulten, R. C.; Whittlesey, M. K., Copper Diamidocarbene Complexes: Characterization of Monomeric to Tetrameric Species. *Inorganic Chemistry* **2014,** *53*, 2699-2707.
52. Hardman, N. J.; Abrams, M. B.; Pribisko, M. A.; Gilbert, T. M.; Martin, R. L.; Kubas, G. J.; Baker, R. T., Molecular and Electronic Structure of Platinum Bis(N-arylamino)phosphenium Complexes including [Pt(phosphane)(phosphenium)(N-heterocyclic carbene)]. *Angewandte Chemie International Edition* **2004,** *43*, 1955-1958.
53. Silbestri, G. F.; Flores, J. C.; de Jesús, E., Water-Soluble N-Heterocyclic Carbene Platinum(0) Complexes: Recyclable Catalysts for the Hydrosilylation of Alkynes in Water at Room Temperature. *Organometallics* **2012,** *31*, 3355-3360.
54. Arduengo, A. J.; Gamper, S. F.; Calabrese, J. C.; Davidson, F., Low-Coordinate Carbene Complexes of Nickel(0) and Platinum(0). *Journal of the American Chemical Society* **1994,** *116*, 4391-4394.
55. Arnold, P. L.; Cloke, F. G. N.; Geldbach, T.; Hitchcock, P. B., Metal Vapor Synthesis as a Straightforward Route to Group 10 Homoleptic Carbene Complexes. *Organometallics* **1999,** *18*, 3228-3233.
56. Fortman, G. C.; Scott, N. M.; Linden, A.; Stevens, E. D.; Dorta, R.; Nolan, S. P., Unusual reactivities of N-heterocyclic carbenes upon coordination to the platinum(ii)–dimethyl moiety. *Chemical Communications* **2010,** *46*, 1050-1052.
57. Bauer, J.; Braunschweig, H.; Brenner, P.; Kraft, K.; Radacki, K.; Schwab, K., Late-Transition-Metal Complexes as Tunable Lewis Bases. *Chemistry – A European Journal* **2010,** *16*, 11985-11992.
58. Bauer, J.; Bertermann, R.; Braunschweig, H.; Gruss, K.; Hupp, F.; Kramer, T., New Metal-Only Lewis Pairs: Elucidating the Electronic Influence of N-Heterocyclic Carbenes and Phosphines on the Dative Pt-Al Bond. *Inorganic Chemistry* **2012,** *51*, 5617-5626.

59. Hupp, F.; Ma, M.; Kroll, F.; Jimenez-Halla, J. O. C.; Dewhurst, R. D.; Radacki, K.; Stasch, A.; Jones, C.; Braunschweig, H., Platinum Complexes Containing Pyramidalized Germanium and Tin Dihalide Ligands Bound through σ,σ M□E Multiple Bonds. *Chemistry – A European Journal* **2014,** *20*, 16888-16898.
60. Şahin-Bölükbaşı, S.; Şahin, N., Novel Silver-NHC complexes: Synthesis and anticancer properties. *Journal of Organometallic Chemistry* **2019,** *891*, 78-84.
61. Haque, R. A.; Ghdhayeb, M. Z.; Budagumpi, S.; Salman, A. W.; Ahamed, M. B. K.; Abdul Majid, A. M. S., Non-symmetrically substituted N-heterocyclic carbene-Ag(I) complexes of benzimidazol-2-ylidenes: Synthesis, crystal structures, anticancer activity and transmetallation studies. *Inorg. Chim. Acta* **2013,** *394*, 519-525.
62. Weiss, D. T.; Altmann, P. J.; Haslinger, S.; Jandl, C.; Poethig, A.; Cokoja, M.; Kuehn, F. E., Structural diversity of late transition metal complexes with flexible tetra-NHC ligands. *Dalton Trans.* **2015,** *44*, 18329-18339.
63. Hameury, S.; de Fremont, P.; Breuil, P.-A. R.; Olivier-Bourbigou, H.; Braunstein, P., Synthesis and characterization of oxygen-functionalised-NHC silver(i) complexes and NHC transmetallation to nickel(ii). *Dalton Trans.* **2014,** *43*, 4700-4710.
64. Lu, Z.; Cramer, S. A.; Jenkins, D. M., Exploiting a dimeric silver transmetallating reagent to synthesize macrocyclic tetracarbene complexes. *Chem. Sci.* **2012,** *3*, 3081-3087.
65. Richeson, D. S. B., P. R. Preparation of carbene ligands and their transition metal complexes useful as catalysts for organic synthesis. 2005.

Chapter 5 : Preparation of N-Heterocyclic Carbene Gold complexes for Collaborative Projects

Abstract

Most of my research over the last five years has been to work with collaborators at the University of Notre Dame (Camden lab) and the University of Tennessee (Sharma lab). Since these projects are highly collaborative, there is a need to synthesize various metal complexes which have been previously published or can be synthesized with a small variation of literature procedures. While these complexes have mostly been reported before, my contribution to be manuscripts were necessary to answer fundamental questions regarding NHC surface chemistry. In addition to the previous published and submitted work (Chapters 2-4), there are three manuscripts in preparation for which I have contributed N-heterocyclic carbene gold complexes. This chapter will discuss the summaries and what I have specifically contributed to each manuscript.

Manuscripts in Preparation

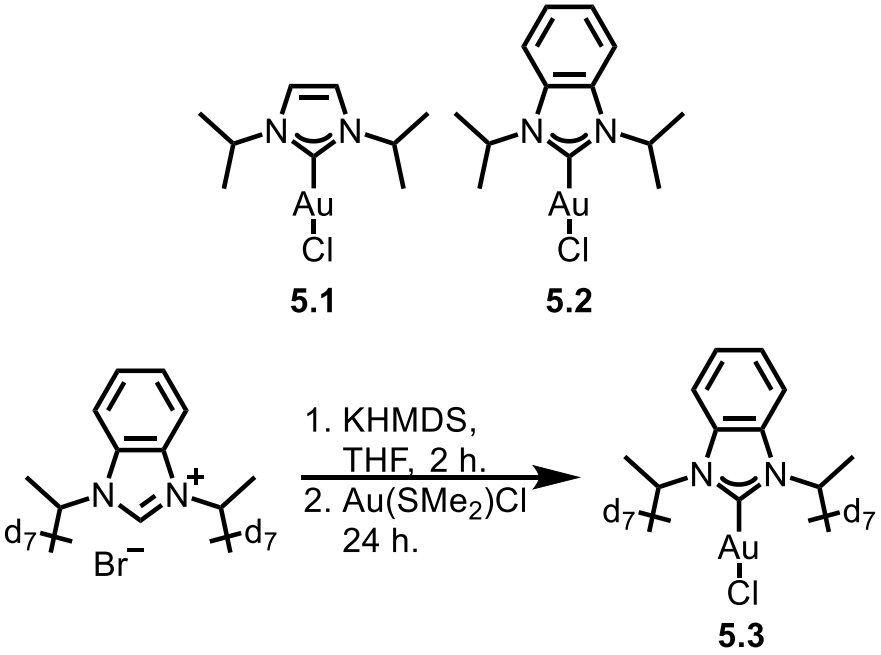
Direct measurement of N-heterocyclic carbenes on Au nanoparticles with laser desorption ionization mass spectrometry

Nathaniel L. Dominique,[†] **Shelby L. Strausser,[‡]** Jacob Olson,[†] Bill Boggess,[†] David M. Jenkins,[‡*] and Jon P. Camden[†*]

Gold surface chemistry lies at the center of advancements in heterogeneous catalysis, biosensors, and drug delivery systems. To utilize these surfaces, a self-assembled monolayer with functional groups is tethered to the surface. General surface functionalization performed using thiol chemistries are limited as thiols degrade in oxidative, thermal and biologically relevant environments. In Crudden, Johnson, and our work, N-Heterocyclic carbenes (NHC) have proved to be superior over thiols due to their great stability in harsh conditions. While NHCs are ideal to functionalize gold surfaces, the characterization methods for such surfaces have been limited to binary techniques (X-ray Photoelectron Microscopy and Scanning Electron Microscopy). Our original reports utilize surface-enhanced Raman spectroscopy (SERS), though this is limited to small molecule binding groups with low background signal to track reactions and in biological applications. In addition, SERS is dependent on the analyte of interest to be close to the surface for signal enhancement, therefore biologically relevant molecules might be too large to see using SERS. One method that is used for thiol coated gold nanoparticles is surface-assisted laser desorption ionization (SALDI) mass spectrometry, though this method has not been explored for NHC gold nanoparticles (AuNPs). With the Camden group at Notre Dame University, we report the synthesis of known and a newly synthesized deuterated isotopologue NHC gold chloride complexes and demonstrate its characterization using SALDI.

My contribution to this manuscript was to synthesize previously published NHC-AuCl complexes (**Scheme 5.1**, top) that were necessary to develop a general method for SALDI to characterize NHC-AuNPs. In addition to previously published complexes, I synthesized and characterized a d_{14}-benzimidazolium gold chloride complex (**Scheme 5.1**, bottom). All complexes were confirmed and characterized through ^{1}H NMR, ^{13}C NMR, HR-MS, and IR. Complexes **5.1**[1] and **5.2**[2] match previous literature. The synthesis of **6.3** starts with the d_{14}-benzimidazolium bromide salt, which was synthesized following our previous publication.[3] In an nitrogen filled glovebox the bromide salt was deprotonated with KHMDS for two hours. Afterwards, the mixture was filtered over Celite to remove KBr from the reaction. This solution was added to a vial containing $Au(SMe_2)Cl$ and stirred for 24 hours. The reaction was worked up in air by removing the solvent, extracting the residue with methylene chloride, and filtering over a Celite pad. The solvent of the filtrate was reduced to 2 mL and was added to hexanes to precipitate the product. The solid was collected, yielding **6.3** as a white solid. Confirmation of the product from the starting bromide salt was shown by the disappearance of the C2 C-H around 9 ppm in the ^{1}H NMR and with the shift of the C2 carbon peak from 130 ppm to 176 ppm in the ^{13}C NMR. This contribution of synthesis allowed for the Camden group to develop a general method for characterization of NHC coated AuNPs using SALDI.

Scheme 5.1: Target molecules previously synthesized (top). Synthesis of **5.3** from previously synthesized benzimidazolium bromide salt.

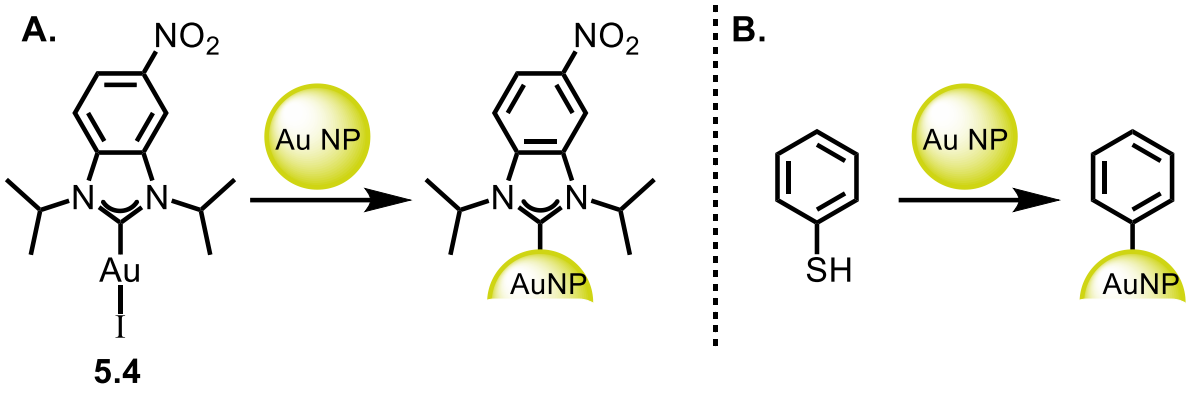


Surface-Enhanced Spatially-Offset Raman Spectroscopy for Non-invasive Deep Tissue Chemical Sensing.

Paula A. Pimiento, **Shelby L. Strausser**, Jon P. Camden, David M. Jenkins,* and Bhavya Sharma*

Optical sensors for *in vivo* sensing are limited to within a few millimeters of depth in tissue, constraining their applications, but, critically, they can provide chemical information by observing chemical phenomena such as bond vibrations. By combining surface-enhanced Raman spectroscopy (SERS) and spatially-offset Raman spectroscopy (SORS), commonly referred to as SESORS, vibrational signatures can be detected, for the first time, up to 26 mm deep in porcine tissue. The SERS probe is a 40 nm gold nanoparticle (AuNP) functionalized with a nitro-N-heterocyclic carbene (NHC) ligand. The NHC ligands show greater stability and robustness compared to traditional thiol-based probes. Furthermore, the SESORS signal of NHC-AuNPs injected at 6 mm depth in tissue is detected immediately after injection and remains detectable in tissue up to 15 hours later. These combined results demonstrate that with appropriate probes SESORS shows great promise for chemical sensing and imaging at tissue depths and time scales that are relevant for medicinal tomography.

My contribution to this manuscript was to synthesize the NO_2-benzimidazolium-AuI complex (**5.4**) and place them onto 40 nm sized nanoparticles. The Au complex was synthesized following our previous publication.[4] I then synthesized 40 nm AuNPs following the method of Frens.[5] The resulting nanoparticles exhibit a plasmon band at 527 nm measured by UV-VIS spectroscopy. The purpose was to test the stability of thiols versus NHCs on AuNPs in tissues. This was done following our previous method[4] keeping the overall concentration of the ligands in solution the same. 1.42 µL of a 1mM solution of **5.4** in CH_2Cl_2 was added to 20 mL of the 40 nm AuNPs. The AuNP solution was agitated on an orbital shaker (MaxQ 2000 Orbital Shaker, Thermo Scientific) at 300 RPM for 10 minutes. After, 3.6 mL of a 1M NaBr solution was added to aggregate the NPs for testing in tissues. The benzene thiol coated nanoparticles were synthesized the same as the NHC AuNPs above. This contribution of synthesis allowed for the Sharma group to test the stability of NHC AuNPs in tissues.



5.4

Scheme 5.2: Functionalization of 40nm gold nanoparticles with A. NO_2-benzimidazolium NHC and B. benzenethiol.

Experimental

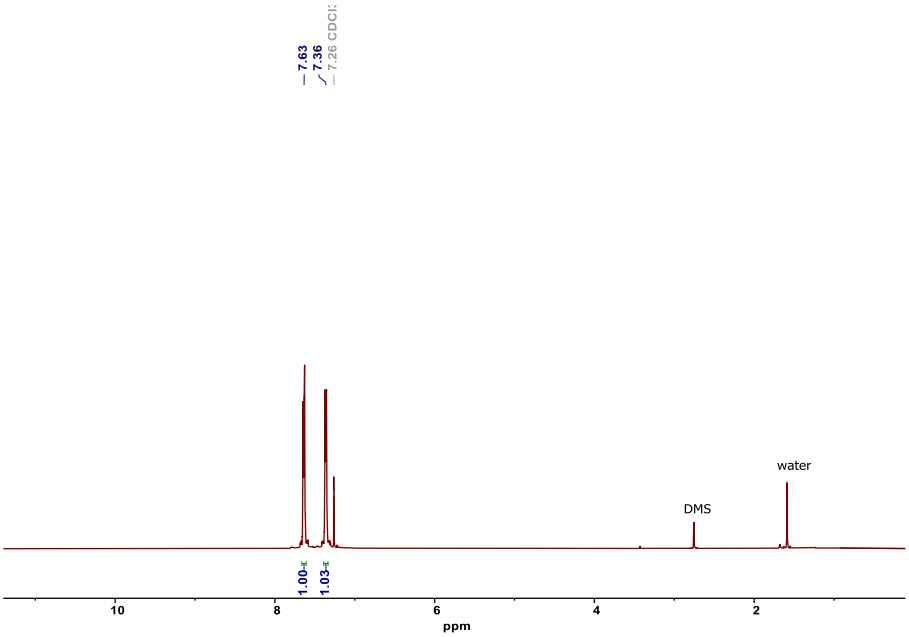
General Considerations

All glassware for air and water sensitive reactions were dried at 170 °C overnight before use. All reactions were stirred vigorously with magnetic stirrers. A glovebox with a dinitrogen atmosphere was used for formation of the gold complexes. Tetrahydrofuran was dried on an Innovative Technologies (Newburyport, MA) Pure Solv MD-7 Solvent Purification System, degassed by three freeze-pump-thaw cycles on a Schlenk line to remove dioxygen and stored under activated 4 Å molecular sieves prior to use. Celite® was dried at 240 °C under vacuum overnight and stored in a dinitrogen glovebox. All other compounds were purchased from commercial vendors at highest available purity and used without any further purification. All deuterium labeling sources were purchased from Cambridge Isotope at a minimum of 98% deuteration. Solution ^{1}H NMR and ^{13}C NMR were performed on a Bruker 500 MHz narrow-bore broadband system 298 K. All ^{1}H and ^{13}C shifts were referenced to the residual solvent.

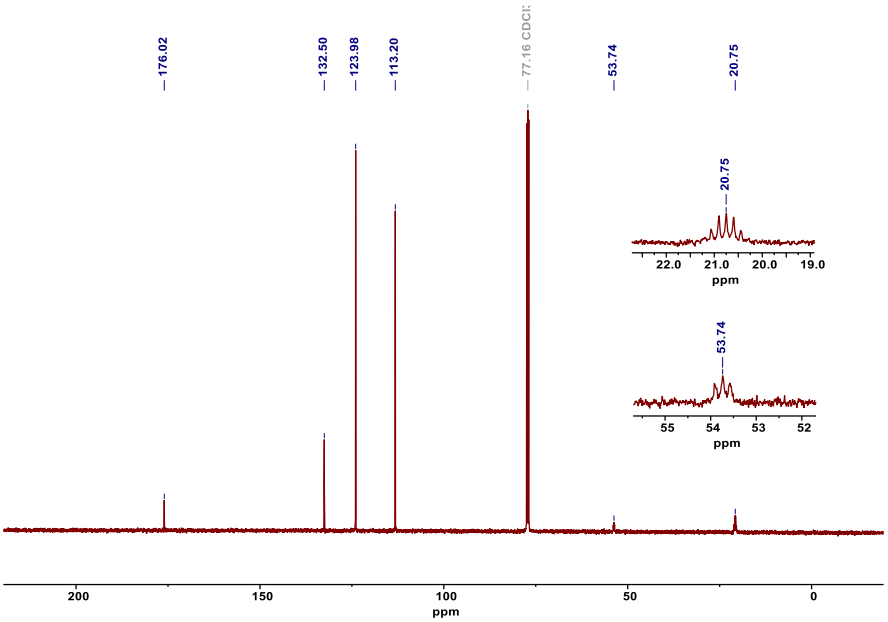
All mass spectrometry analyses were conducted at the Mass Spectrometry Center located in the Department of Chemistry at the University of Tennessee. The MALDI HR-MS analysis of **5.3** was preformed using a Waters Synapt G2-S*i* qTOF instrument with MALDI ion source with a 355 nm laser. A polished steel sample target was employed for all experiments and samples were spotted at a volume of 1µL with no matrix. For positive ion mode scans, the reflector was set to reflector positive mode and data collected from 100-2,000 daltons. In general, 1000 laser shots per spectra was taken with a scan time of 1 second. Solutions for mass spectrometry were prepared in methanol. Infrared spectra were collected on a Thermo Scientific Nicolet iS10 with a Smart iTR accessory for attenuated total reflectance (ATR) using the neat molecules.

Synthesis of d_{14}-benzimidazolium gold(I) chloride (5.3):

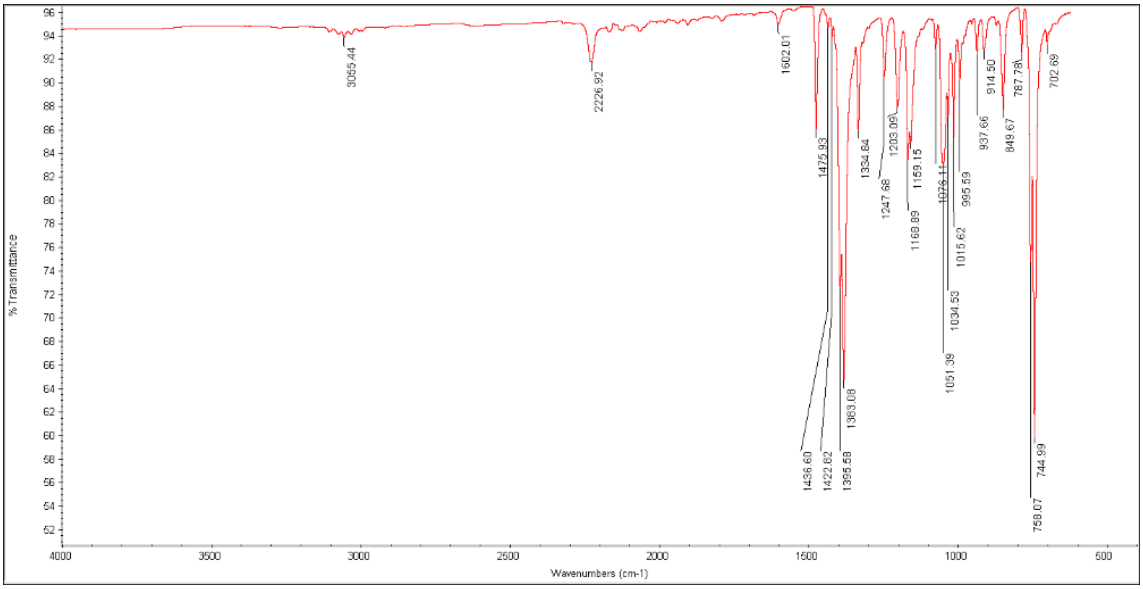
In an inert atmosphere, d_{14}-benzimidazolium bromide salt (0.1625 g, 0.5466 mmols) and KHMDS (0.1090 g, 0.5464 mmols) were measured out into separate vials each equipped with a stir bar. 5 mL of THF was added to each vial and the KHMDS solution was added to the bromide salt suspension and stirred for 1.5 hours. The slurry was then filtered over a pad of Celite into a vial charged with a stir bar and $Au(SMe_2)Cl$ (0.1610 g, 0.5466 mmols). This mixture then stirred overnight at RT. The reaction was then removed from the glovebox and dried under vacuum. The residue was extracted with 40 mL CH_2Cl_2 and filtered over a short Celite plug rinsing with additional CH_2Cl_2 until the filtrate becomes colorless. The volume of the filtrate was reduced to 2 mL and was slowly added to a stirring solution of 80 mL hexanes, over the course of addition a solid precipitated. The solid was collected over a fine frit and dried under vacuum to give a white powder. Yield 0.184 g, 75.0%. ^{1}H NMR ($CDCl_3$, 499.74 MHz): δ 7.63 (m, 2H), 7.36 (m, 2H). ^{13}C NMR ($CDCl_3$, 150.81 MHz): δ 176.02, 132.50, 123.98, 113.20, 53.74 (t, *J* = 19.9 Hz), 20.75 (sept, *J* = 19.08 Hz). IR: 3055, 2227, 1602, 1476, 1437, 1423, 1395, 1383, 1335, 1248, 1203, 1169, 1159, 1076, 1051, 1034, 1015, 996, 938, 915, 850, 788, 758, 745, 70 cm^{-1}. MALDI HR-MS (m/z): $[L_2Au]^+$ 629.4364: (found), $[(C_{13}H_4D_{14}N_2)_2Au]^+$: 629.4357 (calc).



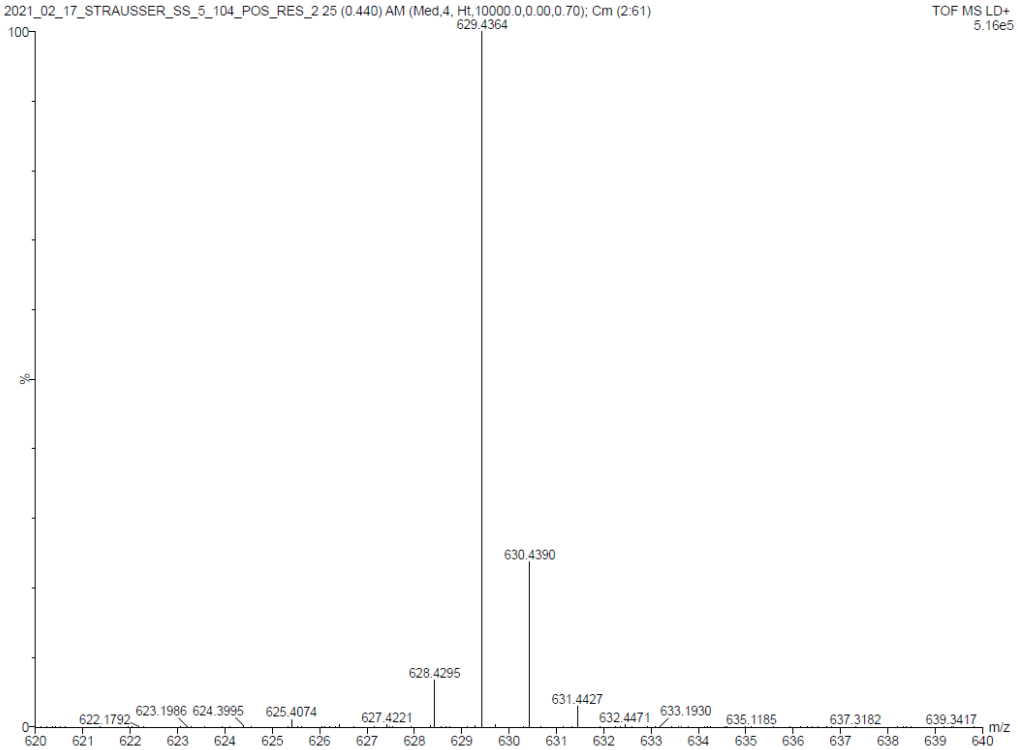
Spectra 5.1. ^{1}H NMR of **5.3** in $CDCl_3$. Dimethyl sulfide (DMS) was residual material from the reaction.



Spectra 5.2. ^{13}C NMR of **5.3** in $CDCl_3$.



Spectra 5.3. IR of **5.3** with C-D stretch at 2227 cm^{-1}.



Spectra 5.4. MS of **5.3**.

References

1. Fèvre, M.; Pinaud, J.; Leteneur, A.; Gnanou, Y.; Vignolle, J.; Taton, D.; Miqueu, K.; Sotiropoulos, J.-M., Imidazol(in)ium Hydrogen Carbonates as a Genuine Source of N-Heterocyclic Carbenes (NHCs): Applications to the Facile Preparation of NHC Metal Complexes and to NHC-Organocatalyzed Molecular and Macromolecular Syntheses. *Journal of the American Chemical Society* **2012,** *134*, 6776-6784.
2. Man, R. W. Y.; Li, C.-H.; MacLean, M. W. A.; Zenkina, O. V.; Zamora, M. T.; Saunders, L. N.; Rousina-Webb, A.; Nambo, M.; Crudden, C. M., Ultrastable Gold Nanoparticles Modified by Bidentate N-Heterocyclic Carbene Ligands. *Journal of the American Chemical Society* **2018,** *140*, 1576-1579.
3. Trujillo, M. J.; Strausser, S. L.; Becca, J. C.; DeJesus, J. F.; Jensen, L.; Jenkins, D. M.; Camden, J. P., Using SERS To Understand the Binding of N-Heterocyclic Carbenes to Gold Surfaces. *The Journal of Physical Chemistry Letters* **2018,** *9*, 6779-6785.
4. DeJesus, J. F.; Sherman, L. M.; Yohannan, D. J.; Becca, J. C.; Strausser, S. L.; Karger, L. F. P.; Jensen, L.; Jenkins, D. M.; Camden, J. P., A Benchtop Method for Appending Protic Functional Groups to N-Heterocyclic Carbene Protected Gold Nanoparticles. **2020,** *59*, 7585-7590.
5. Frens, G., Controlled Nucleation for the Regulation of the Particle Size in Monodisperse Gold Suspensions. *Nature Physical Science* **1973,** *241*, 20-22.

Chapter 6 : Synthesis of “Click” Tagged N-Heterocyclic Carbenes for Post-synthetic Modification of Gold Nanoparticles

Abstract

Gold surfaces have made a critical impact in medicine, particularly due to their non-toxic nature. As a result, gold nanoparticles can be directly injected into the body for sensing of biologically active molecules or for targeted drug delivery. Gold nanoparticles must be functionalized and, traditionally, thiols have served as linkers for the biologically active molecules to the NPs. However, thiols often degrade in ambient conditions and biological media. To combat this problem, N-heterocyclic carbenes (NHCs), which are more stable in various media and conditions on gold surfaces have been employed. Both amide coupling and Click chemistry approached have been used to link biologically active molecules to the NHCs, though these couplings were done before the placement onto the gold surfaces. This method is limited, only allowing for the functionalization of NPs with a limited library of molecules and is not a commercialized process. We propose a more general route to making these compounds by synthesizing alkyne tagged NHC gold nanoparticles (AuNPs), which can be used to react with any biologically active molecule of interest. In collaboration with the Camden group at Notre Dame University, we (the Jenkins group) demonstrate the synthesis and functionalization to provide the first alkyne backed NHC on gold surfaces and which are analyzed through surface-enhanced Raman Spectroscopy.

Introduction

At the present time, cancer, heart disease, and vehicular accidents remain the leading causes of death.[1] Though the technology for detection and treatment is rapidly advancing, the ability to detect cancers, such as pancreatic and ovarian cancer, in the initial asymptomatic stage is highly limited.[2-4] Traditionally, imaging techniques have been used to make these diagnoses, but an advancement has been made so that these cancers can be detected using biosensors equipped with gold nanoparticles.[5-7] In biological sensors, NPs that are functionalized with a binding group targeted for a specific biomarker or antibody will give a response or signal in the presence of the target molecule.[5-7] Due to their non-toxic nature, gold nanoparticles have been exploited for numerous medical applications.[8-12] Gold nanoparticles have also been applied for drug delivery where AuNPs can be injected into the body. The cancerous region can then be targeted with infrared radiation triggering the drug to be released and providing targeted chemotherapy.[13, 14]

In order to facilitate the drug delivery process or biosensors, a tagging agent must be appended to the gold surfaces. The most common tethering method is through thiol self-assembled monolayers (SAMs). Previously, the binding of thiol functionalized DNA moieties to AuNPs has been demonstrated for detection of proteins[15, 16], aptamer-based lateral flow assays[17], and electrochemical biosensors[18]. The main drawback of using thiols is their instability in ambient[19, 20], thermal[21-23], and biological media[24, 25]. This dilemma has lead researchers to seek out a new binding group that is stable in such conditions.

N-heterocyclic carbenes have been utilized as ligands on transition metals for catalysis[26-29] since they are known to be strong σ-donors and results in stronger ligand metal bonds. In recent reports, NHCs have been utilized on noble metal surfaces that include films and nanoparticles.[30-35] NHCs have shown superiority over thiols in their stability in ambient, thermal, extreme pH and reductive conditions.[30, 33] In addition, our research has demonstrated a general approach to append NHCs to pre-synthesized AuNPs of choice, without the use of strong bases or reducing agents.[32] In order to be utilized in the medicinal field as biosensors or drug delivery systems, the NHC ligands need to have an additional functional group that can append a biomolecule onto the surface. This can be done using two different coupling reactions (**Figure 6.1**, **A** and **B** respectively). In our previous report[32], we demonstrate the first amide coupling on an NHC coated surface and which was monitored via surface-enhanced Raman spectroscopy (SERS). While this gave insight into further appending proteins/aptamers to the surface, the most common aptamers that are commercially available are azides. This is because the Click reaction is a biorthogonal coupling reaction. This reaction involves the coupling of an azide and an alkyne typically using a copper catalyst to form a triazole (**Figure 6.1**, **B**). Once an aptamer has been coupled to the surface, the NPs can be used for biomolecule detection, such as biomarkers for cancer (**Figure 6.1**, **C**). Therefore, an alkyne functionalized NHC Au surface is critical to advance the field of gold biosensors.

Johnson and coworkers synthesized an alkyne backed imidazolium bromide salt which reacted with an azide to undergo the Click reaction.[36] After, the triazole containing ligand was used to synthesize a gold complex and then placed on a gold surface. While this was an advancement in the field of NHC gold surfaces, **there have been no reports of alkyne backed NHC Au complexes that have not been previously coupled before being placed on the surface**. The development of an alkyne backed NHC surface would potentially allow for the commercialization of generic NHC-AuNPs to bind any azide functionalized aptamer for detection (**Figure 6.1**, **D**).

In this chapter, we show the pitfalls of synthesizing terminal alkyne backed NHC gold complexes. In addition, we demonstrate the synthesis of the first alkyne backed NHC gold complex for the functionalization of AuNPs. Raman was taken of the alkyne gold complex. Once bound to the surface, we took advantage of the localized surface plasmon resonance (LSPR) effect on noble metal surfaces to provide the first alkyne backed NHC SERS spectra on Au surfaces.

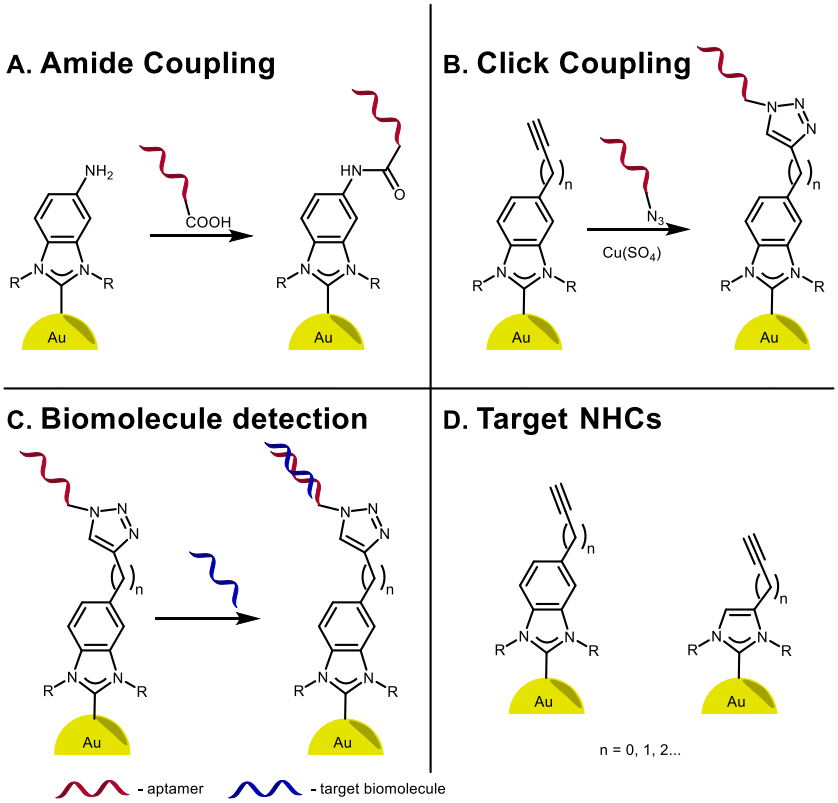


Figure 6.1: Ideal example of aptamer coupling to the NHC coated surface through amide coupling (**A**) and click coupling (**B**). The aptamer bound surface would then react with a target biomolecule of choice (**C**). The ideal NHCs of choice would be the benzimidazolium and imidazolium ligands containing a terminal alkyne (**D**). Ideally, to utilize the LSPR effect of Au NPs the alkyne needs to be closer to the surface (n=0) but other lengths can be explored.

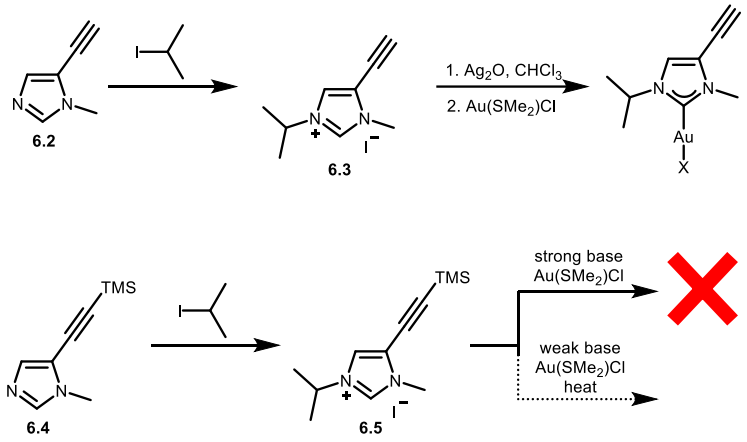
Results and Discussion

Initially, we attempted to synthesize a terminal alkyne backed imidazolium NHC gold complex (**Scheme 6.1,** top). Taking commercially available 5-ethynyl-1-methylimidazole, **6.2**, we alkylated with 2-iodopropane to synthesize the imidazolium iodide salt, **6.3**. There are two main methods to synthesize an imidazolium gold complex: (1) a basic approach or (2) a silver (Ag) transmetallation (**Scheme 6.2**, top and bottom respectively). Since **6.3** possesses an acidic proton on the alkyne, we attempted the Ag approach using Ag_2O in methylene chloride for 3 hours followed by an immediate reaction with $Au(SMe_2)Cl$ following the method of Mazzoni.[37] This reaction was so far unsuccessful. The next attempts should include running the silver reaction for multiple days before reacting with $Au(SMe_2)Cl$. The inclusion of heat in the silver step might be beneficial.

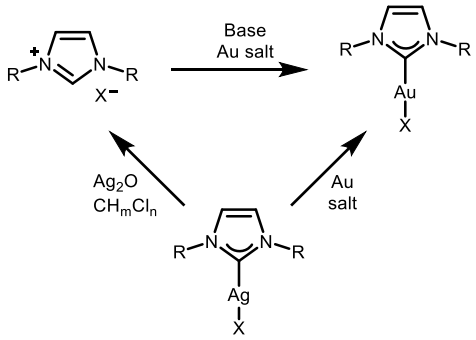
Using the silver method can come with some downsides as the silver products can be unstable. Therefore, instead of the terminal alkyne, we attempted the basic approach of gold complex synthesis on a TMS protected alkyne imidazole(**Scheme 6.1**, bottom). Starting with commercially available 5-[(trimethylsilyl)ethynyl])-1-methylimidazole, **6.4**, we alkylated using 2-iodopropane and heated under pressure to give **6.5**. To synthesize the Au complex, we attempted the basic approach with two different bases. The first approach using a strong base, KHMDS, to deprotonate the imidazolium proton in solution and subsequently adding the resulting free carbene to a vial containing $Au(SMe_2)Cl$. In the deprotonation step, the solution degraded into a black sludge therefore we decided to move away from the strong base approach. The next choice will be to utilize a weak base such as triethyl amine or potassium carbonate for the basic approach with the protected alkyne imidazolium salt to synthesize the gold complex.

Since the methods that would eventually lead to the terminal alkyne were unsuccessful, we moved to the addition of a methyl (the smallest carbon group to prevent steric hindrance) to the alkyne (**Scheme 6.1,** bottom) Starting with **6.5**, the alkyne was deprotected with $Li(NMe_2)$ in THF then followed by the addition of MeI to form the methylated alkyne imidazolium, **6.7**. After **6.7**, was alkylated with neat 2-iodopropane under pressure to form the imidazolium, **6.8**. To form the final gold imidazolium complex, **6.1** was deprotonated with KHMDS and stirred for two hours. After, the reaction was filtered over Celite, to remove the KI salt formed in the reaction, and added into a vial containing $Au(SMe_2)Cl$ and stirred overnight. The reaction was dried and extracted with CH_2Cl_2, then followed by a second filtration over Celite. The volume of the filtrate was reduced to 2 mL and added dropwise to a stirring solution of hexanes. The solid that formed was collected, dried and purified over flash column chromatography to give **6.1** as a white solid. The gold complex was characterized through ^{1}H and ^{13}C NMR. Confirmation of product was shown in the ^{1}H NMR by the absence of the C2 C-H proton in the 8-11 ppm range. In the ^{13}C NMR, we observe the downfield shift of the C2 carbon from 136.24 ppm in the imidazolium salt **6.5** to 170.32 ppm in the Au complex (**6.1**).

Scheme 6.1: Schemes of attempted alkyne imidazolium Au complex.



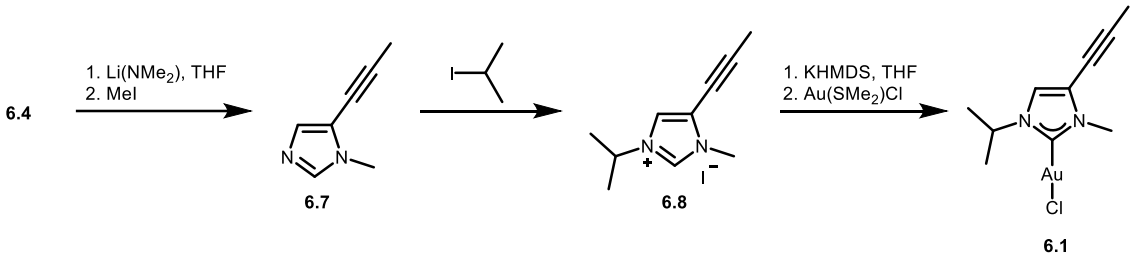
Scheme 6.2: Proposed synthesis of NHC-Au complexes using the basic (top) and Ag_2O (bottom) methods.



Once synthesized, complex **6.1** was bound the complex to AuNPs and observed using SERS. Complex **6.1** was reacted with 24 nm citrate capped AuNPs, by adding 5 µL of a solution containing **6.1** in methylene chloride (1 mM) with 5 mL of the AuNPs following our previously published procedure.[32] The NHC binding to the surface was confirmed using SERS. **Figure 6.2** (bottom, red) shows the Raman of **6.1**. As a complex, this signal was low in intensity but shows a slight peak around 2250 cm^{-1} for the C-C triple bond stretch. Once bound to the NPs, the signal intensity of the complex significantly increased and the C≡C bond stretch is drastically noticeable (**Figure 6.2**, top).

In conclusion, we synthesized three alkyne backed imidazolium iodide complexes. We also attempted the synthesis of a terminal alkyne backed imidazolium NHC using the terminal and protected imidazolium salts. In both cases the Ag_2O and basic approach failed, though other routes need to be explored to synthesize a silver complex using a Cl or Br anionic salt of **6.3**. Finally, we show the synthesis of the first alkyne backed NHC Au complex and AuNPs. The binding of the NHC was confirmed using SERS, where the presence of the alkyne on the surface was clearly visible around 2250 cm^{-1}. The next step is to take the alkyne NHC coated nanoparticles and conduct a Click reaction with an azide and copper catalyst of choice and tracking with SERS, SALDI (referred to Chapter 5), and possibly NMR. In addition, further research needs to be conducted in the synthesis of a terminal backed alkyne NHC-Au complex.

Scheme 6.3: Synthetic route to the methylated alkyne imidazolium gold chloride complex, **6.1**.



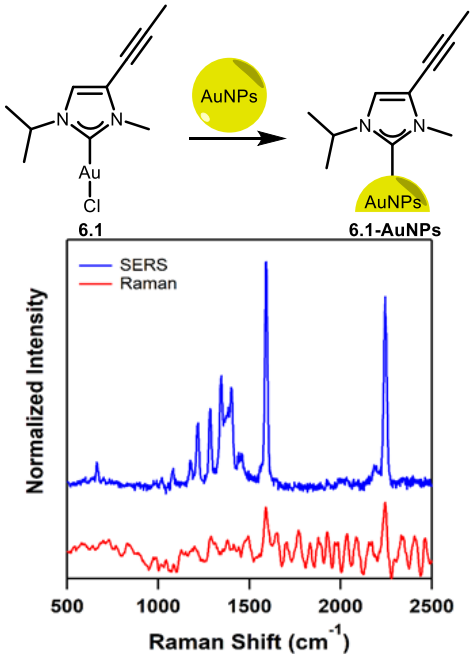


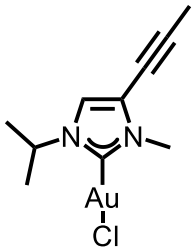
Figure 6.2: Raman (red) of **6.1** and SERS (blue) of **6.1-AuNPs**.

Experimental

General Considerations for Synthesis. All glassware for air and water sensitive reactions were dried at 170 °C overnight before use. All reactions were stirred vigorously with magnetic stirrers. A glovebox with a dinitrogen atmosphere was used for air and water sensitive reactions. Solvents using in dinitrogen atmosphere were dried on an Innovative Technologies (Newburyport, MA) Pure Solv MD-7 Solvent Purification System, degassed by three freeze-pump-thaw cycles on a Schlenk line to remove dioxygen and stored under activated 4 Å molecular sieves prior to use. Celite® was dried at 240 °C under vacuum overnight and stored in a dinitrogen glovebox. All other compounds were purchased from commercial vendors at highest available purity and used without any further purification. Solution ^{1}H NMR and ^{13}C NMR were performed on a Varian VNMRS 500 MHz narrow-bore broadband system and Bruker 500 MHz narrow-bore broadband system at 298 K. All ^{1}H and ^{13}C shifts were referenced to the residual solvent.

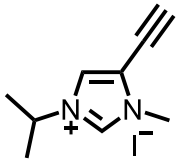
Citrate-capped gold nanoparticles were prepared following the widely-used Lee and Meisel method.[38] The resulting nanoparticles exhibit a plasmon band at 521 nm with a hydrodynamic diameter of 24 nm, measured by UV-VIS spectroscopy and dynamic light scattering respectively. The alkyne-terminated imidazolium NHC Au complex (7.9 mg) was dissolved in dichloromethane (20 mL) to yield a 1 mM solution. The NHC-coated gold nanoparticles are easily prepared by mixing 5 µL of the complex solution with 5 mL of the AuNPs, as confirmed in a previous publication.[32] Raman and SERS spectra are obtained using a 633 nm excitation wavelength (Thor Labs) set at 7 mW and 1 mW of power at the objective (Nikon, 20x, NA = 0.5), respectively. We use a custom-built Raman spectrometer equipped with a deep-depletion CCD detector.

Synthesis of 6.1.



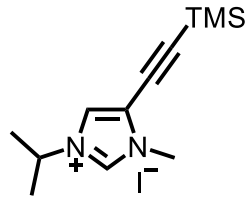
5-([methylethynyl)-3-isopropyl-1-methylimidazolium iodide, **6.8** (0.0520 g, 0.179 mmol), KHMDS (0.0360 g, 0.180 mmol) and 5 mL THF was added to a vial and the reaction was stirred for 3 hours in a glovebox. The mixture was then filtered over a Celite plug and the solution was added into a vial containing $Au(SMe_2)Cl$ (0.0530 g, 0.212 mmol) and stirred at RT overnight. The reaction was removed from the glovebox solvent was removed under vacuum. The residue was extracted with CH_2Cl_2 (50 mL) and filtered over a Celite plug. The filtrate was reduced to approximately 2 mL and pipetted into a 100 mL Erlenmeyer with 50 mL hexanes and a stir bar with vigorous stirring. The precipitate was collected and dried under vacuum to give **6.1** as an off-white powder (0.0540 g, 76.4%). ^{1}H NMR (CD_2Cl_2, 499.74 MHz): □ 7.02 (s, 1H), 4.99 (sept, *J* = 6.81 Hz, 1H), 3.78 (s, 3H), 2.10 (s, 3H), 1.44 (d, *J* = 6.87, 6H). ^{13}C NMR (CD_2Cl_2, 125.66 MHz): □□170.32, 119.15, 118.83, 95.38, 66.06, 54.09, 36.62, 23.40, 4.62.

Synthesis of 6.3.



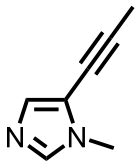
5-ethynyl-1-methylimidazole, **6.2**, (0.5142 g, 4.845 mmol) was measured into a vial with a stir bar. 2-iodopropane (5.000 mL. 50.00 mmol) was added and the vial was capped with a Teflon screw cap and sealed with tape. The reaction was stirred at 87 °C for one day. A solid formed overnight. The reaction cooled and 10 mL ether was added to precipitate more solid. The solid was collected, dissolved in 50 mL acetonitrile, filtered over a Celite pad and rinsed with 20 mL of acetonitrile. The filtrate collected and the solvent was removed. The residue was redissolved in a minimal amount of acetonitrile and titrated with diethyl ether. The resulting precipitate was collected and washed with additional ether (50 mL). The solid was dried under vacuum to give **6.3** as a yellow solid. 0.8747 g, 65.4% yield. ^{1}H NMR (CD_2Cl_2, 499.74 MHz): □ 10.54 (s, 1H), 7.53 (s, 1H), 4.82 (sept, *J* = 6.66 Hz, 1H), 4.05 (s, 3H), 3.78 (s, 1H), 1.63 (d, *J* = 6.68 Hz).^{13}C NMR (CD_2Cl_2, 125.66 MHz): □□137.43, 123.54, 118.45, 89.21, 67.28, 54.59, 35.38, 22.76.

Synthesis of 6.5



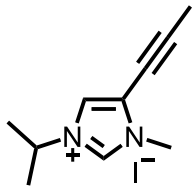
5-[(Trimethylsilyl)ethynyl])-1-methylimidazole, **6.4** (0.1004 g, 0.5631 mmol) was measured into a vial with a stir bar. 2-iodopropane (0.1130 mL. 1.130 mmol) and acetonitrile (15 mL) were added, and the vial was capped with a Teflon screw cap and sealed with tape. The reaction was stirred at 85 °C for one day. After, the reaction was cooled to RT and the solvent was removed. The residue was dissolved in 2 mL of acetonitrile and titrated with diethyl ether. The resulting precipitate was collected and washed with additional ether (10 mL). The solid was dried under vacuum to give **6.5** as a white solid. 0.0503 g, 25.7% yield. ^{1}H NMR (CD_2Cl_2, 499.74 MHz): □ 10.60 (s, 1H), 7.37 (s, 1H), 4.88 (sept, *J* = 6.70 Hz), 4.02 (s, 3H), 1.64 (d, *J* = 6.89, 6H), 0.27 (s, 9H).

Synthesis of 6.7

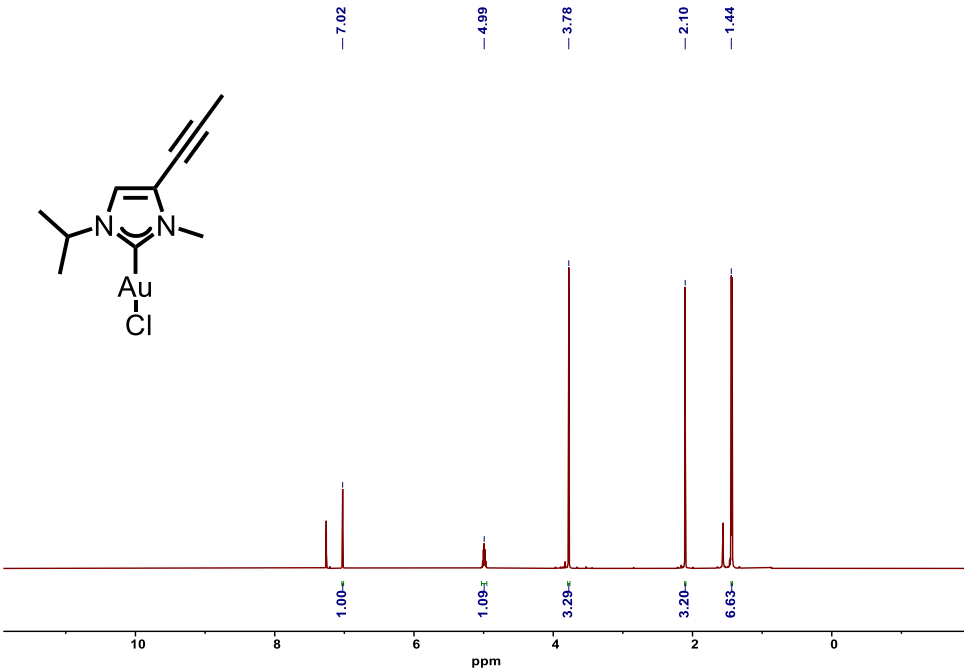


In a glovebox, 5-[(Trimethylsilyl)ethynyl])-1-methylimidazole, **6.4** (0.5374 g, 3.014 mmol), was dissolved in 10 mL THF. Me_2NLi (0.1845 g, 3.616 mmol) in 5 mL THF was added slowing while stirring. After 15 mins., MeI (0.103 g, 3.614 mmol) was added, and the reaction stirred overnight. The reaction was brought out of the glovebox and quenched with 5 mL water. The solution was dried under vacuum, and 25 mL water was added and extracted with 3 x 25mL CH_2Cl_2 fractions. The organic layers were combined, dried with $MgSO_4$, and filtered over a medium porosity frit. The filtrate was collected, and the solvent was removed to give **6.7** as a yellow oil. 0.246 g, 68.0% yield. ^{1}H NMR ($CDCl_3$, 499.74 MHz): □ 7.28 (s, 1H), 7.02 (s, 1H), 3.50 (s, 3H), 1.97 (s, 3H).

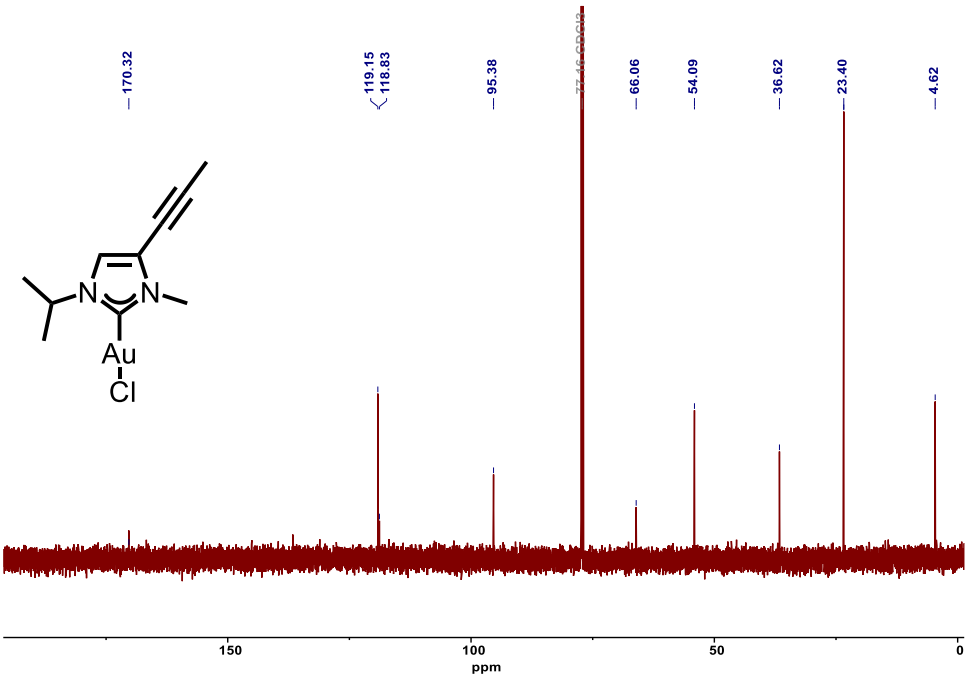
Synthesis of 6.8



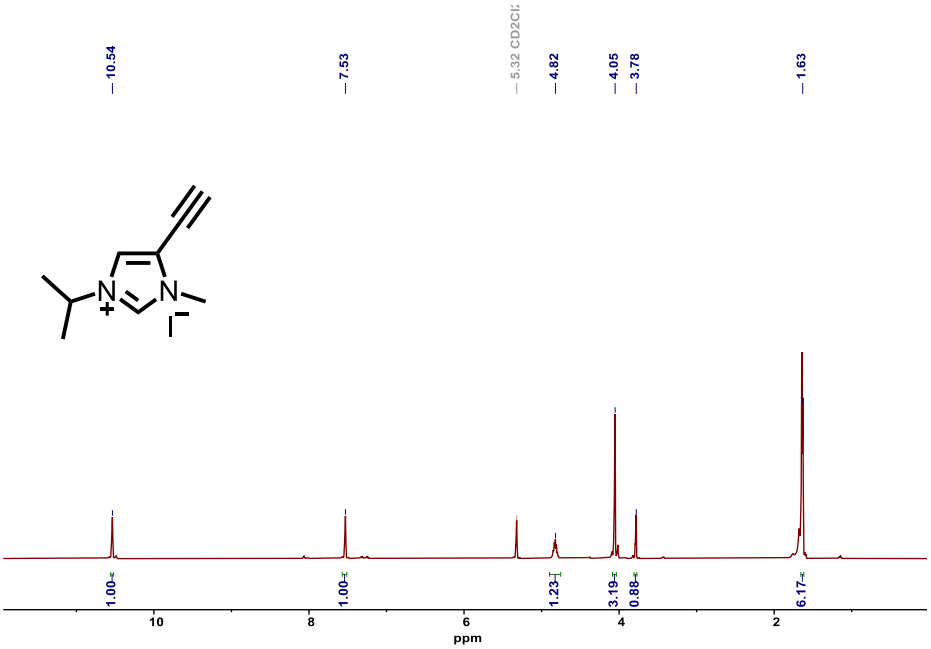
5-([methylethynyl)-1-methylimidazole, **6.7** (0.2391 g, 1.990 mmol) was measured into a vial with a stir bar. 2-iodopropane (7.000 mL, 70.00 mmol) was added and the vial was capped with a Teflon screw cap and sealed with tape. The reaction was stirred at 90 °C for one day. After, the reaction was cooled to RT and the solvent was removed. The residue was extracted with acetonitrile (50 mL) and filtered over a Celite pad. The filtrate was collected, solvent was removed and the residue was redissolved in a minimal amount of acetonitrile and titrated with diethyl ether. The resulting precipitate was collected and washed with additional ether (50 mL). The solid was dried under vacuum to give **6.8** as a yellow solid. 0.460 g, 79.0% yield. ^{1}H NMR (CD_2Cl_2, 499.74 MHz): □ 10.36 (s, 1H), 7.32 (s, 1H), 4.77 (sept., *J* = 6.84Hz, 1H), 3.99 (s, 3H), 2.14 (s, 3H), 1.60 (d, *J* = 6.64Hz).^{13}C NMR (CD_2Cl_2, 125.66 MHz): □□136.24, 121.46, 120.10, 98.84, 89.24, 63.65, 35.11, 23.18, 4.74.



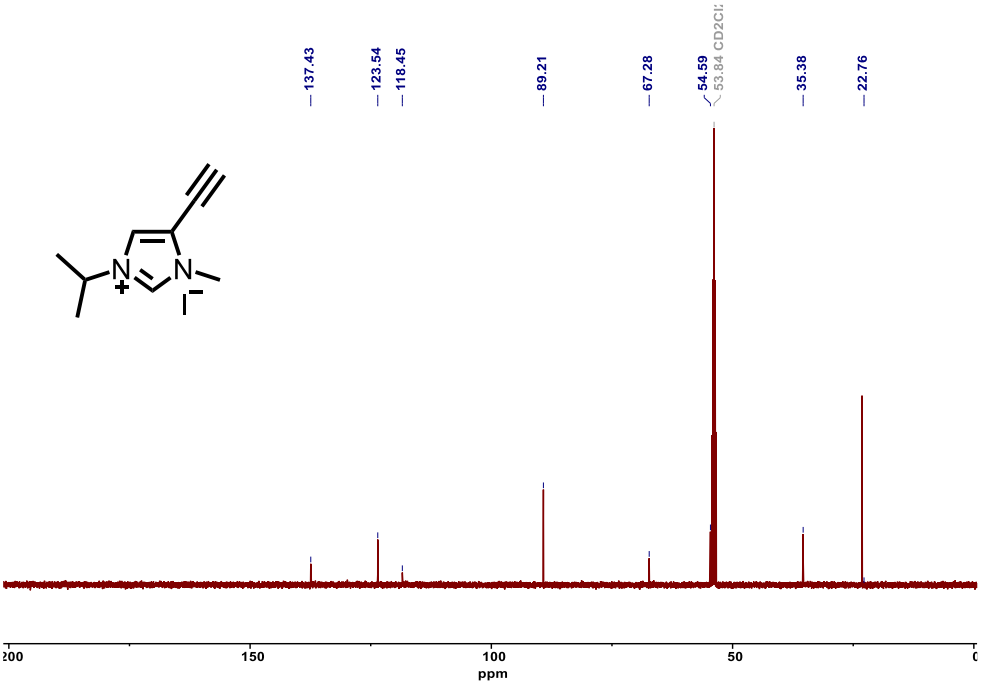
Spectra 6.1: ^{1}H NMR of **6.1** in $CDCl_3$.



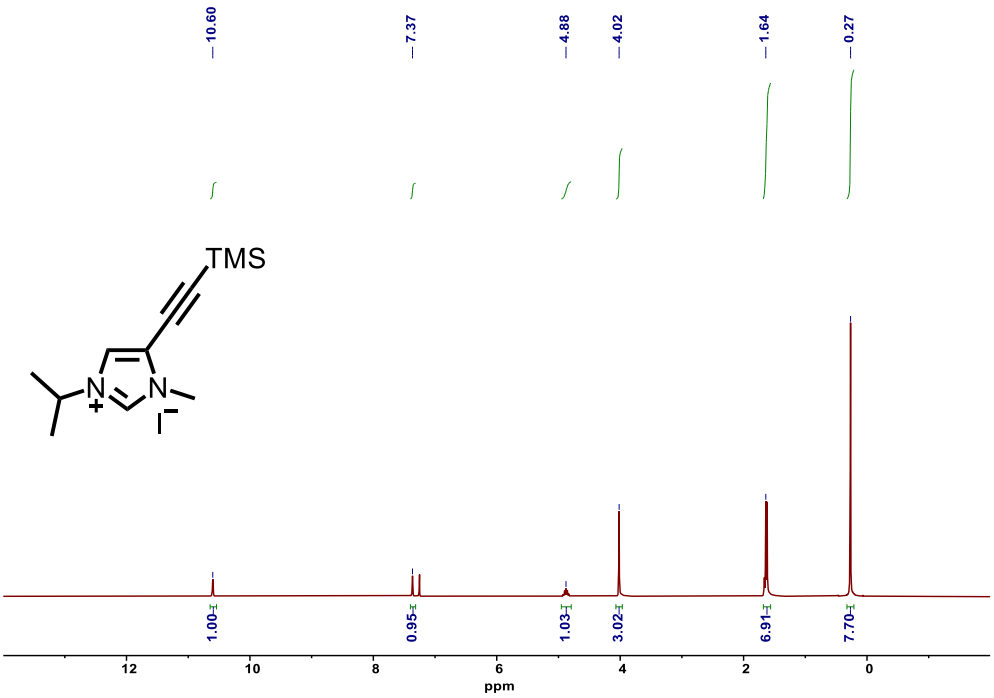
Spectra 6.2: ^{13}C NMR of **6.1** in $CDCl_3$.



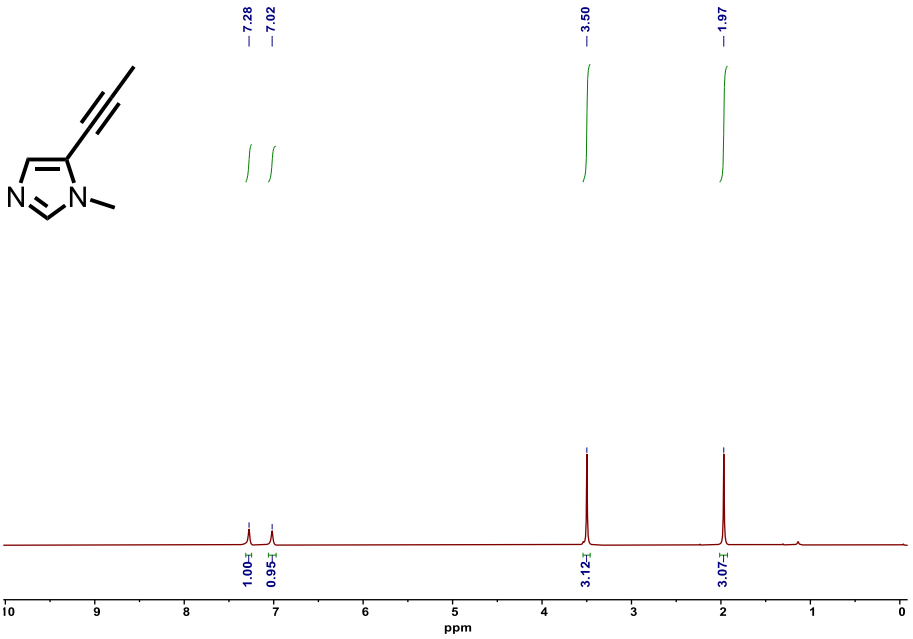
Spectra 6.3: ^{1}H NMR of **6.3** in CD_2Cl_2.



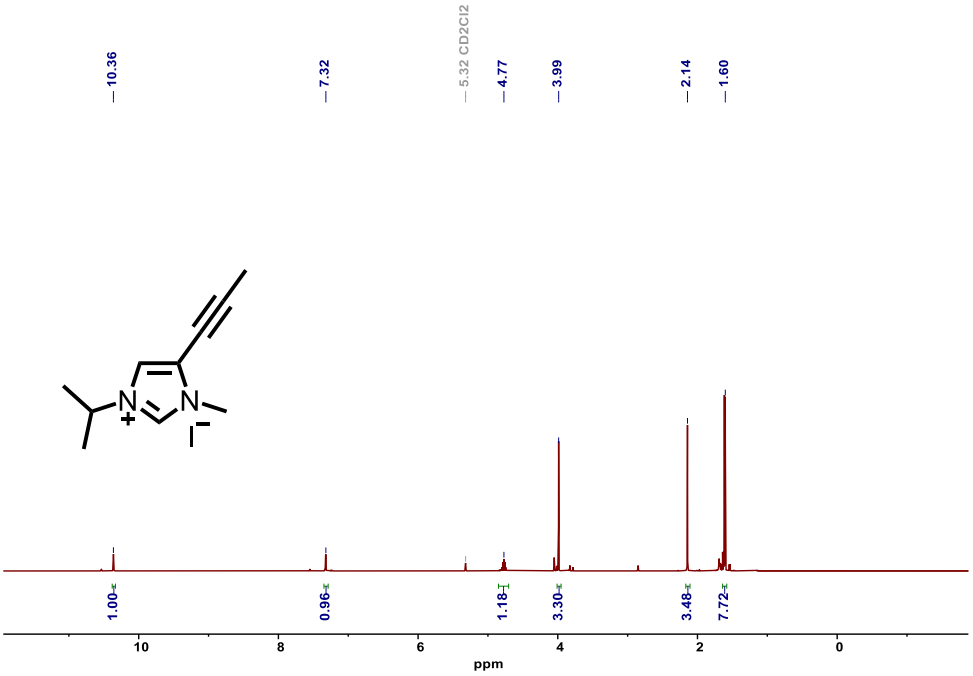
Spectra 6.4: ^{13}C NMR of **6.3** in CD_2Cl_2.



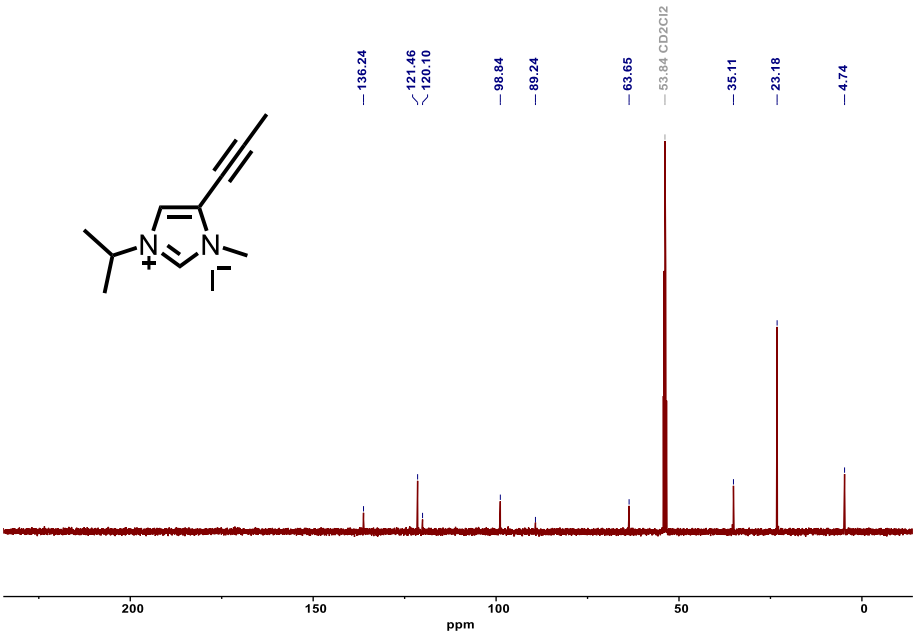
Spectra 6.5: ^{1}H NMR of **6.5** in $CDCl_3$.



Spectra 6.6: ^{1}H NMR of **6.7** in $CDCl_3$.



Spectra 6.7: ^{1}H NMR of **6.8** in CD_2Cl_2.



Spectra 6.8: ^{1}H NMR of **6.8** in CD_2Cl_2.

References

1. Control, C. f. D. Leading Causes of Death. https://www.cdc.gov/nchs/fastats/leading-causes-of-death.htm (accessed March 8, 2021).
2. Chari, S. T., Detecting early pancreatic cancer: problems and prospects. *Semin Oncol* **2007,** *34*, 284-294.
3. Das, P. M.; Bast, R. C., Jr., Early detection of ovarian cancer. *Biomarkers in Medicine* **2008,** *2*, 291-303.
4. Rauh-Hain, J. A.; Krivak, T. C.; Del Carmen, M. G.; Olawaiye, A. B., Ovarian cancer screening and early detection in the general population. *Rev Obstet Gynecol* **2011,** *4*, 15-21.
5. Hamdy, M. E.; Del Carlo, M.; Hussein, H. A.; Salah, T. A.; El-Deeb, A. H.; Emara, M. M.; Pezzoni, G.; Compagnone, D., Development of gold nanoparticles biosensor for ultrasensitive diagnosis of foot and mouth disease virus. *Journal of Nanobiotechnology* **2018,** *16*, 48.
6. Hutter, E.; Maysinger, D., Gold-nanoparticle-based biosensors for detection of enzyme activity. *Trends in Pharmacological Sciences* **2013,** *34*, 497-507.
7. Li, Y.; Schluesener, H. J.; Xu, S., Gold nanoparticle-based biosensors. *Gold Bulletin* **2010,** *43*, 29-41.
8. Chen, P.-C.; Roy, P.; Chen, L.-Y.; Ravindranath, R.; Chang, H.-T., Gold and Silver Nanomaterial-Based Optical Sensing Systems. **2014,** *31*, 917-942.
9. Cordeiro, M.; Ferreira Carlos, F.; Pedrosa, P.; Lopez, A.; Baptista, P. V., Gold Nanoparticles for Diagnostics: Advances towards Points of Care. *Diagnostics (Basel, Switzerland)* **2016,** *6*.
10. Han, G.; Ghosh, P.; Rotello, V. M., Functionalized gold nanoparticles for drug delivery. *Nanomedicine* **2007,** *2*, 113-123.
11. Xu, L.; Liu, Y.; Chen, Z.; Li, W.; Liu, Y.; Wang, L.; Liu, Y.; Wu, X.; Ji, Y.; Zhao, Y.; Ma, L.; Shao, Y.; Chen, C., Surface-Engineered Gold Nanorods: Promising DNA Vaccine Adjuvant for HIV-1 Treatment. *Nano Letters* **2012,** *12*, 2003-2012.
12. Zhao, Y.; Zhou, H.; Zhang, S.; Xu, J., The synthesis of metal nanoclusters and their applications in bio-sensing and imaging. *Methods and Applications in Fluorescence* **2019,** *8*, 012001.
13. Jain, S.; Hirst, D. G.; O'Sullivan, J. M., Gold nanoparticles as novel agents for cancer therapy. *Br J Radiol* **2012,** *85*, 101-113.
14. Mangadlao, J. D.; Wang, X.; McCleese, C.; Escamilla, M.; Ramamurthy, G.; Wang, Z.; Govande, M.; Basilion, J. P.; Burda, C., Prostate-Specific Membrane Antigen Targeted Gold Nanoparticles for Theranostics of Prostate Cancer. *ACS nano* **2018,** *12*, 3714-3725.
15. Wang, W.; Chen, C.; Qian, M.; Zhao, X. S., Aptamer biosensor for protein detection using gold nanoparticles. *Analytical Biochemistry* **2008,** *373*, 213-219.
16. Hu, J.; Zheng, P.-C.; Jiang, J.-H.; Shen, G.-L.; Yu, R.-Q.; Liu, G.-K., Electrostatic Interaction Based Approach to Thrombin Detection by Surface-Enhanced Raman Spectroscopy. *Analytical Chemistry* **2009,** *81*, 87-93.
17. Liu, J.; Mazumdar, D.; Lu, Y., A simple and sensitive "dipstick" test in serum based on lateral flow separation of aptamer-linked nanostructures. *Angewandte Chemie (International ed. in English)* **2006,** *45*, 7955-9.

18. Kang, D.; Sun, S.; Kurnik, M.; Morales, D.; Dahlquist, F. W.; Plaxco, K. W., New Architecture for Reagentless, Protein-Based Electrochemical Biosensors. *Journal of the American Chemical Society* **2017,** *139*, 12113-12116.
19. Schoenfisch, M. H.; Pemberton, J. E., Air Stability of Alkanethiol Self-Assembled Monolayers on Silver and Gold Surfaces. *Journal of the American Chemical Society* **1998,** *120*, 4502-4513.
20. Willey, T. M.; Vance, A. L.; van Buuren, T.; Bostedt, C.; Terminello, L. J.; Fadley, C. S., Rapid degradation of alkanethiol-based self-assembled monolayers on gold in ambient laboratory conditions. *Surface Science* **2005,** *576*, 188-196.
21. Delamarche, E.; Michel, B.; Kang, H.; Gerber, C., Thermal Stability of Self-Assembled Monolayers. *Langmuir* **1994,** *10*, 4103-4108.
22. Garg, N.; Carrasquillo-Molina, E.; Lee, T. R., Self-Assembled Monolayers Composed of Aromatic Thiols on Gold: Structural Characterization and Thermal Stability in Solution. *Langmuir* **2002,** *18*, 2717-2726.
23. Li, F.; Zhang, H.; Dever, B.; Li, X.-F.; Le, X. C., Thermal Stability of DNA Functionalized Gold Nanoparticles. *Bioconjugate Chemistry* **2013,** *24*, 1790-1797.
24. Flynn, N. T.; Tran, T. N. T.; Cima, M. J.; Langer, R., Long-Term Stability of Self-Assembled Monolayers in Biological Media. *Langmuir* **2003,** *19*, 10909-10915.
25. Jans, K.; Bonroy, K.; De Palma, R.; Reekmans, G.; Jans, H.; Laureyn, W.; Smet, M.; Borghs, G.; Maes, G., Stability of mixed PEO-thiol SAMs for biosensing applications. *Langmuir* **2008,** *24*, 3949-54.
26. Hadei, N.; Kantchev, E. A. B.; O'Brie, C. J.; Organ, M. G., The First Negishi Cross-Coupling Reaction of Two Alkyl Centers Utilizing a Pd−N-Heterocyclic Carbene (NHC) Catalyst. *Organic Letters* **2005,** *7*, 3805-3807.
27. Marx, V. M.; Sullivan, A. H.; Melaimi, M.; Virgil, S. C.; Keitz, B. K.; Weinberger, D. S.; Bertrand, G.; Grubbs, R. H., Cyclic Alkyl Amino Carbene (CAAC) Ruthenium Complexes as Remarkably Active Catalysts for Ethenolysis. **2015,** *54*, 1919-1923.
28. McGuinness, D. S.; Suttil, J. A.; Gardiner, M. G.; Davies, N. W., Ethylene Oligomerization with Cr−NHC Catalysts: Further Insights into the Extended Metallacycle Mechanism of Chain Growth. *Organometallics* **2008,** *27*, 4238-4247.
29. Sanford, M. S.; Love, J. A.; Grubbs, R. H., Mechanism and Activity of Ruthenium Olefin Metathesis Catalysts. *Journal of the American Chemical Society* **2001,** *123*, 6543-6554.
30. Crudden, C. M.; Horton, J. H.; Ebralidze, I. I.; Zenkina, O. V.; McLean, A. B.; Drevniok, B.; She, Z.; Kraatz, H.-B.; Mosey, N. J.; Seki, T.; Keske, E. C.; Leake, J. D.; Rousina-Webb, A.; Wu, G., Ultra stable self-assembled monolayers of N-heterocyclic carbenes on gold. *Nature Chemistry* **2014,** *6*, 409-414.
31. Crudden, C. M.; Horton, J. H.; Narouz, M. R.; Li, Z.; Smith, C. A.; Munro, K.; Baddeley, C. J.; Larrea, C. R.; Drevniok, B.; Thanabalasingam, B.; McLean, A. B.; Zenkina, O. V.; Ebralidze, I. I.; She, Z.; Kraatz, H.-B.; Mosey, N. J.; Saunders, L. N.; Yagi, A., Simple direct formation of self-assembled N-heterocyclic carbene monolayers on gold and their application in biosensing. *Nature Communications* **2016,** *7*, 12654.
32. DeJesus, J. F.; Sherman, L. M.; Yohannan, D. J.; Becca, J. C.; Strausser, S. L.; Karger, L. F. P.; Jensen, L.; Jenkins, D. M.; Camden, J. P., A Benchtop Method for Appending Protic Functional Groups to N-Heterocyclic Carbene Protected Gold Nanoparticles. **2020,** *59*, 7585-7590.

33. DeJesus, J. F.; Trujillo, M. J.; Camden, J. P.; Jenkins, D. M., N-Heterocyclic Carbenes as a Robust Platform for Surface-Enhanced Raman Spectroscopy. *Journal of the American Chemical Society* **2018,** *140*, 1247-1250.
34. Trujillo, M. J.; Strausser, S. L.; Becca, J. C.; DeJesus, J. F.; Jensen, L.; Jenkins, D. M.; Camden, J. P., Using SERS To Understand the Binding of N-Heterocyclic Carbenes to Gold Surfaces. *The Journal of Physical Chemistry Letters* **2018,** *9*, 6779-6785.
35. Wang, G.; Rühling, A.; Amirjalayer, S.; Knor, M.; Ernst, J. B.; Richter, C.; Gao, H.-J.; Timmer, A.; Gao, H.-Y.; Doltsinis, N. L.; Glorius, F.; Fuchs, H., Ballbot-type motion of N-heterocyclic carbenes on gold surfaces. *Nature Chemistry* **2016,** *9*, 152.
36. MacLeod, M. J.; Johnson, J. A., PEGylated N-Heterocyclic Carbene Anchors Designed To Stabilize Gold Nanoparticles in Biologically Relevant Media. *Journal of the American Chemical Society* **2015,** *137*, 7974-7977.
37. Cingolani, A.; Cesari, C.; Zacchini, S.; Zanotti, V.; Cassani, M. C.; Mazzoni, R., Straightforward synthesis of iron cyclopentadienone N-heterocyclic carbene complexes. *Dalton Transactions* **2015,** *44*, 19063-19067.
38. Lee, P. C.; Meisel, D., Adsorption and surface-enhanced Raman of dyes on silver and gold sols. *The Journal of Physical Chemistry* **1982,** *86*, 3391-3395.

Chapter 7 : Development of N-Heterocyclic Carbene Ligands for Stability and Modification on Gold Surfaces

Abstract

The previous chapters of this dissertation are based on complete or near complete projects, though the research in N-heterocyclic carbene (NHC) ligands for gold surface modification is still in its infancy. Our previous work focuses on understanding how NHCs bind to gold surfaces, and effects of ligand modification on stability. Now that those questions have been addressed in this dissertation, we wanted to further investigate how ligand modifications, such as how the change of the N-substituents and backbone, impact the NHC-gold surface chemistry for further applications. In this chapter, I will discuss the beginning steps of water solubility modification for gold nanoparticles (AuNPs) and the development of chiral NHC ligands for gold surfaces. All work is intended to be in collaboration with the Camden group at Notre Dame. This work was conducted in collaboration with an undergraduate researcher, Rowan Borsari in the Jenkins group.

Introduction

Changes in N-Substituents to Increase Water Solubility of NHC-AuNPs.

The synthesis of NHC-NPs has generally been achieved in two main approaches: (1) the reduction of NHC-Au-Cl complexes[1, 2] or (2) the deposition of an NHC free carbene onto non-aqueous AuNPs.[3, 4] The reduction method typically yields only 5 nm NPs; this is not large enough to be tracked via SERS which requires NPs between 20 and 60 nm in size.[5] The free carbene method has three main disadvantages. First, the NPs need to be suspended in non-aqueous solutions. Additionally, the NHC starting ligand cannot possess any protic functional groups due to the basic conditions required to form the free carbene, and the NHC must be stable as a free carbene. These complications have led our research to develop a general method to synthesize SERS active AuNPs not using the two previously mentioned methods. In our previous report, we developed a method to generate NHC-AuNPs that used NHC-Au metal complexes which were reacted with pre-synthesized AuNPs. (**Figure 7.1**, top).[6]

The one complication with this method is that we can not have higher concentrations of the NHCs in solution in order to cover the surface as much as possible. The typical amount of the NHC-Au complex added is 1 µL of a 1 mM solution to 5 mL of AuNPs. We speculate that this amount of NHC complex was not enough to completely cover the surface with NHCs. In attempt to achieve full surface coverage, we studied the effects of adding more NHC Au complex solutions to the NPs. In **Figure 7.1** (bottom), the increase from 1 µL to 5 µL of NHC solution starts to cause spontaneous aggregation, which can be observed by the change in color from wine red to darker red and the presence of a black precipitate. We believe this is due to the nonpolar NHC Au complex and that the addition of more complex causes aggregation since they before not soluble in aqueous environments. To confirm this was not due to solvent, we added 5 µL of CH_2Cl_2 and saw no change. After the addition of 25 and 100 µL of NHC solution, we saw complete aggregation of the NPs. In an attempt to mitigate this occurrence, we changed the N-substituents for more water-soluble moieties such as triethylene glycol.

To date there only a few examples of water-soluble NHCs that have been place on AuNPs.[1, 2, 7, 8] These NHCs contain a carboxylic acid, sulfonate or an ethylene glycol unit on either the backbone or as an N-substituent (**Figure 7.2**, **7.2-5-AuNP**). **7.3-AuNP** and **7.5-AuNP** possess a long alkyl chain (which can possibility negate the water-solubility increase of the triethylene glycol (TEG)) or a charged N-substituent, respectively. While **7.2-AuNP** and **7.4-AuNP** are functionalized in the back of the ligand, these ligands would inhibit the ability to append various moieties that can be used in biological applications, particularly **7.4-AuNP** since the functional group is used for placing the PEG on the surface and no other functionality is present.



Figure 7.1: (Top) General approach to functionalize AuNPs with NHC ligands. (**Bottom**) Effects of increasing concentration of NHC-Au complex in AuNPs. From left to right: 1 µL **7.1**, 5 µL CH_2Cl_2, 5 µL **7.1**, 25 µL **7.1**, and 100 µL **7.1** solutions. All **7.1** solutions are a 1mM concentration. Image taken from our Angew. paper.[6]

(refer to Chapter 6). In addition, these NHC coated NPs have not been extensively explored on their true water solubility properties. These examples limit the ability to further impose functionality on the back of the NHC to be viable in biological applications (refer to Chapter 6). Thus, we began to focus on synthesizing NHC ligands that have increased water solubility by incorporating TEG substituents on one or both sides of the NHC nitrogens (**7.6-7.8**). In the case of the addition of only one TEG, our efforts will focus on synthesizing short alkyl chains than **7.3** as this should have a higher solubility than previously published.[8]

In our initial studies, we wanted to focus on benzimidazolium NHCs, due to their robust nature and stronger donation to the gold surface than the imidazolium variant (refer to Chapter 1 & 3). Following the method of Crudden[8], we refluxed benzimidazole (**7.9**) and with 1 equivalent of TEG-Br and Cs_2CO_3, in acetonitrile for one day. We removed the solvent, extracted with methylene chloride, and isolated **7.9a** as a yellow oil. We found that any further attempt to isolate and characterize the intermediate, **7.9a,** resulted in degradation of the compound. Therefore, we alkylated the crude material with three different groups (TEG, isopropyl, and n-hexyl) immediately after synthesis in a pressurized vessel. The TEG variant gave the desired product, though at low yield, and was unable to be purified due to the high polarity of the molecule. The isopropyl case yielded no product. We believe this is due to the low nucleophilic property of the benzimidazole nitrogen and alkylation with a secondary alkyl halide is not viable. Only the *n*-hexyl substituent gave an isolable and purified product, **7.10**. The product was confirmed using ^{1}H and ^{13}C NMR. The main peak to confirm benzimidazolium formation was the presence of the C2 C-H peak at 11.08 ppm. Our next step was to take **7.10** and deprotonate the C2 position with KHMDS and after two hours the reaction was filtered over a celite pad and added to a vial containing $Au(SMe_2)Cl$ and stirred overnight. The reaction is currently under the purification process. In addition, we attempted all reactions with the benzimidazolium starting with alkylation using hydrocarbon substituents, such as isopropyl, hexyl, and dodecane, and then alkylating with TEG but all reactions failed to produce any final product. We believe again this is due to the low nucleophilic properties of the benzimidazole.

Due to the limited benzimidazolium salts that could be synthesized, we then attempted to synthesize water-soluble imidazolium ligands and Au complexes (**Scheme 7.1**, **7.7** and **7.8**). The first step was to synthesize the di-(TEG)imidazolium bromide salt, **7.12**. We started this reaction with imidazole, **7.11**, and TEG-Br following the Crudden method as mentioned previously.[8] We did not isolate the intermediate, **7.11a**, due to our insights from the benzimidazolium case. We then attempted to react **7.11a** with TEG-Br under a pressurized reaction, but this failed as we were not able to isolate the product from the reactants due to its high polarity. Our next approach was to synthesize an asymmetric TEG imidazolium Au complex, **7.8**.

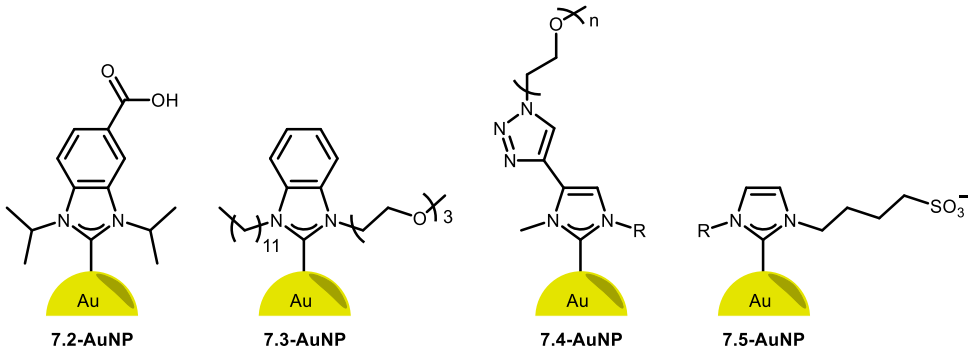
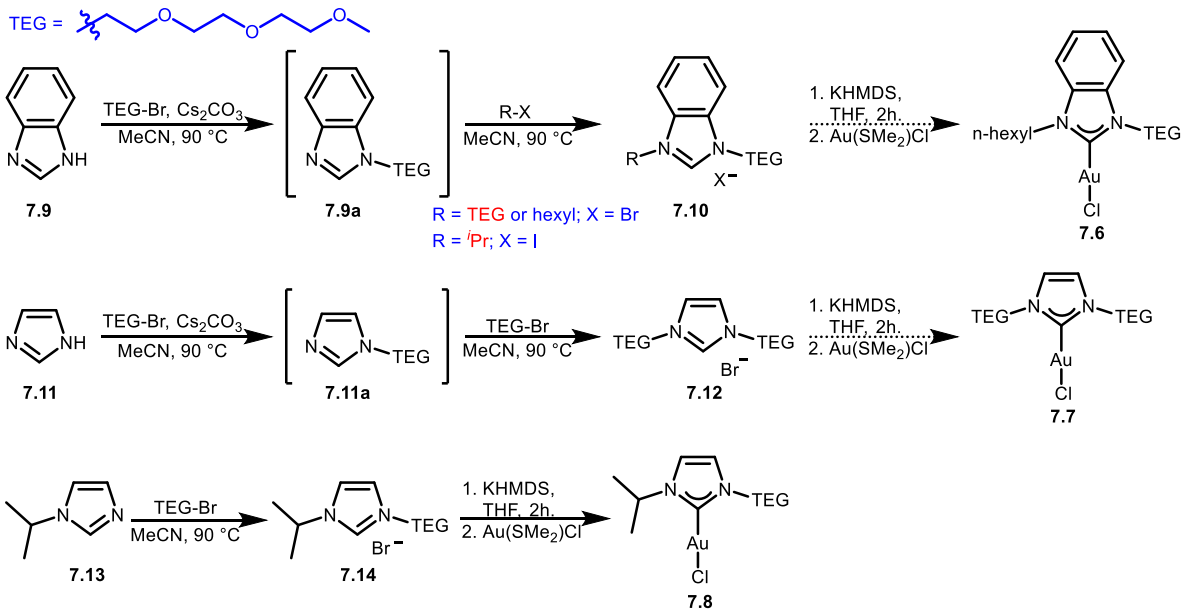


Figure 7.2: Four examples of water-soluble NHCs used on AuNPs.[1, 2, 7, 8]

Scheme 7.1: Synthetic methods to synthesize complexes **7.6** – **7.8**.



We started with commercially available 1-isopropylimidazole, **7.13** and reacted with isopropyl iodide in a pressure vial in acetonitrile overnight. The reaction was then dried and purified through flash column chromatography to give **7.14**. The product was confirmed using ^{1}H and ^{13}C NMR. The main peak to confirm imidazolium formation was the presence of the C2 C-H peak at 10.31 ppm. We then took **7.13** and deprotonated with KHMDS in THF for 2 hours. The solution of the deprotonated complex was filtered over a pad of celite and added to a vial containing $Au(SMe_2)Cl$. This was stirred overnight, then removed from the glovebox and dried. The residue was extracted with methylene chloride, filtered over a Celite pad, and dried to give **7.8** as a light brown oil. The product was confirmed using ^{1}H and ^{13}C NMR. The main confirmation was the lack of the imidazolium C2 C-H peak at 10.31 ppm in the ^{1}H NMR and the presence of the C2 carbon position to 182 ppm indicating a C-Au bond. We did not attempt any reactions with primary alkyl chains for the other side of the isopropyl since the commercially available isopropylimidazole worked with TEG-Br. In addition, the next steps are to research other options for creating symmetric water-soluble groups. This is because if we wanted to further functionalize the back of the benzimidazolium or imidazolium NHCs, the use of two different N-substituents will cause the creation of isomers which might not be able to be separated.

In conclusion, we attempted to synthesize of a variety of benzimidazolium and imidazolium Au complexes. We found that the benzimidazolium required the use of a primary reactant to alkylate after the addition of TEG. That led us to the synthesis of the 3-hexyl-1-(2-(2-(2-methoxyethoxy)ethoxy)ethyl)-1*H*-benzimidazolium bromide, **7.10**. We have begun synthesizing the Au complex of **7.10** which is currently undergoing purification. For the imidazolium variants, we attempted to synthesize the di-TEG-imidazolium salt, but found the salt was unable to be purified. Lastly, we developed a three-step method to synthesize (1-isopropyl-3-(2-(2-(2-methoxyethoxy)ethoxy)ethyl)imidazolium)gold(I) chloride. The next steps are to synthesize other NHC ligands containing water soluble moieties and test their solubility on AuNPs in order to complete full surface coverable.

Development in Chiral-Backed NHC Ligands.

Previously, we have tested the binding and stability of NHCs on gold surfaces. With our methodology developed, the next step was to move into the applying our systems for use in surface chemistry. Though the Click reaction (Chapter 6) functionality is useful for sensors, we wanted to investigate other types of functionality for NHC-gold surface chemistry that can be applied commercially. The introduction of chiral moieties on the NHC may give the ability for chiral molecule detection. Chirality is inherent in the structures of sugars, amino acids, and DNA. The majority of chiral binding groups on gold surfaces for detection are amino acids and their derivatives, all of which link to the surface with a thiol or amine.[9-12] The examples of chiral NHC gold surfaces are limited to a only a few reports that only utilize nanoparticles.[13-16] These reports, primarily by the Reithofer group, demonstrate their development and of NHC-AuCl histidine-derivatives(**Figure 7.3**, **7.15A**). They synthesized NHC-AuNPs by reducing the gold complex with either $NaBH_4$ or $^tBuNH_2{\bullet}BH_3$, which yielded 1-5 nm NPs, which are not large enough to be detected by SERS. The one surface application of chiral detection was reported by Zhang and coworkers, which showed the development of a thin film homochiral metal organic framework (MOF) on a NHC gold surface (**Figure 7.3**, **7.15B-Au**). This example reports the enantioselective absorption of R or *S* 1-phenylethanol.

We have conducted initial studies on NHC ligands besides the imidazolium and benzimidazolium ligands (Chapter 3). We attempted to synthesize chiral backed imidazolinium NHC ligands (**Figure 7.4**, Compounds **7.16-7.17** (*S,S*), (*R,R*), and *meso* isomers). **There have been no examples reported of chiral-backed NHC (imidazolinium) complexes on gold surfaces.** We wanted to have a good handle on binding chiral molecules to gold surfaces and detecting them through SERS. We started with commercially available (1*S*,2*S*)-(−)-1,2-diphenylethylenediamine, **7.18-*(S,S)***, and alkylated each nitrogen using 2-iodopropane and K_2CO_3 in a pressure vial. It is important to note this reaction must be performed in a pressurized vessel, otherwise it does not go to completion and mostly forms a mono substituted product. The reaction was dried, extracted with methylene chloride and filtered over a pad of Celite. The filtrate was dried to give **7.19-(*S,S*)**. We then took **7.19-(*S,S*)** and completed a ring closure to form the imidazolinium salt, **7.20-(*S,S*),** by reacting with triethyl orthoformate and ammonium hexafluorophosphate in a microwave reactor for five minutes at 145 °C.[17] The product precipitates out of solution and can be filtered to give **7.20-(*S,S*)**. The last step was to synthesize the NHC-CO_2 adduct of **7.20-(*S,S*)**. We did this following the method of Bushmeiser[18], by deprotonation if the C2 C-H proton followed by excess of CO_2 gas. **7.16-(*S,S*)** was isolated in a 55 % yield. The complexes were characterized using ^1H and ^{13}C NMR. Confirmation of **7.16-(*S,S*)** was shown by the lack of the imidazolium C2 C-H peak at 8.30 ppm in the ^1H NMR and the presence of the C2 and CO_2 carbon positions to 156.91 and 164.87 ppm, respectively, in the ^{13}C NMR.

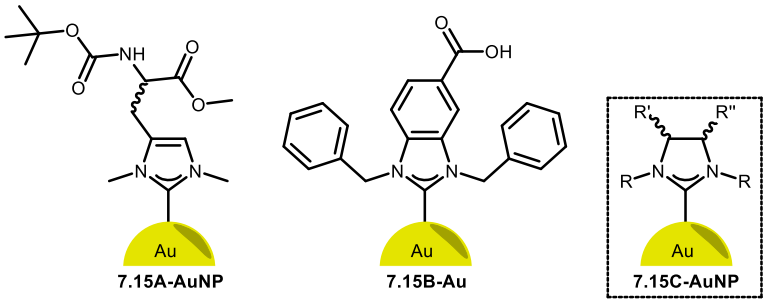


Figure 7.3: Examples of two NHC-Au surfaces that have been employed for chiral detection (**7.15A-AuNP** and **7.15B-Au**)[13, 14] and our proposed chiral imidazolinium NHC on NPs (**7.15C-AuNP**).

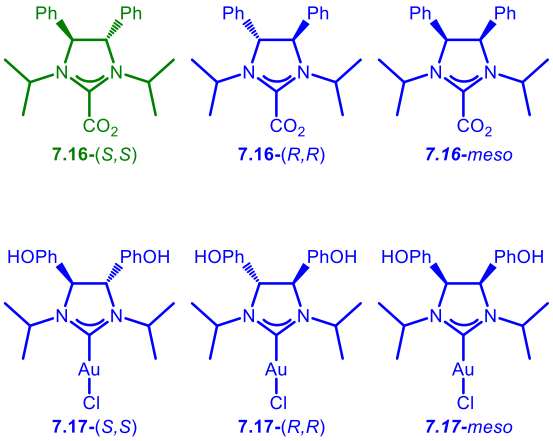
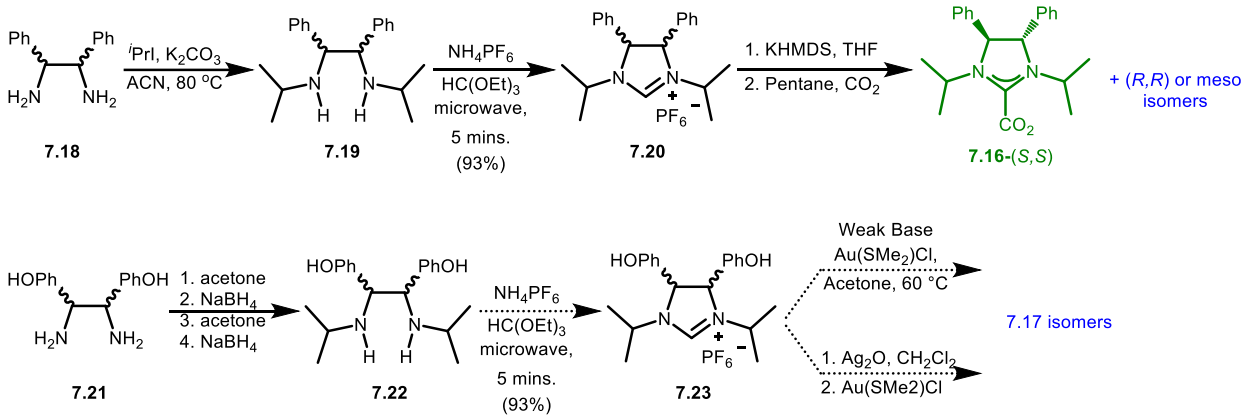


Figure 7.4: Target chiral molecules to bind to gold surfaces. Green molecule has been synthesized. Blue molecules are planned to be synthesized.

Scheme 7.2: Proposed synthetic route to synthesize all isomers of **7.16** and **7.17**.



The next steps are to synthesize the (*R,R*) and *meso* isomers of **7.16-(*S,S*).** We hypothesize this can be done following the methods used for the (*S,S*) enantiomer described above. After all three isomers have been synthesized and characterized, we plan to send the complexes to the Camden group to place the NHCs on gold FONS (film over nanospheres). They will analyze the FONS using SERS following methods previously established by our groups.[19, 20] We expect the different isomers of the complexes to have signature frequencies that will allow us to distinguish between them. This will lead to the next goal of this project, which is the development of functionalized chiral NHC gold surfaces.

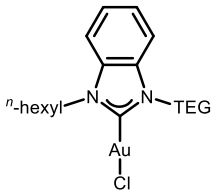
To detect molecules, a functional group that can bind to an analyte needs to be coordinated to the surface. We are choosing a phenol as the starting diamine ((1,2-Bis(2-hydroxyphenyl)ethylenediamine, **7.21)** since the different isomers are all commercially available. The synthesis of the (*R,R*)-N,N'-diisopropyl-((1,2-Bis(2-hydroxyphenyl)ethylenediamine, **7.22-(*R,R*)** has been previously synthesized by Chin.[21] We plan to use this synthesis to synthesize the other isomers of **7.22**. Once we have alkylated the different diamines we will complete a ring closure that was previously discussed above to give, **7.23** isomers. After, we plan to synthesize the gold complexes of **7.23.** Our shift to gold complexes from the CO_2-adducts is due to the acidic proton on the phenol. The synthesis of the gold complexes can be attempted in two ways: (1) a weak base approach[6] or (2) the silver oxide method.[22] After the gold complexes (**7.17**) have been synthesized, we will send the complexes to the Camden group. They will functionalize pre-synthesized gold nanoparticles with the complexes[6] and characterize through SERS. We expect to see signature frequencies of each isomer just as the FONS example above.

In conclusion, we propose a synthesis for six chiral NHC began synthesizing of these complexes and have successfully isolated a chiral NHC-CO_2 adduct. This is the first example of a chiral-backed (imidazolinium) NHC CO_2 adduct. From here we plan to move forward on synthesis of the other CO_2 adducts and gold complexes and to functionalize gold surfaces and FONS.

Experimental

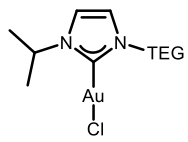
General Considerations for Synthesis. All glassware for air and water sensitive reactions were dried at 170 °C overnight before use. All reactions were stirred vigorously with magnetic stirrers. A glovebox with a dinitrogen atmosphere was used for formation of the free carbenes for NHC-CO_2 adduct synthesis. Tetrahydrofuran used in NHC-CO_2 adduct reactions was dried on an Innovative Technologies (Newburyport, MA) Pure Solv MD-7 Solvent Purification System, degassed by three freeze-pump-thaw cycles on a Schlenk line to remove dioxygen and stored under activated 4 Å molecular sieves prior to use. Carbon dioxide gas was ultra-pure grade from Airgas. Celite was dried at 240 °C under vacuum overnight and stored in a dinitrogen glovebox. All other compounds were purchased from commercial vendors at highest available purity and used without any further purification. All deuterium labeling sources were purchased from Cambridge Isotope at a minimum of 98% deuteration. Solution ^{1}H NMR and ^{13}C NMR were performed on a Varian VNMRS 500 MHz narrow-bore broadband system and Varian VNMRS 600 MHz narrow-bore broadband system at 298 K. All ^{1}H and ^{13}C shifts were referenced to the residual solvent.

Synthesis of 7.6.



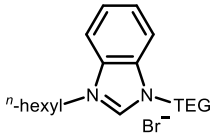
Compound **7.10** (0.1030 g, 0.2399 mmol), KHMDS (0.0564 g, 0.283 mmol), and 5 mL of THF were added to a scintillation vial in a glovebox and stirred for 2 h. at RT. The suspension was filtered over a Celite pad and added to a vial containing $Au(SMe_2)Cl$ (0.05170 g, 0.2410 mmol) and stirred for an additional 24 hours. The reaction was removed from the glovebox and the solvent was removed under vacuum. The product was re-dissolved in methylene chloride and filtered over a Celite pad. The filtrate was collected and dried under vacuum to yield **7.6** as a light brown oil. Purification is currently on-going.

Synthesis of 7.8.



In a 20 mL scintillation vial, **7.14** (0.2581 g, 0.7653 mmol) and KHMDS (0.1536 g, 0.7699 mmol), 10 mL of tetrahydrofuran were added in a glovebox. The reaction was stirred at room temperature for two hours. The suspension was filtered over a Celite pad and added to a vial containing $Au(SMe_2)Cl$ (0.0850 g, 0.3962 mmol) and stirred for an additional 24 hours. The reaction was removed from the glovebox and the solvent was removed under vacuum. The product was re-dissolved in methylene chloride and filtered over a Celite pad. The filtrate was collected and dried under vacuum to yield **7.8** as a light brown oil. 0.249 g, 87.3% yield. ^{1}H NMR (CD_2Cl_2, 499.74 MHz): □ 7.47 (d, *J* = 1.9 Hz, 1H), 7.15 (d, *J* = 1.9 Hz, 1H), 4.86 (h, *J* = 6.8 Hz, 1H), 4.46 (t, *J* = 5.1 Hz, 2H), 3.92 – 3.88 (m, 2H), 3.67 – 3.64 (m, 2H), 3.62 – 3.57 (m, 4H), 3.52 – 3.49 (m, 2H), 3.35 (s, 3H), 1.55 (d, *J* = 6.8 Hz, 6H). ^{13}C NMR (CD_2Cl_2, 125.66 MHz): □□182.21, 123.23, 117.43, 77.28, 71.87, 70.41, 70.29, 58.98, 53.50, 53.42, 51.46, 23.70, 0.98.

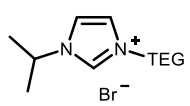
Synthesis of 7.10.



Benzimidazole, **7.9**, (0.3597 g, 3.045 mmol) was added to a 100 mL round bottom flask with TEG-Br (0.7136 g, 3.142 mmol), Cs_2CO_3 (1.0045 g, 3.083 mmol), and 10 mL of acetonitrile. The reaction was refluxed at 90 °C for 24 hours. The following day, the mixture was dried under vacuum, dissolved in 20 mL methylene chloride, and filtered over a Celite pad. The filtrate was dried under vacuum to yield the intermediate as a crude oil and immediately used for the next step. 1-bromohexane (1.290 mL, 9.22 mmol) was combined with intermediate in a 100 mL flask with 20 mL of acetonitrile. The reaction was refluxed overnight at 90 °C. The next day, the reaction was dried under reduced pressure to yield **7.10** as a yellow oil. 0.327 g, 25.0% yield. ^{1}H NMR (CD_2Cl_2, 499.74 MHz): □ 11.08 (s, 1H), 7.96 – 7.92 (m, 1H), 7.75 – 7.71 (m, 1H), 7.65 (dt, *J* = 6.5, 3.7 Hz, 2H), 4.89 – 4.85 (m, 2H), 4.56 (t, *J* = 7.5 Hz, 2H), 4.08 – 4.00 (m, 2H), 3.66 (dd, *J* = 5.5, 3.5 Hz, 2H), 3.56 – 3.48 (m, 4H), 3.44 (dd, *J* = 5.7, 3.4 Hz, 2H), 3.29 (s, 3H), 2.05 (q, *J* = 10.3, 9.0 Hz, 3H), 1.48 – 1.28 (m, 7H), 1.22 (t, *J* = 7.1 Hz, 1H), 0.88 (t, *J* = 7.1 Hz, 3H). ^{13}C NMR (CD_2Cl_2,

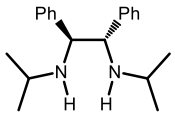
125.66 MHz): □□144.64, 133.98, 133.00, 128.70, 116.13, 114.51, 73.65, 72.42, 72.13, 70.61, 62.04, 60.40, 49.50, 32.97, 31.09, 28.00, 24.26, 15.53.

Synthesis of 7.14.



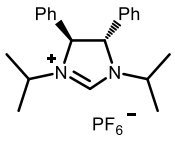
1-isopropylimidazole, **7.13**, (3.0064 g, 4.651 mmol) was combined in a pressure vial with TEG-Br (6.0502 g, 20.67 mmol) and 10 mL of acetonitrile. The vessel was sealed with a Teflon screw cap and stirred at 85 °C for 3 days. During the reaction, a red/orange gum formed. The reaction was cooled and the solvent was removed. The following day, the product was purified using flash chromatography (MeOH in DCM). The product was dried under vacuum to yield **7.14** as a red/orange thick oil. 0.1813 g, 12.0% yield. ^{1}H NMR ($CDCl_3$, 499.74 MHz): □ 10.31 (s, 1H), 7.70 (t, *J* = 1.7 Hz, 1H), 7.39 (d, *J* = 1.8 Hz, 1H), 4.77 (p, *J* = 6.5 Hz, 1H), 4.61 (t, *J* = 4.5 Hz, 2H), 3.85 (t, *J* = 4.5 Hz, 2H), 3.61 – 3.50 (m, 8H), 3.31 (s, 3H), 1.62 (d, *J* = 6.8 Hz, 6H).

Synthesis of 7.19-(*S*,*S*)



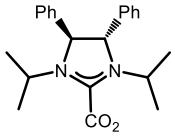
(1*S*,2*S*)-(−)-1,2-diphenylethylenediamine, **7.18-(*S*,*S*)**, (1.013 g, 4.769 mmol), K_2CO_3 (1.652 g, 11.95 mmol), 2-iodopropane (1.19 mL, 11.90 mmol) and 30 mL of acetonitrile were added to a pressure vial and the vessel was sealed with a Teflon screw cap. The reaction was heated at 82 °C and stirred for 48 hours. The reaction was cooled and dried under vacuum. The residue was extracted with methylene chloride and filtered over a Celite pad. The filtrate was collected and the solvent was removed to give **7.19-(*S*,*S*)**, as a yellow solid. 0.330 g, 23.5 % yield. ^{1}H NMR ($CDCl_3$, 499.74 MHz): □□7.25-7.14 (m, 10H), 3.85 (s, 2H), 2.68 (sept, *J* = 5.9 Hz, 2H), 2.14 (bs, 2H), 1.11 (d, *J* = 6.1 Hz, 6H), 1.07 (d, *J* = 6.3 Hz, 6H). ^{13}C NMR ($CDCl_3$, 125.66 MHz): □ 142.17, 127.90, 127.72, 126.59, 66.72, 46.01, 24.51, 22.05.

Synthesis of 7.20-(*S*,*S*)

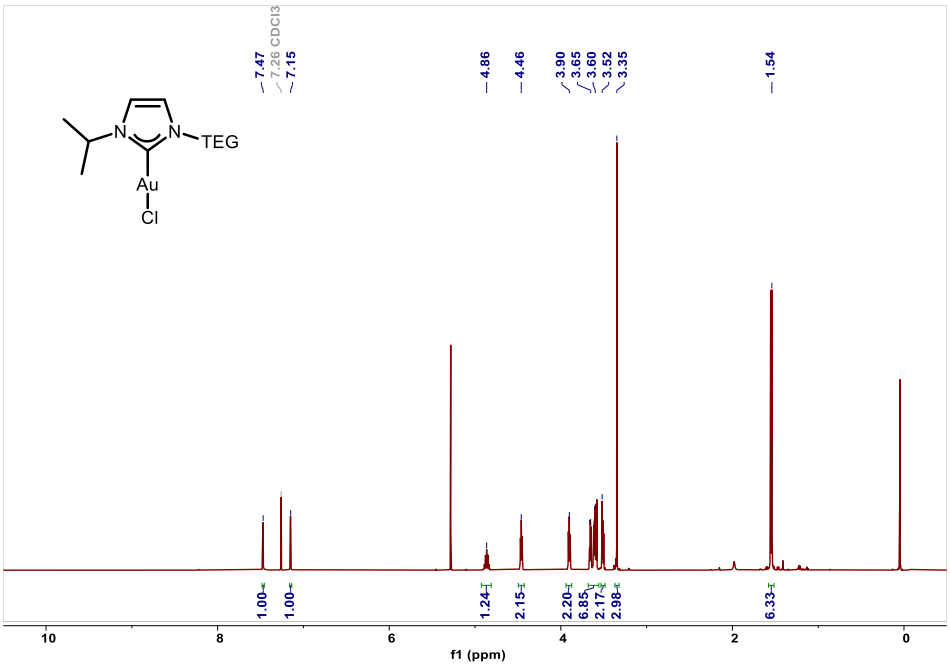


Following the method of Delaude[17], **7.19-(*S*,*S*)** (0.2063 g, 1.430 mmol), NH_4PF_6 (0.233 g, 1.429 mmol), and triethylorthoformate (2.000 mL, 19.51 mmol) were added to a microwave vessel vial with a stir bar. The reaction was sealed and irradiated 5 min at 145 °C (monitored by IR sensor) in a microwave reactor with a 50 W microwave power. Vials were cooled by rapid air cooling by the unit. Precipitate formed after cooling. Diethyl ether was added to precipitate more product. The solid was collected by filtering over a fine frit and washed with additional ether. The solid was dried under vacuum to give **7.20-(*S*,*S*)** as a white solid. 0.4009 g, 93.0 % yield. ^{1}H NMR (CD_2Cl_2, 499.74 MHz): □□8.30 (s, 1H), 7.52-7.50 (m, 5H), 7.27-7.25 (m, 5H), 4.99 (s, 2H), 3.71 (sept, *J* = 6.6 Hz, 2H), 1.46 (d, *J* = 6.8 Hz, 6H), 1.21 (d, *J* = 6.8 Hz, 6H). ^{13}C NMR (CD_2Cl_2, 125.66 MHz): □□153.79, 136.30, 131.60, 130.41, 127.28, 73.13, 50.88, 21.46, 20.70.

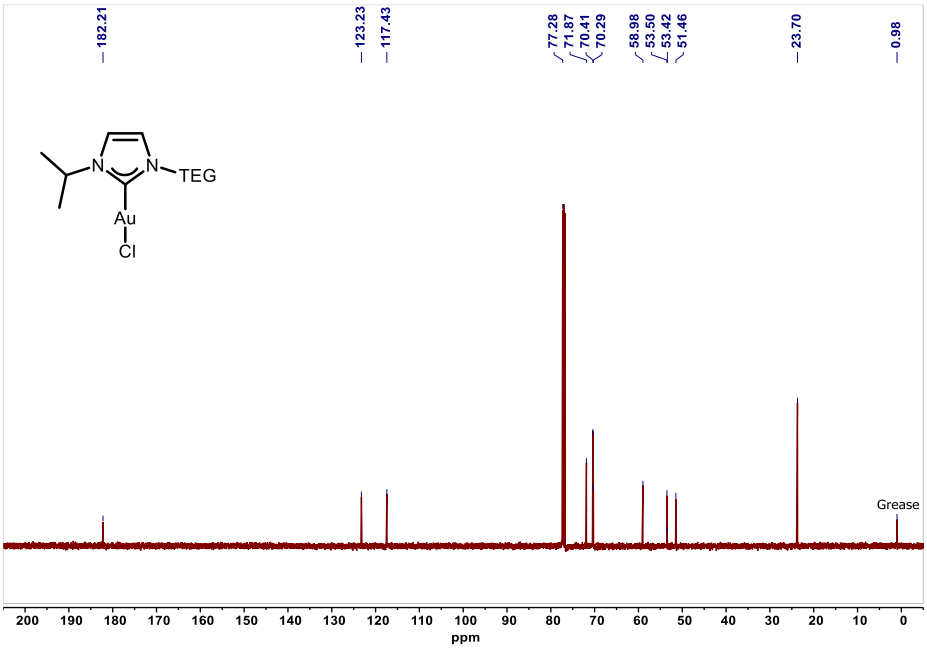
Synthesis of 7.16-(*S*,*S*)



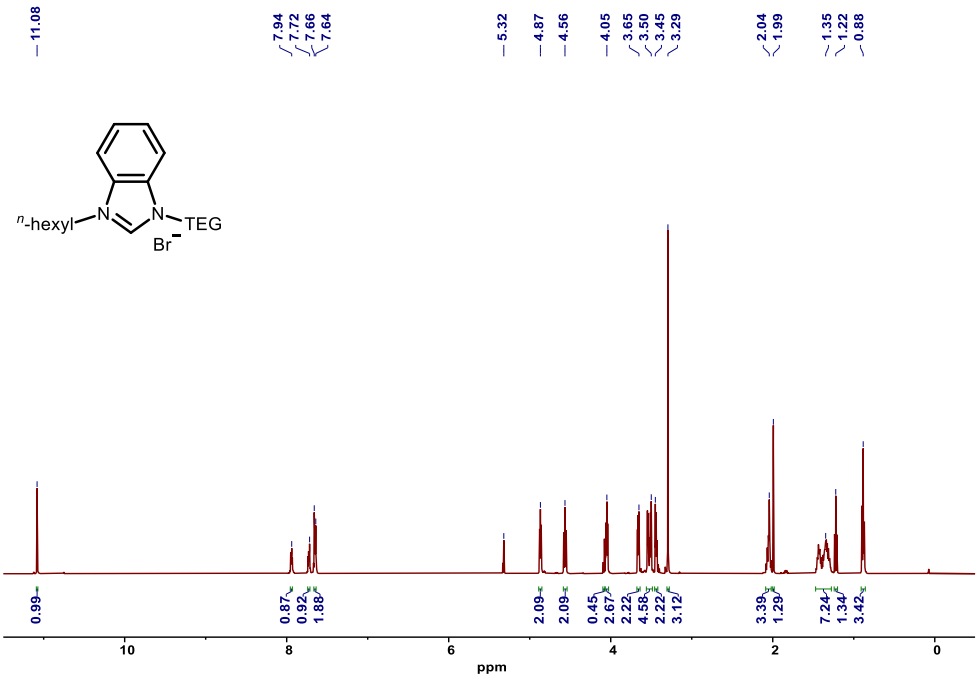
The NHC-CO_2 adduct of **7.20-(*S*,*S*),** (0.1500 g, 0.3315 mmol), was prepared following the method of Bushmeiser[18] by addition of KHMDS (0.0660 g, 0.3308 mmol) and 10 mL of THF followed by excess CO2 gas. 0.0641 g, 55.2 % yield. ^{1}H NMR (CD_2Cl_2, 499.74 MHz): □□7.49-7.43 (m, 6H). 7.32 (d, *J* = 7.1 Hz, 4H), 4.69 (s, 2H), 4.36 (sept, *J* = 6.7 Hz, 2H), 1.32 (d, *J* = 6.4 Hz, 6H), 0.91 (d, *J* = 6.4 Hz, 6H). ^{13}C NMR (CD_2Cl_2, 125.66 MHz): □□164.44, 156.48, 139.46, 129.67, 129.40, 126.00, 69.69, 50.32, 21.74, 20.48.



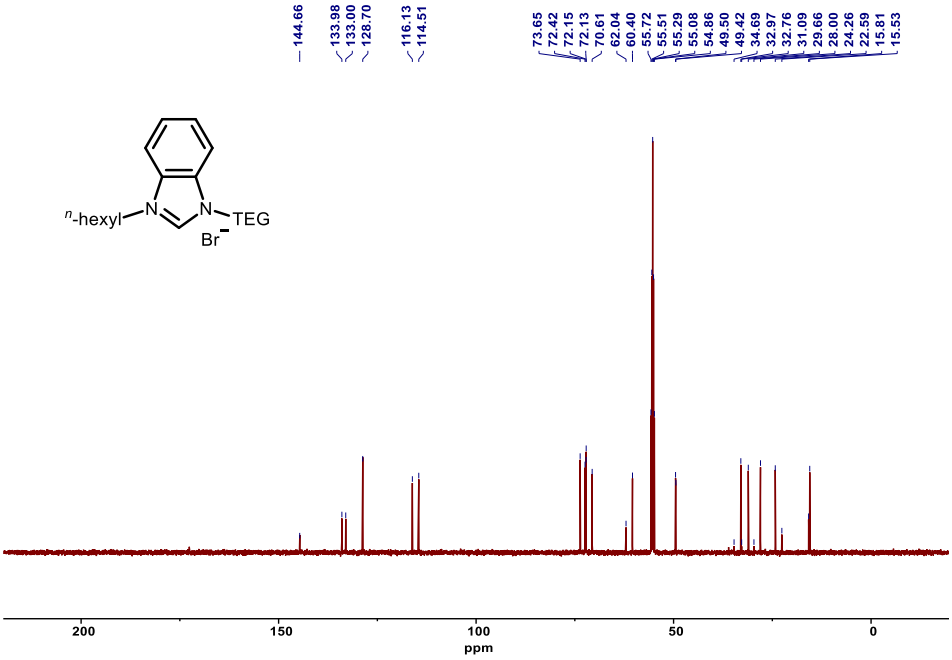
Spectra 7.1: ^{1}H NMR of **7.8** in $CDCl_3$.



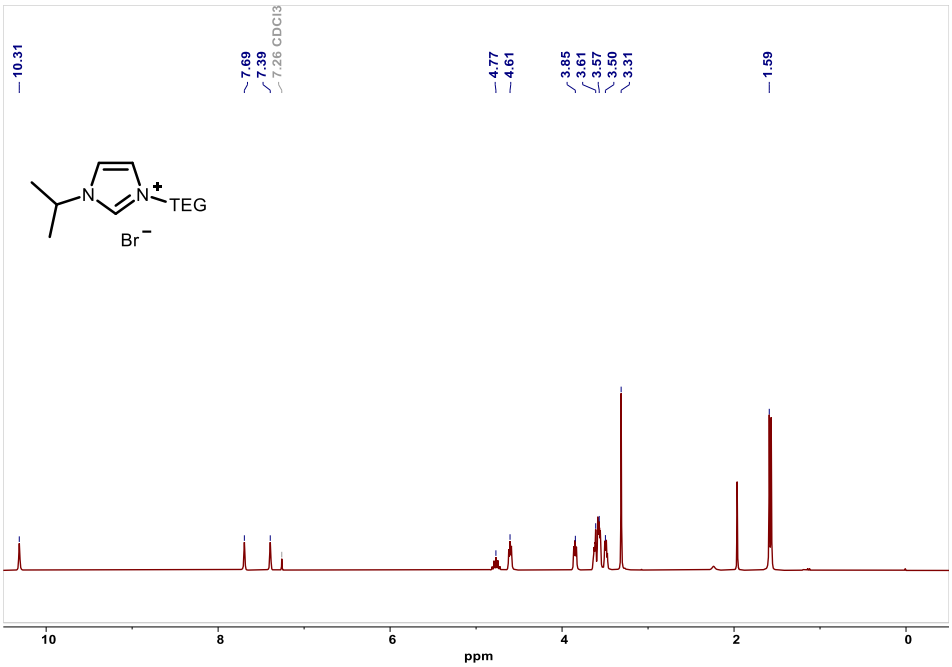
Spectra 7.2: ^{13}C NMR of **7.8** in $CDCl_3$.



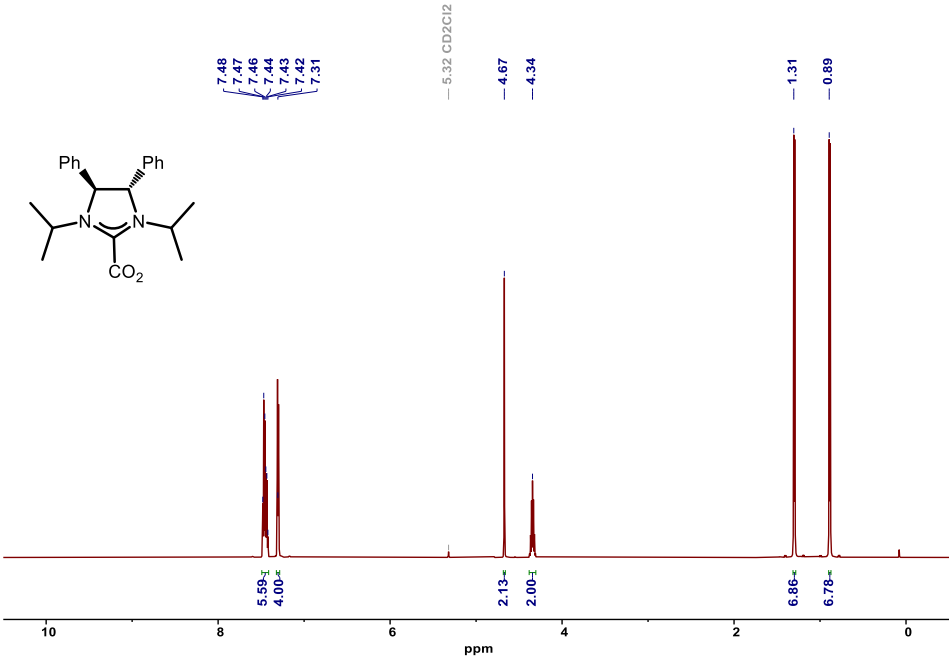
Spectra 7.3: ^{1}H NMR of **7.10** in CD_2Cl_2.



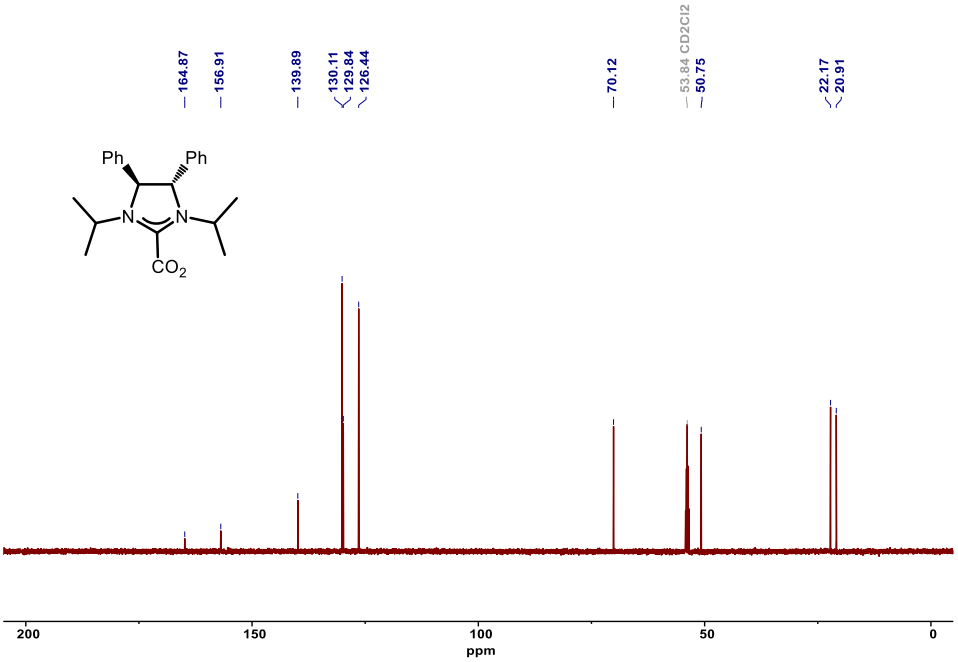
Spectra 7.4: ^{13}C NMR of **7.10** in CD_2Cl_2.



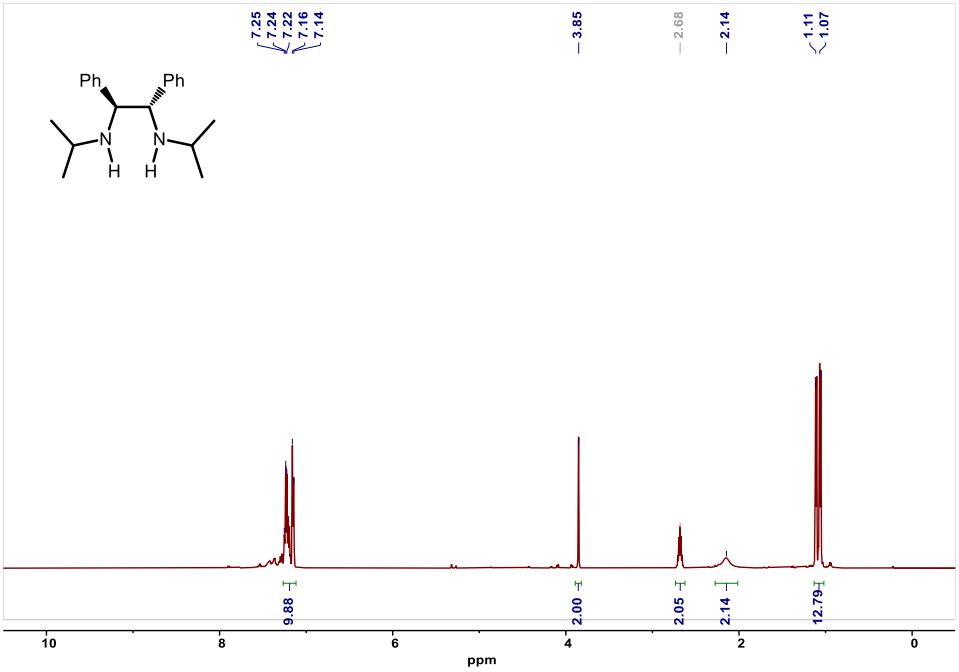
Spectra 7.5: ^{1}H NMR of **7.14** in $CDCl_3$.



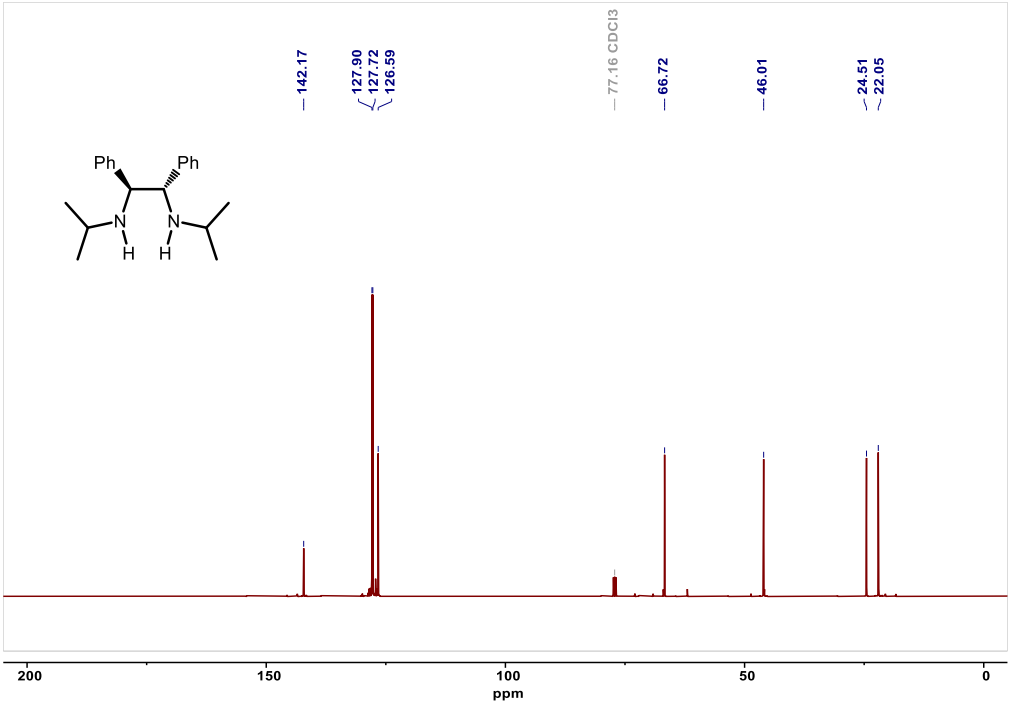
Spectra 7.6: ^{1}H NMR of **7.16-(*S*,*S*)** in CD_2Cl_2.



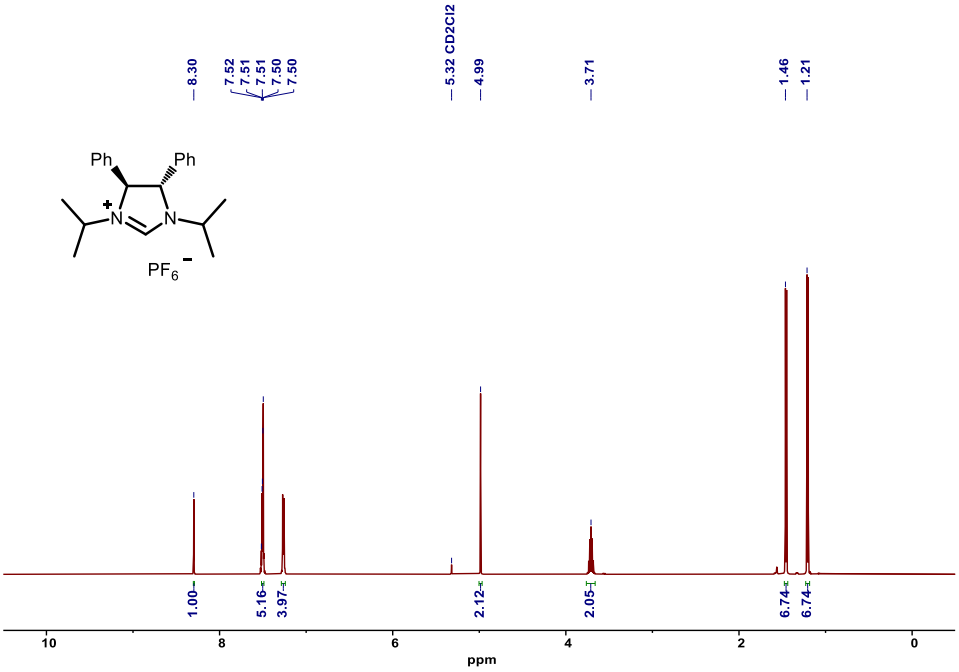
Spectra 7.7: ^{13}C NMR of **7.16-(*S*,*S*)** in $CDCl_3$.



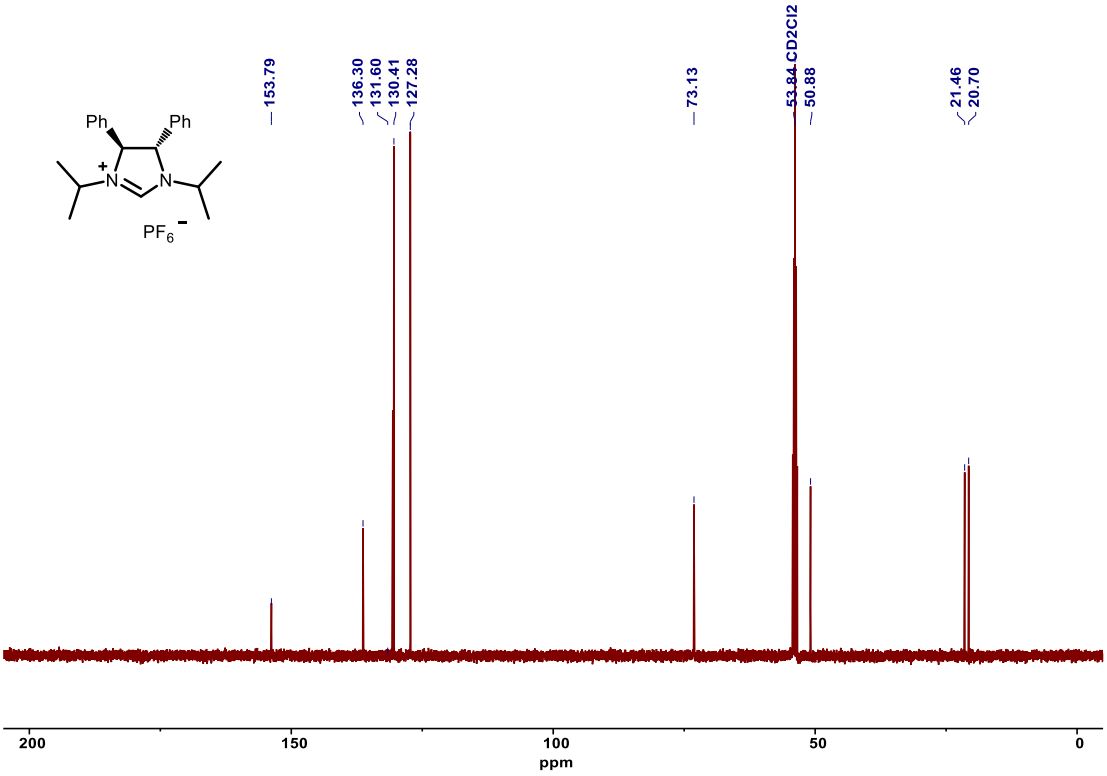
Spectra 7.8: ^{1}H NMR of **7.19-(*S*,*S*)** in $CDCl_3$.



Spectra 7.9: ^{13}C NMR of **7.19-(*S*,*S*)** in $CDCl_3$.



Spectra 7.10: ^{1}H NMR of **7.20-(*S*,*S*)** in CD_2Cl_2.



Spectra 7.11: ^{13}C NMR of **7.20-(*S*,*S*)** in CD_2Cl_2.

References

1. MacLeod, M. J.; Johnson, J. A., PEGylated N-Heterocyclic Carbene Anchors Designed To Stabilize Gold Nanoparticles in Biologically Relevant Media. *Journal of the American Chemical Society* **2015,** *137*, 7974-7977.
2. Salorinne, K.; Man, R. W. Y.; Li, C.-H.; Taki, M.; Nambo, M.; Crudden, C. M., Water-Soluble N-Heterocyclic Carbene-Protected Gold Nanoparticles: Size-Controlled Synthesis, Stability, and Optical Properties. *Angewandte Chemie International Edition* **2017,** *56*, 6198-6202.
3. Hurst, E. C.; Wilson, K.; Fairlamb, I. J. S.; Chechik, V., N-Heterocyclic carbene coated metal nanoparticles. *New Journal of Chemistry* **2009,** *33*, 1837-1840.
4. Man, R. W. Y.; Li, C.-H.; MacLean, M. W. A.; Zenkina, O. V.; Zamora, M. T.; Saunders, L. N.; Rousina-Webb, A.; Nambo, M.; Crudden, C. M., Ultrastable Gold Nanoparticles Modified by Bidentate N-Heterocyclic Carbene Ligands. *Journal of the American Chemical Society* **2018,** *140*, 1576-1579.
5. Israelsen, N. D.; Hanson, C.; Vargis, E., Nanoparticle properties and synthesis effects on surface-enhanced Raman scattering enhancement factor: an introduction. *TheScientificWorldJournal* **2015,** *2015*, 124582.
6. DeJesus, J. F.; Sherman, L. M.; Yohannan, D. J.; Becca, J. C.; Strausser, S. L.; Karger, L. F. P.; Jensen, L.; Jenkins, D. M.; Camden, J. P., A Benchtop Method for Appending Protic Functional Groups to N-Heterocyclic Carbene Protected Gold Nanoparticles. **2020,** *59*, 7585-7590.
7. Ferry, A.; Schaepe, K.; Tegeder, P.; Richter, C.; Chepiga, K. M.; Ravoo, B. J.; Glorius, F., Negatively Charged N-Heterocyclic Carbene-Stabilized Pd and Au Nanoparticles and Efficient Catalysis in Water. *ACS Catalysis* **2015,** *5*, 5414-5420.
8. Narouz, M. R.; Li, C.-H.; Nazemi, A.; Crudden, C. M., Amphiphilic N-Heterocyclic Carbene-Stabilized Gold Nanoparticles and Their Self-Assembly in Polar Solvents. *Langmuir* **2017,** *33*, 14211-14219.
9. Afkhami, A.; Kafrashi, F.; Ahmadi, M.; Madrakian, T., A new chiral electrochemical sensor for the enantioselective recognition of naproxen enantiomers using l-cysteine self-assembled over gold nanoparticles on a gold electrode. *RSC Advances* **2015,** *5*, 58609-58615.
10. Ping, J.; He, Z.; Liu, J.; Xie, X., Smartphone-based colorimetric chiral recognition of ibuprofen using aptamers-capped gold nanoparticles. **2018,** *39*, 486-495.
11. Xie, F.; Bai, Q.; Jiang, X.; Yu, X.; Xia, Z.; Wei, W., Visual and Colorimetric High-Throughput Analysis of Chiral Carboxylic Acids Based on Enantioselective Charge Shielding of Gold Nanoparticles. *ACS Applied Materials & Interfaces* **2018,** *10*, 11872-11879.
12. Zor, E.; Bekar, N., Lab-in-a-syringe using gold nanoparticles for rapid colorimetric chiral discrimination of enantiomers. *Biosensors and Bioelectronics* **2017,** *91*, 211-216.
13. Chang, L.-M.; An, Y.-Y.; Li, Q.-H.; Gu, Z.-G.; Han, Y.-F.; Zhang, J., N-Heterocyclic Carbene as a Surface Platform for Assembly of Homochiral Metal–Organic Framework Thin Films in Chiral Sensing. *ACS Applied Materials & Interfaces* **2020,** *12*, 38357-38364.

14. Young, A. J.; Sauer, M.; Rubio, G. M. D. M.; Sato, A.; Foelske, A.; Serpell, C. J.; Chin, J. M.; Reithofer, M. R., One-step synthesis and XPS investigations of chiral NHC–Au(0)/Au(i) nanoparticles. *Nanoscale* **2019,** *11*, 8327-8333.
15. Young, A. J.; Eisen, C.; Rubio, G. M. D. M.; Chin, J. M.; Reithofer, M. R., pH responsive histidin-2-ylidene stabilized gold nanoparticles. *Journal of Inorganic Biochemistry* **2019,** *199*, 110707.
16. Young, A. J.; Serpell, C. J.; Chin, J. M.; Reithofer, M. R., Optically active histidin-2-ylidene stabilised gold nanoparticles. *Chemical Communications* **2017,** *53*, 12426-12429.
17. Aidouni, A.; Bendahou, S.; Demonceau, A.; Delaude, L., Facile Microwave-Assisted Synthesis of Cyclic Amidinium Salts. *Journal of Combinatorial Chemistry* **2008,** *10*, 886-892.
18. Naumann, S.; Schmidt, F. G.; Schowner, R.; Frey, W.; Buchmeiser, M. R., Polymerization of methyl methacrylate by latent pre-catalysts based on CO2-protected N-heterocyclic carbenes. *Polymer Chemistry* **2013,** *4*, 2731-2740.
19. DeJesus, J. F.; Trujillo, M. J.; Camden, J. P.; Jenkins, D. M., N-Heterocyclic Carbenes as a Robust Platform for Surface-Enhanced Raman Spectroscopy. *Journal of the American Chemical Society* **2018,** *140*, 1247-1250.
20. Trujillo, M. J.; Strausser, S. L.; Becca, J. C.; DeJesus, J. F.; Jensen, L.; Jenkins, D. M.; Camden, J. P., Using SERS To Understand the Binding of N-Heterocyclic Carbenes to Gold Surfaces. *The Journal of Physical Chemistry Letters* **2018,** *9*, 6779-6785.
21. Lee, A.; So, S. M.; Lough, A. J.; Kim, H.; Chin, J., Mother Diamine: A Universal Building Block for Making Chiral Ligands from Daughter Diamines to Binol, Binap and Monophos Analogues. **2014,** *3*, 1102-1107.
22. Cingolani, A.; Cesari, C.; Zacchini, S.; Zanotti, V.; Cassani, M. C.; Mazzoni, R., Straightforward synthesis of iron cyclopentadienone N-heterocyclic carbene complexes. *Dalton Transactions* **2015,** *44*, 19063-19067.

Chapter 8 : Conclusion

The development of gold surfaces has led to great advancements in catalysis, sensors, and medicine, though they are yet to be completely understood. The traditional thiol binding groups have been employed for decades, but their instability on gold surfaces has led researchers to look for a new ligand that is stable in aqueous, oxidative, thermal, and pH-extreme environments, as well as in biological media. The N-heterocyclic carbene (NHC) surpasses thiol ligands by their stability in those conditions. Research by Crudden, Glorius, Johnson, Bertrand, and others has laid the groundwork for NHC gold surfaces, but there is still much to be explored. In this dissertation, we sought to address three primary aspects of NHC gold surface chemistry. (1) How are NHCs oriented on gold surfaces? (2) What are the effects of NHC ligand modifications in regard to their stability on gold surfaces? (3) How do we develop functionalized NHC gold surfaces to be utilized in biological and commercial applications?

To address the first point, we synthesized deuterated isotopologues of imidazolium and benzimidazolium NHC-CO_2 adducts to bind to gold films. Combining the synthesis, surface-enhanced Raman spectroscopy (SERS) analysis, and their agreement with theoretical calculations, we observed that the NHCs cause an adatom to come out of the surface, creating a tip like formation. Furthermore, we found that isopropyl substituents point in a mixture of both up and down in relation to the surface when binding. Finally, we report that the dominating modes (in SERS) are coming from the isopropyl substituents, due to their close proximity to the surface. Additionally, we demonstrate new characterization methods for NHCs on gold surfaces using surface assisted laser desorption ionization (SALDI) and surface enhanced spatially offset Raman spectroscopy (SESORS).

In answering the second question, we first synthesized an imidazolinium with a saturated backbone to bind to gold surfaces. This is the first example of an imidazolinium bound to a roughened surface and characterized through SERS. In addition, we tested the imidazolinium stability against the traditional imidazolium. In this study, we showed that the imidazolium is stripped off the surface upon addition of strong acid, while the imidazolinium is stable under the same conditions. We also explored a perimidinium NHC ligand for the synthesis of a perimidinium gold(I) complex, which could be bound to gold nanoparticles in the future. Furthermore, we demonstrated the synthesis and characterization of three additional d^{10} perimidinium complexes with Cu(I), Ag(I), and Pt(0). To date, there have been no examples of d^{10} perimidinium metal complexes reported.

Finally, we report our first results in the development of functionalized NHC ligands for applications in biological and commercial applications. We first attempted synthesis of a variety of alkyne backed NHC ligands. After much trial and error, we synthesized a methyl-alkyne backed NHC gold complex. This complex was bound to gold nanoparticles and confirmation of the surface functionalization was tracked through SERS, showing the

presence of the C≡C bond stretch in the silent region. Moreover, we began the initial synthesis of increased water-soluble and chiral-backed imidazolinium NHC ligands. We report a TEG functionalized NHC gold complex for applying to gold nanoparticles. We also started the development of a (*S,S*)-diphenylimidazolinium CO_2 adduct for binding to gold films.

The work presented in this dissertation presents a variety of projects that all provide more insights on how NHCs bind to gold surfaces. We synthesized and tested different types of NHCs and found the trend of which ligands are more stable and in what conditions those are. In addition, this work starts the research into using NHC ligands as commercial sensors and for post-synthetic modification. Our hope is that this research provides the background for future biologists and chemists to apply the knowledge of this work to move forward in the field of gold surface chemistry for medicinal applications, like biological sensors and drug delivery systems.

References

Chapter 1:

1.Farooq, M. U.; Novosad, V.; Rozhkova, E. A.; Wali, H.; Ali, A.; Fateh, A. A.; Neogi, P. B.; Neogi, A.; Wang, Z., Gold Nanoparticles-enabled Efficient Dual Delivery of Anticancer Therapeutics to HeLa Cells. *Scientific Reports* **2018,** *8*, 2907.

2. Xu, L.; Liu, Y.; Chen, Z.; Li, W.; Liu, Y.; Wang, L.; Liu, Y.; Wu, X.; Ji, Y.; Zhao, Y.; Ma, L.; Shao, Y.; Chen, C., Surface-Engineered Gold Nanorods: Promising DNA Vaccine Adjuvant for HIV-1 Treatment. *Nano Letters* **2012,** *12*, 2003-2012.

3. Homola, J., Present and future of surface plasmon resonance biosensors. *Anal Bioanal Chem* **2003,** *377*, 528-39.

4. Zhao, Y.; Zhou, H.; Zhang, S.; Xu, J., The synthesis of metal nanoclusters and their applications in bio-sensing and imaging. *Methods and Applications in Fluorescence* **2019,** *8*, 012001.

5. Hutchings, G. J., Vapor phase hydrochlorination of acetylene: Correlation of catalytic activity of supported metal chloride catalysts. *Journal of Catalysis* **1985,** *96*, 292-295.

6. Masatake, H.; Tetsuhiko, K.; Hiroshi, S.; Nobumasa, Y., Novel Gold Catalysts for the Oxidation of Carbon Monoxide at a Temperature far Below 0 °C. **1987,** *16*, 405-408.

7. Chen, P.-C.; Roy, P.; Chen, L.-Y.; Ravindranath, R.; Chang, H.-T., Gold and Silver Nanomaterial-Based Optical Sensing Systems. **2014,** *31*, 917-942.

8. Sener, G.; Uzun, L.; Denizli, A., Lysine-promoted colorimetric response of gold nanoparticles: a simple assay for ultrasensitive mercury(II) detection. *Analytical chemistry* **2014,** *86*, 514-20.

9. Setyawati, M. I.; Fang, W.; Chia, S. L.; Leong, D. T., Nanotoxicology of common metal oxide based nanomaterials: their ROS-y and non-ROS-y consequences. **2013,** *8*, 205-217.

10. Oliver-Meseguer, J.; Doménech-Carbó, A.; Boronat, M.; Leyva-Pérez, A.; Corma, A., Partial Reduction and Selective Transfer of Hydrogen Chloride on Catalytic Gold Nanoparticles. **2017,** *56*, 6435-6439.

11. Lee, J.-S.; Han, M. S.; Mirkin, C. A., Colorimetric Detection of Mercuric Ion (Hg^{2+}) in Aqueous Media using DNA-Functionalized Gold Nanoparticles. **2007,** *46*, 4093-4096.

12. Mout, R.; Moyano, D. F.; Rana, S.; Rotello, V. M., Surface functionalization of nanoparticles for nanomedicine. *Chemical Society Reviews* **2012,** *41*, 2539-2544.

13. Cordeiro, M.; Ferreira Carlos, F.; Pedrosa, P.; Lopez, A.; Baptista, P. V., Gold Nanoparticles for Diagnostics: Advances towards Points of Care. *Diagnostics (Basel, Switzerland)* **2016,** *6*.

14. Vericat, C.; Vela, M. E.; Benitez, G.; Carro, P.; Salvarezza, R. C., Self-assembled monolayers of thiols and dithiols on gold: new challenges for a well-known system. *Chemical Society Reviews* **2010,** *39*, 1805-1834.

15. Vericat, C.; Vela, M. E.; Corthey, G.; Pensa, E.; Cortés, E.; Fonticelli, M. H.; Ibañez, F.; Benitez, G. E.; Carro, P.; Salvarezza, R. C., Self-assembled monolayers of thiolates on metals: a review article on sulfur-metal chemistry and surface structures. *RSC Advances* **2014,** *4*, 27730-27754.

16. de la Llave, E.; Clarenc, R.; Schiffrin, D. J.; Williams, F. J., Organization of Alkane Amines on a Gold Surface: Structure, Surface Dipole, and Electron Transfer. *The Journal of Physical Chemistry C* **2014,** *118*, 468-475.

17. Schoenfisch, M. H.; Pemberton, J. E., Air Stability of Alkanethiol Self-Assembled Monolayers on Silver and Gold Surfaces. *Journal of the American Chemical Society* **1998,** *120*, 4502-4513.
18. Borzenkov, M.; Chirico, G.; D'Alfonso, L.; Sironi, L.; Collini, M.; Cabrini, E.; Dacarro, G.; Milanese, C.; Pallavicini, P.; Taglietti, A.; Bernhard, C.; Denat, F., Thermal and Chemical Stability of Thiol Bonding on Gold Nanostars. *Langmuir* **2015,** *31*, 8081-8091.
19. Delamarche, E.; Michel, B.; Kang, H.; Gerber, C., Thermal Stability of Self-Assembled Monolayers. *Langmuir* **1994,** *10*, 4103-4108.
20. Li, F.; Zhang, H.; Dever, B.; Li, X.-F.; Le, X. C., Thermal Stability of DNA Functionalized Gold Nanoparticles. *Bioconjugate Chemistry* **2013,** *24*, 1790-1797.
21. Huang, J.; Hemminger, J. C., Photooxidation of thiols in self-assembled monolayers on gold. *Journal of the American Chemical Society* **1993,** *115*, 3342-3343.
22. Hutt, D. A.; Leggett, G. J., Influence of Adsorbate Ordering on Rates of UV Photooxidation of Self-Assembled Monolayers. *The Journal of Physical Chemistry* **1996,** *100*, 6657-6662.
23. Zhang, Y.; Terrill, R. H.; Bohn, P. W., Ultraviolet Photochemistry and ex Situ Ozonolysis of Alkanethiol Self-Assembled Monolayers on Gold. *Chemistry of Materials* **1999,** *11*, 2191-2198.
24. Flynn, N. T.; Tran, T. N. T.; Cima, M. J.; Langer, R., Long-Term Stability of Self-Assembled Monolayers in Biological Media. *Langmuir* **2003,** *19*, 10909-10915.
25. Jans, K.; Bonroy, K.; De Palma, R.; Reekmans, G.; Jans, H.; Laureyn, W.; Smet, M.; Borghs, G.; Maes, G., Stability of mixed PEO-thiol SAMs for biosensing applications. *Langmuir* **2008,** *24*, 3949-54.
26. Crudden, C. M.; Horton, J. H.; Ebralidze, I. I.; Zenkina, O. V.; McLean, A. B.; Drevniok, B.; She, Z.; Kraatz, H.-B.; Mosey, N. J.; Seki, T.; Keske, E. C.; Leake, J. D.; Rousina-Webb, A.; Wu, G., Ultra stable self-assembled monolayers of N-heterocyclic carbenes on gold. *Nature Chemistry* **2014,** *6*, 409-414.
27. Crudden, C. M.; Horton, J. H.; Narouz, M. R.; Li, Z.; Smith, C. A.; Munro, K.; Baddeley, C. J.; Larrea, C. R.; Drevniok, B.; Thanabalasingam, B.; McLean, A. B.; Zenkina, O. V.; Ebralidze, I. I.; She, Z.; Kraatz, H.-B.; Mosey, N. J.; Saunders, L. N.; Yagi, A., Simple direct formation of self-assembled N-heterocyclic carbene monolayers on gold and their application in biosensing. *Nature Communications* **2016,** *7*, 12654.
28. DeJesus, J. F.; Trujillo, M. J.; Camden, J. P.; Jenkins, D. M., N-Heterocyclic Carbenes as a Robust Platform for Surface-Enhanced Raman Spectroscopy. *Journal of the American Chemical Society* **2018,** *140*, 1247-1250.
29. Trujillo, M. J.; Strausser, S. L.; Becca, J. C.; DeJesus, J. F.; Jensen, L.; Jenkins, D. M.; Camden, J. P., Using SERS To Understand the Binding of N-Heterocyclic Carbenes to Gold Surfaces. *The Journal of Physical Chemistry Letters* **2018,** *9*, 6779-6785.
30. MacLeod, M. J.; Johnson, J. A., PEGylated N-Heterocyclic Carbene Anchors Designed To Stabilize Gold Nanoparticles in Biologically Relevant Media. *Journal of the American Chemical Society* **2015,** *137*, 7974-7977.
31. Narouz, M. R.; Li, C.-H.; Nazemi, A.; Crudden, C. M., Amphiphilic N-Heterocyclic Carbene-Stabilized Gold Nanoparticles and Their Self-Assembly in Polar Solvents. *Langmuir* **2017,** *33*, 14211-14219.

32. DeJesus, J. F.; Sherman, L. M.; Yohannan, D. J.; Becca, J. C.; Strausser, S. L.; Karger, L. F. P.; Jensen, L.; Jenkins, D. M.; Camden, J. P., A Benchtop Method for Appending Protic Functional Groups to N-Heterocyclic Carbene Protected Gold Nanoparticles. **2020,** *59*, 7585-7590.
33. Marx, V. M.; Sullivan, A. H.; Melaimi, M.; Virgil, S. C.; Keitz, B. K.; Weinberger, D. S.; Bertrand, G.; Grubbs, R. H., Cyclic Alkyl Amino Carbene (CAAC) Ruthenium Complexes as Remarkably Active Catalysts for Ethenolysis. **2015,** *54*, 1919-1923.
34. Melaimi, M.; Jazzar, R.; Soleilhavoup, M.; Bertrand, G., Cyclic (Alkyl)(amino)carbenes (CAACs): Recent Developments. **2017,** *56*, 10046-10068.
35. Garber, S. B.; Kingsbury, J. S.; Gray, B. L.; Hoveyda, A. H., Efficient and Recyclable Monomeric and Dendritic Ru-Based Metathesis Catalysts. *Journal of the American Chemical Society* **2000,** *122*, 8168-8179.
36. Sanford, M. S.; Love, J. A.; Grubbs, R. H., Mechanism and Activity of Ruthenium Olefin Metathesis Catalysts. *Journal of the American Chemical Society* **2001,** *123*, 6543-6554.
37. Herrmann, W. A.; Schütz, J.; Frey, G. D.; Herdtweck, E., N-Heterocyclic Carbenes: Synthesis, Structures, and Electronic Ligand Properties. *Organometallics* **2006,** *25*, 2437-2448.
38. Back, O.; Henry-Ellinger, M.; Martin, C. D.; Martin, D.; Bertrand, G., 31P NMR Chemical Shifts of Carbene–Phosphinidene Adducts as an Indicator of the π-Accepting Properties of Carbenes. **2013,** *52*, 2939-2943.

Chapter 2:

1. Homola, J., Present and future of surface plasmon resonance biosensors. *Analytical and Bioanalytical Chemistry* **2003,** *377*, 528-539.
2. Han, G.; Ghosh, P.; Rotello, V. M., Functionalized gold nanoparticles for drug delivery. *Nanomedicine* **2007,** *2*, 113-123.
3. DiBenedetto, S. A.; Facchetti, A.; Ratner, M. A.; Marks, T. J., Molecular Self-Assembled Monolayers and Multilayers for Organic and Unconventional Inorganic Thin-Film Transistor Applications. *Advanced Materials* **2009,** *21*, 1407-1433.
4. Lv, A.; Freitag, M.; Chepiga, K. M.; Schäfer, A. H.; Glorius, F.; Chi, L., N-Heterocyclic-Carbene-Treated Gold Surfaces in Pentacene Organic Field-Effect Transistors: Improved Stability and Contact at the Interface. *Angewandte Chemie International Edition* **2018,** *57*, 4792-4796.
5. Zamborini, F. P.; Crooks, R. M., Corrosion Passivation of Gold by n-Alkanethiol Self-Assembled Monolayers: Effect of Chain Length and End Group. *Langmuir* **1998,** *14*, 3279-3286.
6. Grzelczak, M.; Pérez-Juste, J.; Mulvaney, P.; Liz-Marzán, L. M., Shape control in gold nanoparticle synthesis. *Chemical Society Reviews* **2008,** *37*, 1783-1791.
7. Hoft, R. C.; Ford, M. J.; McDonagh, A. M.; Cortie, M. B., Adsorption of Amine Compounds on the Au(111) Surface: A Density Functional Study. *The Journal of Physical Chemistry C* **2007,** *111*, 13886-13891.
8. Lavrich, D. J.; Wetterer, S. M.; Bernasek, S. L.; Scoles, G., Physisorption and Chemisorption of Alkanethiols and Alkyl Sulfides on Au(111). *The Journal of Physical Chemistry B* **1998,** *102*, 3456-3465.

9. Srisombat, L.; Jamison, A. C.; Lee, T. R., Stability: A key issue for self-assembled monolayers on gold as thin-film coatings and nanoparticle protectants. *Colloids and Surfaces A: Physicochemical and Engineering Aspects* **2011,** *390*, 1-19.
10. Vericat, C.; Vela, M. E.; Benitez, G.; Carro, P.; Salvarezza, R. C., Self-assembled monolayers of thiols and dithiols on gold: new challenges for a well-known system. *Chemical Society Reviews* **2010,** *39*, 1805-1834.
11. Crudden, C. M.; Horton, J. H.; Ebralidze, I. I.; Zenkina, O. V.; McLean, A. B.; Drevniok, B.; She, Z.; Kraatz, H.-B.; Mosey, N. J.; Seki, T.; Keske, E. C.; Leake, J. D.; Rousina-Webb, A.; Wu, G., Ultra stable self-assembled monolayers of N-heterocyclic carbenes on gold. *Nature Chemistry* **2014,** *6*, 409-414.
12. Hopkinson, M. N.; Richter, C.; Schedler, M.; Glorius, F., An overview of N-heterocyclic carbenes. *Nature* **2014,** *510*, 485-496.
13. Crudden, C. M.; Horton, J. H.; Narouz, M. R.; Li, Z.; Smith, C. A.; Munro, K.; Baddeley, C. J.; Larrea, C. R.; Drevniok, B.; Thanabalasingam, B.; McLean, A. B.; Zenkina, O. V.; Ebralidze, I. I.; She, Z.; Kraatz, H.-B.; Mosey, N. J.; Saunders, L. N.; Yagi, A., Simple direct formation of self-assembled N-heterocyclic carbene monolayers on gold and their application in biosensing. *Nature Communications* **2016,** *7*, 12654.
14. Zhukhovitskiy, A. V.; Mavros, M. G.; Van Voorhis, T.; Johnson, J. A., Addressable Carbene Anchors for Gold Surfaces. *Journal of the American Chemical Society* **2013,** *135*, 7418-7421.
15. Li, Z.; Munro, K.; Ebralize, I. I.; Narouz, M. R.; Padmos, J. D.; Hao, H.; Crudden, C. M.; Horton, J. H., N-Heterocyclic Carbene Self-Assembled Monolayers on Gold as Surface Plasmon Resonance Biosensors. *Langmuir* **2017,** *33*, 13936-13944.
16. Li, Z.; Narouz, M. R.; Munro, K.; Hao, B.; Crudden, C. M.; Horton, J. H.; Hao, H., Carboxymethylated Dextran-Modified N-Heterocyclic Carbene Self-Assembled Monolayers on Gold for Use in Surface Plasmon Resonance Biosensing. *ACS Applied Materials & Interfaces* **2017,** *9*, 39223-39234.
17. Cao, Z.; Derrick, J. S.; Xu, J.; Gao, R.; Gong, M.; Nichols, E. M.; Smith, P. T.; Liu, X.; Wen, X.; Copéret, C.; Chang, C. J., Chelating N-Heterocyclic Carbene Ligands Enable Tuning of Electrocatalytic CO2 Reduction to Formate and Carbon Monoxide: Surface Organometallic Chemistry. *Angewandte Chemie International Edition* **2018,** *57*, 4981-4985.
18. Baquero, E. A.; Tricard, S.; Coppel, Y.; Flores, J. C.; Chaudret, B.; de Jesús, E., Water-soluble platinum nanoparticles stabilized by sulfonated N-heterocyclic carbenes: influence of the synthetic approach. *Dalton Transactions* **2018,** *47*, 4093-4104.
19. Bridonneau, N.; Hippolyte, L.; Mercier, D.; Portehault, D.; Desage-El Murr, M.; Marcus, P.; Fensterbank, L.; Chanéac, C.; Ribot, F., N-Heterocyclic carbene-stabilized gold nanoparticles with tunable sizes. *Dalton Transactions* **2018,** *47*, 6850-6859.
20. MacLeod, M. J.; Johnson, J. A., PEGylated N-Heterocyclic Carbene Anchors Designed To Stabilize Gold Nanoparticles in Biologically Relevant Media. *Journal of the American Chemical Society* **2015,** *137*, 7974-7977.
21. Man, R. W. Y.; Li, C.-H.; MacLean, M. W. A.; Zenkina, O. V.; Zamora, M. T.; Saunders, L. N.; Rousina-Webb, A.; Nambo, M.; Crudden, C. M., Ultrastable Gold Nanoparticles Modified by Bidentate N-Heterocyclic Carbene Ligands. *Journal of the American Chemical Society* **2018,** *140*, 1576-1579.

22. Narouz, M. R.; Li, C.-H.; Nazemi, A.; Crudden, C. M., Amphiphilic N-Heterocyclic Carbene-Stabilized Gold Nanoparticles and Their Self-Assembly in Polar Solvents. *Langmuir* **2017,** *33*, 14211-14219.
23. Salorinne, K.; Man, R. W. Y.; Li, C.-H.; Taki, M.; Nambo, M.; Crudden, C. M., Water-Soluble N-Heterocyclic Carbene-Protected Gold Nanoparticles: Size-Controlled Synthesis, Stability, and Optical Properties. *Angewandte Chemie International Edition* **2017,** *56*, 6198-6202.
24. Vignolle, J.; Tilley, T. D., N-Heterocyclic carbene-stabilized gold nanoparticles and their assembly into 3D superlattices. *Chemical Communications* **2009**, 7230-7232.
25. Larrea, C. R.; Baddeley, C. J.; Narouz, M. R.; Mosey, N. J.; Horton, J. H.; Crudden, C. M., N-Heterocyclic Carbene Self-assembled Monolayers on Copper and Gold: Dramatic Effect of Wingtip Groups on Binding, Orientation and Assembly. *ChemPhysChem* **2017,** *18*, 3536-3539.
26. Wang, G.; Rühling, A.; Amirjalayer, S.; Knor, M.; Ernst, J. B.; Richter, C.; Gao, H.-J.; Timmer, A.; Gao, H.-Y.; Doltsinis, N. L.; Glorius, F.; Fuchs, H., Ballbot-type motion of N-heterocyclic carbenes on gold surfaces. *Nature Chemistry* **2016,** *9*, 152.
27. DeJesus, J. F.; Trujillo, M. J.; Camden, J. P.; Jenkins, D. M., N-Heterocyclic Carbenes as a Robust Platform for Surface-Enhanced Raman Spectroscopy. *Journal of the American Chemical Society* **2018,** *140*, 1247-1250.
28. Allen, C. S.; Van Duyne, R. P., Orientational specificity of Raman scattering from molecules adsorbed on silver electrodes. *Chemical Physics Letters* **1979,** *63*, 455-459.
29. Golab, J. T.; Sprague, J. R.; Carron, K. T.; Schatz, G. C.; Van Duyne, R. P., A surface enhanced hyper-Raman scattering study of pyridine adsorbed onto silver: Experiment and theory. *The Journal of Chemical Physics* **1988,** *88*, 7942-7951.
30. Turley, H. K.; Hu, Z.; Jensen, L.; Camden, J. P., Surface-Enhanced Resonance Hyper-Raman Scattering Elucidates the Molecular Orientation of Rhodamine 6G on Silver Colloids. *The Journal of Physical Chemistry Letters* **2017,** *8*, 1819-1823.
31. Giese, B.; McNaughton, D., Surface-Enhanced Raman Spectroscopic and Density Functional Theory Study of Adenine Adsorption to Silver Surfaces. *The Journal of Physical Chemistry B* **2002,** *106*, 101-112.
32. Chiang, N.; Jiang, N.; Madison, L. R.; Pozzi, E. A.; Wasielewski, M. R.; Ratner, M. A.; Hersam, M. C.; Seideman, T.; Schatz, G. C.; Van Duyne, R. P., Probing Intermolecular Vibrational Symmetry Breaking in Self-Assembled Monolayers with Ultrahigh Vacuum Tip-Enhanced Raman Spectroscopy. *Journal of the American Chemical Society* **2017,** *139*, 18664-18669.
33. Lee, J.; Tallarida, N.; Chen, X.; Jensen, L.; Apkarian, V. A., Microscopy with a single-molecule scanning electrometer. *Science Advances* **2018,** *4*.
34. Blackie, E.; Le Ru, E. C.; Meyer, M.; Timmer, M.; Burkett, B.; Northcote, P.; Etchegoin, P. G., Bi-analyte SERS with isotopically edited dyes. *Physical Chemistry Chemical Physics* **2008,** *10*, 4147-4153.
35. Camden, J. P.; Dieringer, J. A.; Wang, Y.; Masiello, D. J.; Marks, L. D.; Schatz, G. C.; Van Duyne, R. P., Probing the Structure of Single-Molecule Surface-Enhanced Raman Scattering Hot Spots. *Journal of the American Chemical Society* **2008,** *130*, 12616-12617.
36. Kleinman, S. L.; Ringe, E.; Valley, N.; Wustholz, K. L.; Phillips, E.; Scheidt, K. A.; Schatz, G. C.; Van Duyne, R. P., Single-Molecule Surface-Enhanced Raman

Spectroscopy of Crystal Violet Isotopologues: Theory and Experiment. *Journal of the American Chemical Society* **2011,** *133*, 4115-4122.
37. Titus, E. J.; Weber, M. L.; Stranahan, S. M.; Willets, K. A., Super-Resolution SERS Imaging beyond the Single-Molecule Limit: An Isotope-Edited Approach. *Nano Letters* **2012,** *12*, 5103-5110.
38. Campos, J.; Sharninghausen, L. S.; Crabtree, R. H.; Balcells, D., A Carbene-Rich but Carbonyl-Poor $[Ir^6(IMe)^8(CO)^2H^{14}]^{2+}$ Polyhydride Cluster as a Deactivation Product from Catalytic Glycerol Dehydrogenation. *Angewandte Chemie International Edition* **2014,** *53*, 12808-12811.
39. Voutchkova, A. M.; Appelhans, L. N.; Chianese, A. R.; Crabtree, R. H., Disubstituted Imidazolium-2-Carboxylates as Efficient Precursors to N-Heterocyclic Carbene Complexes of Rh, Ru, Ir, and Pd. *Journal of the American Chemical Society* **2005,** *127*, 17624-17625.
40. Van Ausdall, B. R.; Glass, J. L.; Wiggins, K. M.; Aarif, A. M.; Louie, J., A Systematic Investigation of Factors Influencing the Decarboxylation of Imidazolium Carboxylates. *The Journal of Organic Chemistry* **2009,** *74*, 7935-7942.
41. Dzyuba, S. V.; Li, S.; Bartsch, R. A., Convenient syntheses of perdeuterated ionic liquids. *Journal of Heterocyclic Chemistry* **2007,** *44*, 223-225.
42. Fèvre, M.; Pinaud, J.; Leteneur, A.; Gnanou, Y.; Vignolle, J.; Taton, D.; Miqueu, K.; Sotiropoulos, J.-M., Imidazol(in)ium Hydrogen Carbonates as a Genuine Source of N-Heterocyclic Carbenes (NHCs): Applications to the Facile Preparation of NHC Metal Complexes and to NHC-Organocatalyzed Molecular and Macromolecular Syntheses. *Journal of the American Chemical Society* **2012,** *134*, 6776-6784.
43. Lindner, R.; Lejkowski, M. L.; Lavy, S.; Deglmann, P.; Wiss, K. T.; Zarbakhsh, S.; Meyer, L.; Limbach, M., Ring-Opening Polymerization and Copolymerization of Propylene Oxide Catalyzed by N-Heterocyclic Carbenes. *ChemCatChem* **2014,** *6*, 618-625.
44. Ito, N.; Esaki, H.; Maesawa, T.; Imamiya, E.; Maegawa, T.; Sajiki, H., Efficient and Selective Pt/C-Catalyzed H–D Exchange Reaction of Aromatic Rings. *Bulletin of the Chemical Society of Japan* **2008,** *81*, 278-286.
45. Khramov, D. M.; Bielawski, C. W., Donor−Acceptor Triazenes: Synthesis, Characterization, and Study of Their Electronic and Thermal Properties. *The Journal of Organic Chemistry* **2007,** *72*, 9407-9417.
46. Farcau, C.; Astilean, S., Mapping the SERS Efficiency and Hot-Spots Localization on Gold Film over Nanospheres Substrates. *The Journal of Physical Chemistry C* **2010,** *114*, 11717-11722.
47. Péron, O.; Rinnert, E.; Toury, T.; Lamy de la Chapelle, M.; Compère, C., Quantitative SERS sensors for environmental analysis of naphthalene. *Analyst* **2011,** *136*, 1018-1022.
48. Aikens, C. M.; Schatz, G. C., TDDFT Studies of Absorption and SERS Spectra of Pyridine Interacting with Au20. *The Journal of Physical Chemistry A* **2006,** *110*, 13317-13324.
49. Zhao, L.; Jensen, L.; Schatz, G. C., Pyridine−Ag_{20} Cluster: A Model System for Studying Surface-Enhanced Raman Scattering. *Journal of the American Chemical Society* **2006,** *128*, 2911-2919.

50. Li, J.; Li, X.; Zhai, H.-J.; Wang, L.-S., Au_{20}: A Tetrahedral Cluster. *Science* **2003,** *299*, 864-867.
51. Watanabe, H.; Hayazawa, N.; Inouye, Y.; Kawata, S., DFT Vibrational Calculations of Rhodamine 6G Adsorbed on Silver: Analysis of Tip-Enhanced Raman Spectroscopy. *The Journal of Physical Chemistry B* **2005,** *109*, 5012-5020.
52. Gardner, S.; Kawamoto, T.; Curran, D. P., Synthesis of 1,3-Dialkylimidazol-2-ylidene Boranes from 1,3-Dialkylimidazolium Iodides and Sodium Borohydride. *The Journal of Organic Chemistry* **2015,** *80*, 9794-9797.
53. Chen, W.-C.; Lai, Y.-C.; Shih, W.-C.; Yu, M.-S.; Yap, G. P. A.; Ong, T.-G., Mechanistic Study of a Switch in the Regioselectivity of Hydroheteroarylation of Styrene Catalyzed by Bimetallic Ni–Al through C-H Activation. **2014,** *20*, 8099-8105.
54. te Velde, G.; Bickelhaupt, F. M.; Baerends, E. J.; Fonseca Guerra, C.; van Gisbergen, S. J. A.; Snijders, J. G.; Ziegler, T., Chemistry with ADF. **2001,** *22*, 931-967.
55. Lenthe, E. V.; Baerends, E. J.; Snijders, J. G., Relativistic regular two-component Hamiltonians. **1993,** *99*, 4597-4610.
56. Lenthe, E. v.; Ehlers, A.; Baerends, E.-J., Geometry optimizations in the zero order regular approximation for relativistic effects. **1999,** *110*, 8943-8953.
57. Becke, A. D., Density-functional exchange-energy approximation with correct asymptotic behavior. *Physical Review A* **1988,** *38*, 3098-3100.
58. Perdew, J. P., Density-functional approximation for the correlation energy of the inhomogeneous electron gas. *Physical Review B* **1986,** *33*, 8822-8824.

Chapter 3:

1. Engel, S.; Fritz, E.-C.; Ravoo, B. J., New trends in the functionalization of metallic gold: from organosulfur ligands to N-heterocyclic carbenes. *Chemical Society Reviews* **2017,** *46*, 2057-2075.
2. Goddard, Z. R.; Marín, M. J.; Russell, D. A.; Searcey, M., Active targeting of gold nanoparticles as cancer therapeutics. *Chemical Society Reviews* **2020,** *49*, 8774-8789.
3. Heuer-Jungemann, A.; Feliu, N.; Bakaimi, I.; Hamaly, M.; Alkilany, A.; Chakraborty, I.; Masood, A.; Casula, M. F.; Kostopoulou, A.; Oh, E.; Susumu, K.; Stewart, M. H.; Medintz, I. L.; Stratakis, E.; Parak, W. J.; Kanaras, A. G., The Role of Ligands in the Chemical Synthesis and Applications of Inorganic Nanoparticles. *Chemical Reviews* **2019,** *119*, 4819-4880.
4. Smith, C. A.; Narouz, M. R.; Lummis, P. A.; Singh, I.; Nazemi, A.; Li, C.-H.; Crudden, C. M., N-Heterocyclic Carbenes in Materials Chemistry. *Chemical Reviews* **2019,** *119*, 4986-5056.
5. Sun, F.; Galvan, D. D.; Jain, P.; Yu, Q., Multi-functional, thiophenol-based surface chemistry for surface-enhanced Raman spectroscopy. *Chemical Communications* **2017,** *53*, 4550-4561.
6. Zhukhovitskiy, A. V.; MacLeod, M. J.; Johnson, J. A., Carbene Ligands in Surface Chemistry: From Stabilization of Discrete Elemental Allotropes to Modification of Nanoscale and Bulk Substrates. *Chemical Reviews* **2015,** *115*, 11503-11532.
7. Li, Y.; Huang, J.; McIver, R. T.; Hemminger, J. C., Characterization of thiol self-assembled films by laser desorption Fourier transform mass spectrometry. *Journal of the American Chemical Society* **1992,** *114*, 2428-2432.

8. Schoenfisch, M. H.; Pemberton, J. E., Air Stability of Alkanethiol Self-Assembled Monolayers on Silver and Gold Surfaces. *Journal of the American Chemical Society* **1998,** *120*, 4502-4513.
9. Willey, T. M.; Vance, A. L.; van Buuren, T.; Bostedt, C.; Terminello, L. J.; Fadley, C. S., Rapid degradation of alkanethiol-based self-assembled monolayers on gold in ambient laboratory conditions. *Surface Science* **2005,** *576*, 188-196.
10. Andrieux-Ledier, A.; Tremblay, B.; Courty, A., Stability of Self-Ordered Thiol-Coated Silver Nanoparticles: Oxidative Environment Effects. *Langmuir* **2013,** *29*, 13140-13145.
11. Bhatt, N.; Huang, P.-J. J.; Dave, N.; Liu, J., Dissociation and Degradation of Thiol-Modified DNA on Gold Nanoparticles in Aqueous and Organic Solvents. *Langmuir* **2011,** *27*, 6132-6137.
12. Wu, Y.; Lian, J.; Gonçales, V. R.; Pardehkhorram, R.; Tang, W.; Tilley, R. D.; Gooding, J. J., Patterned Molecular Films of Alkanethiol and PLL-PEG on Gold–Silicate Interfaces: How to Add Functionalities while Retaining Effective Antifouling. *Langmuir* **2020,** *36*, 5243-5250.
13. Zhang, J.; Léonard, D.; Yeromonahos, C.; Mazurczyk, R.; Géhin, T.; Monfray, S.; Chevolot, Y.; Cloarec, J.-P., Orthogonal Chemical Functionalization of Au/SiO_2/TiW Patterned Substrates. *Langmuir* **2020,** *36*, 14960-14966.
14. Zhang, D.; Hao, R.; Zhang, L.; You, H.; Fang, J., Ratiometric Sensing of Polycyclic Aromatic Hydrocarbons Using Capturing Ligand Functionalized Mesoporous Au Nanoparticles as a Surface-Enhanced Raman Scattering Substrate. *Langmuir* **2020,** *36*, 11366-11373.
15. Arroyo-Currás, N.; Somerson, J.; Vieira, P. A.; Ploense, K. L.; Kippin, T. E.; Plaxco, K. W., Real-time measurement of small molecules directly in awake, ambulatory animals. *Proceedings of the National Academy of Sciences* **2017,** *114*, 645.
16. Li, H.; Dauphin-Ducharme, P.; Arroyo-Currás, N.; Tran, C. H.; Vieira, P. A.; Li, S.; Shin, C.; Somerson, J.; Kippin, T. E.; Plaxco, K. W., A Biomimetic Phosphatidylcholine-Terminated Monolayer Greatly Improves the In Vivo Performance of Electrochemical Aptamer-Based Sensors. *Angewandte Chemie International Edition* **2017,** *56*, 7492-7495.
17. Crudden, C. M.; Horton, J. H.; Ebralidze, I. I.; Zenkina, O. V.; McLean, A. B.; Drevniok, B.; She, Z.; Kraatz, H.-B.; Mosey, N. J.; Seki, T.; Keske, E. C.; Leake, J. D.; Rousina-Webb, A.; Wu, G., Ultra stable self-assembled monolayers of N-heterocyclic carbenes on gold. *Nature Chemistry* **2014,** *6*, 409.
18. DeJesus, J. F.; Sherman, L. M.; Yohannan, D. J.; Becca, J. C.; Strausser, S. L.; Karger, L. F. P.; Jensen, L.; Jenkins, D. M.; Camden, J. P., A Benchtop Method for Appending Protic Functional Groups to N-Heterocyclic Carbene Protected Gold Nanoparticles. *Angewandte Chemie International Edition* **2020,** *59*, 7585-7590.
19. DeJesus, J. F.; Trujillo, M. J.; Camden, J. P.; Jenkins, D. M., N-Heterocyclic Carbenes as a Robust Platform for Surface-Enhanced Raman Spectroscopy. *Journal of the American Chemical Society* **2018,** *140*, 1247-1250.
20. MacLeod, M. J.; Johnson, J. A., PEGylated N-Heterocyclic Carbene Anchors Designed To Stabilize Gold Nanoparticles in Biologically Relevant Media. *Journal of the American Chemical Society* **2015,** *137*, 7974-7977.
21. Nguyen, D. T.; Freitag, M.; Gutheil, C.; Sotthewes, K.; Tyler, B. J.; Böckmann, M.; Das, M.; Schlüter, F.; Doltsinis, N. L.; Arlinghaus, H. F.; Ravoo, B. J.; Glorius, F.,

An Arylazopyrazole-Based N-Heterocyclic Carbene as a Photoswitch on Gold Surfaces: Light-Switchable Wettability, Work Function, and Conductance. *Angewandte Chemie International Edition* **2020,** *59*, 13651-13656.
22. Li, Z.; Munro, K.; Ebralize, I. I.; Narouz, M. R.; Padmos, J. D.; Hao, H.; Crudden, C. M.; Horton, J. H., N-Heterocyclic Carbene Self-Assembled Monolayers on Gold as Surface Plasmon Resonance Biosensors. *Langmuir* **2017,** *33*, 13936-13944.
23. Mayall, R. M.; Smith, C. A.; Hyla, A. S.; Lee, D. S.; Crudden, C. M.; Birss, V. I., Ultrasensitive and Label-Free Detection of the Measles Virus Using an N-Heterocyclic Carbene-Based Electrochemical Biosensor. *ACS Sensors* **2020,** *5*, 2747-2752.
24. Roland, S.; Ling, X.; Pileni, M.-P., N-Heterocyclic Carbene Ligands for Au Nanocrystal Stabilization and Three-Dimensional Self-Assembly. *Langmuir* **2016,** *32*, 7683-7696.
25. Trujillo, M. J.; Strausser, S. L.; Becca, J. C.; DeJesus, J. F.; Jensen, L.; Jenkins, D. M.; Camden, J. P., Using SERS To Understand the Binding of N-Heterocyclic Carbenes to Gold Surfaces. *The Journal of Physical Chemistry Letters* **2018,** *9*, 6779-6785.
26. Voutchkova, A. M.; Feliz, M.; Clot, E.; Eisenstein, O.; Crabtree, R. H., Imidazolium Carboxylates as Versatile and Selective N-Heterocyclic Carbene Transfer Agents: Synthesis, Mechanism, and Applications. *Journal of the American Chemical Society* **2007,** *129*, 12834-12846.
27. Wang, G.; Rühling, A.; Amirjalayer, S.; Knor, M.; Ernst, J. B.; Richter, C.; Gao, H.-J.; Timmer, A.; Gao, H.-Y.; Doltsinis, N. L.; Glorius, F.; Fuchs, H., Ballbot-type motion of N-heterocyclic carbenes on gold surfaces. *Nature Chemistry* **2017,** *9*, 152-156.
28. Nguyen, D. T.; Freitag, M.; Körsgen, M.; Lamping, S.; Rühling, A.; Schäfer, A. H.; Siekman, M. H.; Arlinghaus, H. F.; van der Wiel, W. G.; Glorius, F.; Ravoo, B. J., Versatile Micropatterns of N-Heterocyclic Carbenes on Gold Surfaces: Increased Thermal and Pattern Stability with Enhanced Conductivity. *Angewandte Chemie International Edition* **2018,** *57*, 11465-11469.
29. Haynes, C. L.; McFarland, A. D.; Van Duyne, R. P., Surface-Enhanced Raman Spectroscopy. *Analytical Chemistry* **2005,** *77*, 338 A-346 A.
30. Schlücker, S., Surface-Enhanced Raman Spectroscopy: Concepts and Chemical Applications. *Angewandte Chemie International Edition* **2014,** *53*, 4756-4795.
31. Hopkinson, M. N.; Richter, C.; Schedler, M.; Glorius, F., An overview of N-heterocyclic carbenes. *Nature* **2014,** *510*, 485-496.
32. Bakker, A.; Freitag, M.; Kolodzeiski, E.; Bellotti, P.; Timmer, A.; Ren, J.; Schulze Lammers, B.; Moock, D.; Roesky, H. W.; Mönig, H.; Amirjalayer, S.; Fuchs, H.; Glorius, F., An Electron-Rich Cyclic (Alkyl)(Amino)Carbene on Au(111), Ag(111), and Cu(111) Surfaces. *Angewandte Chemie International Edition* **2020,** *59*, 13643-13646.
33. Marx, V. M.; Sullivan, A. H.; Melaimi, M.; Virgil, S. C.; Keitz, B. K.; Weinberger, D. S.; Bertrand, G.; Grubbs, R. H., Cyclic Alkyl Amino Carbene (CAAC) Ruthenium Complexes as Remarkably Active Catalysts for Ethenolysis. *Angewandte Chemie International Edition* **2015,** *54*, 1919-1923.
34. Melaimi, M.; Jazzar, R.; Soleilhavoup, M.; Bertrand, G., Cyclic (Alkyl)(amino)carbenes (CAACs): Recent Developments. *Angewandte Chemie International Edition* **2017,** *56*, 10046-10068.

35. Back, O.; Henry-Ellinger, M.; Martin, C. D.; Martin, D.; Bertrand, G., ^{31}P NMR Chemical Shifts of Carbene–Phosphinidene Adducts as an Indicator of the π-Accepting Properties of Carbenes. *Angewandte Chemie International Edition* **2013,** *52*, 2939-2943.
36. Murakami, K.; Tanaka, Y.; Sakai, R.; Hisai, Y.; Hayashi, S.; Mizutani, Y.; Higo, T.; Ogo, S.; Seo, J. G.; Tsuneki, H.; Sekine, Y., Key factor for the anti-Arrhenius low-temperature heterogeneous catalysis induced by H^+ migration: H^+ coverage over support. *Chemical Communications* **2020,** *56*, 3365-3368.
37. Zhao, F.; Bhanage, B. M.; Shirai, M.; Arai, M., Heck Reactions of Iodobenzene and Methyl Acrylate with Conventional Supported Palladium Catalysts in the Presence of Organic and/and Inorganic Bases without Ligands. *Chemistry – A European Journal* **2000,** *6*, 843-848.
38. Borzenkov, M.; Chirico, G.; D'Alfonso, L.; Sironi, L.; Collini, M.; Cabrini, E.; Dacarro, G.; Milanese, C.; Pallavicini, P.; Taglietti, A.; Bernhard, C.; Denat, F., Thermal and Chemical Stability of Thiol Bonding on Gold Nanostars. *Langmuir* **2015,** *31*, 8081-8091.
39. Flynn, N. T.; Tran, T. N. T.; Cima, M. J.; Langer, R., Long-Term Stability of Self-Assembled Monolayers in Biological Media. *Langmuir* **2003,** *19*, 10909-10915.
40. Ma, J.-T.; Cheng, Y., Construction of enantiopure imine bridged benzo[c]azepinones by a silver(I) and chiral N-heterocyclic carbene multicatalytic reaction sequence of N′-(2-alkynylbenzylidene)hydrazides and cyclopropanecarbaldehydes. *Organic Chemistry Frontiers* **2020,** *7*, 3459-3467.
41. Singha, S.; Patra, T.; Daniliuc, C. G.; Glorius, F., Highly Enantioselective [5 + 2] Annulations through Cooperative N-Heterocyclic Carbene (NHC) Organocatalysis and Palladium Catalysis. *Journal of the American Chemical Society* **2018,** *140*, 3551-3554.
42. Thongpaen, J.; E. Schmid, T.; Toupet, L.; Dorcet, V.; Mauduit, M.; Baslé, O., Directed ortho C–H borylation catalyzed using Cp*Rh(III)–NHC complexes. *Chemical Communications* **2018,** *54*, 8202-8205.
43. Chang, L.-M.; An, Y.-Y.; Li, Q.-H.; Gu, Z.-G.; Han, Y.-F.; Zhang, J., N-Heterocyclic Carbene as a Surface Platform for Assembly of Homochiral Metal–Organic Framework Thin Films in Chiral Sensing. *ACS Applied Materials & Interfaces* **2020,** *12*, 38357-38364.
44. Young, A. J.; Sauer, M.; Rubio, G. M. D. M.; Sato, A.; Foelske, A.; Serpell, C. J.; Chin, J. M.; Reithofer, M. R., One-step synthesis and XPS investigations of chiral NHC–Au(0)/Au(I) nanoparticles. *Nanoscale* **2019,** *11*, 8327-8333.
45. Lim, I. I. S.; Mott, D.; Engelhard, M. H.; Pan, Y.; Kamodia, S.; Luo, J.; Njoki, P. N.; Zhou, S.; Wang, L.; Zhong, C. J., Interparticle Chiral Recognition of Enantiomers: A Nanoparticle-Based Regulation Strategy. *Analytical Chemistry* **2009,** *81*, 689-698.
46. Wang, Y.; Yu, Z.; Han, X.; Su, H.; Ji, W.; Cong, Q.; Zhao, B.; Ozaki, Y., Charge-Transfer-Induced Enantiomer Selective Discrimination of Chiral Alcohols by SERS. *The Journal of Physical Chemistry C* **2016,** *120*, 29374-29381.
47. Wang, Y.; Zhao, X.; Yu, Z.; Xu, Z.; Zhao, B.; Ozaki, Y., A Chiral-Label-Free SERS Strategy for the Synchronous Chiral Discrimination and Identification of Small Aromatic Molecules. *Angewandte Chemie International Edition* **2020,** *59*, 19079-19086.

48. Gu, X.; Trujillo, M. J.; Olson, J. E.; Camden, J. P., SERS Sensors: Recent Developments and a Generalized Classification Scheme Based on the Signal Origin. *Annual Review of Analytical Chemistry* **2018,** *11*, 147-169.
49. Willets, K. A.; Van Duyne, R. P., Localized Surface Plasmon Resonance Spectroscopy and Sensing. *Annual Review of Physical Chemistry* **2007,** *58*, 267-297.
50. Zeng, Y.; Hu, R.; Wang, L.; Gu, D.; He, J.; Wu, S.-Y.; Ho, H.-P.; Li, X.; Qu, J.; Gao, B. Z.; Shao, Y., Recent advances in surface plasmon resonance imaging: detection speed, sensitivity, and portability. *Nanophotonics* **2017,** *6*, 1017-1030.
51. Naumann, S.; Schmidt, F. G.; Schowner, R.; Frey, W.; Buchmeiser, M. R., Polymerization of methyl methacrylate by latent pre-catalysts based on CO_2-protected N-heterocyclic carbenes. *Polymer Chemistry* **2013,** *4*, 2731-2740.
52. Zhang, L.; Yang, H.; Jiao, L., Revisiting the Radical Initiation Mechanism of the Diamine-Promoted Transition-Metal-Free Cross-Coupling Reaction. *Journal of the American Chemical Society* **2016,** *138*, 7151-7160.
53. Barry, S. C., T. J.; Coyle, J.; Hastie, J. J. M. Group 11 Mono-Metallic Precursor Compounds and use Thereof in Metal Deposition. 2012.
54. Farcau, C.; Astilean, S., Mapping the SERS Efficiency and Hot-Spots Localization on Gold Film over Nanospheres Substrates. *The Journal of Physical Chemistry C* **2010,** *114*, 11717-11722.
55. Litorja, M.; Haynes, C. L.; Haes, A. J.; Jensen, T. R.; Van Duyne, R. P., Surface-Enhanced Raman Scattering Detected Temperature Programmed Desorption: Optical Properties, Nanostructure, and Stability of Silver Film over SiO2 Nanosphere Surfaces. *The Journal of Physical Chemistry B* **2001,** *105*, 6907-6915.
56. Cao, X.; Coulter, S. K.; Ellison, M. D.; Liu, H.; Liu, J.; Hamers, R. J., Bonding of Nitrogen-Containing Organic Molecules to the Silicon(001) Surface: The Role of Aromaticity. *The Journal of Physical Chemistry B* **2001,** *105*, 3759-3768.
57. Moulder, J. F.; Stickle, W. F.; Sobol, P. E.; Bomben, K. D., *Handbook of X-ray Photoelectron Spectroscopy*. Perkin-Elmer Corporation: 1992.
58. Bridonneau, N.; Hippolyte, L.; Mercier, D.; Portehault, D.; Desage-El Murr, M.; Marcus, P.; Fensterbank, L.; Chanéac, C.; Ribot, F., N-Heterocyclic carbene-stabilized gold nanoparticles with tunable sizes. *Dalton Transactions* **2018,** *47*, 6850-6859.
59. Crudden, C. M.; Horton, J. H.; Narouz, M. R.; Li, Z.; Smith, C. A.; Munro, K.; Baddeley, C. J.; Larrea, C. R.; Drevniok, B.; Thanabalasingam, B.; McLean, A. B.; Zenkina, O. V.; Ebralidze, I. I.; She, Z.; Kraatz, H.-B.; Mosey, N. J.; Saunders, L. N.; Yagi, A., Simple direct formation of self-assembled N-heterocyclic carbene monolayers on gold and their application in biosensing. *Nature Communications* **2016,** *7*, 12654.
60. Shirley, D. A., High-Resolution X-Ray Photoemission Spectrum of the Valence Bands of Gold. *Physical Review B* **1972,** *5*, 4709-4714.
61. Barry, S.; Clark, T. J.; Coyle, J.; Hastie, J. J. M. Group 11 Mono-Metallic Precursor Compounds and use Thereof in Metal Deposition. WO2012155264A1, November 22, 2012.

Chapter 4:

1. Crudden, C. M.; Allen, D. P., Stability and reactivity of N-heterocyclic carbene complexes. *Coordination Chemistry Reviews* **2004,** *248*, 2247-2273.
2. Díez-González, S.; Marion, N.; Nolan, S. P., N-Heterocyclic Carbenes in Late Transition Metal Catalysis. *Chemical Reviews* **2009,** *109*, 3612-3676.

3. Mercs, L.; Albrecht, M., Beyond catalysis: N-heterocyclic carbene complexes as components for medicinal, luminescent, and functional materials applications. *Chemical Society Reviews* **2010,** *39*, 1903-1912.
4. Smith, C. A.; Narouz, M. R.; Lummis, P. A.; Singh, I.; Nazemi, A.; Li, C.-H.; Crudden, C. M., N-Heterocyclic Carbenes in Materials Chemistry. *Chemical Reviews* **2019,** *119*, 4986-5056.
5. De Jesus, J. F.; Sherman, L. M.; Yohannan, D. J.; Becca, J. C.; Strausser, S. L.; Karger, L. F. P.; Jensen, L.; Jenkins, D. M.; Camden, J. P., A Benchtop Method for Appending Protic Functional Groups to N-Heterocyclic Carbene Protected Gold Nanoparticles. *Angew. Chem., Int. Ed.* **2020,** *59*, 7585-7590.
6. Benhamou, L.; Chardon, E.; Lavigne, G.; Bellemin-Laponnaz, S.; César, V., Synthetic Routes to N-Heterocyclic Carbene Precursors. *Chemical Reviews* **2011,** *111*, 2705-2733.
7. Garber, S. B.; Kingsbury, J. S.; Gray, B. L.; Hoveyda, A. H., Efficient and Recyclable Monomeric and Dendritic Ru-Based Metathesis Catalysts. *Journal of the American Chemical Society* **2000,** *122*, 8168-8179.
8. Sanford, M. S.; Love, J. A.; Grubbs, R. H., Mechanism and Activity of Ruthenium Olefin Metathesis Catalysts. *Journal of the American Chemical Society* **2001,** *123*, 6543-6554.
9. Lavallo, V.; Canac, Y.; Präsang, C.; Donnadieu, B.; Bertrand, G., Stable Cyclic (Alkyl)(Amino)Carbenes as Rigid or Flexible, Bulky, Electron-Rich Ligands for Transition-Metal Catalysts: A Quaternary Carbon Atom Makes the Difference. *Angewandte Chemie International Edition* **2005,** *44*, 5705-5709.
10. Schuster, O.; Yang, L.; Raubenheimer, H. G.; Albrecht, M., Beyond Conventional N-Heterocyclic Carbenes: Abnormal, Remote, and Other Classes of NHC Ligands with Reduced Heteroatom Stabilization. *Chemical Reviews* **2009,** *109*, 3445-3478.
11. Wang, F.; Liu, L.-j.; Wang, W.; Li, S.; Shi, M., Chiral NHC–metal-based asymmetric catalysis. *Coordination Chemistry Reviews* **2012,** *256*, 804-853.
12. Marx, V. M.; Sullivan, A. H.; Melaimi, M.; Virgil, S. C.; Keitz, B. K.; Weinberger, D. S.; Bertrand, G.; Grubbs, R. H., Cyclic Alkyl Amino Carbene (CAAC) Ruthenium Complexes as Remarkably Active Catalysts for Ethenolysis. **2015,** *54*, 1919-1923.
13. Melaimi, M.; Jazzar, R.; Soleilhavoup, M.; Bertrand, G., Cyclic (Alkyl)(amino)carbenes (CAACs): Recent Developments. **2017,** *56*, 10046-10068.
14. Ranganath, K. V. S.; Kloesges, J.; Schäfer, A. H.; Glorius, F., Asymmetric Nanocatalysis: N-Heterocyclic Carbenes as Chiral Modifiers of Fe_3O_4/Pd nanoparticles. *Angewandte Chemie International Edition* **2010,** *49*, 7786-7789.
15. Vougioukalakis, G. C.; Grubbs, R. H., Ruthenium-Based Heterocyclic Carbene-Coordinated Olefin Metathesis Catalysts. *Chemical Reviews* **2010,** *110*, 1746-1787.
16. Endo, K.; Grubbs, R. H., Chelated Ruthenium Catalysts for Z-Selective Olefin Metathesis. *Journal of the American Chemical Society* **2011,** *133*, 8525-8527.
17. Moerdyk, J. P.; Schilter, D.; Bielawski, C. W., N,N′-Diamidocarbenes: Isolable Divalent Carbons with Bona Fide Carbene Reactivity. *Accounts of Chemical Research* **2016,** *49*, 1458-1468.
18. Takebayashi, S.; Fayzullin, R. R., $[Co(NHC)(CO)_3]$: Isolation and Reactivity Study of a Model 17-Electron Species in the Oxo Process. *Organometallics* **2021,** *40*, 500-507.

19. Horsley Downie, T. M.; Hall, J. W.; Collier Finn, T. P.; Liptrot, D. J.; Lowe, J. P.; Mahon, M. F.; McMullin, C. L.; Whittlesey, M. K., The first ring-expanded NHC–copper(i) phosphides as catalysts in the highly selective hydrophosphination of isocyanates. *Chemical Communications* **2020,** *56*, 13359-13362.
20. Bermesheva, E. V.; Wozniak, A. I.; Andreyanov, F. A.; Karpov, G. O.; Nechaev, M. S.; Asachenko, A. F.; Topchiy, M. A.; Melnikova, E. K.; Nelyubina, Y. V.; Gribanov, P. S.; Bermeshev, M. V., Polymerization of 5-Alkylidene-2-norbornenes with Highly Active Pd–N-Heterocyclic Carbene Complex Catalysts: Catalyst Structure–Activity Relationships. *ACS Catalysis* **2020,** *10*, 1663-1678.
21. Benedikter, M. J.; Musso, J. V.; Frey, W.; Schowner, R.; Buchmeiser, M. R., Cationic Group VI Metal Imido Alkylidene N-Heterocyclic Carbene Nitrile Complexes: Bench-Stable, Functional-Group-Tolerant Olefin Metathesis Catalysts. *Angewandte Chemie International Edition* **2021,** *60*, 1374-1382.
22. Bazinet, P.; Yap, G. P. A.; Richeson, D. S., Constructing a Stable Carbene with a Novel Topology and Electronic Framework. *Journal of the American Chemical Society* **2003,** *125*, 13314-13315.
23. Bazinet, P.; Ong, T.-G.; O'Brien, J. S.; Lavoie, N.; Bell, E.; Yap, G. P. A.; Korobkov, I.; Richeson, D. S., Design of Sterically Demanding, Electron-Rich Carbene Ligands with the Perimidine Scaffold. *Organometallics* **2007,** *26*, 2885-2895.
24. Lee, S.; Gabidullin, B.; Richeson, D., Distinct Palladium(II) Carbene Complexes Supported by Six-Membered 1,3-Disubstituted Permidin-2-ylidene, Six-Membered N-Heterocyclic Carbenes. *ACS Omega* **2018,** *3*, 6587-6594.
25. Tsurugi, H.; Fujita, S.; Choi, G.; Yamagata, T.; Ito, S.; Miyasaka, H.; Mashima, K., Carboxylate Ligand-Induced Intramolecular C−H Bond Activation of Iridium Complexes with N-Phenylperimidine-Based Carbene Ligands. *Organometallics* **2010,** *29*, 4120-4129.
26. Choi, G.; Tsurugi, H.; Mashima, K., Hemilabile N-Xylyl-N′-methylperimidine Carbene Iridium Complexes as Catalysts for C–H Activation and Dehydrogenative Silylation: Dual Role of N-Xylyl Moiety for ortho-C–H Bond Activation and Reductive Bond Cleavage. *Journal of the American Chemical Society* **2013,** *135*, 13149-13161.
27. Hill, A. F.; McQueen, C. M. A., Dihydroperimidine-Derived N-Heterocyclic Pincer Carbene Complexes via Double C–H Activation. *Organometallics* **2012,** *31*, 8051-8054.
28. McQueen, C. M. A.; Hill, A. F.; Ma, C.; Ward, J. S., Ruthenium and osmium complexes of dihydroperimidine-based N-heterocyclic carbene pincer ligands. *Dalton Transactions* **2015,** *44*, 20376-20385.
29. Hill, A. F.; Ma, C.; McQueen, C. M. A.; Ward, J. S., Iridium complexes of perimidine-based N-heterocyclic carbene pincer ligands via aminal C–H activation. *Dalton Transactions* **2018,** *47*, 1577-1587.
30. Lam, R. H.; McQueen, C. M. A.; Pernik, I.; McBurney, R. T.; Hill, A. F.; Messerle, B. A., Selective formylation or methylation of amines using carbon dioxide catalysed by a rhodium perimidine-based NHC complex. *Green Chemistry* **2019,** *21*, 538-549.
31. Özdemir, İ.; Alıcı, B.; Gürbüz, N.; Çetinkaya, E.; Çetinkaya, B., In situ generated palladium catalysts bearing 1,3-dialkylperimidin-2-yline ligands for Suzuki reactions of aryl chlorides. *Journal of Molecular Catalysis A: Chemical* **2004,** *217*, 37-40.

32. Tu, T.; Malineni, J.; Bao, X.; Dötz, K. H., A Lutidine-Bridged Bis-Perimidinium Salt: Synthesis and Application as a Precursor in Palladium-Catalyzed Cross-Coupling Reactions. *Advanced Synthesis & Catalysis* **2009,** *351*, 1029-1034.
33. Toda, T.; Kuwata, S., Central N-heterocyclic carbene moieties in protic pincer-type bis(pyrazole) ligands: Perturbation on steric and electronic properties of ruthenium center. *Journal of Organometallic Chemistry* **2020,** *917*, 121270.
34. Oehninger, L.; Küster, L. N.; Schmidt, C.; Muñoz-Castro, A.; Prokop, A.; Ott, I., A Chemical–Biological Evaluation of Rhodium(I) N-Heterocyclic Carbene Complexes as Prospective Anticancer Drugs. *Chemistry – A European Journal* **2013,** *19*, 17871-17880.
35. Langbein, S.; Wadepohl, H.; Gade, L. H., Ditopic N-Heterocyclic Pincer Carbene Complexes Containing a Perylene Backbone. *Organometallics* **2016,** *35*, 809-815.
36. Richeson, D. S.; Bazinet, P. R. Preparation of carbene ligands and their transition metal complexes useful as catalysts for organic synthesis. 2005.
37. Krieck, S.; Schulze, D.; Görls, H.; Westerhausen, M., Coordination Chemistry of N,N′-Bis(diphenylphosphanylmethyl)- 2,3-dihydro-1H-perimidine – Lewis Acid-Base Complexes with the d10-Metals Nickel(0) and Gold(I). *Zeitschrift für Naturforschung B* **2014,** *69*, 1299-1305.
38. Akıncı, P. A.; Gülcemal, S.; Kazheva, O. N.; Alexandrov, G. G.; Dyachenko, O. A.; Çetinkaya, E.; Çetinkaya, B., Perimidin-2-ylidene rhodium(I) complexes; unexpected halogen exchange and catalytic activities in transfer hydrogenation reaction. *Journal of Organometallic Chemistry* **2014,** *765*, 23-30.
39. Verlinden, K.; Ganter, C., Converting a perimidine derivative to a cationic N-heterocyclic carbene. *Journal of Organometallic Chemistry* **2014,** *750*, 23-29.
40. Hill, A. F.; McQueen, C. M. A., Dihydroperimidine-Derived PNP Pincer Complexes as Intermediates en Route to N-Heterocyclic Carbene Pincer Complexes. *Organometallics* **2014,** *33*, 1909-1912.
41. Baker, M. V.; Barnard, P. J.; Berners-Price, S. J.; Brayshaw, S. K.; Hickey, J. L.; Skelton, B. W.; White, A. H., Synthesis and structural characterisation of linear Au(I) N-heterocyclic carbene complexes: New analogues of the Au(I) phosphine drug Auranofin. *Journal of Organometallic Chemistry* **2005,** *690*, 5625-5635.
42. Griffiths, M. B. E.; Koponen, S. E.; Mandia, D. J.; McLeod, J. F.; Coyle, J. P.; Sims, J. J.; Giorgi, J. B.; Sirianni, E. R.; Yap, G. P. A.; Barry, S. T., Surfactant Directed Growth of Gold Metal Nanoplates by Chemical Vapor Deposition. *Chemistry of Materials* **2015,** *27*, 6116-6124.
43. Ray, L.; Katiyar, V.; Barman, S.; Raihan, M. J.; Nanavati, H.; Shaikh, M. M.; Ghosh, P., Gold(I) N-heterocyclic carbene based initiators for bulk ring-opening polymerization of l-lactide. *Journal of Organometallic Chemistry* **2007,** *692*, 4259-4269.
44. Sampford, K. R.; Carden, J. L.; Kidner, E. B.; Berry, A.; Cavell, K. J.; Murphy, D. M.; Kariuki, B. M.; Newman, P. D., Twisting the arm: structural constraints in bicyclic expanded-ring N-heterocyclic carbenes. *Dalton Transactions* **2019,** *48*, 1850-1858.
45. Okayama, T.; Watanabe, T.; Hatayama, Y.; Ishihara, S.; Yamaguchi, Y., Transformation of NHC·BEt_3 into AgCl·NHC: Efficiently preparative method for early–late heterobimetallic complexes using indenyl-functionalized N-heterocyclic carbene as a bridging ligand. *Inorganica Chimica Acta* **2016,** *448*, 1-6.

46. Doud, E. A.; Inkpen, M. S.; Lovat, G.; Montes, E.; Paley, D. W.; Steigerwald, M. L.; Vázquez, H.; Venkataraman, L.; Roy, X., In Situ Formation of N-Heterocyclic Carbene-Bound Single-Molecule Junctions. *Journal of the American Chemical Society* **2018,** *140*, 8944-8949.
47. de Frémont, P.; Scott, N. M.; Stevens, E. D.; Ramnial, T.; Lightbody, O. C.; Macdonald, C. L. B.; Clyburne, J. A. C.; Abernethy, C. D.; Nolan, S. P., Synthesis of Well-Defined N-Heterocyclic Carbene Silver(I) Complexes. *Organometallics* **2005,** *24*, 6301-6309.
48. Ogle, J. W.; Zhang, J.; Reibenspies, J. H.; Abboud, K. A.; Miller, S. A., Synthesis of Electronically Diverse Tetraarylimidazolylidene Carbenes via Catalytic Aldimine Coupling. *Organic Letters* **2008,** *10*, 3677-3680.
49. Herrmann, W. A.; Schneider, S. K.; Öfele, K.; Sakamoto, M.; Herdtweck, E., First silver complexes of tetrahydropyrimid-2-ylidenes. *Journal of Organometallic Chemistry* **2004,** *689*, 2441-2449.
50. Humenny, W. J.; Mitzinger, S.; Khadka, C. B.; Najafabadi, B. K.; Vieira, I.; Corrigan, J. F., N-heterocyclic carbene stabilized copper- and silver-phenylchalcogenolate ring complexes. *Dalton Transactions* **2012,** *41*, 4413-4422.
51. Collins, L. R.; Lowe, J. P.; Mahon, M. F.; Poulten, R. C.; Whittlesey, M. K., Copper Diamidocarbene Complexes: Characterization of Monomeric to Tetrameric Species. *Inorganic Chemistry* **2014,** *53*, 2699-2707.
52. Hardman, N. J.; Abrams, M. B.; Pribisko, M. A.; Gilbert, T. M.; Martin, R. L.; Kubas, G. J.; Baker, R. T., Molecular and Electronic Structure of Platinum Bis(N-arylamino)phosphenium Complexes including [Pt(phosphane)(phosphenium)(N-heterocyclic carbene)]. *Angewandte Chemie International Edition* **2004,** *43*, 1955-1958.
53. Silbestri, G. F.; Flores, J. C.; de Jesús, E., Water-Soluble N-Heterocyclic Carbene Platinum(0) Complexes: Recyclable Catalysts for the Hydrosilylation of Alkynes in Water at Room Temperature. *Organometallics* **2012,** *31*, 3355-3360.
54. Arduengo, A. J.; Gamper, S. F.; Calabrese, J. C.; Davidson, F., Low-Coordinate Carbene Complexes of Nickel(0) and Platinum(0). *Journal of the American Chemical Society* **1994,** *116*, 4391-4394.
55. Arnold, P. L.; Cloke, F. G. N.; Geldbach, T.; Hitchcock, P. B., Metal Vapor Synthesis as a Straightforward Route to Group 10 Homoleptic Carbene Complexes. *Organometallics* **1999,** *18*, 3228-3233.
56. Fortman, G. C.; Scott, N. M.; Linden, A.; Stevens, E. D.; Dorta, R.; Nolan, S. P., Unusual reactivities of N-heterocyclic carbenes upon coordination to the platinum(ii)–dimethyl moiety. *Chemical Communications* **2010,** *46*, 1050-1052.
57. Bauer, J.; Braunschweig, H.; Brenner, P.; Kraft, K.; Radacki, K.; Schwab, K., Late-Transition-Metal Complexes as Tunable Lewis Bases. *Chemistry – A European Journal* **2010,** *16*, 11985-11992.
58. Bauer, J.; Bertermann, R.; Braunschweig, H.; Gruss, K.; Hupp, F.; Kramer, T., New Metal-Only Lewis Pairs: Elucidating the Electronic Influence of N-Heterocyclic Carbenes and Phosphines on the Dative Pt-Al Bond. *Inorganic Chemistry* **2012,** *51*, 5617-5626.
59. Hupp, F.; Ma, M.; Kroll, F.; Jimenez-Halla, J. O. C.; Dewhurst, R. D.; Radacki, K.; Stasch, A.; Jones, C.; Braunschweig, H., Platinum Complexes Containing

Pyramidalized Germanium and Tin Dihalide Ligands Bound through σ,σ M□E Multiple Bonds. *Chemistry – A European Journal* **2014,** *20*, 16888-16898.
60. Şahin-Bölükbaşı, S.; Şahin, N., Novel Silver-NHC complexes: Synthesis and anticancer properties. *Journal of Organometallic Chemistry* **2019,** *891*, 78-84.
61. Haque, R. A.; Ghdhayeb, M. Z.; Budagumpi, S.; Salman, A. W.; Ahamed, M. B. K.; Abdul Majid, A. M. S., Non-symmetrically substituted N-heterocyclic carbene-Ag(I) complexes of benzimidazol-2-ylidenes: Synthesis, crystal structures, anticancer activity and transmetallation studies. *Inorg. Chim. Acta* **2013,** *394*, 519-525.
62. Weiss, D. T.; Altmann, P. J.; Haslinger, S.; Jandl, C.; Poethig, A.; Cokoja, M.; Kuehn, F. E., Structural diversity of late transition metal complexes with flexible tetra-NHC ligands. *Dalton Trans.* **2015,** *44*, 18329-18339.
63. Hameury, S.; de Fremont, P.; Breuil, P.-A. R.; Olivier-Bourbigou, H.; Braunstein, P., Synthesis and characterization of oxygen-functionalised-NHC silver(i) complexes and NHC transmetallation to nickel(ii). *Dalton Trans.* **2014,** *43*, 4700-4710.
64. Lu, Z.; Cramer, S. A.; Jenkins, D. M., Exploiting a dimeric silver transmetallating reagent to synthesize macrocyclic tetracarbene complexes. *Chem. Sci.* **2012,** *3*, 3081-3087.
65. Richeson, D. S. B., P. R. Preparation of carbene ligands and their transition metal complexes useful as catalysts for organic synthesis. 2005.

Chapter 5:

1. Fèvre, M.; Pinaud, J.; Leteneur, A.; Gnanou, Y.; Vignolle, J.; Taton, D.; Miqueu, K.; Sotiropoulos, J.-M., Imidazol(in)ium Hydrogen Carbonates as a Genuine Source of N-Heterocyclic Carbenes (NHCs): Applications to the Facile Preparation of NHC Metal Complexes and to NHC-Organocatalyzed Molecular and Macromolecular Syntheses. *Journal of the American Chemical Society* **2012,** *134*, 6776-6784.
2. Man, R. W. Y.; Li, C.-H.; MacLean, M. W. A.; Zenkina, O. V.; Zamora, M. T.; Saunders, L. N.; Rousina-Webb, A.; Nambo, M.; Crudden, C. M., Ultrastable Gold Nanoparticles Modified by Bidentate N-Heterocyclic Carbene Ligands. *Journal of the American Chemical Society* **2018,** *140*, 1576-1579.
3. Trujillo, M. J.; Strausser, S. L.; Becca, J. C.; DeJesus, J. F.; Jensen, L.; Jenkins, D. M.; Camden, J. P., Using SERS To Understand the Binding of N-Heterocyclic Carbenes to Gold Surfaces. *The Journal of Physical Chemistry Letters* **2018,** *9*, 6779-6785.
4. DeJesus, J. F.; Sherman, L. M.; Yohannan, D. J.; Becca, J. C.; Strausser, S. L.; Karger, L. F. P.; Jensen, L.; Jenkins, D. M.; Camden, J. P., A Benchtop Method for Appending Protic Functional Groups to N-Heterocyclic Carbene Protected Gold Nanoparticles. **2020,** *59*, 7585-7590.
5. Frens, G., Controlled Nucleation for the Regulation of the Particle Size in Monodisperse Gold Suspensions. *Nature Physical Science* **1973,** *241*, 20-22.

Chapter 6:

1. CDC. Leading Causes of Death. https://www.cdc.gov/nchs/fastats/leading-causes-of-death.htm (accessed March 8, 2021).
2. Chari, S. T., Detecting early pancreatic cancer: problems and prospects. *Semin Oncol* **2007,** *34*, 284-294.

3. Das, P. M.; Bast, R. C., Jr., Early detection of ovarian cancer. *Biomarkers in Medicine* **2008,** *2*, 291-303.
4. Rauh-Hain, J. A.; Krivak, T. C.; Del Carmen, M. G.; Olawaiye, A. B., Ovarian cancer screening and early detection in the general population. *Rev Obstet Gynecol* **2011,** *4*, 15-21.
5. Hamdy, M. E.; Del Carlo, M.; Hussein, H. A.; Salah, T. A.; El-Deeb, A. H.; Emara, M. M.; Pezzoni, G.; Compagnone, D., Development of gold nanoparticles biosensor for ultrasensitive diagnosis of foot and mouth disease virus. *Journal of Nanobiotechnology* **2018,** *16*, 48.
6. Hutter, E.; Maysinger, D., Gold-nanoparticle-based biosensors for detection of enzyme activity. *Trends in Pharmacological Sciences* **2013,** *34*, 497-507.
7. Li, Y.; Schluesener, H. J.; Xu, S., Gold nanoparticle-based biosensors. *Gold Bulletin* **2010,** *43*, 29-41.
8. Chen, P.-C.; Roy, P.; Chen, L.-Y.; Ravindranath, R.; Chang, H.-T., Gold and Silver Nanomaterial-Based Optical Sensing Systems. **2014,** *31*, 917-942.
9. Cordeiro, M.; Ferreira Carlos, F.; Pedrosa, P.; Lopez, A.; Baptista, P. V., Gold Nanoparticles for Diagnostics: Advances towards Points of Care. *Diagnostics (Basel, Switzerland)* **2016,** *6*.
10. Han, G.; Ghosh, P.; Rotello, V. M., Functionalized gold nanoparticles for drug delivery. *Nanomedicine* **2007,** *2*, 113-123.
11. Xu, L.; Liu, Y.; Chen, Z.; Li, W.; Liu, Y.; Wang, L.; Liu, Y.; Wu, X.; Ji, Y.; Zhao, Y.; Ma, L.; Shao, Y.; Chen, C., Surface-Engineered Gold Nanorods: Promising DNA Vaccine Adjuvant for HIV-1 Treatment. *Nano Letters* **2012,** *12*, 2003-2012.
12. Zhao, Y.; Zhou, H.; Zhang, S.; Xu, J., The synthesis of metal nanoclusters and their applications in bio-sensing and imaging. *Methods and Applications in Fluorescence* **2019,** *8*, 012001.
13. Jain, S.; Hirst, D. G.; O'Sullivan, J. M., Gold nanoparticles as novel agents for cancer therapy. *Br J Radiol* **2012,** *85*, 101-113.
14. Mangadlao, J. D.; Wang, X.; McCleese, C.; Escamilla, M.; Ramamurthy, G.; Wang, Z.; Govande, M.; Basilion, J. P.; Burda, C., Prostate-Specific Membrane Antigen Targeted Gold Nanoparticles for Theranostics of Prostate Cancer. *ACS nano* **2018,** *12*, 3714-3725.
15. Wang, W.; Chen, C.; Qian, M.; Zhao, X. S., Aptamer biosensor for protein detection using gold nanoparticles. *Analytical Biochemistry* **2008,** *373*, 213-219.
16. Hu, J.; Zheng, P.-C.; Jiang, J.-H.; Shen, G.-L.; Yu, R.-Q.; Liu, G.-K., Electrostatic Interaction Based Approach to Thrombin Detection by Surface-Enhanced Raman Spectroscopy. *Analytical Chemistry* **2009,** *81*, 87-93.
17. Liu, J.; Mazumdar, D.; Lu, Y., A simple and sensitive "dipstick" test in serum based on lateral flow separation of aptamer-linked nanostructures. *Angewandte Chemie (International ed. in English)* **2006,** *45*, 7955-9.
18. Kang, D.; Sun, S.; Kurnik, M.; Morales, D.; Dahlquist, F. W.; Plaxco, K. W., New Architecture for Reagentless, Protein-Based Electrochemical Biosensors. *Journal of the American Chemical Society* **2017,** *139*, 12113-12116.
19. Schoenfisch, M. H.; Pemberton, J. E., Air Stability of Alkanethiol Self-Assembled Monolayers on Silver and Gold Surfaces. *Journal of the American Chemical Society* **1998,** *120*, 4502-4513.

20. Willey, T. M.; Vance, A. L.; van Buuren, T.; Bostedt, C.; Terminello, L. J.; Fadley, C. S., Rapid degradation of alkanethiol-based self-assembled monolayers on gold in ambient laboratory conditions. *Surface Science* **2005,** *576*, 188-196.
21. Delamarche, E.; Michel, B.; Kang, H.; Gerber, C., Thermal Stability of Self-Assembled Monolayers. *Langmuir* **1994,** *10*, 4103-4108.
22. Garg, N.; Carrasquillo-Molina, E.; Lee, T. R., Self-Assembled Monolayers Composed of Aromatic Thiols on Gold: Structural Characterization and Thermal Stability in Solution. *Langmuir* **2002,** *18*, 2717-2726.
23. Li, F.; Zhang, H.; Dever, B.; Li, X.-F.; Le, X. C., Thermal Stability of DNA Functionalized Gold Nanoparticles. *Bioconjugate Chemistry* **2013,** *24*, 1790-1797.
24. Flynn, N. T.; Tran, T. N. T.; Cima, M. J.; Langer, R., Long-Term Stability of Self-Assembled Monolayers in Biological Media. *Langmuir* **2003,** *19*, 10909-10915.
25. Jans, K.; Bonroy, K.; De Palma, R.; Reekmans, G.; Jans, H.; Laureyn, W.; Smet, M.; Borghs, G.; Maes, G., Stability of mixed PEO-thiol SAMs for biosensing applications. *Langmuir* **2008,** *24*, 3949-54.
26. Hadei, N.; Kantchev, E. A. B.; O'Brie, C. J.; Organ, M. G., The First Negishi Cross-Coupling Reaction of Two Alkyl Centers Utilizing a Pd−N-Heterocyclic Carbene (NHC) Catalyst. *Organic Letters* **2005,** *7*, 3805-3807.
27. Marx, V. M.; Sullivan, A. H.; Melaimi, M.; Virgil, S. C.; Keitz, B. K.; Weinberger, D. S.; Bertrand, G.; Grubbs, R. H., Cyclic Alkyl Amino Carbene (CAAC) Ruthenium Complexes as Remarkably Active Catalysts for Ethenolysis. **2015,** *54*, 1919-1923.
28. McGuinness, D. S.; Suttil, J. A.; Gardiner, M. G.; Davies, N. W., Ethylene Oligomerization with Cr−NHC Catalysts: Further Insights into the Extended Metallacycle Mechanism of Chain Growth. *Organometallics* **2008,** *27*, 4238-4247.
29. Sanford, M. S.; Love, J. A.; Grubbs, R. H., Mechanism and Activity of Ruthenium Olefin Metathesis Catalysts. *Journal of the American Chemical Society* **2001,** *123*, 6543-6554.
30. Crudden, C. M.; Horton, J. H.; Ebralidze, I. I.; Zenkina, O. V.; McLean, A. B.; Drevniok, B.; She, Z.; Kraatz, H.-B.; Mosey, N. J.; Seki, T.; Keske, E. C.; Leake, J. D.; Rousina-Webb, A.; Wu, G., Ultra stable self-assembled monolayers of N-heterocyclic carbenes on gold. *Nature Chemistry* **2014,** *6*, 409-414.
31. Crudden, C. M.; Horton, J. H.; Narouz, M. R.; Li, Z.; Smith, C. A.; Munro, K.; Baddeley, C. J.; Larrea, C. R.; Drevniok, B.; Thanabalasingam, B.; McLean, A. B.; Zenkina, O. V.; Ebralidze, I. I.; She, Z.; Kraatz, H.-B.; Mosey, N. J.; Saunders, L. N.; Yagi, A., Simple direct formation of self-assembled N-heterocyclic carbene monolayers on gold and their application in biosensing. *Nature Communications* **2016,** *7*, 12654.
32. DeJesus, J. F.; Sherman, L. M.; Yohannan, D. J.; Becca, J. C.; Strausser, S. L.; Karger, L. F. P.; Jensen, L.; Jenkins, D. M.; Camden, J. P., A Benchtop Method for Appending Protic Functional Groups to N-Heterocyclic Carbene Protected Gold Nanoparticles. **2020,** *59*, 7585-7590.
33. DeJesus, J. F.; Trujillo, M. J.; Camden, J. P.; Jenkins, D. M., N-Heterocyclic Carbenes as a Robust Platform for Surface-Enhanced Raman Spectroscopy. *Journal of the American Chemical Society* **2018,** *140*, 1247-1250.
34. Trujillo, M. J.; Strausser, S. L.; Becca, J. C.; DeJesus, J. F.; Jensen, L.; Jenkins, D. M.; Camden, J. P., Using SERS To Understand the Binding of N-Heterocyclic

Carbenes to Gold Surfaces. *The Journal of Physical Chemistry Letters* **2018,** *9*, 6779-6785.
35. Wang, G.; Rühling, A.; Amirjalayer, S.; Knor, M.; Ernst, J. B.; Richter, C.; Gao, H.-J.; Timmer, A.; Gao, H.-Y.; Doltsinis, N. L.; Glorius, F.; Fuchs, H., Ballbot-type motion of N-heterocyclic carbenes on gold surfaces. *Nature Chemistry* **2016,** *9*, 152.
36. MacLeod, M. J.; Johnson, J. A., PEGylated N-Heterocyclic Carbene Anchors Designed To Stabilize Gold Nanoparticles in Biologically Relevant Media. *Journal of the American Chemical Society* **2015,** *137*, 7974-7977.
37. Cingolani, A.; Cesari, C.; Zacchini, S.; Zanotti, V.; Cassani, M. C.; Mazzoni, R., Straightforward synthesis of iron cyclopentadienone N-heterocyclic carbene complexes. *Dalton Transactions* **2015,** *44*, 19063-19067.
38. Lee, P. C.; Meisel, D., Adsorption and surface-enhanced Raman of dyes on silver and gold sols. *The Journal of Physical Chemistry* **1982,** *86*, 3391-3395.

Chapter 7:

1. MacLeod, M. J.; Johnson, J. A., PEGylated N-Heterocyclic Carbene Anchors Designed To Stabilize Gold Nanoparticles in Biologically Relevant Media. *Journal of the American Chemical Society* **2015,** *137*, 7974-7977.
2. Salorinne, K.; Man, R. W. Y.; Li, C.-H.; Taki, M.; Nambo, M.; Crudden, C. M., Water-Soluble N-Heterocyclic Carbene-Protected Gold Nanoparticles: Size-Controlled Synthesis, Stability, and Optical Properties. *Angewandte Chemie International Edition* **2017,** *56*, 6198-6202.
3. Hurst, E. C.; Wilson, K.; Fairlamb, I. J. S.; Chechik, V., N-Heterocyclic carbene coated metal nanoparticles. *New Journal of Chemistry* **2009,** *33*, 1837-1840.
4. Man, R. W. Y.; Li, C.-H.; MacLean, M. W. A.; Zenkina, O. V.; Zamora, M. T.; Saunders, L. N.; Rousina-Webb, A.; Nambo, M.; Crudden, C. M., Ultrastable Gold Nanoparticles Modified by Bidentate N-Heterocyclic Carbene Ligands. *Journal of the American Chemical Society* **2018,** *140*, 1576-1579.
5. Israelsen, N. D.; Hanson, C.; Vargis, E., Nanoparticle properties and synthesis effects on surface-enhanced Raman scattering enhancement factor: an introduction. *TheScientificWorldJournal* **2015,** *2015*, 124582.
6. DeJesus, J. F.; Sherman, L. M.; Yohannan, D. J.; Becca, J. C.; Strausser, S. L.; Karger, L. F. P.; Jensen, L.; Jenkins, D. M.; Camden, J. P., A Benchtop Method for Appending Protic Functional Groups to N-Heterocyclic Carbene Protected Gold Nanoparticles. **2020,** *59*, 7585-7590.
7. Ferry, A.; Schaepe, K.; Tegeder, P.; Richter, C.; Chepiga, K. M.; Ravoo, B. J.; Glorius, F., Negatively Charged N-Heterocyclic Carbene-Stabilized Pd and Au Nanoparticles and Efficient Catalysis in Water. *ACS Catalysis* **2015,** *5*, 5414-5420.
8. Narouz, M. R.; Li, C.-H.; Nazemi, A.; Crudden, C. M., Amphiphilic N-Heterocyclic Carbene-Stabilized Gold Nanoparticles and Their Self-Assembly in Polar Solvents. *Langmuir* **2017,** *33*, 14211-14219.
9. Afkhami, A.; Kafrashi, F.; Ahmadi, M.; Madrakian, T., A new chiral electrochemical sensor for the enantioselective recognition of naproxen enantiomers using l-cysteine self-assembled over gold nanoparticles on a gold electrode. *RSC Advances* **2015,** *5*, 58609-58615.
10. Ping, J.; He, Z.; Liu, J.; Xie, X., Smartphone-based colorimetric chiral recognition of ibuprofen using aptamers-capped gold nanoparticles. **2018,** *39*, 486-495.

11. Xie, F.; Bai, Q.; Jiang, X.; Yu, X.; Xia, Z.; Wei, W., Visual and Colorimetric High-Throughput Analysis of Chiral Carboxylic Acids Based on Enantioselective Charge Shielding of Gold Nanoparticles. *ACS Applied Materials & Interfaces* **2018,** *10*, 11872-11879.
12. Zor, E.; Bekar, N., Lab-in-a-syringe using gold nanoparticles for rapid colorimetric chiral discrimination of enantiomers. *Biosensors and Bioelectronics* **2017,** *91*, 211-216.
13. Chang, L.-M.; An, Y.-Y.; Li, Q.-H.; Gu, Z.-G.; Han, Y.-F.; Zhang, J., N-Heterocyclic Carbene as a Surface Platform for Assembly of Homochiral Metal–Organic Framework Thin Films in Chiral Sensing. *ACS Applied Materials & Interfaces* **2020,** *12*, 38357-38364.
14. Young, A. J.; Sauer, M.; Rubio, G. M. D. M.; Sato, A.; Foelske, A.; Serpell, C. J.; Chin, J. M.; Reithofer, M. R., One-step synthesis and XPS investigations of chiral NHC–Au(0)/Au(i) nanoparticles. *Nanoscale* **2019,** *11*, 8327-8333.
15. Young, A. J.; Eisen, C.; Rubio, G. M. D. M.; Chin, J. M.; Reithofer, M. R., pH responsive histidin-2-ylidene stabilized gold nanoparticles. *Journal of Inorganic Biochemistry* **2019,** *199*, 110707.
16. Young, A. J.; Serpell, C. J.; Chin, J. M.; Reithofer, M. R., Optically active histidin-2-ylidene stabilised gold nanoparticles. *Chemical Communications* **2017,** *53*, 12426-12429.
17. Aidouni, A.; Bendahou, S.; Demonceau, A.; Delaude, L., Facile Microwave-Assisted Synthesis of Cyclic Amidinium Salts. *Journal of Combinatorial Chemistry* **2008,** *10*, 886-892.
18. Naumann, S.; Schmidt, F. G.; Schowner, R.; Frey, W.; Buchmeiser, M. R., Polymerization of methyl methacrylate by latent pre-catalysts based on CO_2-protected N-heterocyclic carbenes. *Polymer Chemistry* **2013,** *4*, 2731-2740.
19. DeJesus, J. F.; Trujillo, M. J.; Camden, J. P.; Jenkins, D. M., N-Heterocyclic Carbenes as a Robust Platform for Surface-Enhanced Raman Spectroscopy. *Journal of the American Chemical Society* **2018,** *140*, 1247-1250.
20. Trujillo, M. J.; Strausser, S. L.; Becca, J. C.; DeJesus, J. F.; Jensen, L.; Jenkins, D. M.; Camden, J. P., Using SERS To Understand the Binding of N-Heterocyclic Carbenes to Gold Surfaces. *The Journal of Physical Chemistry Letters* **2018,** *9*, 6779-6785.
21. Lee, A.; So, S. M.; Lough, A. J.; Kim, H.; Chin, J., Mother Diamine: A Universal Building Block for Making Chiral Ligands from Daughter Diamines to Binol, Binap and Monophos Analogues. **2014,** *3*, 1102-1107.
22. Cingolani, A.; Cesari, C.; Zacchini, S.; Zanotti, V.; Cassani, M. C.; Mazzoni, R., Straightforward synthesis of iron cyclopentadienone N-heterocyclic carbene complexes. *Dalton Transactions* **2015,** *44*, 19063-19067.

Vita

Shelby Strausser grew up in northern Virginia. After graduating from high school, she attended Longwood University receiving a Bachelor of Science in Chemistry with minors in Mathematics and Physics. After college she decided to attend University of Tennessee, Knoxville to obtain a Doctor of Philosophy degree in Chemistry with a concentration in Organic Chemistry. Her research entailed the synthesis of N-heterocyclic carbenes for applications on gold surfaces and their metal complexes. After, graduation she will be moving to Kingston, Ontario to start her new position as a post-doctoral researcher with Dr. Cathleen Crudden at Queens University. She is incredibly grateful for her husband and family as she moves onto the next step in her career.